Distributed Control of Multi-Robot Teleoperation: Connectivity Preservation and Authority Dispatch

by

Yuan Yang
B.Eng., Harbin Institute of Technology, 2015
M.A.Sc., University of Victoria, 2017

A Dissertation Submitted in Partial Fulfillment of the
Requirements for the Degree of

DOCTOR OF PHILOSOPHY

in the Department of Mechanical Engineering

© Yuan Yang, 2021
University of Victoria

All rights reserved. This dissertation may not be reproduced in whole or in part, by photocopying or other means, without the permission of the author.

Distributed Control of Multi-Robot Teleoperation: Connectivity Preservation and Authority Dispatch

by

Yuan Yang
B.Eng., Harbin Institute of Technology, 2015
M.A.Sc., University of Victoria, 2017

Supervisory Committee

Dr. Daniela Constantinescu, Co-Supervisor
(Department of Mechanical Engineering)

Dr. Yang Shi, Co-Supervisor
(Department of Mechanical Engineering)

Dr. Panajotis Agathoklis, Outside Member
(Department of Electrical and Computer Engineering)

ABSTRACT

The frequent occurrences of natural and technological disasters have incurred grave loss of life and damage to property. For mitigating the miserable aftermaths, multi-robot teleoperation systems have been developed and deployed to cooperate with human rescuers in post-earthquake scenarios, and to sample, monitor and clean pollutants in marine environments. With a bidirectional communication channel, human users can deliver commands/requests to guide the motions of the remote robots, and can receive visual/audio feedback to supervise the status of the remote environment, throughout multi-robot teleoperation. Furthermore, the remote robots can send force feedback to human operators to improve their situational awareness and task performance. This way, a closed-loop multi-robot teleoperation system becomes bilateral in which coordinated robots physically interact and exchange energy with human users, and hence needs to be rendered passive for safe human-robot interaction.

Beyond guaranteeing closed-loop passivity, the control of a bilateral multi-robot teleoperation system faces two challenging problems: preserving the communication connectivity of the remote robots; and dispatching the teleoperation authority to multiple human users. Because wireless transmission of radio/acoustic signals between the remote robots is constrained by their distances, bilateral multi-robot teleoperation control must coordinate the motions of the remote robots appropriately so as to maintain their communication network connected. Further, multiple human users can send possibly conflicting teleoperation commands to the remote robots, a distributed authority dispatch algorithm is thus needed for the remote robot network to recognize and follow the most urgent user commands at runtime. This thesis develops an energy shaping strategy to preserve the connectivity of the remote robots, and to dispatch control authority over the remote robots to human users, during bilateral multi-robot teleoperation.

Chapter 1 introduces the application background of multi-robot teleoperation as well as the state-of-the-art development in related research areas. In Chapter 2, a dynamic interconnection and damping strategy is proposed to reduce and constrain the position error between the local and remote robots to any prescribed bound during bilateral teleoperation. Chapter 3 derives a gradient plus damping control from a bounded potential function and then unifies it into an indirect coupling framework to preserve all communication links of an autonomous multi-robot system with

time-varying delays and bounded actuation. On these bases, Chapter 4 develops a dynamic feedforward-feedback passivation strategy to preserve all communication links and thus the connectivity of the tree network of the remote robots while rendering the bilateral multi-robot teleoperation close loop passive. Specifically, by blending the sliding variable in Chapter 2 with the bounded potential function in Chapter 3, the dynamic passivation strategy decomposes the dynamics of the remote robots into a power-preserving interconnection of two subsystems, and regulates the energy behaviour of each subsystem to preserve the tree communication connectivity of the remote robots. To handle time-varying communication delays, the strategy further transforms the communication channels between the local and remote robots into a dynamic controller for passivating bilateral teleoperation. Superior to existing controls, the strategy using a bounded potential function can circumvent numerical instability, reduce noise sensitivity and facilitate future extensions to accommodate robot actuator saturation. On the other side, Chapter 5 designs a distributed and exponentially convergent winners-take-all authority dispatch algorithm that activates the teleoperation of only human users with the most urgent requests in real time. After formulating the problem as a constrained quadratic program, we employ an exact penalty function method to construct a distributed primal-dual dynamical system that can solve the problem at an exponential rate. Because the equilibrium of the system changes with user requests, we then interconnect the dynamical system with physical robot dynamics in a power-preserving way, and passivate closed-loop multi-robot teleoperation using multiple storage functions from a switched system perspective. Finally, Chapter 6 provides some conclusive remarks and two problems regarding connectivity preservation and authority dispatch for future study.

Table of Contents

List of Figures

Acronyms

WTA winners-take-all

EL Euler-Lagrange

IOS input-to-output stable

PD+d Proportional-Derivative plus damping

P+d Proportional plus damping

ISS input-to-state stable

PCA principal component analysis

PD Proportional-Derivative

DOF degree-of-freedom

ROS Robot Operating System

KKT Karush-Kuhn-Tucker

Chapter 1

Introduction

This chapter firstly presents a brief application background of, manipulation- and navigation-oriented control designs for, and open research problems in, multi-robot teleoperation. It then reviews existing control designs for bilateral teleoperation, connectivity-preserving multi-robot coordination, and winners-take-all (WTA) authority dispatch. On these bases, it further discusses the motivations and contributions of this thesis. Some preliminary knowledge of dissipative systems, Euler-Lagrange (EL) robot dynamics and algebraic graph theory, and the notation used in this thesis, are given at the end of this chapter.

1.1 Multi-Robot Teleoperation

1.1.1 Background

Two recent reports of the Emergency Events Database have shown that the total numbers of natural [1] and technological [2] disasters have experienced significant increases over the past forty years. Among these disasters, the Great Sichuan earthquake in 2008 and the MV *Doña Paz* tragedy in 1987 are two terrestrial and marine representatives that are incurred by natural and technological factors, respectively. Due to the lack of precise prediction, effective monitoring and rapid response, it has been reported that over 69000 people lost their lives and 374176 people were injured in the former catastrophe [3], and that 4386 people were presumed dead or missing in the later calamity [4]. Besides the deplorable loss of human lives, these disasters have also caused extremely severe property damage. For example, the Chinese government has invested approximately 441 billion U.S. dollars to the post-earthquake relief and

reconstruction [3]. Therefore, exploring the possibility of, and finding well-grounded solutions for, mitigating the miserable aftermaths of these disasters are highly desired and emergent.

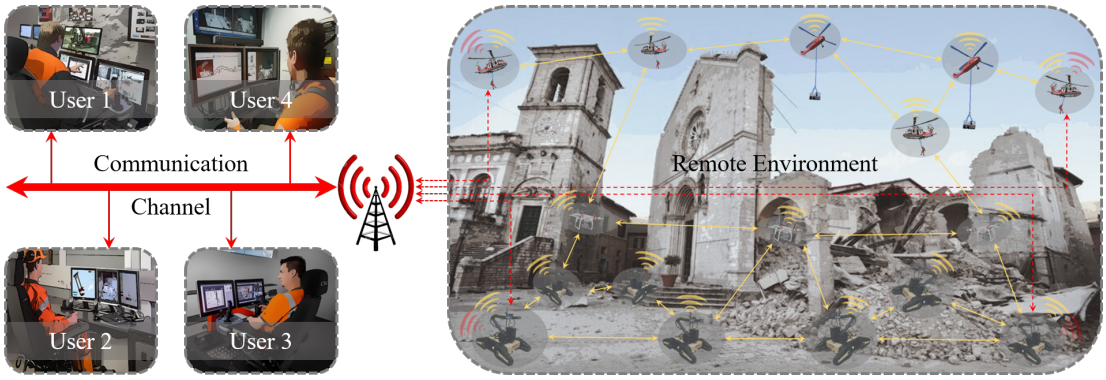

Figure 1.1: Multi-robot teleoperation can be deployed for search and rescue in earthquake ruins.

It is worth noting that disaster areas are hazardous and risky, and that nooks and crannies therein are normally hard-to-access for human rescuers. For example, a series of aftershocks have occurred throughout the rescue of the Great Sichuan earthquake, paths to the earthquake area have been obstructed by collapsed buildings and debris, human divers can possibly get trapped after entering a shipwreck for searching survivors, and the surrounding ocean water can perhaps be polluted by its spilled toxic chemicals. With the great advances of sensing, communication and control techniques, coordinated multi-robot systems, either semi-autonomous or fully autonomous, have been developed and deployed to cooperate with or substitute for human workers in search and rescue missions [5–8], and to sample, monitor and clean pollutants in marine environments [9–13] in recent years. In particular, these prior attempts have practically substantiated that, in comparison with a single complex/bulky robot, a group of appropriately coordinated robots can considerably improve the effectiveness and efficiency of task performance in these large-scale application scenarios, thanks to their higher dexterity, handling capability, loading capacity and robustness.

Despite the progress of robot intelligence, distributing a fully autonomous multi-robot system for trustworthy and comprehensive task executions in a generally dynamic, uncertain and unstructured disaster setting is still far from being reached. For this reason, multi-robot teleoperation, as a specific format of human-robot teaming, has been extensively studied to seamlessly complement the superior capabilities of human participants in cognitive reasoning and decision making, and that of coordinated

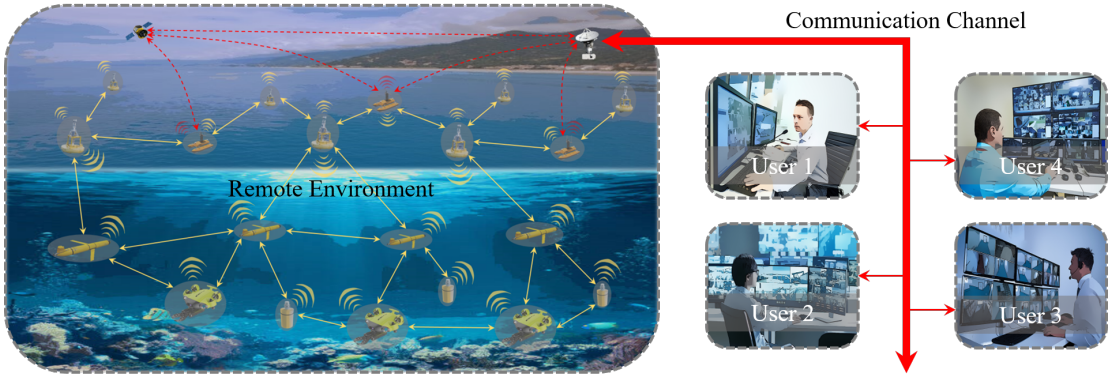

Figure 1.2: Multi-robot teleoperation can be deployed for marine exploration, sampling and monitoring.

robots in repetitive and precise missions [14]. For example, human users can assist in determining a set of attachment points and contact forces for multiple robots to cooperatively and reliably grasp and transport unstructured rubbles, and in identifying a set of positions and orientations for multiple robots to capture informative images of their surrounding environments. In this aspect, a pioneer field implementation of a multi-robot teleoperation system has successfully exploited the heterogeneity of a robot team for simultaneous manipulation and navigation in a shared remote environment [15]. After that, a variety of multi-robot teleoperation control strategies have been designed with special attentions devoted to collaborative manipulation and navigation, as summarized in the following two sections respectively.

1.1.2 Manipulation-Oriented Multi-Robot Teleoperation

A key challenge of the control design and stability analysis for manipulation-oriented multi-robot teleoperation is the kinematic and dynamic couplings among the remote robots. Based on the numbers of the local and remote robots, various earlier teleoperation control architectures for multi-robot cooperative manipulation have been categorized into four groups and systematically reviewed in [16]. Nevertheless, some most recent control designs have not been included. For this reason, this section will briefly overview some representative works on manipulation-oriented multi-robot teleoperation by dividing them into two classes: generic stability analysis and grasp-enforcing control.

1. **Generic Stability Analysis**

Using μ-synthesis, a cooperative tele-manipulation system has been modelled and robustly stabilized in [17] with flow of position and force information among all robots. Accounting for potentially non-passive interactions among the remote robots, a projection-based force reflection approach has rendered a networked multi-robot teleoperation system weakly input-to-output stable (IOS) by appropriate adjustment of local control gains and/or force reflection gains in [18], and has been experimentally validated in a minimally invasive surgical teleoperator in [19]. Focusing on collaboration passivity, an energy monitoring and shaping approach has been developed within the port-Hamiltonian modelling framework in [20]. A two-layer control method has implemented two energy tanks for all local robots and all remote robots, respectively, acting passively while minimizing the conservativeness of the design in [21]. Time-domain passivity approach has passivated dual-user cooperative teleoperation [22] with feedforward transmission of the user-local robot interaction forces and multi-user cooperative teleoperation [23] with unknown time-varying communication delays.

2. **Grasp-Enforcing Control**

   A critical prerequisite for the secure grasping of a rigid object by multiple robots is to maintain their formation shape invariant during cooperative teleoperation. Toward this goal, a passivity-based strategy has firstly been proposed in [24] and then extended in [25] to decompose the dynamics of a holonomic and a non-holonomic robot team, respectively, into a locked system and a shape system. In doing so, the human operator can bilaterally tele-drive the robot team as a whole without interfering with its formation through interconnecting their local robot with the locked system. Later, the strategy has been employed for manipulating microscopic objects in [26] and for fixtureless object grasping/transport from a first-person view in [27]. In the same spirit, a task abstraction concept based on null-space projections has also been designed in [28] and applied in [29] for a remote robot team to prioritize cooperative object manipulation over the teleoperation command. Following the formation-based methodology, the dynamics of the manipulated object have been integrated into the design of a cooperative manipulation system [30], where the human user guides the robot team in a leader-follower modality with no force feedback. Furthermore, a communication-free strategy has aligned the interaction forces of all follower

robots with the steering force of the human user/leader robot for reinforcing their motion intention in [31], and a force regulation control has balanced the interaction forces between the task object and two remote robots in correct directions for tele-grasping the object successfully in [32].

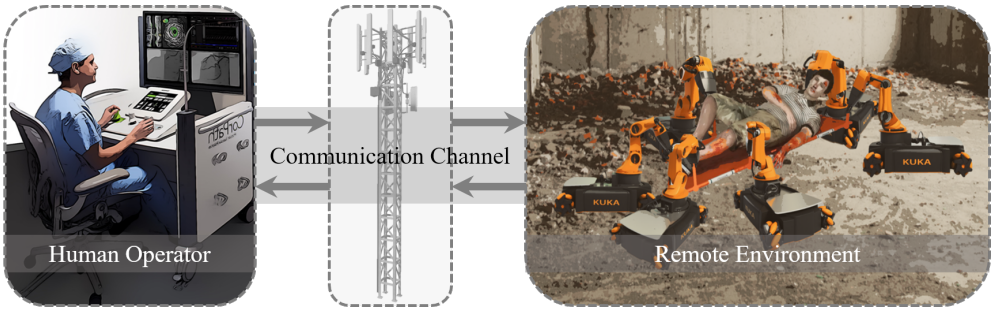

Figure 1.3: An exemplary application of manipulation-oriented multi-robot teleoperation: Cooperative transportation of earthquake survivors.

1.1.3 Navigation-Oriented Multi-Robot Teleoperation

With all remote robots synchronized with the local robots, existing navigation-oriented multi-robot teleoperation designs permit human users to remotely explore and sample data in unknown environments. To facilitate the maneuver of the remote robots and to enhance the telepresence of human users, the local robots have to be connected with the remote robot group appropriately. On the remote side, the remote robots need to measure the relative motion information of, or to transmit their own motion information to, other robots, via onboard sensing/communication modules, which is typically limited by inter-robot distances. In view of this, we will review some representative works on navigation-oriented multi-robot teleoperation by categorizing them into two groups: designing the local robot-remote robot couplings and designing the proximity-limited inter-remote robot couplings.

1. **Designing The Local Robot-Remote Robot Couplings**
   By interconnecting all remote robots with a single local robot, a Proportional-Derivative plus damping (PD+d) control has passivated bilateral teleoperation in the presence of constant communication delays in [33], and a saturated Proportional plus damping (P+d) control has passivated bilateral teleoperation with both time-varying communication delays and actuator saturation in [34]. Similarly, two local robots have been connected to all remote robots in [35] for a

single user to haptically tele-control the translation and expansion/rotation of a bearing-only formation of the remote robots. Further, a unilateral teleoperation architecture in [36] has facilitated tele-switching the remote robot formations by letting the user define and maneuver a virtual structure of which all vertices are tracked by corresponding remote robots. By interconnecting a leader remote robot with a single local robot, an optimization formulation has opportunely enabled multi-robot teleoperation in [37] by including the vision-based coordination of the remote robots as a constraint and the teleoperation command as the objective function. Along this line, a computational trust model has been proposed in [38] and augmented with self-confidence in [39] to reduce the user's workload by dynamically scaling their tele-driving force on, and their received force feedback from, the leader remote robot. Further, the trust model has been utilized in [40] to select a leader among all remote robots on the move for empirically improving the tracking performance. For the same purpose, a periodic leader selection strategy has been derived for a remote robot group with single-integrator [41] and double-integrator [42] dynamics, in accordance with their possibly time-varying communication topology. In addition, the passivity of the decision procedure of the human user in multi-robot teleoperation has been experimentally investigated in [43].

2. **Designing The Proximity-Limited Inter-Remote Robot Couplings**
When the leaders interconnected with the local robots account for only a portion of the remote robots, a shared control framework has been formalized in [44], which abstracts the motion of the remote robot group by a consolidation of tracking the local robots and synchronizing the remote robots. Following the idea, a passivity-based design in [45] has equipped every remote robot with an energy tank for storing and employing the dissipated energy for adding/deleting interconnections between the remote robots in a passive manner. Then, a handshaking mechanism together with a time synchronization algorithm have been integrated into the design for (re)establishing connections between the remote robots with communication delays in [46]. Along this vein, a passivity-constrained optimization has been formulated and solved at leaders for dynamically scaling their couplings with followers within the remote robot group, thereby improving the quality of force feedback displayed to a single [47] and multiple [48] human users. Also, a passivity-based policy in [49] has em-

powered the human user to temporarily detach leaders from followers for, and to promptly restore their connections after, exploring some narrow portions of the remote environment. Beyond exploiting the benefits of establishing/eliminating inter-robot couplings at runtime, existing literature has also inspected the possibility of maintaining them throughout teleoperation. In [50], all interconnections between the remote robots have been preserved by properly restricting the distances between their kinematic virtual proxies using an unbounded potential function. Built on this structure, the impact of various types of force feedback on the maneuverability and perceptual sensitivity of the remote robots and environment, respectively, has been compared via psychophysical experiments in [51]. For the sake of flexibility, in [52], a power iteration algorithm has estimated, and an unbounded potential function has maintained, the global communication connectivity of a teleoperated remote robot network, which permit to maximally create/break interconnections among the remote robots. And as an extension, an additional teleoperation channel has been established in [53], which enables the human user to tele-control the degree of connectivity of, and hence the compression/dispersion of, the remote robot team. A user study in [54] of the design has also experimentally confirmed the superiority of haptic feedback over its visual substitution in raising user's awareness of the communication connectivity of the remote robots.

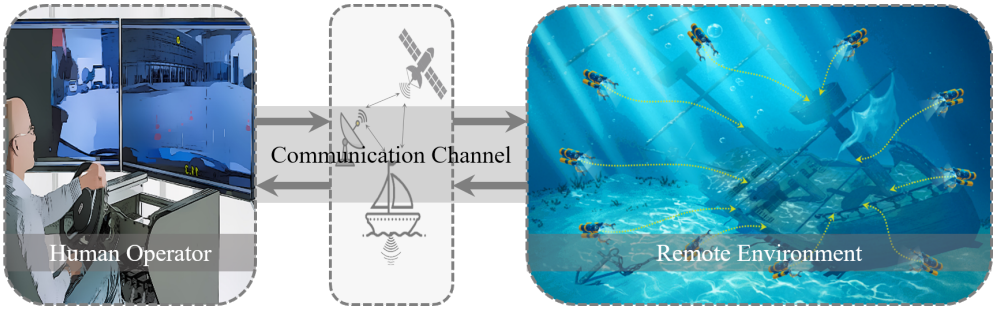

Figure 1.4: An exemplary application of navigation-oriented multi-robot teleoperation: Cooperative marine salvage of shipwrecks.

1.1.4 Open Issues

Being a particular teleoperation formalism, multi-robot teleoperation extends the superior capabilities of human users in cognitive perception and reasoning and dexterous

manipulation to large-scale remote environments. Through a forward communication channel, each human user can operate their local robot in a unique location to send commands/requests to, and hence guides the motion of, the remote robot group in a shared remote environment. Through a backward communication channel, each human user can receive visual/audio signals from the remote robots, thereby supervising the status of the remote environment and robots therein. Preferably, a multi-robot teleoperator, the robotic local robots-communications-remote robots system, can considerably enhance the situational awareness and task performance of human users by delivering also informative force feedback to them via backward communication channels. In doing so, multi-robot teleoperation becomes bilateral, in which the multi-robot teleoperator physically interact and thus exchange energy with human users. For the purpose of human-robot interaction safety [55], a closed-loop multi-robot teleoperation system needs to be rendered passive by designing controllers for the local and remote robots appropriately.

Under the premise of teleoperation passivity, the remote robots in an unstructured environment can perform missions designated by, and respond to requests from, human users by effectively synchronizing themselves with the local robots. Because central communication and control units are expensive and even unavailable in field environments, distributed coordination of the remote robots with 1-hop information exchanges and their onboard controllers becomes thus a favourable, and possibly the only viable, solution in most cases. However, the communications between the remote robots are constrained by their relative distances. For example, dispatching data via radio signals between unmanned aerial and ground vehicles [56–58], and transmitting packets via acoustic signals among autonomous underwater vehicles [10–13], both are restricted by inter-robot distances because of the rapid attenuation of radio and acoustic signals. Given that communications between the local and remote robots are independent of their distances, a connected communication network among the remote robots ensures the needed continuity in the data flow among all robots and thus possibility to share and distribute the needed information over time. As a fundamental topic, maintaining the proximity-limited communication network of the remote robots connected during passive bilateral teleoperation has been investigated in [50, 52–54]. Nevertheless, these multi-robot teleoperation control designs adopt unbounded potential functions to derive inter-robot couplings, which grow infinite as inter-robot distances approach the communication radius, and make these designs numerically unstable and sensitive to noise in practice. For this reason, how to design

distributed controls without using unbounded potentials to preserve the connectivity of the remote robots throughout passive haptic teleoperation is an emergent problem.

When multiple human users are teleoperating a remote robot group in parallel, each of them can explore and surveil a portion of the remote environment by receiving visual/audio/haptic feedback signals from their associated and individual remote robot. Because a number of urgent incidents can occur and be encountered by the remote robots in the remote environment concurrently, in response, multiple human users can separately send multiple requests to the remote robot group in different locations. The level of urgency of every human user's request stands for that of their monitored incident in the remote environment. Yet, due to the limited problem-solving capacity, all remote robots can collaboratively handle only one urgent event each time. As a compromise, the remote robot group is supposed to compare all user requests, identify the most urgent one, and cooperatively transport to the corresponding region for emergency treatment. Furthermore, every remote robot can receive the request from at most an individual human user, it thus demands a distributed WTA authority dispatch algorithm for the remote robot network to pick out winners, human users sending the most urgent requests. More specifically, with a local decision variable adapted with the received user request and messages obtained from communication neighbours, every remote robot can determine if its received user request is the most urgent one by evaluating its own decision variable. And what is more, to activate exclusively the teleoperation of winners, the physical dynamics of all robots have to be coupled with the WTA authority dispatch algorithm to coordinate all remote robots with the local robots of winners. Consequently, the passivity of closed-loop multi-robot teleoperation is influenced by the dynamics of both physical robots and their WTA algorithm. However, how to design such a WTA authority dispatch algorithm and couple it with physical robot dynamics in a distributed manner to compose passive multi-robot teleoperation remains an unanswered problem.

In view of the above two open problems in multi-robot teleoperation, this thesis develops a distributed energy shaping control strategy for rendering bilateral multi-robot teleoperation passive, preserving the communication connectivity of the remote robots and dispatching teleoperation authority equitably and exclusively to winners. Before describing the primal contributions of this thesis, the following section surveys most representative works related to passivity-based bilateral teleoperation, connectivity-preserving multi-robot coordination and distributed WTA authority dispatch.

1.2 Literature Review

This section firstly reviews a number of seminal and state-of-the-art passivity-based bilateral teleoperation control methods by comparing them with finite-gain stability-based designs. Given that the connectivity-preserving multi-robot teleoperation designs [50, 52–54] have been discussed in the last section, it then summarizes some paradigmatic connectivity-preserving coordination methods for autonomous multi-robot systems. Lastly, this section introduces authority dispatch designs in multi-user teleoperation, (k-)WTA neural networks, economic dispatch results in power network research, and passivity-based optimization algorithms because they are closely related to the results in Chapter 5.

1.2.1 Passivity-Based Bilateral Teleoperation

With the dynamics of human users and the robotic teleoperator tightly coupled, the stability analysis and control design for a closed-loop bilateral teleoperation system must take into account the dynamics of human users. Yet, an accurate and generic model of human users is hard and even impossible to be obtained because the biomechanical characteristics vary greatly across human users and specific tasks in practice. Thanks to the compositionality of dissipativity, finite-gain stability and passivity, as two major branches of dissipativity [59], have been extensively employed to guide bilateral teleoperation control designs. By assuming or controlling human users to be finite-gain stable/passive, the modular design lies in rendering the robotic teleoperator finite-gain stable/passive with respect to the physical interaction ports.

Table 1.1: Selected bilateral teleoperation control designs based on finite-gain stability and passivity.

Criteria for Teleoperation Stability		**Related Work**
Finite-Gain Stability		[60-66]
Passivity	Energy Monitoring	[69-78]
	Lyapunov-Like Analysis	[79-91]

Treating the user force as an exogenous input, a projection-based force reflection algorithm in [60] has decomposed the reflected force into "interaction" and "momentum-generating" components with measured user forces, and has attenuated

the latter while displaying the former to the human user. Because the projected force feedback does not incur unwanted motions of the local robot, input-to-state stable (ISS) bilateral teleoperation is ensured without injecting extra damping to the system, thereby mitigating transparency deterioration. A succeeding extension of the algorithm has then eliminated the need for measuring the user forces with an elaborately designed high-gain input observer in [61]. Using the small-gain theorem, an explicit condition on the user force has been derived in [62] for closed-loop stability of bilateral teleoperation with the projection-based force reflection algorithm. Afterwards, first-order filters have been consolidated in the algorithm to enable direct feedback of high-frequency force-reflection signals in [63], thus improving the fidelity of the transient force response. By identifying the $\mathcal{L}_1$ gain of human users, the algorithm has further been practically implemented in a haptics-enabled telerobotic rehabilitation system to deliver resistive/assistive motor therapy in [64]. Built upon $\mathcal{L}_2$-gain stability, a generalized scattering transformation matrix parameterized as the product of two rotation and scaling matrices has encoded power variables into wave variables to robustify communications against constant time delays in [65]. Likely, $\mathcal{L}_2$-gain stable bilateral teleoperator with time-varying communication delays has been established in [66] by transmitting robot positions directly.

Although finite-gain stability-based approaches reviewed in the above favours modular designs, their field implementations require to identify or estimate the input-output gains of human user dynamics in accordance with particular application scenarios. Because human users can be assumed passive [67] or passivated [68], a great deal of passivity-based designs have been reported in the existing literature to facilitate the control of, and to generalize the application of, bilateral teleoperation systems. In the light of this, the following reviews some most seminal works by categorizing them into two classes.

Teleoperation passivity can be ensured using energy monitoring techniques. In [69], a time-domain passivity approach has passivated a bilateral teleoperator by injecting sufficient damping with passivity controllers after measuring excessive energy accumulation with a passivity observer. Later, a two-port augmentation of time-domain passivity approach has been developed in [70] to preserve teleoperation passivity irrespective of the amount of communication time delays. To remedy the position drift problem, time-domain passivity approach has been extended in [71] by transmitting the encodings of robot velocities and positions, and has been utilized in [72] to dissipate the extra energy of the local robot's proxy with only position transmissions.

Recently, time-domain passivity approach has also been blended with tele-impedance control in [73] for mitigating the "phantom force" and thus user fatigue throughout time-delay teleoperation. Unlike time-domain passivity approach, a passive set-position modulation strategy proposed in [74] has preset a fixed amount of damping injection to the local and remote robots and then modulated their proxies in accordance with the passivity margin of the teleoperator, thus bypassing any temporarily active robot behaviours. Within a port-Hamiltonian modelling framework, energy tanks have firstly been proposed in [75] to compensate the position drift caused by the transmission of scattering variables, and have then been formalized in [76] as virtual dynamical systems that are interconnected with physical robots in a power-preserving way to keep track of their dissipated energy. On this basis, a two-layer approach has been developed in [77] to implement any desired teleoperation control in the transparency layer and to regulate the level of system passivity with two energy tanks interconnected in the passivity layer. Restricted to a force-reflection teleoperation architecture, the two-layer approach has been further upgraded in [78] by decoupling the two energy tanks in the passivity layer to reduce the workload of human users.

Teleoperation passivity can also be investigated using Lyapunov-like energy analysis. By encoding power variables into scattering variables and transmitting the latter, the communication channel between the local and remote robots and thus the closed-loop teleoperator have been rendered passive in [79] regardless of constant time delays. With suitable selections of control gains, an extension in [80] of the scattering-based method has matched the impedance of the communication channel with that of the human operator and environment, thereby eliminating wave reflections. As the scattering-based communication channel is physically equivalent to a mass-spring system, a performance index describing its capability of instantaneously transferring energy, and an optimization problem opportunely extracting its energy and computing force/velocity inputs to robots, have been formulated in [81] and [82], respectively, for evaluating and optimizing the teleoperator transparency. By transmitting both robot positions and velocities, in [83], a PD+d control has proven able to passivate teleoperation with bounded constant delays. Along this line, two criteria for selecting gains of a simpler P+d control have been established in [84] and [85] to cope with bounded time-varying delays. In the absence of gravity compensation, adaptive control strategies have also been developed to estimate unknown parameters of the local and remote robot dynamics. Specifically, a sliding variable summing robot velocity

and position has synchronized both the local and remote robots to the origin in [86], and a modified sliding variable has instead achieved mutual synchronization of both robots by adding robot velocities and position errors in [87]. In addition, to exploit the kinematic redundancy of the remote robot, a task-space adaptive synchronization strategy has been derived in [88] accounting for uncertain robot dynamics, and has further been augmented in [89] by incorporating also uncertain robot kinematics into the design. A systematic extension of earlier works using storage function analysis to tackle time-varying communication delays, and a comprehensive review of them, can be referred to [90] and [91], respectively.

1.2.2 Connectivity-Preserving Multi-Robot Coordination

The communication network connectivity is a fundamental condition for distributed coordination of a multi-robot system. With a communication path between every pair of robots, the information of each of them can be explicitly or implicitly propagated to the other, enabling their mutual information exchanges and motion synchronization. However, wireless communications between mobile robots through radio and/or acoustic signals are typically limited by their distances in practice. If controlled inappropriately, the movements of robots can probably grow their distances to break their proximity-limited communications, thereby defeating their distributed coordination. In this respect, substantial attention has been paid to coordinating a multi-robot system while maintaining the underlying communication network connected.

Table 1.2: Selected connectivity-preseving coordination control designs for fully autonomous multi-robot systems.

<table>
<tr><th colspan="4">Types of Robot Network Connectivity</th><th>Related Work</th></tr>
<tr><td rowspan="4">Continuous</td><td rowspan="3">Non-Resilient</td><td colspan="2">Local</td><td>[56,92-99]</td></tr>
<tr><td rowspan="2">Global</td><td>1-hop</td><td>[100-108]</td></tr>
<tr><td>2/k-hop</td><td>[110-112]</td></tr>
<tr><td colspan="3">Resilient</td><td>[113-118]</td></tr>
<tr><td colspan="4">Intermittent</td><td>[58,119-123]</td></tr>
</table>

A simple strategy is local connectivity preservation which aims to maintain all communications of an initially connected robot network. As an initial step, a radio

connectivity map relating the signal strength to inter-robot distances has been built and integrated into a potential function-based reactive control to empirically preserve wireless communications between unmanned ground vehicles in [56]. Motivated by the successful experiment, an unbounded potential function has been proposed to derive interconnections between single-integrator robots with its gradient in [92]. By limiting the distance between every pair of initially adjacent robots to the communication radius, the control can rigorously maintain the robot network connected by sustaining all communication links. Following the design, a generalized unbounded potential function has been characterized for connectivity-preserving coordination of nonholonomic kinematic robots with dynamic link creations in [93]. Nevertheless, the gradients of unbounded potential functions can increase to infinity as inter-robot distances approach the communication radius, leading to infinite control inputs. Given bounded actuation of practical robots, several types of bounded potential functions, including the navigation function in [94] and [95], and the composition function in [96] and [97], have been proposed after that. Uniquely, a bounded potential function evolved from the unbounded one in [92] has been employed to rigorously maintain all communication links between double-integrator robots in [98]. Based on this function, a variety of control approaches have coordinated second-order and even EL robot networks while preserving their connectivity [99].

A more flexible strategy is global connectivity preservation which aims to render the algebraic connectivity of the communication graph positive with link additions/deletions at runtime. On the grounds that the algebraic connectivity is a concave function of the graph Laplacian, a decentralized supergradient algorithm has firstly been developed in [100] to compute the Fidler eigenvector and to maximize the algebraic connectivity of a single-integrator network. For scalability, a power iteration algorithm has been decentralized by a Proportional-Integral average consensus protocol to estimate the algebraic connectivity in [101]. In the same spirit, a decentralized and robust algebraic connectivity estimation and maintenance strategy has been designed in [102] for single-integrator robots with additional bounded control inputs. Further, in [103], the concept of critical robots has been introduced, and the connectivity-preserving control action has been imposed only on critical robots for reducing the control effort and mitigating its interference with other control objectives. Given bounded velocity input, the disturbing impact of the connectivity-preserving control on other control objectives has been quantified in [104] using input-to-state stability analysis. Taking a different path, hybrid approaches have permitted robots

to actively establish or remove communication links without violating network connectivity by synthesizing discrete-time decision-making algorithms, like auction automatons in [105] and [106] and event-driven predictions in [107] and [108], with continuous-time potential-based actuation. However, the integration of discrete-time decision-making algorithms can significantly complicate control designs, performance analyses and practical implementations.

Global connectivity preservation controls, in contrast with their local counterparts, can grant robots with greater freedom of movement and workspace but requires higher bandwidth and thus consumes more power for large-scale communications. Comparative simulations in [109] have demonstrated that, under global connectivity-preserving control, the maximum speed of robots is severely restricted by communication delays. To retain system flexibility while avoiding sluggish robot motions, a supervisory k-hop routing method in [110] has allowed robots to break communication links without destroying network connectivity by detecting an alternative k-hop path. Further, a node permutation approach in [111] has enabled a pair of adjacent robots to swap their neighbours at each time instant while keeping network connectivity invariant. With no algebraic connectivity estimation, a 2-hop communication strategy in [112] has also preserved global connectivity by permitting every robot to predict, at each time step, the next movements of its 1-hop neighbours.

Resilient connectivity preservation against single and multiple robot failures has been explored by enforcing biconnectivity and k-connectivity, respectively, in multi-robot systems. More specifically, a condition on the lower bound of the third smallest eigenvalue of the network Laplacian has been established in [113] for every robot to check biconnectivity, and, based on the condition, a decentralized gradient control law has maintained a robot network biconnected in [114] using eigenvector estimation. In addition, a vulnerability metric has been defined based on 2-hop communications in [115] for empirically optimizing network resilience to a single robot failure. For what concerns k-connectivity maintenance, a subgraph algorithm in [116] has computed a set of inter-robot communication links to be maintained with minimal disruption to primal tasks, and a spanning tree algorithm in [117] has accommodated the possibility that multiple robot subgroups perform different tasks simultaneously. Further, a network reconfiguration strategy in [118] has enabled a multi-robot network to recover k-connectivity in the presence of robot failures.

Rather than keeping the network connected at all times, intermittent connectivity control allows a robot to detach from the remaining group of robots temporarily and

to rejoin at a later time point. In [119], experimental results have confirmed that multi-robot informative path planning with periodic connectivity can facilitate target searching in an outdoor urban environment. After this, formal methods have rendered a network of robots jointly connected over time and infinitely often by constraining them to move forward and backward on links of environmental graphs [120, 121], by forcing them to meet at certain environmental points [122], and by organizing them into connected subgroups [123]. By synchronizing the speed of every robot with that of other robots in neighbouring perimeters, an intermittently connected network has been constructed in [58] with information propagation guarantees. However, these designs require to plan robot motions carefully prior to field deployments.

1.2.3 Winners-Take-All Authority Dispatch

The dexterity, handling capability and redundancy of a multi-robot teleoperation system can be significantly reinforced by permitting multiple human users to participate in the control. Despite these advantages, the controller design and stability analysis of such a multi-user multi-robot teleoperation system need to face and resolve three challenging problems: How to allocate teleoperation control authority over the remote robots to every human user so as to optimize their cooperation; what kind of force feedback every human user should perceive for improving their situational awareness; and how to stabilize the physical interaction between the teleoperator and human users. Because Chapter 5 develops a WTA authority dispatch algorithm for passive multi-robot teleoperation using distributed optimization, the following literature review covers existing designs that are closely related to authority allocation in multi-user teleoperation, (k-)WTA neural networks, economic dispatch in power networks, and passivity-based optimization.

The problem of sharing teleoperation control authority between two/multiple human operators has primarily been studied for expert-in-the-loop supervised hands-on training in medical robotics [124]. Starting with dual-user teleoperation, a pioneer design in [125] has enabled two human users to share the control authority with a dominance factor and its complement while keeping the linear teleoperator robustly stable via H_∞ control. However, the teleoperator offers each user the force of the other rather than forces from the remote site. With regard to this, two control architectures inheriting the concept of dominance factor have been proposed in [126] for providing each user with a force feedback informative of the action of the other

Table 1.3: Selected designs for teleoperation authority sharing, (k-)WTA neural networks, economic dispatch and passivity-based optimization.

Research Topics in WTA Authority Dispatch		**Related Work**
Authority Sharing in Teleoperation	Static	[125-130]
	Dynamic	[131-135]
(k-)WTA Neural Networks	Centralized	[136-138]
	Distributed	[139-143]
Economic Dispatch in Power Networks	Decoupled	[144-150]
	Coupled	[151-153]
Passivity-Based Optimization	Krasovskii Passivity	[154-156]
	Equilibrium-Independent Passivity	[159-167]

as well as the remote robot-environment interaction. Regarding the environment as a load termination, unconditional stability of the resulting system has been established by applying Llewellyn's criterion to its two-port network equivalent. Following the design, four measures based on the transmitted impedance have been adopted in [127] to analyse and evaluate its kinesthetic performance, and an extension of the Zeheb-Walach criteria has been applied in [128] for enlarging the stability margin. To expand the authority-sharing scheme to a multi-user context, an unconditional stability criterion has further been characterized in [129] by converting the n-port network model of the resulting system into a two-port network, and a small-gain approach in [130] has guaranteed IOS teleoperation in the presence of nonlinear robot dynamics and time-varying communication delays.

However, the aforementioned designs are limited to fixed (invariant) dominance factors. In view of this, a dynamic authority distribution strategy has been devised in [131], which builds a kinesthetic coupling between two users, classifies their energy interaction into leader/follower behaviour, and then adapts their control authority accordingly. Thereafter, intrinsically passive control has been blended with time-domain passivity approach to accomplish passive authority sharing for single-trainee [132] and multi-trainee [133] haptic training. A fuzzy logic interface has been integrated into a dual-user surgical training system in [134] for empirically evaluating the proficiency level of, and for adjusting the haptic guidance provided to, the trainee surgeon in

real time. With an emphasis on the supervisory role of the trainer surgeon, the ISS teleoperator in [135] has enabled them to manually transfer task authority to/from the trainee by changing the magnitude of their force.

In Chapter 5, a WTA algorithm is devised for allocating control authority to multiple human users in distributed multi-robot teleoperation, of which the theoretical foundation is k-WTA neural networks. In [136], a zero-one integer linear program has been formulated to activate exactly k neurons receiving the k largest inputs. On this basis, in [137], a convex linear program has been rigorously proven to fulfill the same purpose by relaxing binary constraints to be continuous. Assuming a proper gap between the k-th and the $k+1$-st inputs, a quadratic program with the same constraints has also been introduced in [138] with global convergence guarantees. Besides these centralized designs, distributed WTA neural networks have also been explored. In [139], a nonsmooth model has been constructed to perform WTA computation over a star communication network. In [140], a smooth WTA model has been developed based on a consensus protocol, and has been proven to work over any connected network by Lyapunov's indirect method. In the same spirit, a k-WTA computational model has been designed in [141], of which the convergence is shown by Lasalle's invariant principle. On the application side, two k-WTA algorithms have enabled a group of redundant robot manipulators in [142] and a group of wheeled-mobile robots in [143] to elect the k fittest members for tracking a moving target. However, all these distributed WTA algorithms enjoy only asymptotic convergence.

Interestingly, the convex quadratic programming of WTA computation [138] coincides with the economic dispatch problem of distributed power networks. With nontrivial initialization, a Laplacian-nonsmooth-gradient algorithm has been derived from an exact penalty function in [144] to search the optimal solution. Afterwards, the initialization requirement has been eliminated by upgrading the design with a dynamic average consensus-based estimator in [145] and by employing projected gradient flow dynamics in [146,147]. Some trendy designs also attempt to reduce the communication and computational burden incurred by the algorithm dynamics. For example, a dual-gradient-based method [148] and a singular perturbation method [149] have been constructed to reach suboptimal solutions. In particular, incremental passivity has been leveraged in [150] to simplify the algorithm in [146] via removing the Proportional term in the dual dynamics therein. To provide holistic economic dispatch, in [151], a primal-dual algorithm has been coupled with a tree power network as a dynamic feedback controller. In [152], the power system dynamics have been

reverse-engineered and unified into the optimization-based formulation to derive a partial primal-dual controller. Also, the port-Hamiltonian modelling framework has been adopted in [153] to explore the power-preserving interconnection between the passive primal-dual dynamics and the passive power system.

A variety of primal-dual algorithms have been reported for solving convex optimization problems. Among them, some passivity-based designs have enlightened the WTA algorithm in Chapter 5. Specifically, a Krasovskii function has firstly been proposed in [154] to demonstrate the passivity of a projected primal-dual algorithm solving inequality-constrained convex program. Later, the internal power-preserving interconnection between the primal and dual dynamics of the algorithm has been revealed in [155]. Built upon the algorithm, a distributed control has been developed and coupled with a microgrid for current sharing and voltage regulation in [156], and the concept of Krasovskii passivity has been formally defined in [157]. Alternatively, equilibrium-independent passivity [158] has guided the design of another type of storage functions for studying the passivity of primal-dual algorithms. In this context, the source and link update laws in passivity-based network flow control have been reformulated as primal and dual dynamics interconnected for optimizing network utility in [159]. Later, the asymptotic convergence of primal-dual algorithms for solving strictly convex programming problems with equality [160] and inequality [161] constraints has been established. On top of this, a distributed algorithm has been implemented in conjunction with scattering-based communications for solving a constrained program over an undirected network with constant delays in [162], and a distributed algorithm has been decomposed into an output feedback interconnection of several input feedforward passive subsystems for solving an unconstrained program over a jointly connected balanced network in [163]. To asymptotically solve non-strictly convex programs, a generalized primal-dual algorithm has been developed by the phase lead compensation in [164], and has been implemented with scattering-based communications over a network with constant delays in [165]. With every agent estimating the actions of all other agents, in [166] and [167], passive primal-dual algorithms have also been applied to distributed Nash equilibrium seeking over networks.

1.3 Research Motivations and Contributions

In spite of the above-reviewed designs, preserving the communication connectivity of, and dispatching control authority to multiple human users over, a distributed remote robot network impose several unique challenges on passive multi-robot teleoperation.

For connectivity preservation, the distances between, and hence the energy stored in, the remote robots need to be bounded appropriately, while human users can inject an unknown amount of energy into the remote robot group for teleoperation. Existing multi-robot teleoperation designs [50, 52–54] have attempted to unify connectivity-preserving coordination of the remote robots and passive bilateral teleoperation by deriving the inter-remote robot couplings from unbounded potential functions. When the distances between the remote robots approach the communication distance, or when the remote robot communication network is about to get disconnected, the connectivity-preserving actions produced by these designs become infinitely large and thus cannot be fully executed by physical robots due to their limited actuation in practice. Moreover, the excessively high gains of these connectivity-preserving controls make them sensitive and vulnerable to the noises contained in the position and velocity measurements of robots. For these reasons, it is more desirable to maintain the communication network of the remote robots connected and to render closed-loop bilateral teleoperation passive without using unbounded potential functions.

For authority dispatch, the remote robot group ought to adapt their behaviours in a well-defined and distributed way in response to the actions/commands/requests of multiple human users. Available authority allocation approaches [125–135] are developed mostly for the purpose of hand-by-hand haptic training, ignoring the distributed implementation of multi-robot teleoperation systems. More precisely, predetermined and fixed authority allocations in [125–130] cannot react to the variations of user intentions during teleoperation, adjustable but manually-controlled authority allocations in [132, 133, 135] require a single user to supervise the entire system and to tune the task authorities of every other users, and autonomous authority allocations in [131, 134] are heuristically designed and empirically validated, lacking strict performance guarantees. For these reasons, it is essential to tailor an authority dispatch algorithm to multi-robot teleoperation, which can adapt to time-varying user intentions, favours distributed implementation, and is provably functional. On top of this, suitable force feedback should be delivered to every human user to inform them about the actions of other users and/or the motions of the remote robots, and the passivity

of the closed-loop teleoperator should be rendered to ensure the safety of its physical interactions with human users.

This thesis develops an energy shaping strategy to preserve the connectivity of the remote robots based on a bounded potential function, and to dispatch control authority over the remote robots to human users with the most urgent request, while ensuring the closed-loop passivity of distributed multi-robot teleoperation. Toward this goal, the main ingredients of this thesis, Chapters 2-5, contrive an exponentially ISS teleoperator, an autonomous connectivity-preserving multi-robot system, a passive multi-robot teleoperation system with connectivity-preserving containment, and a multi-robot teleoperation system with online WTA authority dispatch, respectively. Figure 1.5 provides a map of the thesis[1].

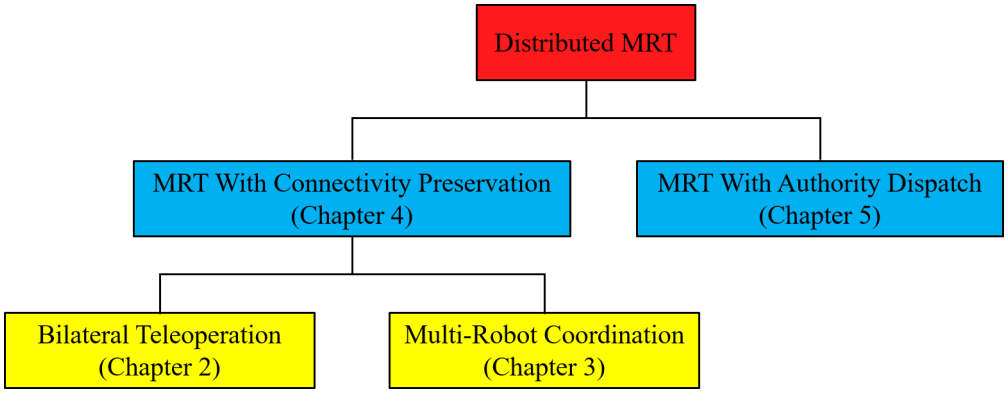

Figure 1.5: An outline for this thesis.

Chapter 2 proposes a dynamic interconnection and damping injection strategy for reducing and constraining the position error between the local and remote robots to any prescribed bound during bilateral teleoperation with time-varying delays. At each robot, a sliding surface adding its velocity and its displacement from the other firstly transforms the EL robot dynamics into a first-order system. Based upon this, a dynamic feedback control is designed for each robot, and, by updating its gains with the robot velocity, is proven to render the teleoperator exponentially ISS. Rewriting the dynamic control illustrates that it essentially adapts the interconnection between, and the local damping of, both robots with their velocities. Accounting for time-varying communication delays, every robot is dynamically interconnected with a second-order proxy, and both sides are then coupled by static P+d control. By rigorous Lyapunov-like analysis, it proves that the resulting teleoperator is exponentially ISS even with

[1]In Figure 1.5, MRT means multi-robot teleoperation.

time-varying communication delays. As a result, the proposed strategy can steer the position error between the local and remote robots arbitrarily close to zero under the human and environment perturbations.

Chapter 3 establishes a connectivity-preserving synchronization control for autonomous multi-robot systems with time-varying communication delays and bounded actuation. For every pair of initially adjacent robots, a gradient plus damping control firstly couples them using the gradient of a bounded potential function and injects into each of them a constant amount of damping. By selecting parameters for the bounded potential function and gains for the control appropriately, the distance between every pair of initially adjacent robots can be sufficiently constrained, and all time-delay communication links in the robot network can thus be maintained. Considering bounded robot actuation, a second-order proxy is simulated at, and coupled via P+d control with, each robot locally, and the proxies of every two initially adjacent robots are interconnected through a gradient plus damping control. The energy analysis of the entire robot network indicates that the proposed indirect coupling control can preserve all time-delay communication links between robots regardless of their actuator saturation, and can thus better exploit robot actuation for rapid synchronization.

Chapter 4 contributes a passive multi-robot teleoperation system that enables multiple human users to cooperatively tele-transport a remote robot group with connectivity maintenance while receiving informative force feedback over time-delay communication channels. Inspired by the sliding variable in Chapter 2 and the bounded potential function in Chapter 3, the dynamics of the tree network of the remote robots are firstly decomposed into a power-preserving interconnection of two subsystems. Then, by regulating the energy behaviour of each subsystem, all communication links in the tree network of the remote robots can be preserved under bounded perturbations. On this basis, each local robot is coupled with a unique remote robot via saturated Proportional control to close the force feedback loop, and is damped for passivating the teleoperator. In the presence of communication delays, a kinematic proxy is simulated at each leader remote robot as a medium for interconnecting the leader with an associated local robot, recasting the teleoperator into a "control as interconnection" paradigm. Because the dynamic feedforward-feedback passivation strategy is developed using a bounded potential function, it can sidestep the numerical instability and reduce the noise sensitivity of unbounded potential function-based multi-robot teleoperation designs.

Chapter 5 formulates an online WTA authority dispatch algorithm to permit exclusively human users with the most urgent requests to collaboratively teleoperate a remote robot group in a distributed fashion while preserving the passivity of the closed-loop system. Based on the Oja's rule for principal component analysis (PCA), it firstly constructs a preliminary WTA algorithm using a distributed consensus protocol. With the vector of all decision variables exponentially convergent to a hypersphere, a quotient function illustrates that the preliminary WTA algorithm can identify a single winner at an exponential rate. However, the passivity of the algorithm is unclear, impeding its integration into passive teleoperation. We therefore resort to a constrained quadratic program for WTA authority dispatch. After proving the correctness of program, Chapter 5 converts the program into an equivalent strongly convex optimization problem using an exact penalty function method, and further derives a distributed primal-dual algorithm for solving the problem. Because the WTA algorithm is not only exponentially convergent but also equilibrium-independent passive with respect to a customized power port, it is elaborately interconnected with physical robot dynamics through the port in a power-preserving way, acting as a dynamic feedback controller. Given that the equilibrium of the algorithm varies with users' requests, the passivity of the closed-loop teleoperation system is studied with multiple storage functions from a time-dependent switched system point of view.

1.4 Preliminaries

To streamline the presentation, this section introduces some prerequisite information of dissipative systems, EL robot dynamics and algebraic graph theory, and unifies the notation to be used in the remainder of this thesis.

1.4.1 Dissipative Systems

Consider a continuous-time dynamical system,

$$\dot{\mathbf{x}}(t) = f(\mathbf{x}(t), \mathbf{u}(t)), \tag{1.1a}$$

$$\mathbf{y}(t) = h(\mathbf{x}(t), \mathbf{u}(t)), \tag{1.1b}$$

where $\mathbf{x}(t) \in \mathbb{R}^n$, $\mathbf{u}(t) \in \mathbb{R}^m$ and $\mathbf{y}(t) \in \mathbb{R}^p$ are its state, input and output, respectively, and $f: \mathbb{R}^n \times \mathbb{R}^m \mapsto \mathbb{R}^n$ and $h: \mathbb{R}^n \times \mathbb{R}^m \mapsto \mathbb{R}^p$ are continuously differentiable

mappings. Given the input $\mathbf{u}(\cdot)$ and the initial condition $\mathbf{x}(t_0)$, the solution state trajectory $\mathbf{x}(\cdot)$ of (1.1a) and the resulting output $\mathbf{y}(\cdot)$ of (1.1b) are unique on the infinite time interval $[0, +\infty)$.

Definition 1.1. *[59, Chapter 3.1] The dynamical system* (1.1) *is dissipative with respect to the supply rate* $s(\mathbf{u}(t), \mathbf{y}(t)) \in \mathbb{R}$ *if there is a positive semi-definite function* $V : \mathbb{R}^n \mapsto \mathbb{R}_{\geq 0}$*, called the storage function, such that for every initial condition* $\mathbf{x}(t_0) \in \mathbb{R}^n$ *at any time* t_0*, and for every input* $\mathbf{u}(\cdot)$ *and all* $t_1 \geq t_0$*, such that*

$$V(\mathbf{x}(t_1)) \leq V(\mathbf{x}(t_0)) + \int_{t_0}^{t_1} s(\mathbf{u}(\tau), \mathbf{y}(\tau)) d\tau. \tag{1.2}$$

The dissipation inequality (1.2) describes the fact that $V(\mathbf{x}(t_1))$, the "stored energy" of the dynamical system (1.1) at any future time t_1, is at most equal to $V(\mathbf{x}(t_0))$, the energy storage at present time t_0, plus $\int_{t_0}^{t_1} s(\mathbf{u}(\tau), \mathbf{y}(\tau)) d\tau$, the total externally supplied energy during the time interval $[t_0, t_1]$. Based on Definition 1.1, finite-gain $\mathcal{L}_2$ stability and passivity, as two important types of dissipativity, can be characterized by the following choices of supply rates.

A first class of supply rates is

$$s(\mathbf{u}(t), \mathbf{y}(t)) = \gamma^2 \|\mathbf{u}(t)\|^2 - \|\mathbf{y}(t)\|^2,$$

where $\gamma > 0$, and $\|\mathbf{u}(t)\|$ and $\|\mathbf{y}(t)\|$ are Euclidian norms of $\mathbf{u}(t)$ and $\mathbf{y}(t)$, respectively. It defines finite-gain $\mathcal{L}_2$ stability of the system (1.1) as follows.

Definition 1.2. *[59, Chapter 3.1] The dynamical system* (1.1) *has* $\mathcal{L}_2$ *gain no greater than* γ *if it is dissipative with respect to the supply rate* $s(\mathbf{u}(t), \mathbf{y}(t)) = \gamma^2 \|\mathbf{u}(t)\|^2 - \|\mathbf{y}(t)\|^2$*. The* $\mathcal{L}_2$ *gain of* (1.1) *is defined by*

$$\gamma^* = \inf\{\gamma \mid (1.1) \text{ has } \mathcal{L}_2 \text{ gain no larger than } \gamma\}.$$

A second class of supply rates is

$$s(\mathbf{u}(t), \mathbf{y}(t)) = \mathbf{u}^{\mathsf{T}}(t)\mathbf{y}(t)$$

if the dimensions of the input $\mathbf{u}(t)$ and the output $\mathbf{y}(t)$ are equal, i.e., $m = p$. It defines passivity of the system (1.1) as follows.

Definition 1.3. *[59, Chapter* 3.1*] The dynamical system* (1.1) *with $m = p$ is passive if it is dissipative with respect to the supply rate $s(\mathbf{u}(t), \mathbf{y}(t)) = \mathbf{u}^{\mathsf{T}}(t)\mathbf{y}(t)$, is (δ-)input strictly passive if there exists $\delta > 0$ such that* (1.1) *is dissipative with respect to $s(\mathbf{u}(t), \mathbf{y}(t)) = \mathbf{u}^{\mathsf{T}}(t)\mathbf{y}(t) - \delta\|\mathbf{u}(t)\|^2$, and is (ϵ-)output strictly passive if there exists $\epsilon > 0$ such that* (1.1) *is dissipative with respect to $s(\mathbf{u}(t), \mathbf{y}(t)) = \mathbf{u}^{\mathsf{T}}(t)\mathbf{y}(t) - \epsilon\|\mathbf{y}(t)\|^2$.*

Indeed, output strict passivity implies finite-gain $\mathcal{L}_2$ stability:

Proposition 1.1. *[59, Chapter* 4.2*] If the dynamical system* (1.1) *is ϵ-output strictly passive, then it has $\mathcal{L}_2$ gain no greater than $1/\epsilon$.*

Further, the dynamical system (1.1) is is said to be zero-state detectable if $\mathbf{u}(t) = \mathbf{0}$ and $\mathbf{y}(t) = \mathbf{0}$ for any $t \geq 0$ implies that $\lim_{t\to+\infty} \mathbf{x}(t) = \mathbf{0}$. The following then establishes a connection between the dissipativity of the system (1.1) and the stability of its autonomous configuration with $\mathbf{u}(t) = \mathbf{0}$.

Proposition 1.2. *[59, Chapter* 3.2*] Let the system* (1.1) *be zero-state detectable and dissipative as in Definition 1.1. Suppose further that the storage function $V(\mathbf{x}(t))$ is continuously differentiable and positive definite, and the supply rate $s(\mathbf{u}(t), \mathbf{y}(t))$ satisfies that $s(\mathbf{0}, \mathbf{y}(t)) \leq 0$ and that $s(\mathbf{0}, \mathbf{y}(t)) = 0$ implies $\mathbf{y}(t) = \mathbf{0}$. Then, $\mathbf{x}^* = \mathbf{0}$ is an asymptotically stable equilibrium of the system* (1.1) *with $\mathbf{u}(t) = \mathbf{0}$ for any $t \geq 0$. If additionally, the storage function $V(\mathbf{x}(t))$ is radially unbounded, then the equilibrium $\mathbf{x}^* = \mathbf{0}$ is globally asymptotically stable.*

An alternative approach to studying the stability of the non-autonomous system (1.1) is provided by the theory of input-to-state stability. A continuous function $\alpha : [0, a) \mapsto [0, \infty)$ belongs to class $\mathcal{K}$ if it is strictly increasing and $\alpha(0) = 0$. Further, the function α belongs to class $\mathcal{K}_\infty$ if it belongs to class $\mathcal{K}$, $a = \infty$ and $\lim_{r\to\infty} \alpha(r) = \infty$. A continuous function $\beta : [0, a) \times [0, \infty) \mapsto [0, \infty)$ belongs to class $\mathcal{KL}$ if: the function $\beta(r, s)$ belongs to class $\mathcal{K}$ for each fixed s; and the function $\beta(r, s)$ is decreasing with respect to s and $\lim_{s\to\infty} \beta(r, s) = 0$ for each fixed r.

Definition 1.4. *[168] A controllable continuous-time dynamical system,*

$$\dot{\mathbf{x}}(t) = f(\mathbf{x}(t), \mathbf{u}(t)), \tag{1.3}$$

is ISS with the input $\mathbf{u}(t)$ and the state $\mathbf{x}(t)$ if there exist some functions $\alpha(\cdot) \in \mathcal{K}$

and $\beta(\cdot,\cdot) \in \mathcal{KL}$ *such that*

$$\|\mathbf{x}(t_1)\| \leq \beta(\|\mathbf{x}(t_0)\|, t_1 - t_0) + \alpha\left(\sup_{t_0 \leq \tau \leq t_1} \|\mathbf{u}(\tau)\|\right), \quad \forall t_1 \geq t_0 \geq 0.$$

By Definition 1.4, the following proposition indicates the close relationship between input-to-state stability and finite-gain $\mathcal{L}_2$ stability.

Proposition 1.3. *[59, Chapter* 8.5*] The dynamical system* (1.1) *is ISS if there exist some functions* $\psi(\cdot) \in \mathcal{K}_\infty$ *and* $\phi(\cdot) \in \mathcal{K}_\infty$ *such that the system with the output* $\mathbf{y}(t) = h(\mathbf{x}(t), \mathbf{u}(t)) = \mathbf{x}(t)$ *is dissipative with respect to the supply rate* $s(\mathbf{u}(t), \mathbf{y}(t)) = \psi(\|\mathbf{u}(t)\|) - \phi(\|\mathbf{y}(t)\|)$ *with a continuously differentiable, radially unbounded and positive definite storage function* $V(\mathbf{x}(t))$*.*

Note that the supply rate $s(\mathbf{u}(t), \mathbf{y}(t))$ in the above proposition can be regarded as a generalization of the $\mathcal{L}_2$-gain supply rate in Definition 1.2. Letting $\psi(\cdot)$ and $\phi(\cdot)$ be quadratic functions $\psi(\|\mathbf{u}(t)\|) = \gamma\|\mathbf{u}(t)\|^2$ and $\phi(\|\mathbf{y}(t)\|) = \|\mathbf{y}(t)\|^2$ recovers the case with $\mathcal{L}_2$-gain no greater than γ for $\mathbf{y}(t) = \mathbf{x}(t)$.

Despite the connection to $\mathcal{L}_2$-gain stability, the input-to-state stability of time-delay systems is defined in a slightly different way.

Definition 1.5. *[169] A controllable continuous-time time-delay dynamical system,*

$$\dot{\mathbf{x}}(t) = f(\mathbf{x}_t, \mathbf{u}(t)), \quad t \geq t_0 \text{ a.e.}, \tag{1.4a}$$

$$\mathbf{x}(\sigma) = \boldsymbol{\xi}_0(\sigma), \quad \sigma \in \left[t_0 - \overline{T}, t_0\right], \tag{1.4b}$$

with $\mathbf{x}_t : [-\overline{T}, 0] \mapsto \mathbb{R}^n$ *the standard function* $\mathbf{x}_t(\tau) = \mathbf{x}(t+\tau)$*, and* $\overline{T}$ *the maximum involved time delay, and* $\boldsymbol{\xi}_0 : [t_0 - \overline{T}, t_0] \mapsto \mathbb{R}^n$*, is ISS with the input* $\mathbf{u}(t)$ *and the state* $\mathbf{x}(t)$ *if there exist some functions* $\alpha(\cdot) \in \mathcal{K}$ *and* $\beta(\cdot,\cdot) \in \mathcal{KL}$ *such that*

$$\|\mathbf{x}(t_1)\| \leq \beta(|\boldsymbol{\xi}_0|_{\overline{T}}, t_1 - t_0) + \alpha\left(\sup_{t_0 \leq \tau \leq t_1} \|\mathbf{u}(\tau)\|\right), \quad t_1 \geq t_0 \geq 0.$$

In addition, the following two theorems facilitate proving ISS systems without delays and with time-varying delays, respectively.

Theorem 1.1. *[168] The delay-free dynamical system* (1.3) *is ISS if and only if there exist an ISS-Lyapunov function* $V : \mathbb{R}^n \mapsto \mathbb{R}_{\geq 0}$*, and some functions* $\alpha_1(\cdot), \alpha_2(\cdot) \in \mathcal{K}_\infty$ *and* $\alpha_3(\cdot), \rho(\cdot) \in \mathcal{K}$ *such that:*

(a) $\alpha_1(\|\mathbf{x}(t)\|) \leq V(\mathbf{x}(t)) \leq \alpha_2(\|\mathbf{x}(t)\|)$, $\forall \mathbf{x} \in \mathbb{R}^n$;

(b) $\dot{V}(\mathbf{x}(t)) \leq -\alpha_3(\|\mathbf{x}(t)\|)$, $\forall \mathbf{x} \in \mathbb{R}^n$ *and* $\mathbf{u}(t) \in \mathbb{R}^m$ *with* $\|\mathbf{x}(t)\| \geq \rho(\|\mathbf{u}(t)\|)$.

Let $\mathcal{C}([-\overline{T}, 0]; \mathbb{R}^n)$ denote the set of continuous functions defined on $[-\overline{T}, 0]$ and with values in $\mathbb{R}^n$. For any essentially bounded function $\eta(\cdot) \in \mathcal{C}([-\overline{T}, 0]; \mathbb{R}^n)$, let $|\eta|_{\overline{T}} = \sup_{-\overline{T} \leq \tau \leq 0} \|\eta(\tau)\|$ and $|\eta|_a$ be a norm of η such that $k_l \|\eta(0)\| \leq |\eta|_a \leq k_u |\eta|_{\overline{T}}$ for some positive reals k_l and k_u.

Theorem 1.2. *[169] The time-delay system* (1.4) *is ISS if there exist a Lyapunov-Krasovskii functional* $V : \mathcal{C}([-\overline{T}, 0]; \mathbb{R}^n) \mapsto \mathbb{R}_{\geq 0}$, *some functions* $\alpha_1(\cdot), \alpha_2(\cdot) \in \mathcal{K}_\infty$ *and* $\alpha_3(\cdot), \rho(\cdot) \in \mathcal{K}$ *such that:*

(a) $\alpha_1(\|\mathbf{x}(t)\|) \leq V(\mathbf{x}_t) \leq \alpha_2(|\mathbf{x}_t|_a)$, $\forall \mathbf{x}_t \in \mathcal{C}([-\overline{T}, 0]; \mathbb{R}^n)$;

(b) $\dot{V}(\mathbf{x}_t) \leq -\alpha_3(|\mathbf{x}_t|_a)$, $\forall \mathbf{x}_t \in \mathcal{C}([-\overline{T}, 0]; \mathbb{R}^n)$ *and* $\mathbf{u}(t) \in \mathbb{R}^m$ *with* $|\mathbf{x}_t|_a \geq \rho(\|\mathbf{u}(t)\|)$.

1.4.2 Robot Dynamics

Throughout the thesis, we assume that every robot with n degrees of freedom possesses the following EL dynamics with gravity compensated:

$$\mathbf{M}_R(\mathbf{x}_R)\ddot{\mathbf{x}}_R + \mathbf{C}_R(\mathbf{x}_R, \dot{\mathbf{x}}_R)\dot{\mathbf{x}}_R = \mathbf{f}_R, \tag{1.5}$$

where the subscript R is the index of the robot, $\mathbf{x}_R$, $\dot{\mathbf{x}}_R$ and $\ddot{\mathbf{x}}_R$ are n-dimensional position, velocity and acceleration vectors of the robot, $\mathbf{M}_R(\mathbf{x}_R)$ and $\mathbf{C}_R(\mathbf{x}_R, \dot{\mathbf{x}}_R)$ are its matrices of inertia and of Coriolis and centrifugal effects, and $\mathbf{f}_R$ is its control input, respectively. For example, for the two types of experimental robots, the Geomagic Touch[2] and Novint Falcon[3] haptic devices in Figure 1.6, their end-effector motions under task-space controls can be described by the dynamics (1.5) with $\mathbf{x}_R = (x, y, z)^\mathsf{T}$.

Some properties of the robot dynamics (1.5) are adopted from [170, Chapter 2] and listed as follows to facilitate the control designs and stability analyses in Chapters 2-5.

Property 1.1. *The matrix of inertia,* $\mathbf{M}_R(\mathbf{x}_R)$, *is symmetric, positive definite and uniformly bounded by* $\mathbf{0} \prec \lambda_{*1}\mathbf{I} \preceq \mathbf{M}_R(\mathbf{x}_R) \preceq \lambda_{*2}\mathbf{I} \prec +\boldsymbol{\infty}$, *where* $\lambda_{*2} \geq \lambda_{*1} > 0$.

Property 1.2. *The matrix* $\dot{\mathbf{M}}_R(\mathbf{x}_R) - 2\mathbf{C}_R(\mathbf{x}_R, \dot{\mathbf{x}}_R)$ *is skew-symmetric.*

[2] `https://www.3dsystems.com/haptics-devices/touch`

[3] `https://en.wikipedia.org/wiki/Novint_Technologies`

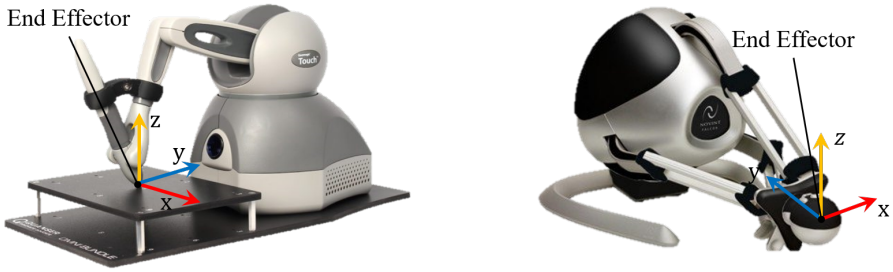

(a) A Geomagic Touch robot. (b) A Novint Falcon robot.

Figure 1.6: Two types of haptic robots that have end-effector dynamics in the form of (1.5) with $\mathbf{x}_R = (x, y, z)^\mathsf{T}$.

Property 1.3. *There exists* $c_R > 0$ *such that* $\|\mathbf{C}_R(\mathbf{x}_R, \mathbf{y})\mathbf{z}\| \leq c_R\|\mathbf{y}\|\|\mathbf{z}\|$, $\forall \mathbf{x}_R, \mathbf{y}, \mathbf{z}$.

In particular, Properties 1.1 and 1.2 together imply the open-loop passivity of the robot. Let the storage function of the robot be defined by

$$V_k = \frac{1}{2}\dot{\mathbf{x}}_R^\mathsf{T}\mathbf{M}_R(\mathbf{x}_R)\dot{\mathbf{x}}_R.$$

Along the dynamics (1.5), the storage function V_k changes with

$$\begin{aligned}\dot{V}_k =& \frac{1}{2}\ddot{\mathbf{x}}_R^\mathsf{T}\mathbf{M}_R(\mathbf{x}_R)\dot{\mathbf{x}}_R + \frac{1}{2}\dot{\mathbf{x}}_R^\mathsf{T}\dot{\mathbf{M}}_R(\mathbf{x}_R)\dot{\mathbf{x}}_R + \frac{1}{2}\dot{\mathbf{x}}_R^\mathsf{T}\mathbf{M}_R(\mathbf{x}_R)\ddot{\mathbf{x}}_R \\ =& \frac{1}{2}\dot{\mathbf{x}}_R^\mathsf{T}\mathbf{M}_R(\mathbf{x}_R)\dot{\mathbf{x}}_R + \dot{\mathbf{x}}_R^\mathsf{T}\mathbf{M}_R(\mathbf{x}_R)\ddot{\mathbf{x}}_R = \frac{1}{2}\dot{\mathbf{x}}_R^\mathsf{T}\mathbf{M}_R(\mathbf{x}_R)\dot{\mathbf{x}}_R - \dot{\mathbf{x}}_R^\mathsf{T}\mathbf{C}_R(\mathbf{x}_R, \dot{\mathbf{x}}_R)\dot{\mathbf{x}}_R + \dot{\mathbf{x}}_R^\mathsf{T}\mathbf{f}_R \\ =& \frac{1}{2}\dot{\mathbf{x}}_R^\mathsf{T}\left[\dot{\mathbf{M}}_R(\mathbf{x}_R) - 2\mathbf{C}_R(\mathbf{x}_R, \dot{\mathbf{x}}_R)\right]\dot{\mathbf{x}}_R + \dot{\mathbf{x}}_R\mathbf{f} = \dot{\mathbf{x}}_R^\mathsf{T}\mathbf{f}_R,\end{aligned}$$

which means that the robot is passive (lossless) with the input $\mathbf{f}_R$ and the output $\dot{\mathbf{x}}_R$.

A classical and elegant application of passivity is the position regulation of the robot via Proportional-Derivative (PD) control. Suppose that the target point of the robot is $\mathbf{x}^*$. Designing a PD control by

$$\mathbf{f}_R = \mathbf{P}(\mathbf{x}^* - \mathbf{x}_R) + \mathbf{D}(\dot{\mathbf{x}}^* - \dot{\mathbf{x}}_R)$$

with $\mathbf{P}$ and $\mathbf{D}$ symmetric and positive definite can then steer the robot to its target location. To show this, let the storage function of the system be

$$V_{kp} = \frac{1}{2}\dot{\mathbf{x}}_R^\mathsf{T}\mathbf{M}(\mathbf{x}_R)\dot{\mathbf{x}}_R + \frac{1}{2}(\mathbf{x}_R - \mathbf{x}^*)^\mathsf{T}\mathbf{P}(\mathbf{x}_R - \mathbf{x}^*),$$

of which the derivative along (1.5) is

$$\begin{aligned}\dot{V}_{kp} =&\dot{\mathbf{x}}_R^\mathsf{T}\mathbf{f}_R + \frac{1}{2}(\dot{\mathbf{x}}_R - \dot{\mathbf{x}}^*)^\mathsf{T}\mathbf{P}(\mathbf{x}_R - \mathbf{x}^*) + \frac{1}{2}(\mathbf{x}_R - \mathbf{x}^*)^\mathsf{T}\mathbf{P}(\dot{\mathbf{x}}_R - \dot{\mathbf{x}}^*)\\ =&\dot{\mathbf{x}}_R^\mathsf{T}\mathbf{P}(\mathbf{x}^* - \mathbf{x}_R) + \dot{\mathbf{x}}_R^\mathsf{T}\mathbf{D}(\dot{\mathbf{x}}^* - \dot{\mathbf{x}}_R) + (\dot{\mathbf{x}}_R - \dot{\mathbf{x}}^*)^\mathsf{T}\mathbf{P}(\mathbf{x}_R - \mathbf{x}^*)\\ =&\dot{\mathbf{x}}_R^\mathsf{T}\mathbf{D}(\dot{\mathbf{x}}^* - \dot{\mathbf{x}}_R) - \dot{\mathbf{x}}^{*\mathsf{T}}\mathbf{P}(\mathbf{x}_R - \mathbf{x}^*) = -\dot{\mathbf{x}}_R^\mathsf{T}\mathbf{D}\dot{\mathbf{x}}_R\end{aligned}$$

because $\dot{\mathbf{x}}^* = \mathbf{0}$ for fixed $\mathbf{x}^*$. The time integration of both sides from t_0 to t_1 leads to

$$V_{kp}(t_1) = V_{kp}(t_0) - \int_{t_0}^{t_1} \dot{\mathbf{x}}_R^\mathsf{T}(\tau)\mathbf{D}\dot{\mathbf{x}}_R(\tau)d\tau,$$

which implies that the closed-loop system is passive with the supply rate $-\dot{\mathbf{x}}_R^\mathsf{T}\mathbf{D}\dot{\mathbf{x}}_R$ according to Definition 1.3. It can then conclude from Proposition 1.2 that $\dot{\mathbf{x}}_R$ globally asymptotically converges to $\mathbf{0}$. Because $\ddot{\mathbf{x}}_R$ is bounded by the derivative of (1.5), using Barbalat's lemma then gives that $\ddot{\mathbf{x}}_R$ also converges to $\mathbf{0}$. From (1.5), they together result in the convergence of $\mathbf{f}_R$ and thus of $\mathbf{x}^* - \mathbf{x}_R$ to $\mathbf{0}$.

1.4.3 Algebraic Graph Theory

A time-varying undirected graph $\mathcal{G}(t) = \{\mathcal{V}, \mathcal{E}(t)\}$ can encode all interactions within a multi-robot system. Specifically, the vertex set $\mathcal{V} = \{1, \cdots, N\}$ collects the indices of all robots. The edge set $\mathcal{E}(t) \subset \mathcal{V} \times \mathcal{V}$ includes all bidirectional communication links (i, j) between pairs of distinct robots i and j at time t. Let $\mathcal{N}_i(t) = \{j \in \mathcal{V} |\ (i, j) \in \mathcal{E}(t)\}$ be the set of the neighbours j of the robot i at time t. The degree of the robot i, $d_i(t)$, is then the cardinality of $\mathcal{N}_i(t)$, $d_i(t) = |\mathcal{N}_i(t)|$. The $N \times N$ diagonal degree matrix $\mathbf{D}(t)$ has $d_i(t)$ as its i-th diagonal element. If the robot j is a neighbour of the robot i, i.e., $j \in \mathcal{N}_i(t)$, the robot j is said to be adjacent to the robot i. Let $a_{ij}(t) = 1$ if $j \in \mathcal{N}_i(t)$, and $a_{ij}(t) = 0$ otherwise. The $N \times N$ adjacency matrix $\mathbf{A}(t)$ has $a_{ij}(t)$ as its (i, j)-th component. Then $\overline{\mathbf{L}}(t) = \mathbf{D}(t) - \mathbf{A}(t)$ is the unweighted Laplacian matrix of the graph. Because $\mathcal{G}(t)$ is undirected, $\mathbf{A}(t)$ and $\overline{\mathbf{L}}(t)$ both are symmetric.

Example 1.1. *In Figure 1.7(a), the graph $\mathcal{G}$ has a vertex set $\mathcal{V} = \{1, 2, 3, 4, 5\}$ and an edge set $\mathcal{E} = \{(1, 2), (1, 3), (2, 3), (3, 4), (4, 5)\}$. The neighbourhood of the vertex 3 is $\mathcal{N}_3 = \{1, 2, 4\}$ and thus the degree of the vertex 3 is $d_3 = 3$. The adjacency matrix*

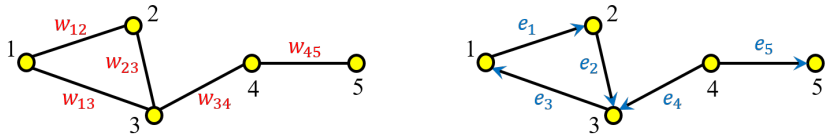

(a) A connected graph $\mathcal{G}$. (b) An oriented version of $\mathcal{G}$.

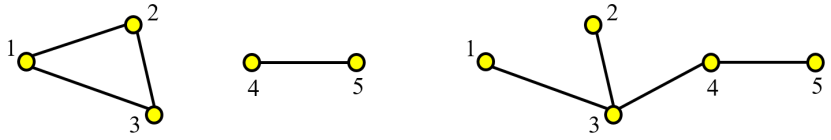

(c) A disconnected graph $\mathcal{G}_d$. (d) A spanning tee $\mathcal{T}$ of $\mathcal{G}$.

Figure 1.7: Different types of graphs of 5 vertices: (a) a connected graph $\mathcal{G}$; (b) an oriented version of $\mathcal{G}$; (c) a disconnected graph $\mathcal{G}_{dis}$; and (d) a spanning tree $\mathcal{T}$ of $\mathcal{G}$.

and the unweighted Laplacian matrix of $\mathcal{G}$ are defined, respectively, by

$$\mathbf{A} = \begin{bmatrix} 0 & 1 & 1 & 0 & 0 \\ 1 & 0 & 1 & 0 & 0 \\ 1 & 1 & 0 & 1 & 0 \\ 0 & 0 & 1 & 0 & 1 \\ 0 & 0 & 0 & 1 & 0 \end{bmatrix}, \quad \overline{\mathbf{L}} = \begin{bmatrix} 2 & -1 & -1 & 0 & 0 \\ -1 & 2 & -1 & 0 & 0 \\ -1 & -1 & 3 & -1 & 0 \\ 0 & 0 & -1 & 2 & -1 \\ 0 & 0 & 0 & -1 & 1 \end{bmatrix}.$$

Let there be M pairs of mutually adjacent robots. The cardinality of the edge set $\mathcal{E}(t)$ is then $|\mathcal{E}(t)| = M$. An oriented version of $\mathcal{G}(t)$ can be derived by assigning a unique index e_k with the subscript $k = 1, \cdots, M$ and an arbitrary orientation to every link $(i, j) \in \mathcal{E}(t)$. Then, an $N \times M$ incidence matrix $\mathbf{B}(t)$ associated with the oriented version of the graph $\mathcal{G}(t)$ can be defined by letting its (i, k)-th element be

$$b_{ik} = \begin{cases} 1 & \text{if vertex } i \text{ is the head of oriented edge } e_k, \\ -1 & \text{if vertex } i \text{ is the tail of oriented edge } e_k, \\ 0 & \text{otherwise,} \end{cases}$$

and the edge Laplacian matrix $\mathbf{L}_e(t)$ of $\mathcal{G}(t)$ can be defined by $\mathbf{L}_e(t) = \mathbf{B}^{\mathsf{T}}(t)\mathbf{B}(t)$. Further, associating a weight w_{ij} to every edge (i, j) of $\mathcal{G}$ introduces an $N \times N$ weighted

Laplacian matrix $\mathbf{L}(t)$ with its (i,j)-th entry being

$$l_{ij} = \begin{cases} -w_{ij} & \text{if } j \neq i \text{ and } j \in \mathcal{N}_i, \\ 0 & \text{if} j \neq i \text{ and } j \notin \mathcal{N}_i, \\ \sum_{h \in \mathcal{N}_i} w_{ih} & \text{if } j = i. \end{cases}$$

Let an $M \times M$ diagonal matrix $\mathbf{\Xi}(t)$ collect every edge weight w_{ij} corresponding to e_k by its k-th diagonal component with $k = 1, \cdots, M$. The following proposition regarding $\mathbf{B}(t)$, $\overline{\mathbf{L}}(t)$, $\mathbf{\Xi}(t)$ and $\mathbf{L}(t)$ is instrumental to the designs in Chapters 5 and 6.

Proposition 1.4. *For any undirected graph $\mathcal{G}(t)$, its incidence matrix $\mathbf{B}(t)$ can decompose its unweighted Laplacian matrix into $\overline{\mathbf{L}}(t) = \mathbf{B}(t)\mathbf{B}^{\mathsf{T}}(t)$ and its weighted Laplacian matrix into $\mathbf{L}(t) = \mathbf{B}(t)\mathbf{\Xi}(t)\mathbf{B}^{\mathsf{T}}(t)$.*

To better understand the incidence matrix, we give an example as follows.

Example 1.2. *The graph $\mathcal{G}$ in Figure 1.7(a) has $M = 5$ edges weighted by $w_{12} = w_{23} = 2$, $w_{13} = w_{34} = 1$ and $w_{45} = 3$. An oriented version of $\mathcal{G}$ is obtained by assigning an arbitrary orientation and a unique index e_k to every edge of $\mathcal{G}$, see Figure 1.7(b). Then, the associated incidice matrix and the weighted Laplacian matrix of $\mathcal{G}$ are*

$$\mathbf{B} = \begin{bmatrix} -1 & 0 & 1 & 0 & 0 \\ 1 & -1 & 0 & 0 & 0 \\ 0 & 1 & -1 & 1 & 0 \\ 0 & 0 & 0 & -1 & -1 \\ 0 & 0 & 0 & 0 & 1 \end{bmatrix}, \quad \mathbf{L} = \begin{bmatrix} 3 & -2 & -1 & 0 & 0 \\ -2 & -2 & 4 & 0 & 0 \\ -1 & -2 & 4 & -1 & 0 \\ 0 & 0 & -1 & 4 & -3 \\ 0 & 0 & 0 & -3 & 3 \end{bmatrix},$$

respectively. It can also verify that $\overline{\mathbf{L}} = \mathbf{B}\mathbf{B}^{\mathsf{T}}$ and $\mathbf{L} = \mathbf{B}\mathbf{\Xi}\mathbf{B}^{\mathsf{T}}$.

A path in $\mathcal{G}(t)$ is a sequence of edges that joins a sequence of distinct vertices. If a path exists between every pair of distinct vertices, then $\mathcal{G}(t)$ is connected. A tree is a connected graph with the minimum number of edges.

Proposition 1.5. *If $\mathcal{G}(t)$ is a tree, the smallest eigenvalue of its edge Laplacian $\mathbf{L}_e(t)$ is positive, $\lambda_L > 0$.*

Example 1.3. *The graph $\mathcal{G}$ in Figure 1.7(a) is connected, while the graph $\mathcal{G}_d$ in Figure 1.7(c) is disconnected because of no path between the vertices 3 and 4. In Figure 1.7(d), the spanning tree $\mathcal{T}$ of $\mathcal{G}$ is obtained by removing the edge $(1,2)$ from $\mathcal{G}$, of which the edge Laplacian matrix $\mathbf{L}_e$ has the smallest eigenvalue $\lambda_L = 0.5188 > 0$.*

Refer to [171, Chapter 2] for more details on graph theory.

1.4.4 Notation

In the remainder of the thesis: bolded upper- and lower-case letters indicate matrices and vectors, respectively; regular fonts denote scalars; the superscript $^\mathsf{T}$ transposes a matrix or vector; $\mathbf{A} \otimes \mathbf{B}$ is the Kronecker product of $\mathbf{A}$ and $\mathbf{B}$; $\mathbf{A} \succeq \mathbf{B}$ and $\mathbf{A} \succ \mathbf{B}$ imply that $\mathbf{A} - \mathbf{B}$ is positive semidefinite and positive definite, respectively; $\mathbf{A}^p$ is the product matrix taking $\mathbf{A}$ and multiplying it by itself p-times; $\mathbf{I}$ ($\mathbf{I}_n$) is the identity matrix of proper dimensions (dimension $n \times n$); $\mathbf{0}$ ($\mathbf{0}_{n_r \times n_c}$) denotes a matrix of appropriate dimensions (dimension $n_r \times r_c$) with all entries 0; $\mathbf{0}_n$ is a column vector of dimension n with all components 0; $\mathbf{1}$ ($\mathbf{1}_n$) is a column vector of proper dimension (dimension n) with all elements 1; $\text{Diag}\{\mathbf{M}_i\}$ is a block diagonal matrix with $\mathbf{M}_i$ the i-th diagonal block; $\|\mathbf{v}\|$ is the Euclidean norm of $\mathbf{v} = (v_1, \cdots, v_n)^\mathsf{T}$; $|\mathbf{v}| = \big(|v_1|, \cdots, |v_n|\big)^\mathsf{T}$; $\mathbf{v} \geq \mathbf{0}$ and $\mathbf{v} > \mathbf{0}$ indicate that $v_i \geq 0$ and $v_i > 0$ for all $i = 1, \cdots, n$, respectively; $\text{diag}\{\mathbf{v}\}$ is a diagonal matrix with v_i the i-th diagonal element; $\text{sign}(\mathbf{v}) = (\text{sign}(v_1), \cdots, \text{sign}(v_n))^\mathsf{T}$ with $\text{sign}(v_i) = \{1\}$ if $v_i > 0$, $\text{sign}(v_i) = [-1, 1]$ if $v_i = 0$, and $\text{sign}(v_i) = \{-1\}$ if $v_i < 0$; $\text{S}_b(\mathbf{v}) = \mathbf{v}$ if $\|\mathbf{v}\| \leq b$, and $\text{S}_b(\mathbf{v}) = b\mathbf{v}/\|\mathbf{v}\|$ if $\|\mathbf{v}\| > b$, for $b > 0$; for two vectors $\mathbf{v}_1$ and $\mathbf{v}_2$ having the same dimension, $\mathbf{v}_1 \circ \mathbf{v}_2$ is the Hadamard product of $\mathbf{v}_1$ and $\mathbf{v}_2$; for any set $\mathcal{C} \in \mathbb{R}^n$, its algebraic operation with the vector $\mathbf{v}$ is imposed on all its elements, forming a new set; $\mathcal{C} \geq 0$ and $\mathcal{C} > 0$ indicate that all elements of $\mathcal{C}$ are nonnegative and positive, respectively; for $\mathcal{C}$ closed and bounded, $\text{int}(\mathcal{C})$ and $\partial\mathcal{C}$ are the interior and boundary of $\mathcal{C}$, respectively; if $\mathcal{C}$ is countable, $|\mathcal{C}|$ is its cardinality; $\mathcal{C}_1 \ominus \mathcal{C}_2$ is the Minkovski difference of $\mathcal{C}_1$ and $\mathcal{C}_2$; and the time argument is omitted when clear from the context.

Given a closed convex set $\mathcal{C} \in \mathbb{R}^n$ with $n = 1, 2, 3, \cdots$, a vector $\mathbf{n}$ is a normal vector of $\mathcal{C}$ at the point $\mathbf{c} \in \mathcal{C}$ if $\mathbf{n}^\mathsf{T}(\mathbf{z} - \mathbf{c}) \leq 0$ for any $\mathbf{z} \in \mathcal{C}$. Further, the normal cone $\mathcal{N}_\mathcal{C}(\mathbf{c})$ of $\mathcal{C}$ at $\mathbf{c}$ is the collection of all normal vectors $\mathbf{n}$, i.e., $\mathcal{N}_\mathcal{C}(\mathbf{c}) = \big\{\mathbf{n} \in \mathbb{R}^n |\ \mathbf{n}^\mathsf{T}(\mathbf{z} - \mathbf{c}) \leq 0,\ \forall \mathbf{z} \in \mathcal{C}\big\}$. Let $\mathcal{N}^*_\mathcal{C}(\mathbf{c}) = \{\mathbf{0}\}$ if $\mathcal{N}_\mathcal{C}(\mathbf{c}) = \{\mathbf{0}\}$, and $\mathcal{N}^*_\mathcal{C}(\mathbf{c}) = \{\mathbf{n} \in \mathbb{R}^n |\ \|\mathbf{n}\| = 1 \text{ and } \mathbf{n}^\mathsf{T}(\mathbf{z} - \mathbf{c}) \leq 0,\ \forall \mathbf{z} \in \mathcal{C}\}$ if $\mathcal{N}_\mathcal{C}(\mathbf{c}) \neq \{\mathbf{0}\}$. Then, for any vector $\mathbf{g} \in \mathbb{R}^n$, the projection operator $\text{Proj}_\mathcal{C}(\mathbf{c}, \mathbf{g})$ on $\mathcal{C}$ is defined by $\text{Proj}_\mathcal{C}(\mathbf{c}, \mathbf{g}) = \big(\mathbf{I} - \mathbf{n}_*\mathbf{n}_*^\mathsf{T}\big)\,\mathbf{g}$, where $\mathbf{n}_* \in \mathcal{N}^*_\mathcal{C}(\mathbf{c})$ is given by $\mathbf{n}_* = \arg \max_{\mathbf{n} \in \mathcal{N}^*_\mathcal{C}(\mathbf{c})} \mathbf{n}^\mathsf{T}\mathbf{g}$. That is, $\text{Proj}_\mathcal{C}(\mathbf{c}, \mathbf{g}) = \mathbf{g}$ if $\mathcal{N}^*_\mathcal{C}(\mathbf{c}) = \{\mathbf{0}\}$, and $\mathbf{n}_*^\mathsf{T}\mathbf{g} \geq 0$ if $\mathcal{N}^*_\mathcal{C}(\mathbf{c}) \neq \{\mathbf{0}\}$ because $\mathbf{0} \in \mathcal{N}^*_\mathcal{C}(\mathbf{c})$.

Chapter 2

Input-to-State Stable Bilateral Teleoperation By Dynamic Interconnection and Damping Injection

This chapter introduces a novel strategy for ISS time-delay bilateral teleoperation. The new strategy blends a dynamic local robot-remote robot interconnection with dynamic damping injection to each robot. Although force-reflection [78] architectures can improve transparency, the force and acceleration measurements are unavailable or noisy for many commercial robots. Therefore, the proposed strategy relies on a position-position structure. Its controllers require only the position and velocity of each robot, plus the delayed position of the other robot. Compared to conventional controllers based on Lyapunov-like analysis [91] or energy-monitoring [77], which stably connect the local and remote robots but cannot quantify their error a priori, the proposed strategy can limit the impact of the user and environment on it. A key design step to bring about this property is the transformation of the system dynamics into a first-order form through some properly designed sliding variables. The proposed strategy then suppresses the Coriolis and centrifugal effects of the EL dynamics without compensation, by simply and locally modulating the Proportional and damping gains according to the velocities of robots, making time-delay teleoperation exponentially ISS based on damping injection control.

2.1 Teleoperation Controller Designs

This section presents the control design and stability analysis for ISS bilateral teleoperation, considering communications both without, and with time-varying, delays.

Let the local and remote robots have n-degree-of-freedom (n-DOF) dynamics:

$$\begin{aligned} \mathbf{M}_l(\mathbf{x}_l)\ddot{\mathbf{x}}_l + \mathbf{C}_l(\mathbf{x}_l, \dot{\mathbf{x}}_l)\dot{\mathbf{x}}_l &= \mathbf{f}_l + \mathbf{f}_h, \\ \mathbf{M}_r(\mathbf{x}_r)\ddot{\mathbf{x}}_r + \mathbf{C}_r(\mathbf{x}_r, \dot{\mathbf{x}}_r)\dot{\mathbf{x}}_r &= \mathbf{f}_r + \mathbf{f}_e, \end{aligned} \tag{2.1}$$

where the subscript $i = l, r$ indexes the local and remote robots, $\mathbf{f}_i$ are the control inputs, and $\mathbf{f}_h$ and $\mathbf{f}_e$ are the user and environment forces.

The following assumptions on communication delays and on the user and environment forces facilitate the later control design and stability analysis.

Assumption 2.1. *The time-varying communication delays $T_i(t)$ from the robot indexed by i to the robot indexed by j are bounded by $0 \leq T_i(t) \leq \overline{T}_i$, for $i, j = l, r$.*

Assumption 2.2. *The user and environment forces are bounded by $\|\mathbf{f}_k\| \leq \overline{f}_k$, for $k = h, e$.*

2.1.1 Teleoperation Without Time Delays

Define the sliding variables for the local and remote robots by

$$\mathbf{s}_i = \dot{\mathbf{x}}_i + \sigma(\mathbf{x}_i - \mathbf{x}_j), \tag{2.2}$$

where $i, j = l, r$ and $i \neq j$, and $\sigma > 0$ is a constant to be determined. Then, the teleoperator dynamics (2.1) can be transformed into

$$\mathbf{M}_i(\mathbf{x}_i)\dot{\mathbf{s}}_i + \mathbf{C}_i(\mathbf{x}_i, \dot{\mathbf{x}}_i)\mathbf{s}_i = \mathbf{f}_i + \mathbf{f}_k + \sigma\boldsymbol{\Delta}_i(t), \tag{2.3}$$

where $i = l, r$ and $k = h, e$, respectively, and the state-dependent mismatched dynamics $\boldsymbol{\Delta}_i(t)$ of the local and remote robots are

$$\boldsymbol{\Delta}_i(t) = \mathbf{M}_i(\mathbf{x}_i)(\dot{\mathbf{x}}_i - \dot{\mathbf{x}}_j) + \mathbf{C}_i(\mathbf{x}_i, \dot{\mathbf{x}}_i)(\mathbf{x}_i - \mathbf{x}_j), \tag{2.4}$$

with $i, j = l, r$ and $i \neq j$. Given that the local and remote robots receive each other's position instantly, their dynamic interconnection and damping injection controllers

are designed by

$$\mathbf{f}_i = -\mathbf{K}_i(t)\mathbf{s}_i - \mathbf{P}(\mathbf{x}_i - \mathbf{x}_j) - \mathbf{D}_i\dot{\mathbf{x}}_i, \tag{2.5}$$

where $i, j = l, r$ and $i \neq j$, and $\mathbf{K}_i(t)$, $\mathbf{P}$ and $\mathbf{D}_i$ are diagonal positive definite gain matrices to be determined.

The velocity-dependent gains $\mathbf{K}_i(t)$ are designed to suppress the state-dependent mismatch $\boldsymbol{\Delta}_i(t)$ in (2.4). Rewritting (2.5) in the form:

$$\mathbf{f}_i = -\big[\mathbf{P} + \sigma\mathbf{K}_i(t)\big](\mathbf{x}_i - \mathbf{x}_j) - \big[\mathbf{D}_i + \mathbf{K}_i(t)\big]\dot{\mathbf{x}}_i,$$

where $i, j = l, r$ and $i \neq j$, reveals that the controller dynamically modulates the local robot-remote robot interconnection and the local damping through $\mathbf{K}_i(t)$. The transformed system dynamics (2.3) are input-output passive with the input $\mathbf{f}_i + \mathbf{f}_k + \sigma\boldsymbol{\Delta}_i(t)$ and the output $\mathbf{s}_i$, where $i = l, r$ and $k = h, e$, respectively. However, the teleoperator (2.1) in closed-loop with the controller (2.5) is not guaranteed stable because the modulated interconnection between the local and remote robots, shown in Figure 2.1, may not be passive. The following rigorous analysis is required to show ISS teleoperation.

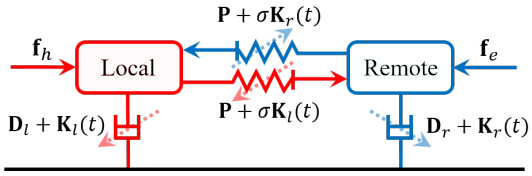

Figure 2.1: The diagram of the teleoperator (2.1) in closed-loop with the control (2.5).

The following Lyapunov candidate:

$$V = \frac{1}{2}\sum_{i=l,r}\mathbf{s}_i^{\mathsf{T}}\mathbf{M}_i(\mathbf{x}_i)\mathbf{s}_i + \frac{1}{2}(\mathbf{x}_l - \mathbf{x}_r)^{\mathsf{T}}\mathbf{P}(\mathbf{x}_l - \mathbf{x}_r), \tag{2.6}$$

serves to evaluate stability. After using Property 1.2, the time derivative of V along the transformed dynamics (2.3) in closed-loop with the control (2.5) can be evaluated by

$$\begin{aligned}\dot{V} = &\sum_{i=l,r}\big[\sigma\mathbf{s}_i^{\mathsf{T}}\boldsymbol{\Delta}_i - \mathbf{s}_i^{\mathsf{T}}\mathbf{K}_i(t)\mathbf{s}_i - \mathbf{s}_i^{\mathsf{T}}\mathbf{D}_i\dot{\mathbf{x}}_i\big] + \mathbf{s}_l^{\mathsf{T}}\mathbf{f}_h + \mathbf{s}_r^{\mathsf{T}}\mathbf{f}_e \\ &+ \dot{\mathbf{x}}_l^{\mathsf{T}}\mathbf{P}(\mathbf{x}_l - \mathbf{x}_r) - \mathbf{s}_l^{\mathsf{T}}\mathbf{P}(\mathbf{x}_l - \mathbf{x}_r) + \dot{\mathbf{x}}_r^{\mathsf{T}}\mathbf{P}(\mathbf{x}_r - \mathbf{x}_l) - \mathbf{s}_r^{\mathsf{T}}\mathbf{P}(\mathbf{x}_r - \mathbf{x}_l).\end{aligned} \tag{2.7}$$

The definitions of $\mathbf{\Delta}_i(t)$ in (2.4) together with Properties 1.1 and 1.3 lead to the following inequalities for $i = l, r$:

$$\begin{aligned}\mathbf{s}_i^{\mathsf{T}}\mathbf{\Delta}_i(t) \leq & \left|\mathbf{s}_i^{\mathsf{T}}\mathbf{M}_i(\mathbf{x}_i)(\dot{\mathbf{x}}_l - \dot{\mathbf{x}}_r)\right| + \left|\mathbf{s}_i^{\mathsf{T}}\mathbf{C}_i(\mathbf{x}_i, \dot{\mathbf{x}}_i)(\mathbf{x}_l - \mathbf{x}_r)\right| \\ \leq & \frac{\lambda_{i2}}{2}\left(2\mathbf{s}_i^{\mathsf{T}}\mathbf{s}_i + \dot{\mathbf{x}}_l^{\mathsf{T}}\dot{\mathbf{x}}_l + \dot{\mathbf{x}}_r^{\mathsf{T}}\dot{\mathbf{x}}_r\right) + \frac{c_i}{4}\left(4\|\dot{\mathbf{x}}_i\|^2\mathbf{s}_i^{\mathsf{T}}\mathbf{s}_i + \|\mathbf{x}_l - \mathbf{x}_r\|^2\right).\end{aligned} \tag{2.8}$$

The inequalities (2.8) reveal that the impact of the local and remote robot mismatches can be upper-bounded using the velocities of the two robots and their position error. Thus, they indicate the demand for a dynamic interconnection and damping injection strategy. More specifically, as will be illustrated in Equations (2.11)-(2.12), $\|\dot{\mathbf{x}}_i\|^2\mathbf{s}_i^{\mathsf{T}}\mathbf{s}_i$ in the inequalities (2.8) can be dominated by selecting the velocity-dependent gains $\mathbf{K}_i(t)$ in the control forces $\mathbf{f}_i$. Alternatively, $\mathbf{s}_i^{\mathsf{T}}\mathbf{C}_i(\mathbf{x}_i, \dot{\mathbf{x}}_i)(\mathbf{x}_l - \mathbf{x}_r)$ can be bounded by $(c_i/4)\left(4\|\mathbf{x}_l - \mathbf{x}_r\|^2\mathbf{s}_i^{\mathsf{T}}\mathbf{s}_i + \dot{\mathbf{x}}_i^{\mathsf{T}}\dot{\mathbf{x}}_i\right)$, and the gains $\mathbf{K}_i(t)$ can be updated based on the local robot-remote robot position error. Therefore, the velocities of both the local and remote robots and their position error can be used to dynamically modulate their coupling and local damping injection, to achieve ISS bilateral teleoperation.

The definitions of the sliding variables $\mathbf{s}_i$ in (2.2) lead to

$$\begin{aligned}& -\mathbf{s}_i^{\mathsf{T}}\mathbf{P}(\mathbf{x}_i - \mathbf{x}_j) - \mathbf{s}_i^{\mathsf{T}}\mathbf{D}_i\dot{\mathbf{x}}_i + \dot{\mathbf{x}}_i^{\mathsf{T}}\mathbf{P}(\mathbf{x}_i - \mathbf{x}_j) \\ = & -\sigma(\mathbf{x}_i - \mathbf{x}_j)^{\mathsf{T}}\mathbf{P}(\mathbf{x}_i - \mathbf{x}_j) - \dot{\mathbf{x}}_i^{\mathsf{T}}\mathbf{D}_i\dot{\mathbf{x}}_i - \sigma(\mathbf{x}_i - \mathbf{x}_j)^{\mathsf{T}}\mathbf{D}_i\dot{\mathbf{x}}_i \\ \leq & -\frac{\sigma}{4}(\mathbf{x}_i - \mathbf{x}_j)^{\mathsf{T}}\left(4\mathbf{P} - \mu_i\mathbf{D}_i\right)(\mathbf{x}_i - \mathbf{x}_j) - \frac{1}{\mu_i}(\mu_i - \sigma)\dot{\mathbf{x}}_i^{\mathsf{T}}\mathbf{D}_i\dot{\mathbf{x}}_i,\end{aligned} \tag{2.9}$$

where $i, j = l, r$, $i \neq j$ and $\mu_i > 0$. Further algebraic manipulations yield

$$\mathbf{s}_l^{\mathsf{T}}\mathbf{f}_h + \mathbf{s}_r^{\mathsf{T}}\mathbf{f}_e \leq \sum_{i=l,r}\omega_i\mathbf{s}_i^{\mathsf{T}}\mathbf{s}_i + \frac{\|\mathbf{f}_h\|^2}{4\omega_l} + \frac{\|\mathbf{f}_e\|^2}{4\omega_r}, \tag{2.10}$$

where $\omega_i > 0$, $i = l, r$.

After substitutions from Equations (2.8)-(2.10), the time derivative of the Lyapunov candidate $\dot{V}$ in (2.7) can then be bounded by

$$\dot{V} \leq -\sum_{i=l,r}\left[\mathbf{s}_i^{\mathsf{T}}\overline{\mathbf{K}}_i(t)\mathbf{s}_i + \dot{\mathbf{x}}_i^{\mathsf{T}}\overline{\mathbf{D}}_i\dot{\mathbf{x}}_i\right] - (\mathbf{x}_l - \mathbf{x}_r)^{\mathsf{T}}\overline{\mathbf{P}}(\mathbf{x}_l - \mathbf{x}_r) + \frac{\|\mathbf{f}_h\|^2 + \|\mathbf{f}_e\|^2}{4\omega}, \tag{2.11}$$

where $\omega = \min(\omega_l, \omega_r)$ and

$$\begin{aligned}\overline{\mathbf{K}}_i(t) =& \mathbf{K}_i(t) - \big(\omega_i + \sigma\lambda_{i2} + \sigma c_i\|\dot{\mathbf{x}}_i\|^2\big)\mathbf{I},\\ \overline{\mathbf{D}}_i =& \big(1-\sigma/\mu_i\big)\mathbf{D}_i - \big[\sigma\big(\lambda_{l2}+\lambda_{r2}\big)/2\big]\mathbf{I},\\ \overline{\mathbf{P}} =& 2\sigma\mathbf{P} - (\sigma/4)\sum_{i=l,r}\big(\mu_i\mathbf{D}_i + c_i\mathbf{I}\big).\end{aligned}$$

Theorem 2.1. *The bilateral teleoperator* (2.1) *under the control* (2.5) *is ISS with respect to the input* $\mathbf{u} = \big(\mathbf{f}_h^\mathsf{T}\ \mathbf{f}_e^\mathsf{T}\big)^\mathsf{T}$ *and the state* $\mathbf{x} = \big(\dot{\mathbf{x}}_l^\mathsf{T}\ \dot{\mathbf{x}}_r^\mathsf{T}\ (\mathbf{x}_l - \mathbf{x}_r)^\mathsf{T}\big)^\mathsf{T}$ *if the control gains* $\mathbf{K}_i(t)$, $\mathbf{D}_i$, $\mathbf{P}$, σ *and the positive parameters* μ_i, ω_i, κ, $i = l, r$, *are selected to satisfy that*

$$2\overline{\mathbf{P}} \succeq \kappa\mathbf{P}, \quad 2\overline{\mathbf{K}}_i(t) \succeq \kappa\lambda_{i2}\mathbf{I} \quad \textit{and} \quad \overline{\mathbf{D}}_i \succeq \mathbf{0}. \tag{2.12}$$

Proof. The definitions of the sliding variables $\mathbf{s}_i$ in (2.2) imply that $\|\dot{\mathbf{x}}_i\|^2 \le 2\|\dot{\mathbf{s}}_i\|^2 + 2\sigma^2\|\mathbf{x}_l - \mathbf{x}_r\|^2$ and $\|\mathbf{s}_i\|^2 \le 2\|\dot{\mathbf{x}}_i\|^2 + 2\sigma^2\|\mathbf{x}_l - \mathbf{x}_r\|^2$. Let $p\mathbf{I} \preceq \mathbf{P} \preceq P\mathbf{I}$. Then, Property 1.1 and Equations (2.6) and (2.2) together lead to

$$V \ge \sum_{i=l,r}\frac{\lambda_{i1}}{2}\|\mathbf{s}_i\|^2 + \frac{p}{2}\|\mathbf{x}_l - \mathbf{x}_r\|^2 \ge \alpha_1(\|\mathbf{x}\|), \tag{2.13}$$

where $\alpha_1(\|\mathbf{x}\|) = a_1\|\mathbf{x}\|^2$ with

$$\frac{1}{a_1} = \frac{4}{\lambda_{l1}} + \frac{4}{\lambda_{r1}} + \frac{8\sigma^2+2}{p},$$

and also to

$$V \le \sum_{i=l,r}\frac{\lambda_{i2}}{2}\|\mathbf{s}_i\|^2 + \frac{P}{2}\|\mathbf{x}_l - \mathbf{x}_r\|^2 \le \alpha_2(\|\mathbf{x}\|), \tag{2.14}$$

where $\alpha_2(\|\mathbf{x}\|) = (a_2/2)\|\mathbf{x}\|^2$ with $a_2 = \max\big[2\lambda_{l2}, 2\lambda_{r2}, P + 2\sigma^2(\lambda_{l2}+\lambda_{r2})\big]$. Because the functions α_1 and α_2 are of class $\mathcal{K}_\infty$, V satisfies the condition (a) of Theorem 1.1. If the condition (2.12) is satisfied, $\dot{V}$ in (2.11) can be further upper-bounded by

$$\dot{V} \le -\kappa V + \frac{\|\mathbf{u}\|^2}{4\omega}. \tag{2.15}$$

Choosing the class $\mathcal{K}$ functions $\alpha_3(\|\mathbf{x}\|) = (a_1\kappa/2)\|\mathbf{x}\|^2$ and $\rho(\|\mathbf{u}\|) = \sqrt{1/(2a_1\kappa\omega)}\|\mathbf{u}\|$ ensures that V in (2.6) also satisfies the condition (b) of Theorem 1.1 and thus, that the teleoperator is ISS. ■

Corollary 2.1. *Let* $d_I = (2/p)\big[V(0) + \overline{f}^2/(4\kappa\omega)\big]$ *and* $d_A = \overline{f}^2/(2p\kappa\omega)$ *with* $\overline{f}^2 = \bar{f}_h^2 + \bar{f}_e^2$. *ISS teleoperation renders the set* $\mathcal{S}_I = \big\{\mathbf{x}_l - \mathbf{x}_r \in \mathbb{R}^n \mid \|\mathbf{x}_l - \mathbf{x}_r\|^2 \leq d_I\big\}$ *invariant and the set* $\mathcal{S}_A = \big\{\mathbf{x}_l - \mathbf{x}_r \in \mathbb{R}^n \mid \|\mathbf{x}_l - \mathbf{x}_r\|^2 \leq d_A\big\}$ *globally exponentially attractive.*

Proof. Apllying Grönwall's inequality to the time integration of $\dot{V}$ in (2.15) yields

$$\begin{aligned} V(t) \leq & \exp(-\kappa t) \cdot V(0) + \frac{1}{4\omega}\int_0^t \exp[-\kappa(t-\tau)] \cdot \|\mathbf{u}(\tau)\|^2 d\tau \\ \leq & \exp(-\kappa t) \cdot V(0) + \frac{\overline{f}^2}{4\omega}\int_0^t \exp[-\kappa(t-\tau)] d\tau \leq \exp(-\kappa t) \cdot V(0) + \frac{\overline{f}^2}{4\kappa\omega}, \end{aligned}$$

which, together with (2.13), completes the proof. ■

2.1.2 Teleoperation With Time-Varying Delays

For each robot, construct the following auxiliary system (virtual proxy):

$$\begin{aligned} \widehat{\mathbf{M}}_i\ddot{\widehat{\mathbf{x}}}_i = & -\widehat{\mathbf{K}}_i\big[\dot{\widehat{\mathbf{x}}}_i + \widehat{\sigma}\big(\mathbf{P}_i(\widehat{\mathbf{x}}_i - \mathbf{x}_i) + \widehat{\mathbf{P}}(\widehat{\mathbf{x}}_i - \widehat{\mathbf{x}}_{jd})\big)\big] \\ & - \widehat{\mathbf{D}}_i\dot{\widehat{\mathbf{x}}}_i - \mathbf{P}_i(\widehat{\mathbf{x}}_i - \mathbf{x}_i) - \widehat{\mathbf{P}}(\widehat{\mathbf{x}}_i - \widehat{\mathbf{x}}_{jd}), \end{aligned} \tag{2.16}$$

where $i, j = l, r$ with $i \neq j$, $\widehat{\sigma} > 0$, $\widehat{\mathbf{M}}_i$, $\widehat{\mathbf{K}}_i$, $\widehat{\mathbf{D}}_i$, $\mathbf{P}_i$ and $\widehat{\mathbf{P}}$ are diagonal positive definite matrices to be determined; and $\widehat{\mathbf{x}}_{jd} = \widehat{\mathbf{x}}_j(t - T_j(t))$ is the output of the auxiliary system of the robot indexed by j received with a time-varying delay $T_j(t)$ by the other robot indexed by i. Define a sliding variable $\widehat{\mathbf{s}}_i$ for the proxy of the robot indexed by i by

$$\widehat{\mathbf{s}}_i = \dot{\widehat{\mathbf{x}}}_i + \widehat{\sigma}\widehat{\mathbf{e}}_i, \tag{2.17}$$

in which $\widehat{\mathbf{e}}_i = \mathbf{P}_i\left(\widehat{\mathbf{x}}_i - \mathbf{x}_i\right) + \widehat{\mathbf{P}}\left(\widehat{\mathbf{x}}_i - \widehat{\mathbf{x}}_j\right)$. Then, the dynamics (2.16) of the auxiliary systems can be rearranged in the form:

$$\begin{aligned} \widehat{\mathbf{M}}_i\dot{\widehat{\mathbf{s}}}_i = & \widehat{\sigma}\widehat{\mathbf{M}}_i\big[\mathbf{P}_i\big(\dot{\widehat{\mathbf{x}}}_i - \dot{\mathbf{x}}_i\big) + \widehat{\mathbf{P}}\big(\dot{\widehat{\mathbf{x}}}_i - \dot{\widehat{\mathbf{x}}}_j\big)\big] - \widehat{\mathbf{e}}_i \\ & - \widehat{\mathbf{K}}_i\widehat{\mathbf{s}}_i - \big(\widehat{\sigma}\widehat{\mathbf{K}}_i + \mathbf{I}\big)\widehat{\mathbf{P}}\left(\widehat{\mathbf{x}}_j - \widehat{\mathbf{x}}_{jd}\right) - \widehat{\mathbf{D}}_i\dot{\widehat{\mathbf{x}}}_i. \end{aligned} \tag{2.18}$$

Define a sliding variable for the robot indexed by i by

$$\mathbf{s}_i = \dot{\mathbf{x}}_i + \sigma(\mathbf{x}_i - \widehat{\mathbf{x}}_i) \tag{2.19}$$

with $\sigma > 0$. As in Section 2.1.1, the local and remote robot dynamics (2.1) can be

transformed into (2.3) but with the mismatched dynamics redefined by

$$\boldsymbol{\Delta}_i(t) = \mathbf{M}_i(\mathbf{x}_i)\big(\dot{\mathbf{x}}_i - \dot{\widehat{\mathbf{x}}}_i\big) + \mathbf{C}_i(\mathbf{x}_i, \dot{\mathbf{x}}_i)(\mathbf{x}_i - \widehat{\mathbf{x}}_i). \tag{2.20}$$

Correspondingly, the local and remote robot controllers are designed by

$$\mathbf{f}_i = -\mathbf{K}_i(t)\mathbf{s}_i - \mathbf{P}_i(\mathbf{x}_i - \widehat{\mathbf{x}}_i) - \mathbf{D}_i\dot{\mathbf{x}}_i \tag{2.21}$$

with $\mathbf{K}_i(t)$ and $\mathbf{D}_i$ diagonal positive definite gain matrices to be determined.

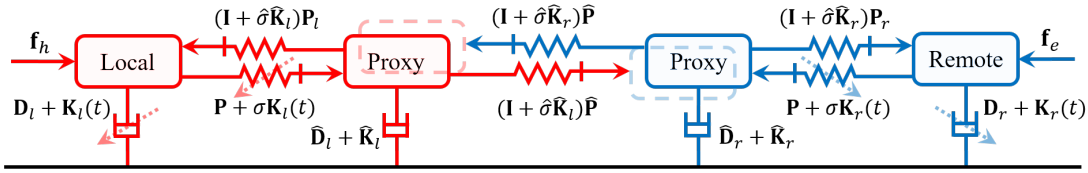

Figure 2.2: The diagram of the teleoperator (2.1) in closed-loop with the proxies (2.16) and the control (2.21).

As shown in Figure 2.2, the auxiliary systems (2.16) have inertia $\widehat{\mathbf{M}}_i$, are connected to each other through static Proportional control, and are driven by the local and remote robots through a static interconnection and damping control. In contrast, the local and remote robots are connected to their proxies by the dynamic interconnection and damping injection controls (2.21), which are updated according to each robot's velocity $\dot{\mathbf{x}}_i$. Because the communication delays distort only the information transmitted between the statically coupled proxies, classical damping injection [84] can overcome their destabilizing effect. The state-dependent mismatches $\boldsymbol{\Delta}_i(t)$ in (2.20) affect only the local and remote robots, as in the case of non-delayed communications in Section 2.1.1. The dynamic control strategy (2.21) will be designed in Theorem 2.2 to address these mismatches.

The stability is validated using the Lyapunov candidate $V = V_1 + V_2$ with

$$\begin{aligned} V_1 =& \frac{1}{2}\sum_{i=l,r}\left[\mathbf{s}_i^{\mathsf{T}}\mathbf{M}_i(\mathbf{x}_i)\mathbf{s}_i + (\mathbf{x}_i - \widehat{\mathbf{x}}_i)^{\mathsf{T}}\mathbf{P}_i(\mathbf{x}_i - \widehat{\mathbf{x}}_i)\right] \\ &+ \frac{1}{2}\sum_{i=l,r}\widehat{\mathbf{s}}_i^{\mathsf{T}}\widehat{\mathbf{M}}_i\widehat{\mathbf{s}}_i + \frac{1}{2}(\widehat{\mathbf{x}}_l - \widehat{\mathbf{x}}_r)^{\mathsf{T}}\widehat{\mathbf{P}}(\widehat{\mathbf{x}}_l - \widehat{\mathbf{x}}_r), \end{aligned} \tag{2.22a}$$

$$V_2 = \sum_{i=l,r}\int_{-\overline{T}_i}^{0}\int_{t+\tau}^{t}\exp[-\gamma(t-\theta)]\cdot\dot{\widehat{\mathbf{x}}}_i^{\mathsf{T}}(\theta)\mathbf{Q}_i\dot{\widehat{\mathbf{x}}}_i(\theta)d\theta d\tau \tag{2.22b}$$

accounting for the kinetic and potential energy of the overall system, and the energy injected by time-varying delays, respectively, where $\mathbf{Q}_i \succ \mathbf{0}$, $i = l, r$.

Using Property 1.2, the time derivative of V_1 along the transformed local and remote robot dynamics (2.3) and their auxiliary dynamics (2.18) is

$$\begin{aligned}\dot{V}_1 = &\sum_{i=l,r} \Big[\sigma \mathbf{s}_i^{\mathsf{T}} \boldsymbol{\Delta}_i(t) - \mathbf{s}_i^{\mathsf{T}} \mathbf{K}_i(t) \mathbf{s}_i - \mathbf{s}_i^{\mathsf{T}} \mathbf{P}_i(\mathbf{x}_i - \widehat{\mathbf{x}}_i) - \mathbf{s}_i^{\mathsf{T}} \mathbf{D}_i \dot{\mathbf{x}}_i - \widehat{\mathbf{s}}_i^{\mathsf{T}} \widehat{\mathbf{K}}_i \widehat{\mathbf{s}}_i - \widehat{\mathbf{s}}_i^{\mathsf{T}} \widehat{\mathbf{e}}_i \\ &\qquad - \widehat{\mathbf{s}}_i^{\mathsf{T}} \widehat{\mathbf{D}}_i \dot{\widehat{\mathbf{x}}}_i + \widehat{\sigma} \widehat{\mathbf{s}}_i^{\mathsf{T}} \widehat{\mathbf{M}}_i \mathbf{P}_i \big(\dot{\widehat{\mathbf{x}}}_i - \dot{\mathbf{x}}_i\big) - \widehat{\mathbf{s}}_i^{\mathsf{T}} \big(\widehat{\sigma} \widehat{\mathbf{K}}_i + \mathbf{I}\big) \widehat{\mathbf{P}} (\widehat{\mathbf{x}}_j - \widehat{\mathbf{x}}_{jd}) \Big] \\ &+ \sum_{i=l,r} \widehat{\sigma} \widehat{\mathbf{s}}_i^{\mathsf{T}} \widehat{\mathbf{M}}_i \widehat{\mathbf{P}} \big(\dot{\widehat{\mathbf{x}}}_i - \dot{\widehat{\mathbf{x}}}_j\big) + \dot{\widehat{\mathbf{x}}}_i^{\mathsf{T}} \widehat{\mathbf{P}} (\widehat{\mathbf{x}}_i - \widehat{\mathbf{x}}_j) \\ &+ \sum_{i=l,r} \Big[\dot{\mathbf{x}}_i^{\mathsf{T}} \mathbf{P}_i (\mathbf{x}_i - \widehat{\mathbf{x}}_i) + \dot{\widehat{\mathbf{x}}}_i^{\mathsf{T}} \mathbf{P}_i (\widehat{\mathbf{x}}_i - \mathbf{x}_i)\Big] + \mathbf{s}_l^{\mathsf{T}} \mathbf{f}_h + \mathbf{s}_r^{\mathsf{T}} \mathbf{f}_e,\end{aligned} \tag{2.23}$$

where $j = r, l$ for $i = l, r$, respectively. The time derivative of V_2 is bounded by

$$\begin{aligned}\dot{V}_2 \leq &- \gamma V_2 + \sum_{i=l,r} \overline{T}_i \dot{\widehat{\mathbf{x}}}_i^{\mathsf{T}} \mathbf{Q}_i \dot{\widehat{\mathbf{x}}}_i - \sum_{i=l,r} \int_{t-\overline{T}_i}^{t} \exp[-\gamma(t-\theta)] \cdot \dot{\widehat{\mathbf{x}}}_i^{\mathsf{T}}(\theta) \mathbf{Q}_i \dot{\widehat{\mathbf{x}}}_i(\theta) d\theta \\ \leq &- \gamma V_2 + \sum_{i=l,r} \overline{T}_i \dot{\widehat{\mathbf{x}}}_i^{\mathsf{T}} \mathbf{Q}_i \dot{\widehat{\mathbf{x}}}_i - \sum_{i=l,r} \exp(-\gamma \overline{T}_i) \int_{t-T_i(t)}^{t} \dot{\widehat{\mathbf{x}}}_i^{\mathsf{T}}(\theta) \mathbf{Q}_i \dot{\widehat{\mathbf{x}}}_i(\theta) d\theta.\end{aligned} \tag{2.24}$$

By Property 1.3, the definitions of the mismatches $\boldsymbol{\Delta}_i(t)$ in (2.20) further lead to

$$\begin{aligned}\mathbf{s}_i^{\mathsf{T}} \boldsymbol{\Delta}_i(t) \leq &\big|\mathbf{s}_i^{\mathsf{T}} \mathbf{M}_i(\mathbf{x}_i) \big(\dot{\mathbf{x}}_i - \dot{\widehat{\mathbf{x}}}_i\big)\big| + \big|\mathbf{s}_i^{\mathsf{T}} \mathbf{C}_i(\mathbf{x}_i, \dot{\mathbf{x}}_i)(\mathbf{x}_i - \widehat{\mathbf{x}}_i)\big| \\ \leq &\frac{\lambda_{i2}}{2} \big(2\mathbf{s}_i^{\mathsf{T}} \mathbf{s}_i + \dot{\mathbf{x}}_i^{\mathsf{T}} \dot{\mathbf{x}}_i + \dot{\widehat{\mathbf{x}}}_i^{\mathsf{T}} \dot{\widehat{\mathbf{x}}}_i\big) + \frac{c_i}{4} \big(4\|\dot{\mathbf{x}}_i\|^2 \mathbf{s}_i^{\mathsf{T}} \mathbf{s}_i + \|\mathbf{x}_i - \widehat{\mathbf{x}}_i\|^2\big).\end{aligned} \tag{2.25}$$

The sliding variables $\mathbf{s}_i$ designed in (2.19) imply that

$$\begin{aligned}&\dot{\mathbf{x}}_i^{\mathsf{T}} \mathbf{P}_i (\mathbf{x}_i - \widehat{\mathbf{x}}_i) - \mathbf{s}_i^{\mathsf{T}} \mathbf{P}_i (\mathbf{x}_i - \widehat{\mathbf{x}}_i) - \mathbf{s}_i^{\mathsf{T}} \mathbf{D}_i \dot{\mathbf{x}}_i \\ \leq &- \frac{\sigma}{4} (\mathbf{x}_i - \widehat{\mathbf{x}}_i)^{\mathsf{T}} \big(4\mathbf{P}_i - \mu_i \mathbf{D}_i\big)(\mathbf{x}_i - \widehat{\mathbf{x}}_i) - \frac{1}{\mu_i} (\mu_i - \sigma) \dot{\mathbf{x}}_i^{\mathsf{T}} \mathbf{D}_i \dot{\mathbf{x}}_i\end{aligned} \tag{2.26}$$

with $\mu_i > 0$. Similarly, the sliding variables $\widehat{\mathbf{s}}_i$ designed in (2.17) imply that

$$\begin{aligned}&\dot{\widehat{\mathbf{x}}}_i^{\mathsf{T}} \mathbf{P}_i (\widehat{\mathbf{x}}_i - \mathbf{x}_i) - \widehat{\mathbf{s}}_i^{\mathsf{T}} \widehat{\mathbf{e}}_i - \widehat{\mathbf{s}}_i^{\mathsf{T}} \widehat{\mathbf{D}}_i \dot{\widehat{\mathbf{x}}}_i + \dot{\widehat{\mathbf{x}}}_i^{\mathsf{T}} \widehat{\mathbf{P}} (\widehat{\mathbf{x}}_i - \widehat{\mathbf{x}}_j) \\ \leq &- \frac{1}{\nu_i} (\nu_i - \widehat{\sigma}) \dot{\widehat{\mathbf{x}}}_i^{\mathsf{T}} \widehat{\mathbf{D}}_i \dot{\widehat{\mathbf{x}}}_i - \frac{\widehat{\sigma}}{4} \widehat{\mathbf{e}}_i^{\mathsf{T}} \big(4\mathbf{I} - \nu_i \widehat{\mathbf{D}}_i\big) \widehat{\mathbf{e}}_i,\end{aligned} \tag{2.27}$$

$$\begin{aligned}&\widehat{\mathbf{s}}_i^{\mathsf{T}}\widehat{\mathbf{M}}_i\widehat{\mathbf{P}}\big(\dot{\widehat{\mathbf{x}}}_i-\dot{\widehat{\mathbf{x}}}_j\big)+\widehat{\mathbf{s}}_i^{\mathsf{T}}\widehat{\mathbf{M}}_i\mathbf{P}_i\big(\dot{\widehat{\mathbf{x}}}_i-\dot{\mathbf{x}}_i\big)\\ \leq&\zeta_i\widehat{\mathbf{s}}_i^{\mathsf{T}}\big(\widehat{\mathbf{P}}\widehat{\mathbf{P}}+\mathbf{P}_i\mathbf{P}_i\big)\widehat{\mathbf{s}}_i+\frac{\widehat{\lambda}_{i2}^2}{2\zeta_i}\big(2\dot{\widehat{\mathbf{x}}}_i^{\mathsf{T}}\dot{\widehat{\mathbf{x}}}_i+\dot{\widehat{\mathbf{x}}}_j^{\mathsf{T}}\dot{\widehat{\mathbf{x}}}_j+\dot{\mathbf{x}}_i^{\mathsf{T}}\dot{\mathbf{x}}_i\big)\end{aligned}\tag{2.28}$$

with ν_i, ζ_i positive and $\widehat{\lambda}_{i2}\mathbf{I}\succeq\widehat{\mathbf{M}}_i$. Thereafter, Lemma 1 in [85] yields

$$\begin{aligned}&-\widehat{\mathbf{s}}_i^{\mathsf{T}}\big(\widehat{\sigma}\widehat{\mathbf{K}}_i+\mathbf{I}\big)\widehat{\mathbf{P}}\big(\widehat{\mathbf{x}}_j-\widehat{\mathbf{x}}_{jd}\big)-\exp(-\gamma\overline{T}_j)\int_{t-T_j(t)}^{t}\dot{\widehat{\mathbf{x}}}_j^{\mathsf{T}}(\theta)\mathbf{Q}_j\dot{\widehat{\mathbf{x}}}_j(\theta)d\theta\\ \leq&\frac{\overline{T}_j}{4}\exp(-\gamma\overline{T}_j)\cdot\widehat{\mathbf{s}}_i^{\mathsf{T}}\big(\widehat{\sigma}\widehat{\mathbf{K}}_i+\mathbf{I}\big)\widehat{\mathbf{P}}\mathbf{Q}_j^{-1}\widehat{\mathbf{P}}\big(\widehat{\sigma}\widehat{\mathbf{K}}_i+\mathbf{I}\big)\widehat{\mathbf{s}}_i.\end{aligned}\tag{2.29}$$

After substitutions from (2.25)-(2.29) and (2.10), the sum of (2.23) and (2.24) is

$$\begin{aligned}\dot{V}\leq&-\sum_{i=l,r}\Big[\mathbf{s}_i^{\mathsf{T}}\overline{\mathbf{K}}_i(t)\mathbf{s}_i+\widehat{\mathbf{s}}_i^{\mathsf{T}}\widetilde{\mathbf{K}}_i\widehat{\mathbf{s}}_i+\dot{\mathbf{x}}_i^{\mathsf{T}}\overline{\mathbf{D}}_i\dot{\mathbf{x}}_i+\dot{\widehat{\mathbf{x}}}_i^{\mathsf{T}}\widetilde{\mathbf{D}}_i\dot{\widehat{\mathbf{x}}}_i\Big]-\gamma V_2\\ &-\frac{1}{4}\sum_{i=l,r}\Big[4(\mathbf{x}_i-\widehat{\mathbf{x}}_i)^{\mathsf{T}}\overline{\mathbf{P}}_i(\mathbf{x}_i-\widehat{\mathbf{x}}_i)+\widehat{\sigma}\widehat{\mathbf{e}}_i^{\mathsf{T}}\big(4\mathbf{I}-\nu_i\widehat{\mathbf{D}}_i\big)\widehat{\mathbf{e}}_i\Big]+\frac{\|\mathbf{f}_h\|^2+\|\mathbf{f}_e\|^2}{4\omega},\end{aligned}\tag{2.30}$$

where $\chi_{ij}=\sigma\lambda_{i2}+2\widehat{\sigma}\widehat{\lambda}_{i2}^2/\zeta_i+\widehat{\sigma}\widehat{\lambda}_{j2}^2/\zeta_j$ and

$$\begin{aligned}\overline{\mathbf{K}}_i(t)=&\mathbf{K}_i(t)-\big(\sigma\lambda_{i2}+\sigma c_i\|\dot{\mathbf{x}}_i\|^2+\omega_i\big)\mathbf{I},\\ \overline{\mathbf{P}}_i=&\sigma\mathbf{P}_i-(\sigma/4)\big(c_i\mathbf{I}+\mu_i\mathbf{D}_i\big),\\ \overline{\mathbf{D}}_i=&(1-\sigma/\mu_i)\mathbf{D}_i-\big[\sigma\lambda_{i2}/2+\widehat{\sigma}\widehat{\lambda}_{i2}^2/(2\zeta_i)\big]\mathbf{I},\\ \widetilde{\mathbf{K}}_i=&\widehat{\mathbf{K}}_i-\widehat{\sigma}\zeta_i\big(\widehat{\mathbf{P}}\widehat{\mathbf{P}}+\mathbf{P}_i\mathbf{P}_i\big)-e^{\gamma\overline{T}_j}(\overline{T}_j/4)\big(\widehat{\sigma}\widehat{\mathbf{K}}_i+\mathbf{I}\big)\widehat{\mathbf{P}}\mathbf{Q}_j^{-1}\widehat{\mathbf{P}}\big(\widehat{\sigma}\widehat{\mathbf{K}}_i+\mathbf{I}\big),\\ \widetilde{\mathbf{D}}_i=&(1-\widehat{\sigma}/\nu_i)\widehat{\mathbf{D}}_i-\overline{T}_i\mathbf{Q}_i-(\chi_{ij}/2)\mathbf{I}.\end{aligned}$$

Letting $\widetilde{\mathbf{x}}=\big((\mathbf{x}_l-\widehat{\mathbf{x}}_l)^{\mathsf{T}}\ (\mathbf{x}_r-\widehat{\mathbf{x}}_r)^{\mathsf{T}}\ (\widehat{\mathbf{x}}_l-\widehat{\mathbf{x}}_r)^{\mathsf{T}}\big)^{\mathsf{T}}$ and using $\widehat{\mathbf{e}}_i$ in (2.17) lead to

$$\sum_{i=l,r}\Big[4(\mathbf{x}_i-\widehat{\mathbf{x}}_i)^{\mathsf{T}}\overline{\mathbf{P}}_i(\mathbf{x}_i-\widehat{\mathbf{x}}_i)+\widehat{\sigma}\widehat{\mathbf{e}}_i^{\mathsf{T}}\big(4\mathbf{I}-\nu_i\widehat{\mathbf{D}}_i\big)\widehat{\mathbf{e}}_i\Big]=\widetilde{\mathbf{x}}^{\mathsf{T}}\widetilde{\mathbf{P}}\widetilde{\mathbf{x}},\tag{2.31}$$

in which $\widetilde{\mathbf{P}}=[\mathbf{B}_{ij}]$ with the (i,j)-th blocks $\mathbf{B}_{ij}$ defined by $\mathbf{B}_{11}=\mathbf{P}_l\big(4\mathbf{I}-\nu_l\widehat{\mathbf{D}}_l\big)\mathbf{P}_l+4\overline{\mathbf{P}}_l$, $\mathbf{B}_{12}=\mathbf{B}_{21}=\mathbf{0}$, $\mathbf{B}_{13}=\mathbf{B}_{31}=\mathbf{P}_l\big(4\mathbf{I}-\nu_l\widehat{\mathbf{D}}_l\big)\widehat{\mathbf{P}}$, $\mathbf{B}_{22}=\mathbf{P}_r\big(4\mathbf{I}-\nu_r\widehat{\mathbf{D}}_r\big)\mathbf{P}_r+4\overline{\mathbf{P}}_r$, $\mathbf{B}_{23}=\mathbf{B}_{32}=\mathbf{P}_r\big(4\mathbf{I}-\nu_r\widehat{\mathbf{D}}_r\big)\widehat{\mathbf{P}}$ and $\mathbf{B}_{33}=\widehat{\mathbf{P}}\big(8\mathbf{I}-\nu_l\widehat{\mathbf{D}}_l-\nu_r\widehat{\mathbf{D}}_r\big)\widehat{\mathbf{P}}$. The following proposition about $\widetilde{\mathbf{P}}$ contributes to ISS teleoperation in Theorem 2.2.

Proposition 2.1. *Let* $\mathbf{P}_i=\mathbf{P}$, $\widehat{\mathbf{D}}_i=\widehat{\mathbf{D}}$, $\nu_i=\nu$, $\overline{\mathbf{P}}_i\succ\mathbf{0}$, *and* $4\mathbf{I}-\nu\widehat{\mathbf{D}}\succ\mathbf{0}$ *for* $i=l,r$. *Then there exists* $\delta>0$ *such that* $2\widetilde{\mathbf{P}}\succeq\delta\cdot\max\big(\mathbf{P},\widehat{\mathbf{P}}\big)$.

Proof. It suffices to show that $\widetilde{\mathbf{P}} \succ \mathbf{0}$. Using the Schur complement decomposition, $\widetilde{\mathbf{P}} \succ \mathbf{0}$ if and only if $\mathbf{B}_{33} \succ \mathbf{0}$ and

$$\begin{bmatrix} \mathbf{B}_{11} & \mathbf{0} \\ \mathbf{0} & \mathbf{B}_{22} \end{bmatrix} - \begin{bmatrix} \mathbf{B}_{13} \\ \mathbf{B}_{23} \end{bmatrix} \mathbf{B}_{33}^{-1} \begin{bmatrix} \mathbf{B}_{13}^{\mathsf{T}} \ \mathbf{B}_{23}^{\mathsf{T}} \end{bmatrix} \succ \mathbf{0}.$$

From Equations (2.30)-(2.31), it follows that $\mathbf{B}_{33} \succ \mathbf{0}$, that

$$\begin{bmatrix} \mathbf{B}_{13} \\ \mathbf{B}_{23} \end{bmatrix} \mathbf{B}_{33}^{-1} \begin{bmatrix} \mathbf{B}_{13}^{\mathsf{T}} \ \mathbf{B}_{23}^{\mathsf{T}} \end{bmatrix} = \frac{1}{8} \begin{bmatrix} 1 & 1 \\ 1 & 1 \end{bmatrix} \otimes \left[\big(4\mathbf{I} - \upsilon \widehat{\mathbf{D}}\big) \mathbf{P}^2 \right],$$

and, further that

$$\begin{bmatrix} \mathbf{B}_{11} & \mathbf{0} \\ \mathbf{0} & \mathbf{B}_{22} \end{bmatrix} - \begin{bmatrix} \mathbf{B}_{13} \\ \mathbf{B}_{23} \end{bmatrix} \mathbf{B}_{33}^{-1} \begin{bmatrix} \mathbf{B}_{13}^{\mathsf{T}} \ \mathbf{B}_{23}^{\mathsf{T}} \end{bmatrix} = \begin{bmatrix} \overline{\mathbf{P}}_l & \mathbf{0} \\ \mathbf{0} & \overline{\mathbf{P}}_r \end{bmatrix} + \frac{1}{8} \begin{bmatrix} 1 & -1 \\ -1 & 1 \end{bmatrix} \otimes \left[\big(4\mathbf{I} - \upsilon \widehat{\mathbf{D}}\big) \mathbf{P}^2 \right]$$

is positive definite. ■

Theorem 2.2. *The teleoperator* (2.1) *in closed-loop with the proxies* (2.16) *and the control* (2.21) *is ISS with the input* $\mathbf{u} = \big(\mathbf{f}_h^{\mathsf{T}} \ \mathbf{f}_e^{\mathsf{T}}\big)^{\mathsf{T}}$ *and the state* $\mathbf{x} = \big(\dot{\mathbf{x}}_l^{\mathsf{T}} \ \dot{\mathbf{x}}_r^{\mathsf{T}} \ \dot{\widehat{\mathbf{x}}}_l^{\mathsf{T}} \ \dot{\widehat{\mathbf{x}}}_r^{\mathsf{T}} \ (\mathbf{x}_l - \widehat{\mathbf{x}}_l)^{\mathsf{T}} \ (\mathbf{x}_r - \widehat{\mathbf{x}}_r)^{\mathsf{T}} \ (\widehat{\mathbf{x}}_l - \widehat{\mathbf{x}}_r)^{\mathsf{T}}\big)^{\mathsf{T}}$ *if the parameters and control gains satisfy the conditions in Proposition 2.1 and*

$$2\overline{\mathbf{K}}_i(t) \succeq \psi \lambda_{i2} \mathbf{I}, \quad 2\widetilde{\mathbf{K}}_i \succeq \psi \widehat{\lambda}_{i2} \mathbf{I}, \quad \overline{\mathbf{D}}_i \succeq \mathbf{0}, \quad \widetilde{\mathbf{D}}_i \succeq \mathbf{0}, \tag{2.32}$$

where $i = l, r$ *and* $\psi > 0$.

Proof. The definitions of $\widehat{\mathbf{s}}_i$ and $\mathbf{s}_i$, $i = l, r$, imply that $\|\dot{\widehat{\mathbf{x}}}_i\|^2 \leq 2\|\widehat{\mathbf{s}}_i\|^2 + 2\widehat{\sigma}^2 \|\widehat{\mathbf{e}}_i\|^2$, $\|\widehat{\mathbf{s}}_i\|^2 \leq 2\|\dot{\widehat{\mathbf{x}}}_i\|^2 + 2\widehat{\sigma}^2 \|\widehat{\mathbf{e}}_i\|^2$, $\|\dot{\mathbf{x}}_i\|^2 \leq 2\|\mathbf{s}_i\|^2 + 2\sigma^2 \|\mathbf{x}_i - \widehat{\mathbf{x}}_i\|^2$ and $\|\mathbf{s}_i\|^2 \leq 2\|\dot{\mathbf{x}}_i\|^2 + 2\sigma^2 \|\mathbf{x}_i - \widehat{\mathbf{x}}_i\|^2$. Given that $V_2 \geq 0$, $p\mathbf{I} \preceq \mathbf{P} \preceq P\mathbf{I}$ and $\widehat{p}\mathbf{I} \preceq \widehat{\mathbf{P}} \preceq \widehat{P}\mathbf{I}$, it follows that $\|\widehat{\mathbf{e}}_i\|^2 \leq 2P^2 \|\mathbf{x}_i - \widehat{\mathbf{x}}_i\|^2 + 2\widehat{P}^2 \|\widehat{\mathbf{x}}_l - \widehat{\mathbf{x}}_r\|$, and thus that the Lyapunov candidate V can be lower-bounded by

$$V \geq \frac{1}{2} \sum_{i=l,r} \big(\lambda_{i1} \|\mathbf{s}_i\|^2 + \widehat{\lambda}_{i1} \|\widehat{\mathbf{s}}_i\|^2 + p \|\mathbf{q}_i - \widehat{\mathbf{q}}_i\|^2 \big) + \frac{\widehat{p}}{2} \|\widehat{\mathbf{q}}_l - \widehat{\mathbf{q}}_r\|^2 \geq \widehat{\alpha}_3(\|\mathbf{x}\|), \tag{2.33}$$

where $\lambda_{i1} \preceq \mathbf{M}_i(\mathbf{x}_i)$, $\widehat{\lambda}_{i1}\mathbf{I} \preceq \widehat{\mathbf{M}}_i$, and $\widehat{\alpha}_3(\|\mathbf{x}\|) = a_3 \|\mathbf{x}\|^2$ is a function of class $\mathcal{K}_\infty$ with

$$\frac{1}{a_3} = \frac{4}{\lambda_{l1}} + \frac{4}{\widehat{\lambda}_{l1}} + \frac{4}{\lambda_{r1}} + \frac{4}{\widehat{\lambda}_{r1}} + \frac{4\sigma^2 + 8\widehat{\sigma}^2 P^2}{p} + \frac{16\widehat{\sigma}^2 \widehat{P}^2}{\widehat{p}}.$$

Further, the definition of V_2 indicates that

$$V_2 \leq \sum_{i=l,r} Q_i |\dot{\widehat{\mathbf{x}}}_i|^2_{\overline{T}_i} \int_{-\overline{T}_i}^{0} \int_{t+\tau}^{t} \exp[-\gamma(t-\theta)] d\theta d\tau \leq \frac{1}{2} \sum_{i=l,r} \overline{T}_i^2 Q_i |\dot{\widehat{\mathbf{x}}}_i|^2_{\overline{T}_i}, \tag{2.34}$$

where $Q_i \mathbf{I} \succeq \mathbf{Q}_i$. Then V can be upper-bounded by

$$V \leq \frac{1}{2} \sum_{i=l,r} \left(\lambda_{i2} \|\mathbf{s}_i\|^2 + \widehat{\lambda}_{i2} \|\widehat{\mathbf{s}}_i\|^2 + P \|\mathbf{x}_i - \widehat{\mathbf{x}}_i\|^2 \right) + \frac{\widehat{P}}{2} \|\widehat{\mathbf{x}}_l - \widehat{\mathbf{x}}_r\|^2 + V_2 \leq \widehat{\alpha}_4(|\mathbf{x}|_{\overline{T}}), \tag{2.35}$$

where $\lambda_{i2} \mathbf{I} \succeq \mathbf{M}_i(\mathbf{x}_i)$, $\widehat{\lambda}_{i2} \succeq \widehat{\mathbf{M}}_i$, $\widehat{\alpha}_4(|\mathbf{x}|_{\overline{T}}) = (a_4/2)|\mathbf{x}|^2_{\overline{T}}$ with

$$a_4 = \max_{i=l,r} \left[\max \left(2\lambda_{i2}, 2\widehat{\lambda}_{i2} + \overline{T}_i^2 \overline{Q}_i, 4\widehat{\lambda}_{i2} \widehat{\sigma}^2 \widehat{P}^2 + \widehat{P}, 2\lambda_{i2}\sigma^2 + 4\widehat{\lambda}_{i2} \widehat{\sigma}^2 P^2 + P \right) \right]$$

Let $\gamma_a = \sqrt{a_3}$ and $\overline{\gamma}_a = \sqrt{a_4}$, define $|\mathbf{x}_t|_a = \sqrt{V(\mathbf{x}_t)}$, and select $\alpha_1(\|\mathbf{x}\|) = \widehat{\alpha}_3(\|\mathbf{x}\|)$ and $\alpha_2(|\mathbf{x}_t|_a) = |\mathbf{x}_t|_a^2$ of class $\mathcal{K}_\infty$ to trivially ensure the condition (a) of Theorem 1.2.

After the substitution from (2.31) in (2.30), using the condition (2.32) and setting $\kappa = \min(\psi, \delta, \gamma)$, $\dot{V}$ can be upper-bounded by

$$\dot{V} \leq -\kappa V + \frac{\|\mathbf{u}\|^2}{4\omega}. \tag{2.36}$$

Then the functions $\alpha_3(|\mathbf{x}_t|_a) = (\kappa/2)|\mathbf{x}_t|_a^2$ and $\rho(\|\mathbf{u}\|) = \sqrt{1/(2\kappa\omega)}\|\mathbf{u}\|$ of class $\mathcal{K}$ ensure the condition (b) of Theorem 1.2.

Thus, the Lyapunov candidate V obeys both conditions of Theorem 1.2 and the teleoperator (2.1) in closed-loop with the proxies (2.16) and the control (2.21) is exponentially ISS. ■

Corollary 2.2. *Let* $d_I = 4V(0)/p' + \overline{f}^2/(p'\kappa\omega)$ *and* $d_A = \overline{f}^2/(p'\kappa\omega)$ *with* $\overline{f}^2 = \overline{f}_h^2 + \overline{f}_e^2$ *and* $p' = \min(p_l, p_r, \widehat{p})$. *ISS teleoperation renders the set* $\mathcal{S}_I = \left\{ \mathbf{x}_l - \mathbf{x}_r \in \mathbb{R}^n \mid \|\mathbf{x}_l - \mathbf{x}_r\|^2 \leq d_I \right\}$ *invariant and the set* $\mathcal{S}_A = \left\{ \mathbf{x}_l - \mathbf{x}_r \in \mathbb{R}^n \mid \|\mathbf{x}_l - \mathbf{x}_r\|^2 \leq d_A \right\}$ *globally attractive.*

Proof. Applying Grönwall's inequality to the time integration of (2.36) leads to

$$V(t) \leq \exp(-\kappa t) \cdot V(0) + \frac{\overline{f}^2}{4\kappa\omega},$$

while the definition of V implies that

$$V \geq \sum_{i=l,r} \frac{p_i}{2}\|\mathbf{x}_i - \widehat{\mathbf{x}}_i\|^2 + \frac{\widehat{p}}{2}\|\widehat{\mathbf{x}}_l - \widehat{\mathbf{x}}_r\|^2 \geq \frac{p'}{4}\|\mathbf{x}_l - \mathbf{x}_r\|^2,$$

and completes the proof. ■

2.1.3 Discussion

Closed-loop bilateral teleoperation includes uncertain and practically uncontrollable user and environment dynamics. To robustly stabilize closed-loop teleoperation, this chapter regards the user and environment forces as time-varying and unpredictable teleoperator inputs, and designs controllers to render the teleoperator ISS. It guarantees robust position synchronization of the local and remote robots under the user and environment perturbations [172], and thus, reflects the remote robot-environment interaction to the operator [78]. According to Definition 1.5, ISS teleoperation implies: (i) $\{\dot{\mathbf{x}}_l, \dot{\mathbf{x}}_r, \mathbf{x}_l - \mathbf{x}_r\} \in \mathcal{L}_\infty$; and (ii) $\{\dot{\mathbf{x}}_l, \dot{\mathbf{x}}_r, \mathbf{x}_l - \mathbf{x}_r\} \to \mathbf{0}$ if $\mathbf{f}_h = \mathbf{f}_e = \mathbf{0}$.

By Corollary 2.1 and Corollary 2.2, an invariant set $\mathcal{S}_I$ and a globally attractive set $\mathcal{S}_A$ characterize the local robot-remote robot position error $\mathbf{x}_l(t) - \mathbf{x}_r(t)$ of ISS teleoperation: the error stays in $\mathcal{S}_I$ and exponentially approaches $\mathcal{S}_A$ for $t \geq 0$. The Lebesgue measures of $\mathcal{S}_I$ and $\mathcal{S}_A$ can be reduced by increasing p_i, $\widehat{p}$, ω and κ. The speed of (exponential) convergence to $\mathcal{S}_A$ is determined by κ. When the user and environment forces disappear, the steady-state position error becomes zero by the definition of input-to-state stability.

2.2 Experiments

In this section, four experiments[1] with a pair of 3-DOF Geomagic Touch haptic devices displayed in Figure 2.3 compare the dynamic interconnection and damping injection strategy to three position-based approaches: P+d control [84], two-layer control [77] and passive set-position modulation control [74]. The human user seeks to drive the local robot along the same Cartesian path in each successive experiment. The time-varying communication delays obey $\overline{T}_i = 5$ ms with $i = l, r$. The robust position tracking performance of the teleoperator with the four controllers is illustrated

[1] `https://youtu.be/xBXDh5BX3uY`

by plotting the Cartesian paths of the local and remote robot end-effectors, and is quantitatively evaluated through their maximum and average position errors.

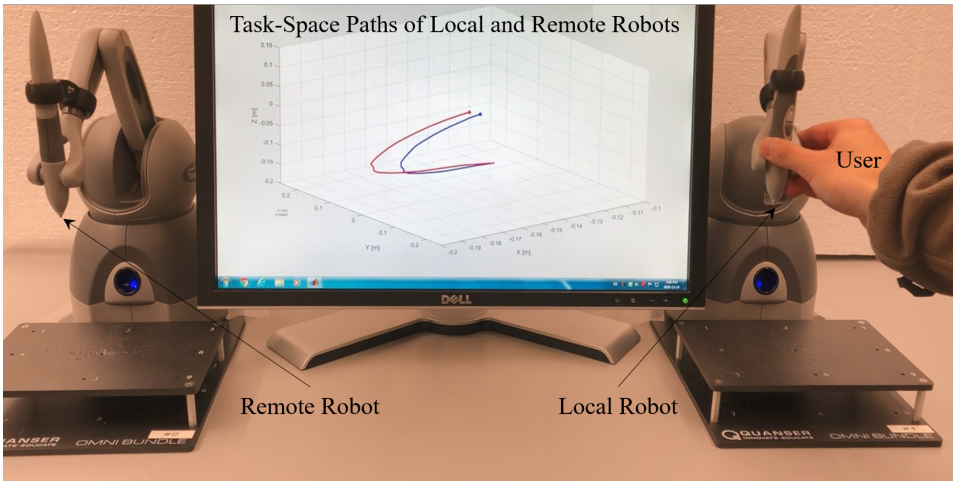

Figure 2.3: The experimental setup for ISS teleoperation with time-varying delays.

All parameters are selected heuristically for optimal performance of each controller. All controllers connect the local and remote robots by Proportional control and stabilize the teleoperator by local damping injection. The robot joint positions are measured by encoders, and their joint velocities are estimated by second-order low-pass filters with the recommended cut-off frequency 200 rad/s and damping ratio 1. The damping injection for all four controllers is then restricted by the unreliable velocity estimation in experiments. In turn, the limited damping injection constrains the Proportional gain of each controller by their design criteria. Because larger Proportional gains generally decrease position errors, the parameters of all controllers are tuned to maximize their Proportional gains for the damping gains that practically stabilizes the system. Basically, the coupling between the local and remote robots of each controller is maximally tightened without destabilizing the teleoperation experiments.

P+d Control [84]

After choosing the damping gain $B_i = 0.01$, a maximum Proportional gain $K_i = 3.5$ can couple the local and remote robots stably. Figure 2.4(a) depicts the paths of the local and remote robot end-effectors. It shows that the remote robot follows the local robot with increasing tracking errors and vibrations during the changes of the direction of motion.

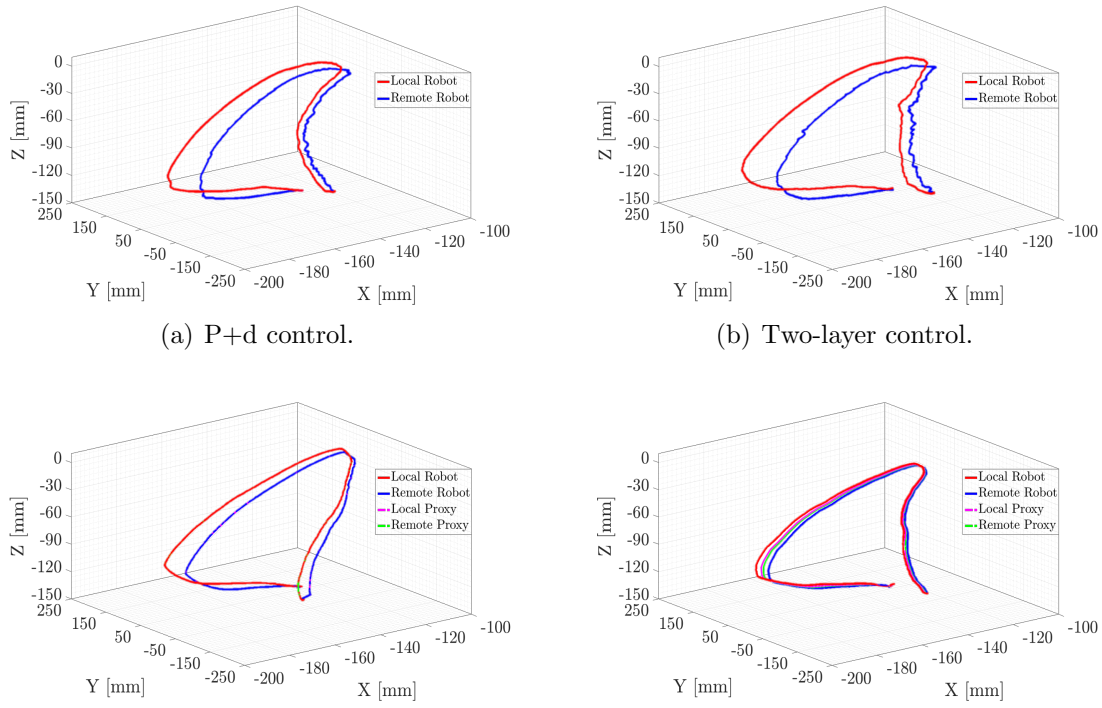

(a) P+d control.

(b) Two-layer control.

(c) Passive set-position modulation control.

(d) The proposed control (2.16) and (2.21).

Figure 2.4: The task-space paths of the local and remote robot end-effectors under P+d control, two-layer control, passive set-position modulation control and the proposed control (2.16) and (2.21).

Two-Layer Control [77]

Selecting an identical threshold $H_D = 0.3$ J and $\beta = 0.01$ for the energy tanks of the local and remote robots firstly synchronizes them quickly. Then, a Proportional gain $K_i = 3$ in the transparency layer and a nonlinear local robot damper with $\alpha = 0.3$ in the passivity layer maximally stiffen the coupling between the local and remote robots without destabilizing the teleoperator. The experimental end-effector paths in Figure 2.4(b) indicate a position tracking performance similar to P+d control. Yet, the momentarily active behaviours lead to more severe vibrations in the final phase of this experiment.

Passive Set-Position Modulation Control [74]

For an energy tank with the capacity $\overline{E}_i = 0.3$ J and the initially stored energy $E_i(0) = 0.15$ J, the coupling and damping gains $K_i = 5$ and $B_i = 0.1$, respectively, guarantee agile and oscillation-free position tracking. The experimental

results in Figure 2.4(c) show that the set-position (proxy) of each robot is exactly the position of the other robot. The controller does not modulate the reference signal of either robot, but is a static P+d controller during the experiment. Nevertheless, its triggering mechanism with a time period of 0.01 s permits larger K_i and B_i gains than P+d control and, hence, couples the local and remote robots tighter.

The Proposed Control (2.16) **and** (2.21)

From the EL model of the haptic device in [173], $\lambda_{i2} = 1.6$ and $c_i = 0.1$ are employed in the design. After choosing $\sigma = 0.01$, $\widehat{\sigma} = 0.001$, $\mu_i = 10$ and $\zeta_i = 0.1$, each robot is connected to its proxy tightly and damped suitably while guaranteeing $\overline{\mathbf{P}}_i \succ \mathbf{0}$ and $\overline{\mathbf{D}}_i \succeq \mathbf{0}$ by setting $\mathbf{D}_i = 0.08\mathbf{I}$ and $\mathbf{P}_i = 20\mathbf{I}$. With $\nu_i = 0.25$, $\psi = 0.001$, $\gamma = 0.1$, $\widehat{\mathbf{M}}_i = 0.01\mathbf{I}$ and $\mathbf{Q}_i = 50\mathbf{I}$, selecting $\widehat{\mathbf{P}}_i = 50\mathbf{I}$, $\widehat{\mathbf{D}}_i = 0.275\mathbf{I}$ and $\widehat{\mathbf{K}}_i = 0.01\mathbf{I}$ then makes $\widetilde{\mathbf{K}}_i \succeq (\psi\widehat{\lambda}_{i2}/2)\mathbf{I}$ and $\widetilde{\mathbf{D}}_i \succeq \mathbf{0}$ and connects the proxies of the local and remote robots tightly. Given $\omega_i = 0.01$, $\mathbf{K}_i(t)$ can be updated according to (2.32) to stabilize the teleoperator. Figure 2.4(d), which plots the experimental paths of the local and remote robot end-effectors and of their proxies, indicates that: (i) compared to P+d (Figure 2.4(a)) and two-layer (Figure 2.4(b)) control, the proposed dynamic interconnection and damping injection control eliminates vibrations when the local robot slows down; and (ii) compared to passive set-position modulation control (Figure 2.4(c)), it synchronizes the local and remote robots better, through larger static Proportional gains $\mathbf{P}_i$, $\widehat{\mathbf{P}}_i$ and $\widehat{\mathbf{K}}_i$ and dynamically updated gains $\mathbf{K}_i(t)$.

Table 2.1 evaluates the robust position tracking performance of the time-delay teleoperator under the four controllers through the maximum tracking error:

$$\Xi_{\max} = \max_{k=1,\cdots,N} \|\mathbf{x}_l^t(k) - \mathbf{x}_r^t(k)\|,$$

and the average tracking error:

$$\Xi_{\text{ave}} = \frac{1}{N}\sum_{k=1}^{N} \|\mathbf{x}_l^t(k) - \mathbf{x}_r^t(k)\|,$$

where $\mathbf{x}_i^t(k)$ is the end-effector position of the robot indexed by i in its task space at the k-th sampling instant, and N is the number of sampling instants. It illustrates that the proposed dynamic interconnection and damping injection control can reduce both the maximum and the average position errors between the local and remote robots during the experiments. By Corollary 2.2, the position error between the local and

remote robots can be reduced by increasing the Proportional gains. Then, a greater amount of physical damping injection is needed to practically stabilize the system. However, the unreliable velocity estimations limit the amount of injected damping and hence the coupling stiffness between the local and remote robots by Theorem 2.2. Therefore, the average position error Ξ_{ave} remains 1.8 mm even though the parameters of the proposed control have been opportunely tuned in the experiment.

Table 2.1: The position tracking errors during teleoperation under four controllers.

Controller	Ξ_{max}	Ξ_{ave}
P+d Control	25.4 mm	3.3 mm
Two-Layer Control	30.1 mm	3.6 mm
Passive Set-Position Modulation Control	18.5 mm	2.6 mm
The Proposed Control (2.16) (2.21)	10.8 mm	1.8 mm

The proposed dynamic interconnection and damping injection control has force feedback performance similar to passive set-position modulation control, and has the average and maximum local robot control forces approximately 40% larger than P+d and two-layer control. The larger forces incured by the larger damping injection are needed to stabilize the stiffer interconnection between the local and remote robots.

2.3 Conclusion

This chapter has presented a constructive dynamic interconnection and damping injection strategy for robust stabilization of bilateral teleoperation without, and with, time-varying delays. Lyapunov stability analysis has proven that the proposed strategy renders bilateral teleoperation exponentially ISS, even in the presence of time-varying delays. Using an invariant set and a globally attractive set, it has also characterized the position error between the local and remote robots during teleoperation under the proposed control. Suitable selection and update of the control gains can reduce the position error between the local and remote robots to any prescribed level with a certain rate of convergence and, thus, can improve the robust position tracking performance. The experiments have illustrated that, compared to state-of-the-art controllers, the proposed control can reduce both the maximum and the average position tracking errors during teleoperation with time-varying delays.

Chapter 3

Connectivity-Preserving Synchronization of Time-Delay Robot Networks with Bounded Actuation

This chapter proposes a strategy to overcome the threats posed to connectivity-preserving synchronization of robot networks by time-varying delays and bounded actuation. It first introduces a suitable distributed gradient plus damping control, based on which it establishes that the local connectivity of time-delay robot networks can be preserved by appropriately regulating the interconnections between robots and increasing their local damping injection. Yet, actuator saturation may impede the proper modulation of inter-robot connections and the injection of sufficient damping and, thus, may threaten the maintenance of connectivity. The chapter then develops an indirect coupling control which accommodates bounded robot actuation. The design endows every robot with a virtual proxy and couples initially adjacent robots through their virtual proxies. The inter-proxy couplings then tackle time-varying delays and robot-proxy couplings account for the saturation of actuators. By Lyapunov-Krasovskii analysis, it proves that the indirect coupling strategy can drive time-delay robot networks with bounded actuation to connectivity-preserving synchronization by limiting the energy of the robot-proxy and inter-proxy couplings according to actuation constraints. Three experiments validate the proposed designs compared to P+d control [174].

3.1 Connectivity-Preserving Controller Designs

This section first develops a gradient plus damping control for connectivity-preserving synchronization of time-delay robot networks with unbounded actuation. Then, it integrates the gradient-based control into an indirect coupling framework that provably copes with saturating actuators.

Consider a network of N robots with EL dynamics:

$$\mathbf{M}_i(\mathbf{x}_i)\ddot{\mathbf{x}}_i + \mathbf{C}_i(\mathbf{x}_i, \dot{\mathbf{x}}_i)\dot{\mathbf{x}}_i = \mathbf{f}_i, \tag{3.1}$$

where $i = 1, \cdots, N$ are indices of robots. Further, consider that each robot of (3.1) can both send and receive information from other robots that are closer than the distance r from it. The robots i and j are called adjacent, or neighbours, at time t if they exchange information at all times until t. Note that, to be adjacent at time t, the robots i and j must have been within the communication distance r of each other, and thus neighbours, at all times, i.e., $\|\mathbf{x}_{ij}(\tau)\| = \|\mathbf{x}_i(\tau) - \mathbf{x}_j(\tau)\| < r$, $\forall \tau \in [0, t]$. The communication graph $\mathcal{G}(t) = \{\mathcal{V}, \mathcal{E}(t)\}$ of the robot network (3.1) consists of a set of vertices $\mathcal{V} = \{1, \cdots, N\}$, each associated with one robot in the network, and a set of communication edges $\mathcal{E}(t) = \big\{(i, j) \in \mathcal{V} \times \mathcal{V} \;\big|\; \|\mathbf{x}_{ij}(\tau)\| < r \;\forall \tau \in [0, t]\big\}$, each associated with a communication link in the network.

In [98], the connectivity-preserving synchronization of delay-free EL networks has been formulated as follows:

Definition 3.1. *For the robot network* (3.1)*, find a distributed control such that: (1)* $\|\mathbf{x}_{ij}(t)\| < r$*,* $\forall t \geq 0$ *and* $\forall (i, j) \in \mathcal{E}(0)$*; and (2)* $\|\mathbf{x}_{ij}(t)\| \to 0$ *as* $t \to \infty$ $\forall (i, j) \in \mathcal{E}(0)$*.*

A connected communication graph is sufficient for synchronizing an EL network. In practical applications in which robots can exchange information only when they are sufficiently close to each other, graph edges and, with them, graph connectivity may be destroyed during control. Then, the synchronization task may fail due to the disconnection of the communication graph. The threat posed to synchronization by a limited inter-robot communication distance r can be overcome by preserving local connectivity during synchronization, i.e., by guaranteeing $\mathcal{E}(t) = \mathcal{E}(0)$, $\forall t \geq 0$. In the absence of communication delays, all initial edges of the communication graph are maintained at all times iff all pairs of initially adjacent robots are kept within their communication distance r at all times, i.e., iff $\|\mathbf{x}_{ij}(t)\| < r$, $\forall (i, j) \in \mathcal{E}(0)$ and $\forall t \geq 0$. Compared to conventional consensus, in Definition 3.1, the connectivity-

preserving synchronization problem imposes an additional constraint (1) on the inter-robot distances $\|\mathbf{x}_{ij}(t)\|$.

To preserve the connectivity of the robot network (3.1) in the presence of time-varying communication delays and bounded actuation, this chapter relies on the following three assumptions.

Assumption 3.1. *The transmission of information from the robot i to the robot j is affected by the time-varying delay $T_{ij}(t)$ upper-bounded by $T_{ij}(t) \leq \overline{T}_{ij}$, for any $i, j \in \mathcal{V}$.*

Assumption 3.2. *Initially, every robot i of the network* (3.1) *is at rest, and has been at rest longer than the maximum transmission delay from it to its neighbours j, i.e., $\dot{\mathbf{x}}_i(\tau) = \mathbf{0}$, $\forall \tau \in \left[-\overline{T}_i, 0\right]$ and $\forall i \in \mathcal{V}$, where $\overline{T}_i = \max_{(i,j)\in\mathcal{E}(0)} \overline{T}_{ij}$.*

Assumption 3.3. *The initial communication graph of the network* (3.1) *is undirected and connected, and each pair of initially adjacent robots (i, j) is strictly within their communication distance r at $t = 0$, i.e., $\|\mathbf{x}_{ij}(0)\| = \|\mathbf{x}_{ji}(0)\| < r - \epsilon$ for some $\epsilon > 0$ if $(i, j) \in \mathcal{E}(0)$.*

3.1.1 Time-Delay Network With Unbounded Actuation

Let the following potential function describe the energy stored in each initial communication link $(i, j) \in \mathcal{E}(0)$ at time t:

$$\psi(\|\mathbf{x}_{ij}\|) = \frac{P\|\mathbf{x}_{ij}\|^2}{r^2 - \|\mathbf{x}_{ij}\|^2 + Q}, \tag{3.2}$$

where $P > 0$ and $Q > 0$ are to be determined, and $\|\mathbf{x}_{ij}\|$ is used in place of $\|\mathbf{x}_{ij}(t)\|$ to simplify notation. Then, let the connectivity-preserving control of the robot i be

$$\mathbf{f}_i = -\sum_{j\in\mathcal{N}_i} \nabla_i \psi(\|\mathbf{x}_{ij}^d\|) - K_i \dot{\mathbf{x}}_i, \tag{3.3}$$

where $K_i > 0$, $\mathbf{x}_{ij}^d = \mathbf{x}_i - \mathbf{x}_{jd}$ with $\mathbf{x}_{jd} = \mathbf{x}_j(t - T_{ji}(t))$ the delayed data received by the robot i from the robot j, and

$$\nabla_i \psi(\|\mathbf{x}_{ij}^d\|) = \frac{2P(r^2 + Q)}{\left(r^2 - \|\mathbf{x}_{ij}^d\|^2 + Q\right)^2} (\mathbf{x}_i - \mathbf{x}_{jd})$$

is the gradient of $\psi(\|\mathbf{x}_{ij}^d\|)$ with respect to $\mathbf{x}_i$.

The potential function $\psi(\|\mathbf{x}_{ij}\|)$ in (3.2) is continuous, positive definite and strictly increasing with respect to $\|\mathbf{x}_{ij}\| \in [0, r]$. Using Assumption 3.3, $\|\mathbf{x}_{ij}(0)\| < r - \epsilon < r$ for every $(i, j) \in \mathcal{E}(0)$, it can be shown that the controller (3.3) can be designed to guarantee $\psi(\|\mathbf{x}_{ij}(t)\|) < \psi(r) = Pr^2/Q$, $\forall t \geq 0$. In turn, this condition implies that the robots i and j are within the communication distance r of each other at all times in the absence of time-varying transmission delays [98].

For delay-free communications, $\|\mathbf{x}_{ij}(t)\| < r$ for all $t \geq 0$ is a sufficient condition for preserving the undirected communication link between the robots i and j during synchronization, i.e., $(i, j) \in \mathcal{E}(0) \Rightarrow (i, j) \in \mathcal{E}(t)$, $\forall t \geq 0$. For delayed communications, at time t, the robot i receives the information sent by the robot j at time $t - T_{ji}(t)$ and the robot j receives the information sent by the robot i at time $t - T_{ij}(t)$. The undirected communication link between the robots i and j exists at time t, i.e., $(i, j) \in \mathcal{E}(t)$, iff $\|\mathbf{x}_i(t) - \mathbf{x}_j(t - T_{ji}(t))\| \leq r$ and $\|\mathbf{x}_j(t) - \mathbf{x}_i(t - T_{ij}(t))\| \leq r$. To account for bounded time-varying communication delays, this chapter defines the set of neighbours of the robot i at time t by $\mathcal{N}_i = \{j \in \mathcal{V} \mid (i, j) \in \mathcal{E}(0) \text{ and } |\mathbf{x}_{ij}|_T < r\}$, where

$$|\mathbf{x}_{ij}|_T = \sup_{-\overline{T}_{ji} \leq \tau \leq 0} \|\mathbf{x}_i(t) - \mathbf{x}_j(t + \tau)\|.$$

Connectivity-preserving synchronization can then be analyzed using the following Lyapunov candidate:

$$V = V_k + V_p + \omega V_d, \tag{3.4}$$

where $\omega > 0$, and

$$\begin{aligned}
V_k =& \frac{1}{2} \sum_{i=1}^{N} \dot{\mathbf{x}}_i^{\mathsf{T}} \mathbf{M}_i(\mathbf{x}_i) \dot{\mathbf{x}}_i, \\
V_p =& \frac{1}{2} \sum_{i=1}^{N} \sum_{j \in \mathcal{N}_i(0)} \psi(\|\mathbf{x}_{ij}\|), \\
V_d =& \sum_{i=1}^{N} \sum_{j \in \mathcal{N}_i(0)} \overline{T}_{ji} \int_{t - \overline{T}_{ji}}^{t} \|\dot{\mathbf{x}}_j(\theta)\|^2 d\theta.
\end{aligned}$$

with $j \in \mathcal{N}_i(0)$ if and only if $(i, j) \in \mathcal{E}(0)$ by Assumptions 3.2-3.3. In Equation (3.4), V_k is the kinetic energy of the robot network; V_p is the potential energy of all initial

inter-robot links $(i,j) \in \mathcal{E}(0)$; and V_d measures the impact of time-varying delays on connectivity maintenance.

The analysis is facilitated by the following lemma.

Lemma 3.1. *Let the robot network* (3.1) *satisfy Assumptions 3.1 and 3.3, let* $\overline{r} = r - \kappa\epsilon$ *with* $0 < \kappa < 1$, *and select* P, Q *and* ω *by* $[\overline{r}^2 - M(r-\epsilon)^2]\,Q \geq [\overline{r}^2 + M(r-\overline{r})^2]\,(r-\epsilon)^2 - \overline{r}^2 r^2$, *where* $M = |\mathcal{E}(0)|$ *is the size of* $\mathcal{G}(0)$, *and by* $\omega \geq P\overline{r}^2/[\kappa^2\epsilon^2(r^2-\overline{r}^2+Q)]$. *If* $V(\tau) \leq V(0)$, $\forall \tau \in [0,t]$, *then* $|\mathbf{x}_{ij}|_T < r$ *and thus* $\|\mathbf{x}_{ij}^d\| < r$, $\forall (i,j) \in \mathcal{E}(0)$, *namely, all initial links are preserved regardless of communication delays.*

Proof. Assumption 3.2 on zero initial velocities of the network implies that $V_k(0) = V_d(0) = 0$, and thus $V(0) = V_p(0)$. Choosing Q as required leads to $V_p(0) < MP(r-\epsilon)^2/[r^2-(r-\epsilon)^2+Q] \leq P\overline{r}^2/(r^2-\overline{r}^2+Q)$. Because V_k and V_d are non-negative, it follows that $V_p(\tau) \leq V(\tau)$ for every $\tau \in [0,t]$. Therefore, if $V(\tau) \leq V(0)$, then $V_p(\tau) \leq V(\tau) \leq V(0) = V_p(0) < P\overline{r}^2/(r^2-\overline{r}^2+Q)$.

From $\psi(\|\mathbf{x}_{ij}\|)$ continuous, positive definite and strictly increasing on $\|\mathbf{x}_{ij}\| \in [0,r]$, it follows that $0 \leq \psi(\|\mathbf{x}_{ij}(0)\|) < P(r-\epsilon)^2/[r^2-(r-\epsilon)^2+Q] < P\overline{r}^2/(r^2-\overline{r}^2+Q)$ by Assumption 3.3 and the definition of $\psi(\|\mathbf{x}_{ij}\|)$ in (3.2). Suppose that, at time t, the link with maximal length among all initial links is (l,m) with $\|\mathbf{x}_{lm}(t)\| = \overline{r}$. It follows then that $\psi(\|\mathbf{x}_{lm}(t)\|) = P\overline{r}^2/(r^2-\overline{r}^2+Q)$. Since $\|\mathbf{x}_{ij}(t)\| \leq \|\mathbf{x}_{lm}(t)\|$, $\forall (i,j) \in \mathcal{E}(0) - \{(l,m)\}$, it further follows that $0 \leq \psi(\|\mathbf{x}_{ij}(t)\|) \leq P\overline{r}^2/(r^2-\overline{r}^2+Q)$, $\forall (i,j) \in \mathcal{E}(0) - \{(l,m)\}$, and that $V_p(t) \geq P\overline{r}^2/(r^2-\overline{r}^2+Q)$, which contradicts (3.11). Thus, $0 \leq \psi(\|\mathbf{x}_{ij}(t)\|) \leq V_p(t) < P\overline{r}^2/(r^2-\overline{r}^2+Q)$, $\forall (i,j) \in \mathcal{E}(0)$, and further that $\|\mathbf{x}_{ij}(t)\| < \overline{r}$, $\forall (i,j) \in \mathcal{E}(0)$.

The application of the Cauchy-Schwarz inequality leads to

$$\begin{aligned}
&\int_{t-\overline{T}_{ji}}^{t} \|\dot{\mathbf{x}}_j(\theta)\|^2 d\theta = \sum_{k=1}^{n} \int_{t-\overline{T}_{ji}}^{t} |\dot{x}_j^k(\theta)|^2 d\theta = \frac{1}{\overline{T}_{ji}} \sum_{k=1}^{n} \int_{t-\overline{T}_{ji}}^{t} |\dot{x}_j^k(\theta)|^2 d\theta \int_{t-\overline{T}_{ji}}^{t} 1^2 d\theta \\
\geq &\frac{1}{\overline{T}_{ji}} \sum_{k=1}^{n} \left(\int_{t-\overline{T}_{ji}}^{t} |\dot{x}_j^k(\theta)| d\theta \right)^2 \geq \frac{1}{\overline{T}_{ji}} \sum_{k=1}^{n} \left[\sup_{-\overline{T}_{ji} \leq \tau \leq 0} x_j^k(t+\tau) - \inf_{-\overline{T}_{ji} \leq \tau \leq 0} x_j^k(t+\tau) \right]^2 \\
\geq &\frac{1}{\overline{T}_{ji}} \cdot \sup_{-\overline{T}_{ji} \leq \tau_1, \tau_2 \leq 0} \|\mathbf{x}_j(t+\tau_1) - \mathbf{x}_j(t+\tau_2)\|^2 \geq \frac{1}{\overline{T}_{ji}} \cdot \sup_{-\overline{T}_{ji} \leq \tau \leq 0} \|\mathbf{x}_j(t) - \mathbf{x}_j(t+\tau)\|^2,
\end{aligned}$$

where $\dot{x}_j^k$ is the k-th element of $\dot{\mathbf{x}}_j$. Thus, V_d can be lower-bounded by

$$V_d(t) \geq \sum_{i=1}^{N} \sum_{j \in \mathcal{N}_i(0)} \sup_{-\overline{T}_{ji} \leq \tau \leq 0} \|\mathbf{x}_j(t) - \mathbf{x}_j(t+\tau)\|^2.$$

With ω selected as required, it follows that

$$\begin{aligned}&\sup_{-\overline{T}_{ji}\le\tau\le 0}\|\mathbf{x}_j(t)-\mathbf{x}_j(t+\tau)\|\le\sqrt{V_d(t)}\le\sqrt{\frac{V(t)}{\omega}}\\ \le&\sqrt{\frac{V(0)}{\omega}}=\sqrt{\frac{V_p(0)}{\omega}}<\sqrt{\frac{P\overline{r}^2}{\omega(r^2-\overline{r}^2+Q)}}=\kappa\epsilon,\end{aligned}$$

which, together with $\|\mathbf{x}_{ij}(t)\|<\overline{r}$ and the definition of $|\mathbf{x}_{ij}|_T$, lead to

$$\begin{aligned}|\mathbf{x}_{ij}|_T=&\sup_{-\overline{T}_{ji}\le\tau\le 0}\|\mathbf{x}_i(t)-\mathbf{x}_j(t)+\mathbf{x}_j(t)-\mathbf{x}_j(t+\tau)\|\\ \le&\|\mathbf{x}_{ij}(t)\|+\sup_{-\overline{T}_{ji}\le\tau\le 0}\|\mathbf{x}_j(t)-\mathbf{x}_j(t+\tau)\|<\overline{r}+\kappa\epsilon=r\quad\forall(i,j)\in\mathcal{E}(0).\end{aligned}$$

Therefore, all initial links are preserved regardless of communication delays. ■

The above proof of Lemma 3.1 is in four steps: (i) given $V(t)\le V(0)$ and the selection of Q, $V_k\ge 0$, $V_d\ge 0$ and $V(0)=V_p(0)$ imply that $V_p(\tau)<P\overline{r}^2/(r^2-\overline{r}^2+Q)$; (ii) because $\psi(\|\mathbf{x}_{ij}\|)$ is continuous, positive definite and strictly increasing on $\|\mathbf{x}_{ij}\|\in[0,r]$, Assumption 3.3 together with (i) then imply that $\|\mathbf{x}_{ij}(t)\|<\overline{r}$ by contradiction; (iii) the application of the Cauchy-Schwarz inequality bounds V_d and, together with (i) and the selection of ω, leads to $\sup_{-\overline{T}_{ji}\le\tau\le 0}\|\mathbf{x}_j(t)-\mathbf{x}_j(t+\tau)\|<\kappa\epsilon$; (iv) lastly, the definition of $|\mathbf{x}_{ij}|_T$ and the triangle inequality imply $|\mathbf{x}_{ij}|_T<r$. The proof of $\|\mathbf{x}_{ij}(t)\|<\overline{r}$ by contradiction in (ii) has been developed in [98] for mobile robots with delay-free communications. By contrast, the proof of Lemma 3.1 is for time-delay EL networks. Connectivity preservation in time-delay networks must account for the delay-induced distortions $\mathbf{x}_j(t)-\mathbf{x}_j(t+T_{ji}(t))$. In the proof, the function V_d in the Lyapunov candidate V serves to bound $\mathbf{x}_j(t)-\mathbf{x}_j(t+T_{ji}(t))$ and further $|\mathbf{x}_{ij}|_T$.

Theorem 3.1. *Let the robot network* (3.1) *satisfy Assumptions 3.1-3.3. Then, the controls* (3.3) *preserve all initial communication links and synchronize the network if the parameters P, Q and ω are selected as in Lemma 3.1, and the control gains K_i are chosen by*

$$\overline{K}_i=K_i-\frac{1}{2}\sum_{j\in\mathcal{N}_i(0)}\left[(2\omega+\upsilon)\overline{T}_{ij}+\upsilon\overline{T}_{ji}\right]>0, \tag{3.5}$$

where $\upsilon=2PQ^{-3}\left(r^2+Q\right)\left(4r^2+Q\right)$.

Proof. By Property 1.2, the time derivative of V_k is

$$\dot{V}_k = \sum_{i=1}^{N} \dot{\mathbf{x}}_i^{\mathsf{T}} \mathbf{u}_i = -\sum_{i=1}^{N} \dot{\mathbf{x}}_i^{\mathsf{T}} \sum_{j \in \mathcal{N}_i} \nabla_i \psi(\|\mathbf{x}_{ij}^d\|) - \sum_{i=1}^{N} K_i \|\dot{\mathbf{x}}_i\|^2. \tag{3.6}$$

The initially undirected network by Assumption 3.3 implies that $j \in \mathcal{N}_i(0)$ iff $i \in \mathcal{N}_j(0)$, and thus that

$$\dot{V}_p = \frac{1}{2} \sum_{i=1}^{N} \sum_{j \in \mathcal{N}_i(0)} \left[\dot{\mathbf{x}}_i^{\mathsf{T}} \nabla_i \psi(\|\mathbf{x}_{ij}\|) + \dot{\mathbf{x}}_j^{\mathsf{T}} \nabla_j \psi(\|\mathbf{x}_{ij}\|) \right] = \sum_{i=1}^{N} \sum_{j \in \mathcal{N}_i(0)} \dot{\mathbf{x}}_i^{\mathsf{T}} \nabla_i \psi(\|\mathbf{x}_{ij}\|). \tag{3.7}$$

The bounds $\overline{T}_{ji}$ of time delays then lead to

$$\dot{V}_d = \sum_{i=1}^{N} \sum_{j \in \mathcal{N}_i(0)} \overline{T}_{ji} \left[\|\dot{\mathbf{x}}_j\|^2 - \|\dot{\mathbf{x}}_j(t - \overline{T}_{ji})\|^2 \right]. \tag{3.8}$$

Because $\mathcal{N}_i(t) = \mathcal{N}_i(0)$ for all $i = 1, \cdots, N$ at time $t = 0$, $V(\tau) \leq V(0)$, $\forall \tau \in [0, t]$ implies by Lemma 3.1 that $\mathcal{N}_i(t) = \mathcal{N}_i(0)$, i.e., that all initial links are maintained $\forall \tau \in [0, t]$. Set invariance [175] can then be leveraged to prove connectivity maintenance by induction on time [98]. Let $V(\tau) \leq V(0)$ and thus $\mathcal{N}_i(\tau) = \mathcal{N}_i(0)$, $\forall \tau \in [0, t)$ in (3.6). It then suffices to prove that $V(t) \leq V(0)$ as follows.

After adding (3.6)-(3.8), the time derivative of V becomes

$$\dot{V} \leq \sum_{i=1}^{N} \sum_{j \in \mathcal{N}_i(0)} \left[\dot{\mathbf{x}}_i^{\mathsf{T}} \nabla_i \psi(\|\mathbf{x}_{ij}\|) - \dot{\mathbf{x}}_i^{\mathsf{T}} \nabla_i \psi(\|\mathbf{x}_{ij}^d\|) \right] - \sum_{i=1}^{N} \left(K_i \|\dot{\mathbf{x}}_i\|^2 - \sum_{j \in \mathcal{N}_i(0)} \omega \overline{T}_{ji} \|\dot{\mathbf{x}}_j\|^2 \right).$$

By the definition of $\mathcal{N}_i$, $j \in \mathcal{N}_i \Rightarrow |\mathbf{x}_{ij}|_T < r$, and thence $\|\mathbf{x}_{ij}\| \leq |\mathbf{x}_{ij}|_T < r$ and $\|\mathbf{x}_{ij}^d\| \leq |\mathbf{x}_{ij}|_T < r$. It follows from Appendix A that

$$\dot{\mathbf{x}}_i^{\mathsf{T}} \nabla_i \psi(\|\mathbf{x}_{ij}\|) - \dot{\mathbf{x}}_i^{\mathsf{T}} \nabla_i \psi(\|\mathbf{x}_{ij}^d\|) \leq \upsilon \|\dot{\mathbf{x}}_i\| \|\mathbf{x}_j - \mathbf{x}_{jd}\| \tag{3.9}$$

and further that $\dot{V}$ is upper-bounded by

$$\dot{V} \leq \sum_{i=1}^{N} \sum_{j \in \mathcal{N}_i(0)} \upsilon \|\dot{\mathbf{x}}_i\| \|\mathbf{x}_j - \mathbf{x}_{jd}\| - \sum_{i=1}^{N} K_i \|\dot{\mathbf{x}}_i\|^2 + \sum_{i=1}^{N} \sum_{j \in \mathcal{N}_i(0)} \omega \overline{T}_{ij} \|\dot{\mathbf{x}}_i\|^2. \tag{3.10}$$

In (3.10), the first double summation captures, linearizes and upper-bounds the im-

pact of the delay-induced distortions $\mathbf{x}_j - \mathbf{x}_{jd}$ on connectivity-preserving synchronization. As shown below, this property is key to determining how much damping to inject locally to overcome the threat posed by delay-induced distortions.

By Lemma 1 in [84], the Cauchy-Schwarz inequality helps bound the cumulative effect of delay-incurred distortions as follows:

$$\int_0^t \|\dot{\mathbf{x}}_i(\theta)\|\|\mathbf{x}_j(\theta) - \mathbf{x}_{jd}(\theta)\|d\theta \leq \frac{\overline{T}_{ji}}{2}\left[\int_0^t \|\dot{\mathbf{x}}_i(\theta)\|^2 d\theta + \int_0^t \|\dot{\mathbf{x}}_j(\theta)\|^2 d\theta\right],$$

where Assumption 3.2, i.e., $\dot{\mathbf{x}}_i(\theta) = \mathbf{0}$ for $\theta \in [-\overline{T}_{ji}, 0]$, has been used. Then, the time integration of $\dot{V}$ from 0 to t leads to

$$\begin{aligned} V(t) \leq & \sum_{i=1}^{N} \sum_{j\in\mathcal{N}_i(0)} \left[\frac{\upsilon\overline{T}_{ji}}{2}\int_0^t \left(\|\dot{\mathbf{x}}_i(\theta)\|^2 + \|\dot{\mathbf{x}}_j(\theta)\|^2\right) d\theta + \omega\overline{T}_{ij}\int_0^t \|\dot{\mathbf{x}}_i(\theta)\|^2 d\theta\right] \\ & + V(0) - \sum_{i=1}^{N} K_i \int_0^t \|\dot{\mathbf{x}}_i(\theta)\|^2 d\theta = V(0) - \sum_{i=1}^{N} \overline{K}_i \int_0^t \|\dot{\mathbf{x}}_i(\theta)\|^2 d\theta. \end{aligned} \tag{3.11}$$

The selection of $\overline{K}_i > 0$ in (3.5) guarantees that: (i) $V(t) \leq V(0)$, $\forall t \geq 0$; and (ii) $\dot{\mathbf{x}}_i \in \mathcal{L}_2 \cap \mathcal{L}_\infty$ for $i = 1, \cdots, N$.

With the parameters P, Q and ω selected as required, Lemma 3.1 together with $V(t) \leq V(0)$ $\forall t \geq 0$ prove that all initial communication links are preserved, i.e., $\mathcal{N}_i(t) = \mathcal{N}_i(0)$ for all $t \geq 0$ and $i = 1, \cdots, N$. By Barbalat's lemma, $\dot{\mathbf{x}}_i \in \mathcal{L}_2 \cap \mathcal{L}_\infty$ for $i = 1, \cdots, N$ implies the synchronization of the robot network (3.1) [174]. ■

The proof of Theorem 3.1 above is by making $\mathcal{N}_i(\tau)$ forward invariant [175]: assume that $\mathcal{N}_i(t^-) = \mathcal{N}_i(0)$ and $V(\tau) \leq V(0)$ for all $\tau \in [0, t)$ and obtain that $V(t) \leq V(0)$ which, in turn, implies that $\mathcal{N}_i(t) = \mathcal{N}_i(0)$. The connectivity-preserving synchronization controllers (3.3) can be designed by selecting Q and setting ω after choosing P heuristically to satisfy the conditions in Lemma 3.1, and then by injecting sufficient local damping according to (3.5).

Practical robot networks have limited actuation and the controls (3.3) may saturate it and become invalid. Existing work has proposed controllers for connectivity-preserving consensus of first-order [176] and second-order multi-robot systems [98]. Connectivity-preserving consensus of first-order networks with bounded actuation has been studied in [97]. Connectivity-preserving consensus of EL networks with time-varying delays and bounded actuation has remained an open question. The key

challenge in this question is the saturated actuation. Given unlimited actuation, this section has shown that proper modulation of the inter-robot couplings together with sufficient local damping injection can preserve the local connectivity of time-delay EL networks during synchronization. Actuator saturation, however, limits the coupling stiffness and the injected damping. Thereby, it prevents existing controllers from guaranteeing connectivity and, implicitly, synchronization. The following section develops an indirect coupling control framework to integrate the constraints due to bounded actuation into the controller design.

3.1.2 Time-Delay Network With Bounded Actuation

The indirect coupling framework proposed in this section: (i) endows every robot with a second-order virtual proxy; (ii) interconnects the proxies of initially adjacent robots; and (iii) couples all robots to their proxies. As shown below, the intervening dynamics of virtual proxies permit to decouple time-varying delays from actuator saturation because they can tackle time delays in the inter-proxy couplings and actuation bounds in the robot-proxy couplings.

The designed dynamics of the virtual proxy of the robot i are

$$\widehat{\mathbf{M}}_i\ddot{\widehat{\mathbf{x}}}_i = \mathrm{Sat}_i\left(P_i\widetilde{\mathbf{x}}_i\right) - \sum_{j\in\mathcal{N}_i}\nabla_i\widehat{\psi}(\|\widehat{\mathbf{x}}_{ij}^d\|) - \widehat{K}_i\dot{\widehat{\mathbf{x}}}_i, \tag{3.12}$$

where $\widetilde{\mathbf{x}}_i = \mathbf{x}_i - \widehat{\mathbf{x}}_i$, $\widehat{\mathbf{x}}_{ij}^d = \widehat{\mathbf{x}}_i - \widehat{\mathbf{x}}_{jd}$ with $\widehat{\mathbf{x}}_{jd} = \widehat{\mathbf{x}}_j(t - T_{ji}(t))$, $\mathrm{Sat}_i(\cdot)$ is a vector-valued saturation function with bounds to be determined, $\widehat{\mathbf{M}}_i$ is a tunable positive diagonal matrix, P_i and $\widehat{K}_i$ are positive constants, $\mathcal{N}_i$ is to be defined, and the potential function $\widehat{\psi}(\|\widehat{\mathbf{x}}_{ij}\|)$ is defined by

$$\widehat{\psi}(\|\widehat{\mathbf{x}}_{ij}\|) = \frac{\widehat{P}\|\widehat{\mathbf{x}}_{ij}\|^2}{\widehat{r}^2 - \|\widehat{\mathbf{x}}_{ij}\|^2 + \widehat{Q}}, \tag{3.13}$$

with $\widehat{r} = r - 2\epsilon/3$, and $\widehat{P}$ and $\widehat{Q}$ positive constants to be determined. The gradient of $\widehat{\psi}(\|\widehat{\mathbf{x}}_{ij}^d\|)$ with respect to $\widehat{\mathbf{x}}_i$,

$$\nabla_i\widehat{\psi}(\|\widehat{\mathbf{x}}_{ij}^d\|) = \frac{2\widehat{P}\left(\widehat{r}^2 + \widehat{Q}\right)}{\left(\widehat{r}^2 - \|\widehat{\mathbf{x}}_{ij}^d\|^2 + \widehat{Q}\right)^2}\left(\widehat{\mathbf{x}}_i - \widehat{\mathbf{x}}_{jd}\right),$$

provides the coupling between the proxies of two initially adjacent robots i and j.

The nominal control:

$$\widehat{\mathbf{f}}_i = -P_i\widetilde{\mathbf{x}}_i - K_i\dot{\mathbf{x}}_i, \tag{3.14}$$

where K_i is a non-negative constant, connects each robot i to its virtual proxy, and completes the design of the indirect coupling framework.

Let the actuation bound of each robot i be $\overline{\mathbf{f}}_i = \begin{bmatrix}\overline{f}_i^1 & \cdots & \overline{f}_i^n\end{bmatrix}^\mathsf{T}$. The actual control input $\mathbf{f}_i$ is then a saturated version of the nominal control $\widehat{\mathbf{f}}_i$, typically modelled by $\mathbf{f}_i = \mathrm{Sat}_i\big(\widehat{\mathbf{f}}_i\big) = \big[\mathrm{sat}_i^1\big(\widehat{f}_i^1\big) \ \cdots \ \mathrm{sat}_i^n\big(\widehat{f}_i^n\big)\big]^\mathsf{T}$, refer to [177]. In (3.14), $\mathrm{Sat}_i(\cdot)$ saturates $\widehat{\mathbf{f}}_i$ component-wisely by the standard saturation functions $\mathrm{sat}_i^k(\cdot)$ with the bounds $\overline{f}_i^k$, $k = 1, \cdots, n$. Because the Proportional gains P_i and the damping gains K_i can be tuned freely, independent of time-varying delays and actuator saturation, the controller (3.14) can exploit the available bounded actuation more fully, as discussed in [177–179].

The virtual proxy designed in (3.12) can be regarded as a virtual inertia $\widehat{\mathbf{M}}_i$ with the position $\widehat{\mathbf{x}}_i$ and forced by the right-hand side of (3.12). The saturated Proportional term $\mathrm{Sat}_i\left(P_i\widetilde{\mathbf{x}}_i\right)$ in (3.12) connects the proxy to its robot i passively. The gradient term $-\nabla_i\widehat{\psi}(\|\widehat{\mathbf{x}}_{ij}^d\|)$ connects the proxies of two adjacent robots i and j via time-delay communications. Because every two neighbouring robots i and j are connected to their proxies and the proxies, in turn, are connected to each other, the adjacent robots are indirectly coupled through their proxies.

For delay-free communications, connectivity preservation requires that $\|\mathbf{x}_{ij}(t)\| < r$, $\forall (i,j) \in \mathcal{E}(0)$ and $\forall t \geq 0$. By the triangle inequality $\|\mathbf{x}_{ij}\| \leq \|\widetilde{\mathbf{x}}_i\| + \|\widehat{\mathbf{x}}_{ij}\| + \|\widetilde{\mathbf{x}}_j\|$, it suffices to guarantee that $\|\widehat{\mathbf{x}}_{ij}(t)\| < \widehat{r}$, $\forall (i,j) \in \mathcal{E}(0)$, and that $\|\widetilde{\mathbf{x}}_i(t)\| \leq \epsilon/3$, $\forall i = 1, \cdots, N$. For delayed communications, $\|\widehat{\mathbf{x}}_{ij}(t)\| < \widehat{r}$ does not guarantee that the proxy of the robot i can receive at time t the information sent by the proxy of the robot j at time $t - T_{ji}(t)$. Thus, $\|\widehat{\mathbf{x}}_{ij}(t)\| < \widehat{r}$ is not sufficient for connectivity preservation. To account for the delay-induced mismatches $\|\widehat{\mathbf{x}}_j(t) - \widehat{\mathbf{x}}_j(t - T_{ji}(t))\|$, the set of neighbours of the robot i is re-defined by $\mathcal{N}_i = \big\{j \in \mathcal{V} \mid (i,j) \in \mathcal{E}(0) \text{ and } |\widehat{\mathbf{x}}_{ij}|_T < \widehat{r}\big\}$, where

$$|\widehat{\mathbf{x}}_{ij}|_T = \sup_{-\overline{T}_{ji} \leq \tau \leq 0} \|\widehat{\mathbf{x}}_i(t) - \widehat{\mathbf{x}}_j(t+\tau)\|.$$

Assumption 3.3 implies that $\|\mathbf{x}_{ij}(0)\| < r - \epsilon < \widehat{r}$, $\forall (i,j) \in \mathcal{E}(0)$. Letting the initial state of the virtual proxy (3.12) be $\widehat{\mathbf{x}}_i(\tau) = \mathbf{x}_i(\tau)$ and $\dot{\widehat{\mathbf{x}}}_i(\tau) = \mathbf{0}$, $\forall \tau \in [-\overline{T}_i, 0]$, ensures that $j \in \mathcal{N}_i(0)$ if and only if $(i,j) \in \mathcal{E}(0)$. Then, the connectivity of the time-delay

robot network with bounded actuation is preserved if the set $\mathcal{N}_i$ is rendered invariant, i.e., $\mathcal{N}_i(t) = \mathcal{N}_i(0)$, and if $\|\widetilde{\mathbf{x}}_i(t)\| \leq \epsilon/3$, $\forall i = 1, \cdots, N$, $\forall t \geq 0$. More specifically, the undirected communication link between the robots i and j exists at time t, namely, $(i,j) \in \mathcal{E}(t)$, iff $\|\mathbf{x}_i(t) - \mathbf{x}_j(t - T_{ji}(t))\| \leq r$ and $\|\mathbf{x}_j(t) - \mathbf{x}_i(t - T_{ij}(t))\| \leq r$. With $\mathcal{N}_i(t) = \mathcal{N}_i(0)$ and $\|\widetilde{\mathbf{x}}_i(t) \leq \epsilon/3\|$, it ensures that

$$\begin{aligned}|\mathbf{x}_{ij}|_T \leq & \|\widetilde{\mathbf{x}}_i(t)\| + \sup_{-\overline{T}_{ji} \leq r \leq 0} \|\widehat{\mathbf{x}}_i(t) - \widehat{\mathbf{x}}_j(t+\tau)\| + \sup_{-\overline{T}_{ji} \leq \tau \leq 0} \|\widetilde{\mathbf{x}}_j(t+\tau)\| \\ = & \|\widetilde{\mathbf{x}}_i(t)\| + |\widehat{\mathbf{x}}_{ij}|_T + \sup_{-\overline{T}_{ji} \leq \tau \leq 0} \|\widetilde{\mathbf{x}}_j(t+\tau)\| < \frac{\epsilon}{3} + \widehat{r} + \frac{\epsilon}{3} = r,\end{aligned}$$

where $\forall (i,j) \in \mathcal{E}(0)$, and is thus sufficient to maintain the connectivity of the time-delay robot network with bounded actuation.

By the design of the virtual proxies (3.12), actuator saturation makes the robot-proxy couplings dynamic but symmetric and thus passive. The potential energy stored in the coupling between the robot i and its proxy is

$$\phi_i(\widetilde{\mathbf{x}}_i) = \int_{\mathbf{0}}^{\widetilde{\mathbf{x}}_i} \mathrm{Sat}_i(P_i \boldsymbol{\sigma})^{\mathsf{T}} d\boldsymbol{\sigma}. \tag{3.15}$$

Then, the following three propositions combined give an optimal ϕ^* such that $\|\widetilde{\mathbf{x}}_i(t)\| \leq \epsilon/3$ is guaranteed if $\phi_i(\widetilde{\mathbf{x}}_i) \leq \phi^*$.

Proposition 3.1. *The potential function $\phi_i(\widetilde{\mathbf{x}}_i)$ is convex with respect to $\widetilde{\mathbf{x}}_i$ on $\mathbb{R}^n$.*

Proof. The gradient of $\phi_i(\widetilde{\mathbf{x}}_i)$ with respect to $\widetilde{\mathbf{x}}_i$ is $\nabla \phi_i(\widetilde{\mathbf{x}}_i) = \mathrm{Sat}_i(P_i \widetilde{\mathbf{x}}_i)$. Let $\mathbf{y} \in \mathbb{R}^n$ and $\mathbf{z} \in \mathbb{R}^n$. Then, it holds that $\big[\nabla \phi_i(\mathbf{y}) - \nabla_i \phi(\mathbf{z})\big]^{\mathsf{T}} (\mathbf{y} - \mathbf{z}) = \big[\mathrm{Sat}_i(P_i \mathbf{y}) - \mathrm{Sat}_i(P_i \mathbf{z})\big]^{\mathsf{T}} (\mathbf{y} - \mathbf{z}) = \sum_{k=1}^n \big[\mathrm{sat}_i^k(P_i y^k) - \mathrm{sat}_i^k(P_i z^k)\big](y^k - z^k) \geq 0$, because $\mathrm{sat}_i^k(\cdot)$ are non-decreasing. By the first-order convexity condition, $\phi_i(\widetilde{\mathbf{x}}_i)$ is convex on $\mathbb{R}^n$. ■

Proposition 3.2. *On the ball $B(\mathbf{0}, \epsilon/3) = \{\widetilde{\mathbf{x}}_i \in \mathbb{R}^n \mid \|\widetilde{\mathbf{x}}_i\| \leq \epsilon/3\}$, the potential function $\phi_i(\widetilde{\mathbf{x}}_i)$ is maximum on the boundary $\|\widetilde{\mathbf{x}}_i\| = \epsilon/3$ and minimum at the origin $\widetilde{\mathbf{x}}_i = \mathbf{0}$.*

Proof. The potential function $\phi_i(\widetilde{\mathbf{x}}_i)$ is continuous on the ball $B(\mathbf{0}, \epsilon/3) \subseteq \mathbb{R}^n$. Therefore, by the Weierstrass theorem, $\phi_i(\widetilde{\mathbf{x}}_i)$ attains its global minimum and maximum on $B(\mathbf{0}, \epsilon/3)$. Further, $\phi_i(\widetilde{\mathbf{x}}_i)$ is convex on $\mathbb{R}^n$. Hence, on the ball $B(\mathbf{0}, \epsilon/3)$, $\phi_i(\widetilde{\mathbf{x}}_i)$ attains its global maximum on the boundary of $B(\mathbf{0}, \epsilon/3)$, and its global minimum at the point with $\nabla \phi_i(\widetilde{\mathbf{x}}_i) = \mathrm{Sat}_i(P_i \widetilde{\mathbf{x}}_i) = \mathbf{0}$, that is at $\widetilde{\mathbf{x}}_i = \mathbf{0}$. ■

Proposition 3.3. *Let ϕ_i^* be the minimum of $\phi_i(\widetilde{\mathbf{x}}_i)$ on the boundary of $B(\mathbf{0}, \epsilon/3)$,*

$$\begin{aligned} \phi_i^* = \underset{\widetilde{\mathbf{x}}_i \in \mathbb{R}^n}{minimize} \quad & \phi_i(\widetilde{\mathbf{x}}_i) = \int_{\mathbf{0}}^{\widetilde{\mathbf{x}}_i} Sat_i(P_i \boldsymbol{\sigma})^{\mathsf{T}} d\boldsymbol{\sigma} \\ subject\ to \quad & \|\widetilde{\mathbf{x}}_i\| = \epsilon/3. \end{aligned}$$

If $\phi_i(\widetilde{\mathbf{x}}_i) \leq \phi_i^*$, then $\widetilde{\mathbf{x}}_i \in B(\mathbf{0}, \epsilon/3)$.

Proof. Suppose there exists $\widetilde{\mathbf{x}}_i \notin B(\mathbf{0}, \epsilon/3)$ such that $\phi_i(\widetilde{\mathbf{x}}_i) \leq \phi_i^*$. Then, there exists $0 < \lambda < 1$ such that $\mathbf{x} = \lambda \mathbf{0} + (1-\lambda)\widetilde{\mathbf{x}}_i$ is on the boundary of $B(\mathbf{0}, \epsilon/3)$, namely, $\|\mathbf{x}\| = \epsilon/3$. By the convexity of $\phi_i(\cdot)$, it follows that $\phi_i(\mathbf{x}) = \phi_i\left(\lambda \mathbf{0} + (1-\lambda)\widetilde{\mathbf{x}}_i\right) \leq \lambda \phi_i(\mathbf{0}) + (1-\lambda)\phi_i(\widetilde{\mathbf{x}}_i) = (1-\lambda)\phi_i(\widetilde{\mathbf{x}}_i) < \phi_i^*$, which contradicts $\phi_i(\mathbf{x}) \geq \phi_i^*$. Therefore, $\phi_i(\widetilde{\mathbf{x}}_i) \leq \phi_i^*$ implies that $\widetilde{\mathbf{x}}_i \in B(\mathbf{0}, \epsilon/3)$. ■

The Lyapunov candidate used to investigate connectivity-preserving synchronization of the time-delay robot network (3.1) with limited actuation is

$$V = V_k + V_p + \widehat{\omega} V_d, \tag{3.16}$$

where $\widehat{\omega} > 0$ and

$$\begin{aligned} V_k =& \frac{1}{2} \sum_{i=1}^{N} \left[\dot{\mathbf{x}}_i^{\mathsf{T}} \mathbf{M}_i(\mathbf{x}_i) \dot{\mathbf{x}}_i + \dot{\widehat{\mathbf{x}}}_i^{\mathsf{T}} \widehat{\mathbf{M}}_i \dot{\widehat{\mathbf{x}}}_i \right], \\ V_p =& \frac{1}{2} \sum_{i=1}^{N} \sum_{j \in \mathcal{N}_i(0)} \widehat{\psi}(\|\widehat{\mathbf{x}}_{ij}\|) + \sum_{i=1}^{N} \phi_i(\widetilde{\mathbf{x}}_i), \\ V_d =& \sum_{i=1}^{N} \sum_{j \in \mathcal{N}_i(0)} \overline{T}_{ji} \int_{t-\overline{T}_{ji}}^{t} \|\dot{\widehat{\mathbf{x}}}_j(\theta)\|^2 d\theta. \end{aligned}$$

Compared to that in (3.4), the Lyapunov candidate V in (3.16) accounts for the kinetic energy of the robot network plus all proxies in V_k, the potential energy of all robot-proxy and inter-proxy couplings in V_p, and the impact of time-varying delays on the constraints imposed on the inter-proxy distances by connectivity preservation in V_d.

Then, the following lemma facilitates the proof of connectivity maintenance.

Lemma 3.2. *Let the robot network* (3.1) *satisfy Assumptions 3.1-3.3, and let $\widetilde{r} = \widehat{r} - \kappa\epsilon/3$ with $0 < \kappa < 1$, $M = |\mathcal{E}(0)|$, and $\phi^* = \min_{i=1\cdots,N} \phi_i^*$. Choose the parameters $\widehat{P}$, $\widehat{Q}$*

and $\widehat{\omega}$ *such that* $[\widetilde{r}^2 - M(r-\epsilon)^2]\,\widehat{Q} \geq [\widetilde{r}^2 + M(\widehat{r}^2 - \widetilde{r}^2)]\,(r-\epsilon)^2 - \widehat{r}^2\widetilde{r}^2$, $\widetilde{r}^2\widehat{P} = \phi^*\big(\widehat{r}^2 - \widetilde{r}^2 + \widehat{Q}\big)$ *and* $\kappa^2\epsilon^2\widehat{\omega} \geq 9\phi^*$. *Then* $V(\tau) \leq V(0)$, $\forall \tau \in [0,t]$, *implies that* $\mathcal{N}_i(t) = \mathcal{N}_i(0)$ *and* $\|\widetilde{\mathbf{x}}_i(t)\| \leq \epsilon/3$, $\forall i = 1, \cdots, N$ *and* $\forall t \geq 0$, *and further that* $|\mathbf{x}_{ij}|_T < r$, $\forall (i,j) \in \mathcal{E}(0)$. *That is, all initial communication links are maintained regardless of time delays.*

Proof. By Assumption 3.2 and the initial state variables $\widehat{\mathbf{x}}_i(0) = \mathbf{x}_i(0)$ and $\dot{\widehat{\mathbf{x}}}_0(0) = \mathbf{0}$ of the proxy of every robot i, it follows that $V_k(0) = V_d(0) = 0$ and $\phi_i(\widetilde{\mathbf{x}}_i(0)) = 0$ for $i = 1, \cdots, N$. Then, selecting $\widehat{Q}$ and $\widehat{P}$ as required leads to $V(0) < M\widehat{P}(r-\epsilon)^2/\big[\widehat{r}^2 - (r-\epsilon)^2 + \widehat{Q}\big] \leq \widehat{P}\widetilde{r}^2/\big[\widehat{r}^2 - \widetilde{r}^2 + \widehat{Q}\big] = \phi^*$. If $V(t) \leq V(0)$ for any $t \geq 0$, then $V_k(t) \geq 0$ and $V_d \geq 0$ imply that $V_p(t) < \phi^*$. Further, $\phi_i(\widetilde{\mathbf{x}}_i) \geq 0$ by (3.15), and thus V_p defined in (3.16) implies that

$$\frac{1}{2}\sum_{i=1}^{N}\sum_{j\in\mathcal{N}_i(0)}\widehat{\psi}(\|\widehat{\mathbf{x}}_{ij}\|) < \phi^* = \frac{\widehat{P}\widetilde{r}^2}{\widehat{r}^2 - \widetilde{r}^2 + \widehat{Q}}$$

An analysis by contradiction similar to the analysis in Lemma 3.1 leads to

$$0 \leq \widehat{\psi}(\|\widehat{\mathbf{x}}_{ij}(t)\|) = \frac{\widehat{P}\|\widehat{\mathbf{x}}_{ij}(t)\|^2}{\widehat{r}^2 - \|\widehat{\mathbf{x}}_{ij}(t)\|^2 + \widehat{Q}} < \phi^*$$

and thus to $\|\widehat{\mathbf{x}}_{ij}(t)\| < \widetilde{r}$, $\forall (i,j) \in \mathcal{E}(0)$. Because $\widehat{\psi}(\|\widehat{\mathbf{x}}_{ij}(t)\|) \geq 0$, $V_p(t) < \phi^*$ implies that $\phi_i(\widetilde{\mathbf{x}}_i) < \phi^*$ and, by Proposition 3.3, that $\|\widetilde{\mathbf{x}}_i(t)\| < \epsilon/3$, $\forall i = 1, \cdots, N$.

With $\widehat{\omega}$ selected as required, $\widehat{\psi}(\|\widehat{\mathbf{x}}_{ij}(t)\|) \geq 0$, $\phi_i(\widetilde{\mathbf{x}}_i) > 0$ and $V(t) \leq V(0) = \phi^*$ lead to $V_d(t) \leq \phi^*/\widehat{\omega} \leq \kappa^2\epsilon^2/9$. Similarly to the proof of Lemma 3.1, the Cauchy-Schwarz inequality can be applied to lower-bound V_d by

$$V_d(t) \geq \sum_{i=1}^{N}\sum_{j\in\mathcal{N}_i(0)}\sup_{-\overline{T}_{ji}\leq\tau\leq 0}\|\widehat{\mathbf{x}}_j(t) - \widehat{\mathbf{x}}_j(t+\tau)\|^2.$$

Hence, it follows that

$$\sup_{-\overline{T}_{ji}\leq\tau\leq 0}\|\widehat{\mathbf{x}}_j(t) - \widehat{\mathbf{x}}_j(t+\tau)\| \leq \sqrt{V_d(t)} \leq \frac{\kappa\epsilon}{3},$$

which, together with $\|\mathbf{x}_i(t)\| < \epsilon/3$ and the definition of $|\widehat{\mathbf{x}}_{ij}(t)|_T$, leads to

$$|\widehat{\mathbf{x}}_{ij}(t)|_T \leq \|\widehat{\mathbf{x}}_{ij}(t)\| + \sup_{-\overline{T}_{ji}\leq\tau\leq 0}\|\widehat{\mathbf{x}}_j(t) - \widehat{\mathbf{x}}_j(t+\tau)\| < \widetilde{r} + \frac{\kappa\epsilon}{3} = \widehat{r},$$

to $\|\widehat{\mathbf{x}}_{ij}^d\| < \widehat{r}$, $\forall (i,j) \in \mathcal{E}(0)$, and, with $\|\widetilde{\mathbf{x}}_i\| < \epsilon/3$, $\forall i = 1, \cdots, N$, to the maintenance of all communication links regardless of time delays. ■

The following proposition facilitates the proof of connectivity-preserving synchronization in Theorem 3.2.

Proposition 3.4. *Let $Sat(\cdot)$ be a standard vector valued saturation function. For any $\mathbf{x} \in \mathbb{R}^n$, $\mathbf{y} \in \mathbb{R}^n$, it follows that $-\mathbf{x}^{\mathsf{T}} Sat(\mathbf{x}+\mathbf{y}) \leq -\mathbf{x}^{\mathsf{T}} Sat(\mathbf{y})$.*

Proof. The proof is by enumeration and is omitted. ■

Theorem 3.2. *Let the time-delay robot network* (3.1) *with bounded actuation satisfy Assumptions 3.1-3.3. Then, the controls* (3.12) *and* (3.14) *preserve all initial communication links and synchronize the network if the parameters $\widehat{P}$, $\widehat{Q}$ and $\widehat{\omega}$ are selected as in Lemma 3.2, and the gains P_i, K_i and $\widehat{K}_i$ satisfy that*

$$\widetilde{K}_i = \widehat{K}_i - \frac{1}{2} \sum_{j \in \mathcal{N}_i(0)} \left[(2\widehat{\omega} + \widehat{\upsilon}) \overline{T}_{ij} + \widehat{\upsilon} \overline{T}_{ji} \right] > 0, \tag{3.17}$$

where $\widehat{\upsilon} = 2\widehat{P}\widehat{Q}^{-3}\big(\widehat{r}^2 + \widehat{Q}\big)\big(4\widehat{r}^2 + \widehat{Q}\big)$.

Proof. By Property 1.2 and Proposition 3.4, the time derivative of V_k becomes

$$\begin{aligned}
\dot{V}_k =& \sum_{i=1}^{N} \left[\dot{\mathbf{x}}_i^{\mathsf{T}} \mathrm{Sat}_i \left(-P_i \widetilde{\mathbf{x}}_i - K_i \dot{\mathbf{x}}_i \right) + \dot{\widehat{\mathbf{x}}}_i^{\mathsf{T}} \mathrm{Sat}_i \left(P_i \widetilde{\mathbf{x}}_i \right) - \dot{\widehat{\mathbf{x}}}_i^{\mathsf{T}} \sum_{j \in \mathcal{N}_i} \nabla_i \widehat{\psi}(\|\widehat{\mathbf{x}}_{ij}^d\|) - \widehat{K}_i \|\dot{\widehat{\mathbf{x}}}_i\|^2 \right] \\
\leq& \sum_{i=1}^{N} \left[\dot{\mathbf{x}}_i^{\mathsf{T}} \mathrm{Sat}_i \left(-P_i \widetilde{\mathbf{x}}_i + \dot{\widehat{\mathbf{x}}}_i^{\mathsf{T}} \mathrm{Sat}_i \left(P_i \widetilde{\mathbf{x}}_i \right) \right) - \dot{\widehat{\mathbf{x}}}_i^{\mathsf{T}} \sum_{j \in \mathcal{N}_i} \nabla_i \widehat{\psi}(\|\widehat{\mathbf{x}}_{ij}^d\|) - \widehat{K}_i \|\dot{\widehat{\mathbf{x}}}_i\|^2 \right] \\
=& - \sum_{i=1}^{N} \dot{\widetilde{\mathbf{x}}}_i^{\mathsf{T}} \mathrm{Sat}_i \left(P_i \widetilde{\mathbf{x}}_i \right) - \sum_{i=1}^{N} \widehat{K}_i \|\dot{\widehat{\mathbf{x}}}_i\|^2 - \sum_{i=1}^{N} \sum_{j \in \mathcal{N}_i} \dot{\widehat{\mathbf{x}}}_i^{\mathsf{T}} \nabla_i \widehat{\psi}(\|\widehat{\mathbf{x}}_{ij}^d\|).
\end{aligned} \tag{3.18}$$

Assumption 3.3 and the definitions of $\widehat{\psi}(\|\widehat{\mathbf{x}}_{ij}\|)$ in (3.13) and $\phi_i(\widetilde{\mathbf{x}}_i)$ in (3.15) lead to

$$\dot{V}_p = \sum_{i=1}^{N} \sum_{j \in \mathcal{N}_i(0)} \dot{\widehat{\mathbf{x}}}_i^{\mathsf{T}} \nabla_i \widehat{\psi}(\|\widehat{\mathbf{x}}_{ij}\|) + \sum_{i=1}^{N} \dot{\widetilde{\mathbf{x}}}_i^{\mathsf{T}} \mathrm{Sat}_i \left(P_i \widetilde{\mathbf{x}}_i \right). \tag{3.19}$$

The upper-bounds $\overline{T}_{ji}$ of time delays indicate that

$$\dot{V}_d = \sum_{i=1}^{N} \sum_{j \in \mathcal{N}_i(0)} \overline{T}_{ji} \Big[\|\dot{\widehat{\mathbf{x}}}_j(t)\|^2 - \|\dot{\widehat{\mathbf{x}}}_j(t - \overline{T}_{ji})\|^2 \Big]. \tag{3.20}$$

Because $\mathcal{N}_i(t) = \mathcal{N}_i(0)\ \forall i = 1, \cdots, N$ at time $t = 0$, and $V(\tau) \leq V(0)$, $\forall \tau \in [0, t]$, implies that $\mathcal{N}_i(t) = \mathcal{N}_i(0)$ and $\|\widetilde{\mathbf{x}}_i(t)\| \leq \epsilon/3$, $\forall t \geq 0$ and $\forall i = 1, \cdots, N$, by Lemma 3.2, set invariance [175] can again be leveraged to prove connectivity maintenance by induction on time [98]. Let $V(\tau) \leq V(0)$ and thus $\mathcal{N}_i = \mathcal{N}_i(0)$, $\forall \tau \in [0, t)$, in (3.18). It then suffices to prove $V(t) \leq V(0)$ as follows.

The definition of $\mathcal{N}_i$ implies that $|\widehat{\mathbf{x}}_{ij}|_T < \widehat{r}$, and thus, that $\|\widehat{\mathbf{x}}_{ij}\| < \widehat{r}$ and $\|\widehat{\mathbf{x}}_{ij}^d\| < \widehat{r}$. Then, adding (3.18)-(3.20) and using $\dot{\widehat{\mathbf{x}}}_i^{\mathsf{T}} \nabla_i \widehat{\psi}(\|\widehat{\mathbf{x}}_{ij}\|) - \dot{\widehat{\mathbf{x}}}_i^{\mathsf{T}} \nabla_i \widehat{\psi}(\|\widehat{\mathbf{x}}_{ij}^d\|) \leq \widehat{v}\|\dot{\widehat{\mathbf{x}}}_i\|\|\widehat{\mathbf{x}}_j - \widehat{\mathbf{x}}_{jd}\|$, $\forall j \in \mathcal{N}_i(0)$, yield

$$\begin{aligned}\dot{V} \leq & \sum_{i=1}^{N} \sum_{j \in \mathcal{N}_i(0)} \Big[\dot{\widehat{\mathbf{x}}}_i^{\mathsf{T}} \nabla_i \widehat{\psi}(\|\widehat{\mathbf{x}}_{ij}\|) - \dot{\widehat{\mathbf{x}}}_i^{\mathsf{T}} \nabla_i \widehat{\psi}(\|\widehat{\mathbf{x}}_{ij}^d\|) + \widehat{\omega}\overline{T}_{ji}\|\dot{\widehat{\mathbf{x}}}_j(t)\|^2\Big] - \sum_{i=1}^{N} \widehat{K}_i \|\dot{\widehat{\mathbf{x}}}_i\|^2 \\ \leq & \sum_{i=1}^{N} \sum_{j \in \mathcal{N}_i(0)} \big(\widehat{v}\|\dot{\widehat{\mathbf{x}}}_i\|\|\widehat{\mathbf{x}}_j - \widehat{\mathbf{x}}_{jd}\| + \widehat{\omega}\overline{T}_{ij}\|\dot{\widehat{\mathbf{x}}}_i\|^2\big) - \sum_{i=1}^{N} \widehat{K}_i \|\dot{\widehat{\mathbf{x}}}_i\|^2.\end{aligned} \tag{3.21}$$

Applying the Cauchy-Schwarz inequality as in (3.11) leads to

$$\int_0^t \|\dot{\widehat{\mathbf{x}}}_i(\theta)\|\|\widehat{\mathbf{x}}_j(\theta) - \widehat{\mathbf{x}}_{jd}(\theta)\| d\theta \leq \frac{\overline{T}_{ji}}{2}\Big[\int_0^t \|\dot{\widehat{\mathbf{x}}}_i(\theta)\|^2 d\theta + \int_0^t \|\dot{\widehat{\mathbf{x}}}_j(\theta)\|^2 d\theta\Big].$$

Then, the time integration of (3.21) from 0 to t gives that

$$\begin{aligned}V(t) \leq & \sum_{i=1}^{N} \sum_{j \in \mathcal{N}_i(0)} \Big[\frac{\widehat{v}\overline{T}_{ji}}{2} \int_0^t \big(\|\dot{\widehat{\mathbf{x}}}_i(\theta)\|^2 + \|\dot{\widehat{\mathbf{x}}}_j(\theta)\|^2\big) d\theta + \widehat{\omega}\overline{T}_{ij} \int_0^t \|\dot{\widehat{\mathbf{x}}}_i(\theta)\|^2 d\theta\Big] \\ & + V(0) - \sum_{i=1}^{N} \widehat{K}_i \int_0^t \|\dot{\widehat{\mathbf{x}}}_i(\theta)\|^2 d\theta = V(0) - \sum_{i=1}^{N} \widetilde{K}_i \int_0^t \|\dot{\widehat{\mathbf{x}}}_i(\theta)\|^2 d\theta.\end{aligned} \tag{3.22}$$

Because $\widetilde{K}_i$ are positive, Equation (3.22) guarantees that $V(t) \leq V(0)$ and, by Lemma 3.2, that all initial communication links are preserved.

Synchronization can be concluded by noting that (3.22) also yields that $\dot{\widehat{\mathbf{x}}}_i \in \mathcal{L}_2 \cap \mathcal{L}_\infty$, which implies that $\dot{\widehat{\mathbf{x}}}_i \to \mathbf{0}$. After obtaining the time derivative of $\ddot{\widehat{\mathbf{x}}}_i$ in (3.12), Barbalat's lemma yields $\ddot{\widehat{\mathbf{x}}}_i \to \mathbf{0}$. The bounded second derivative of $\ddot{\widehat{\mathbf{x}}}_i$ leads to $\dddot{\widehat{\mathbf{x}}}_i \to \mathbf{0}$ and further to $\dot{\widehat{\mathbf{x}}}_i \to \dot{\mathbf{x}}_i \to \mathbf{0}$ and $\widehat{\mathbf{x}}_{ij} \to \mathbf{0}$. The derivative of (3.1) gives $\ddot{\mathbf{x}}_i \to \mathbf{0}$ and thus $\mathrm{Sat}_i\left[P_i(\widehat{\mathbf{x}}_i - \mathbf{x}_i)\right] \to \mathbf{0}$. Together, all the above inferences lead to $\widetilde{\mathbf{x}}_i \to \mathbf{0}$ and $\widehat{\mathbf{x}}_{ij} \to \mathbf{0}$, i.e., to $\mathbf{x}_i \to \mathbf{x}_j$. ■

The first stepping-stone in the proposed indirect coupling framework is to connect

all robots only to their proxies through saturated P+d control. The regulation control of a single robot in [177] provides the impetus for employing saturated P+d terms for robot control, by showing that the control exploits actuator capabilities better than other saturating controllers, potentially speeding up the convergence. These virtual proxies decouple the actuator saturation and time-varying delays in the robot-proxy and inter-proxy couplings, respectively, thereby permitting the control design to tackle them separately. The second stepping-stone of the framework is to convert the impact of limited actuation on connectivity maintenance to a constraint on the time-delay inter-proxy couplings. A single Lyapunov candidate V in (3.16) can then verify all constraints after synchronizing the upper bounds of their potential functions.

3.1.3 Discussion

This chapter focuses on connectivity-preserving synchronization of time-delay EL robot networks without and with bounded actuation.

1. Given unbounded actuation (Section 3.1.1), a gradient-based control couples every two initially adjacent robots symmetrically. In particular, $-\nabla_i \psi(\|\mathbf{x}_{ij}^d\|)$ in the control $\mathbf{f}_i$ designed in (3.3) connects the robot i to the robot j. Correspondingly, $-\nabla_j \psi(\|\mathbf{x}_{ji}^d\|)$ in the control $\mathbf{f}_j$ connects the robot j to the robot i because $i \in \mathcal{N}_j$ iff $j \in \mathcal{N}_i$ for undirected communications.

2. Given bounded actuation (Section 3.1.2), a saturated Proportional control interconnects each robot with its proxy while a gradient-based control couples the proxies of two initially adjacent robots symmetrically. In particular, the saturated Proportional control $-P_i\widetilde{\mathbf{x}}_i$ in (3.14) and $\mathrm{Sat}_i(P_i\widetilde{\mathbf{x}}_i)$ in (3.12) interconnect the robot i with its proxy. Further, the gradient terms $-\nabla_i\widehat{\psi}(\|\widehat{\mathbf{x}}_{ij}^d\|)$ and $-\nabla_j\widehat{\psi}(\|\widehat{\mathbf{x}}_{ij}^d\|)$ mutually couple the proxies of the initially adjacent robots i and j according to (3.12). In this context, the adjacent robots are interconnected indirectly through their proxies.

3.2 Experiments

This section compares the controllers, proposed in (3.3) for time-delay robot networks with full actuation, and in (3.12) plus (3.14) for time-delay robot networks with

limited actuation, to conventional P+d control [174] through experiments[1] with $N = 3$ Geomagic Touch haptic robots shown in Figure 3.1. Each robot can drive its end-effector with 3 actuated joints: An inner-loop controller for gravity compensation in joint space; and an outer-loop controller for synchronization in task space.

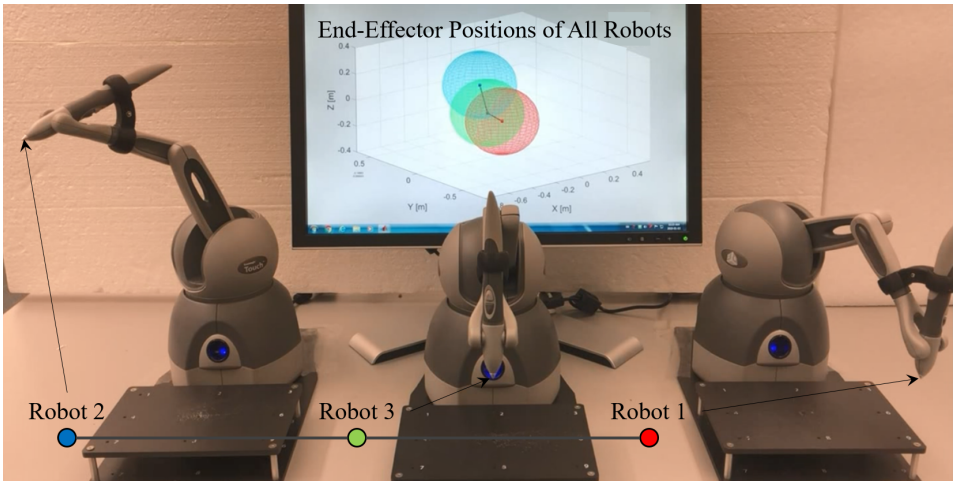

Figure 3.1: The experimental setup for connectivity-preserving synchronization of time-delay robot networks.

The experimental robots are initially at rest at $\mathbf{x}_1(0) = (-150, -100, -100)^\mathsf{T}$ mm, $\mathbf{x}_2(0) = (-150, 150, 120)^\mathsf{T}$ mm, $\mathbf{x}_3(0) = (-200, 0, -50)^\mathsf{T}$ mm. Their communication radius is $r = 250$ mm. Hence, the robots 1 and 3, and the robots 2 and 3 are initially adjacent, i.e., $\mathcal{E}(0) = \{(1, 3), (2, 3)\}$, see the dark grey lines in Figure 3.1. The time-varying communication delays $T_{ij}(t)$ are up to $\overline{T}_{ij} = 5$ ms.

P+d Control [174]

Let the parameters giving the synchronizing Proportional gains be $p_i = 1$, $\omega_{13} = \omega_{31} = 200$ and $\omega_{23} = \omega_{32} = 0.5$. If the communication distances of robots are unlimited, conventional P+d control with the damping gains $d_1 = 8$, $d_2 = 5$ and $d_3 = 3$ stably synchronizes the robot network. However, it cannot synchronize the three robots with the given communication radius $r = 250$ mm. Because the robot 3 has a much stiffer coupling to the robot 1 than to the robot 2, it moves away from the robot 2 so quickly that the distance between them increases to about 300 mm before the robot 2 can track it, see Figure 3.2. The controller cannot maintain the initial communication link $(2, 3)$. As a result, the network loses connectivity. The robot 2

[1] `https://youtu.be/P5sY_8l0ihw`

becomes isolated and the controller cannot synchronize it with the other two robots, as seen in Figure 3.2(b). This experiment verifies that the connectivity of robot networks whose robots have limited communication distances must be guaranteed during synchronization.

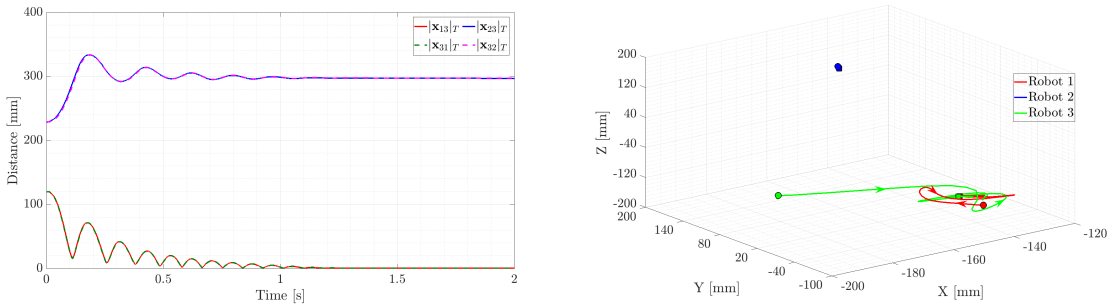

(a) The inter-robot distances.

(b) The end-effector paths.

Figure 3.2: The experimental inter-robot distances and end-effector paths of three robots under conventional P+d synchronization control.

The Proposed Control (3.3)

After setting $Q = 0.0047$ as required in Lemma 3.1, $P = 0.2$ is tuned heuristically to couple all initially adjacent robots. In the presence of friction in joints and inaccurate velocity measurements, the local damping gains which practically stabilize robots are selected by $K_1 = K_2 = 3$ and $K_3 = 6$. Figure 3.3(a) verifies that the proposed gradient plus damping control (3.3) restricts the distances between the robots 1 and 3, and between the robots 2 and 3, below r. Hence, it preserves all initial links, $(1, 3)$ and $(2, 3)$, during synchronization. Its gradient terms $\nabla_i \psi(\|\mathbf{x}_{ij}^d\|)$ make the inter-robot couplings more compliant when the inter-robot distances decrease. The parameters P and Q can reduce overshoots by weakening initially stiff couplings. However, they make the inter-robot couplings over-compliant when the inter-robot distances become small. The compliant inter-robot couplings demand relatively large position errors to balance gravity compensation errors and intrinsic friction in robot joints. Therefore, the three robots can only be driven close to each other in Figure 3.3(b), with steady-state position errors smaller than 30 mm.

The Proposed Control (3.12)-(3.14)

The control force in each direction $k = x, y, z$ is bounded by $\overline{f}_i^k = 0.5$ N for all robots. Each robot $i = 1, 2, 3$ is tightly connected to its proxy by $P_i = 500$ and

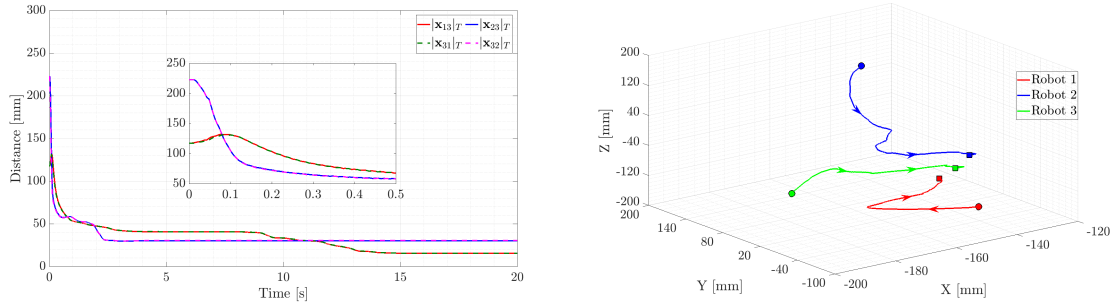

(a) The inter-robot distances. (b) The end-effector paths.

Figure 3.3: The experimental inter-robot distances and end-effector paths of three robots under the proposed gradient plus damping control (3.3).

$K_i = 5$. Given $\widehat{r} = 240$ mm, the selection of $\widehat{Q} = 0.0013$ guarantees the conditions in Lemma 3.2. Then, $\widehat{P} = 0.2$ and $\widehat{K}_i = 24$ practically stabilize the system. All actuators of robots saturate for a certain time during the first 10 s of the synchronization. The actuator force time histories are presented in Figure 3.4. Although the saturation of actuators makes the inter-robot distances fluctuate during the first 10 s, the indirect coupling strategy maintains the distances between the robots 1 and 3 (the red solid line and the green dashed line in Figure 3.5(a)), and between the robots 2 and 3 (the blue solid line and the pink dashed line in Figure 3.5(a)), strictly smaller than their communication distance r and thus, preserves the connectivity of the network. Compared to Figure 3.3(b), it synchronizes all robot end-effectors better, with steady-state errors reduced to about 20 mm in Figure 3.5(b). The parameters $\widehat{P}$ and $\widehat{Q}$ can be selected to stiffen the inter-proxy couplings even for small inter-proxy distances, and the virtual damping with $\widehat{K}_i$ can be injected to address the delay-induced instability regardless of inaccurate robot velocity measurements.

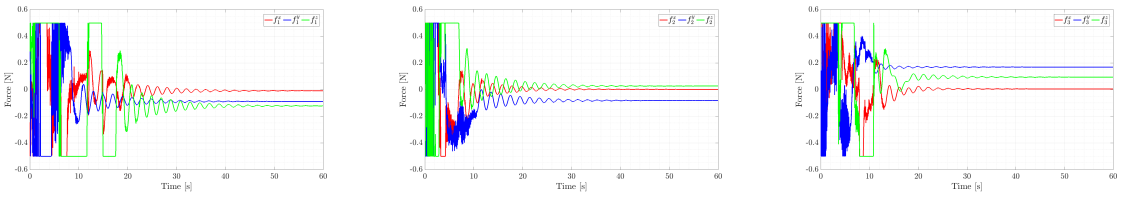

(a) $\mathbf{f}_1 = \left(f_1^x, f_1^y, f_1^z\right)^\mathsf{T}$. (b) $\mathbf{f}_2 = \left(f_2^x, f_2^y, f_2^z\right)^\mathsf{T}$. (c) $\mathbf{f}_3 = \left(f_3^x, f_3^y, f_3^z\right)^\mathsf{T}$.

Figure 3.4: The control forces $\mathbf{f}_i = \left(f_i^x, f_i^y, f_i^z\right)^\mathsf{T}$ of all robots $i = 1, 2, 3$.

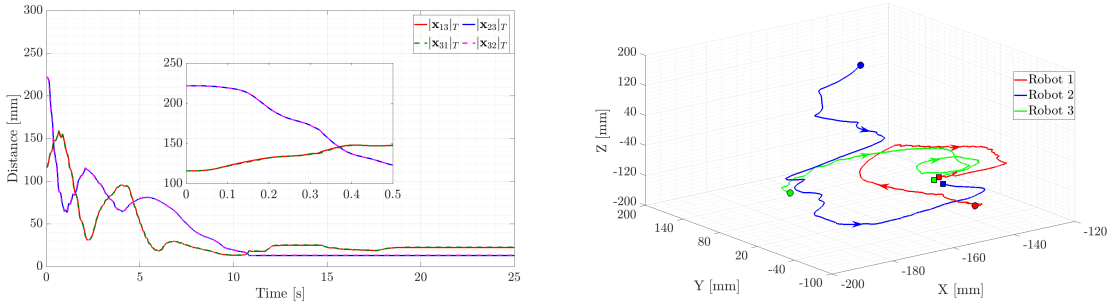

(a) The inter-robot distances.

(b) The end-effector paths.

Figure 3.5: The experimental inter-robot distances and end-effector paths of three robots under the proposed indirect coupling strategy (3.12)-(3.14).

3.3 Conclusions

This chapter has investigated the impact of time-varying delays and actuator saturation on connectivity-preserving synchronization of EL robot networks. For time-delay robot networks with unbounded actuation, this chapter has proposed a gradient plus damping control that modulates the inter-robot connections dynamically and injects damping locally to preserve connectivity during synchronization. For time-delay robot networks with bounded actuation, this chapter has developed an indirect coupling strategy that decomposes the inter-robot couplings into the robot-proxy and inter-proxy couplings, and overcomes actuator saturation in the former and time-varying delays in the latter. The experiments with three Geomagic Touch haptic robots have validated the proposed designs.

Chapter 4

Passive Multi-User Teleoperation of a Multi-Robot System With Connectivity-Preserving Containment

This chapter enables multi-user teleoperation of a remote multi-robot system through a control strategy that: robustly synchronizes a multi-robot system with a tree topology and proximity-limited 1-hop intra-network communications; permits multiple users to tele-guide the multi-robot system and to feel actions of other users over time-delay communication channels between the users' local robots and the remote multi-robot system; and enforces steady-state containment by driving the multi-robot system to the convex hull spanned by all local robots held stationary by users. A control design, proactively addressing practical requirements on the connectivity of the multi-robot system and on the passivity of the multi-local robot-remote multi-robot system teleoperator, ensures effective coordination and safe teleoperation. A suitable decomposition of the teleoperator into interconnected subsystems facilitates a dynamic feedforward-feedback passivation strategy that guarantees stable teleoperation and steady-state containment. The analysis of storage functions, and thus input-output relations, of all subsystems and their interconnections proves fruitful properties of the design. Two comparative experiments in a teleoperation testbed with 4 local and 10 remote robots validate its practical efficacy.

4.1 Dynamic Feedforward-Feedback Passivation

An innovative decomposition of the overall teleoperator dynamics permits to integrate the connectivity of the remote robot network and the passivity of the closed-loop teleoperation system into a unified paradigm. This section introduces the new decomposition in steps, starting with a control design for delay-free teleoperation. It then augments the design to incorporate time-delay communications between local robots and the remote multi-robot system. The analyses of steady-state teleoperation and of containment control end this section.

Let a bilateral teleoperator have N_l local robots and a remote multi-robot system with N_r remote robots, $N_r \geq N_l \geq 1$. The communication network of the multi-robot system is encoded by $\mathcal{G}(t) = \{\mathcal{V}, \mathcal{E}(t)\}$, in which $\mathcal{V} = \{1, \cdots, N_r\}$ collects indices of all remote robots. Further, let the local robot i be connected to the remote robot i across the Internet. Then, the first N_l remote robots are leaders and the remaining $N_r - N_l$ remote robots are followers. With local gravity compensation, the EL dynamics of the local robots are

$$\mathbf{M}_{li}(\mathbf{x}_{li})\ddot{\mathbf{x}}_{li} + \mathbf{C}_{li}(\mathbf{x}_{li}, \dot{\mathbf{x}}_{li})\dot{\mathbf{x}}_{li} = \mathbf{f}_{li} + \mathbf{f}_{hi} \tag{4.1}$$

for $i = 1, \cdots, N_l$, and the EL dynamics of the remote robots are

$$\mathbf{M}_{ri}(\mathbf{x}_{ri})\ddot{\mathbf{x}}_{ri} + \mathbf{C}_{ri}(\mathbf{x}_{ri}, \dot{\mathbf{x}}_{ri})\dot{\mathbf{x}}_{ri} = \mathbf{f}_{ri} \tag{4.2}$$

for $i = 1, \cdots, N_r$, where $\mathbf{f}_*$ with the subscript $* \in \{li, ri\}$ are the control inputs of corresponding robots; and $\mathbf{f}_{hi}$ is the force applied by the human user i on their local robot $i = 1, \cdots, N_l$.

Let the communication range of all remote robots be $r > 0$. Then, the remote robots i and j can exchange information at time $t \geq 0$ if they are within the distance $\|\mathbf{x}_{rij}(t)\| < r$ of each other, where $\mathbf{x}_{rij}(t) = \mathbf{x}_{ri}(t) - \mathbf{x}_{rj}(t)$. Notably, every two initially non-adjacent remote robots $(i, j) \notin \mathcal{E}(0)$ are not allowed to interact at a later time $t \geq 0$ even if $\|\mathbf{x}_{rij}(t)\| < r$. This condition streamlines the presentation, although is not required by the proposed design. Instead, the design relies on the following assumptions.

Assumption 4.1. *The human users are passive, i.e.,* $\int_0^t \dot{\mathbf{x}}_{li}^{\mathsf{T}}(\tau)\mathbf{f}_{hi}(\tau)d\tau < +\infty$ *for* $i = 1, \cdots, N_l$ *and* $t \geq 0$.

Assumption 4.2. *The user forces are bounded by* $|\mathbf{f}_{hi}(t)| \leq \overline{\mathbf{f}}_{hi}$ *component-wisely, and have finite time derivatives* $\left\|\dot{\mathbf{f}}_{hi}(t)\right\| < +\infty$, $\forall i = 1, \cdots, N_l$.

Assumption 4.3. *The remote multi-robot system is initially at rest, i.e.,* $\dot{\mathbf{x}}_{ri}(0) = \mathbf{0}$, $\forall i = 1, \cdots, N_r$.

Assumption 4.4. *The initial communication network* $\mathcal{G}(0)$ *of the remote multi-robot system is a tree, and* $\|\mathbf{x}_{rij}(0)\| < r - \epsilon$ *with* $\epsilon > 0$ *for all* $(i, j) \in \mathcal{E}(0)$.

Assumption 4.5. *The time-varying communication delays* $T_*(t)$ *between the local robots and the remote multi-robot system are bounded and have finite time derivatives, i.e.,* $0 \leq T_*(t) \leq \overline{T}_* < +\infty$ *and* $\left|\dot{T}_*(t)\right| < +\infty$ *for* $* = li, ri$ *with* $\forall i = 1, \cdots, N_l$ *and* $\forall t \geq 0$.

Because the proposed design preserves all initial communication links, the communication network of the remote multi-robot system is invariant, $\mathcal{G}(t) = \mathcal{G}(0)$, $\forall t \geq 0$. Hence, the remainder of this chapter indicates the degree, adjacency, incidence and edge Laplacian matrices of the remote multi-robot network $\mathcal{G}(t)$ by $\mathbf{D}$, $\mathbf{A}$, $\mathbf{B}$ and $\mathbf{L}_e$, respectively, without time arguments.

4.1.1 Teleoperation With No Delay

This section develops a passivity-based control that ensures the connectivity of the remote multi-robot system and the passivity of the teleoperator in this order of priority. Two lemmas summarize conditions for selecting and updating various control gains.

4.1.1.1 Controller Design

For every remote robot $i = 1, \cdots, N_r$, define a sliding variable $\mathbf{s}_i$ by

$$\mathbf{s}_i = \begin{cases} \dot{\mathbf{x}}_{ri} + \sigma\boldsymbol{\theta}_{ri} + \eta\boldsymbol{\theta}_{lri}, & i = 1, \cdots, N_l, \\ \dot{\mathbf{x}}_{ri} + \sigma\boldsymbol{\theta}_{ri}, & i = N_l + 1, \cdots, N_r, \end{cases} \tag{4.3}$$

where σ and η are positive constants, $\boldsymbol{\theta}_{lri}$ connects the leader remote robot i to its associated local robot i by $\boldsymbol{\theta}_{lri} = \overline{\mathbf{F}}_{hi} \cdot \tanh\left[K_{lri}(\mathbf{x}_{ri} - \mathbf{x}_{li})\right]$ with $\overline{\mathbf{F}}_{hi} = \operatorname{diag}\left\{\overline{\mathbf{f}}_{hi}\right\}$, $K_{lri} > 0$, and $\boldsymbol{\theta}_{ri}$ couples the remote robot i to its neighbours $j \in \mathcal{N}_i$ by $\boldsymbol{\theta}_{ri} =$

$\sum_{j\in\mathcal{N}_i}\nabla_i\psi(\|\mathbf{x}_{rij}\|)$ with the partial derivative of $\psi(\|\mathbf{x}_{rij}\|)$ with respect to $\mathbf{x}_{ri}$,

$$\nabla_i\psi(\|\mathbf{x}_{rij}\|)=\frac{2P(r^2+Q)}{\left(r^2-\|\mathbf{x}_{rij}\|^2+Q\right)^2}(\mathbf{x}_{ri}-\mathbf{x}_{rj}),$$

$P>0$ and $Q>0$, where the potential function $\psi(\|\mathbf{x}_{rij}\|)$, similar to (3.2), is given by

$$\psi(\|\mathbf{x}_{rij}\|)=\frac{P\|\mathbf{x}_{rij}\|^2}{r^2-\|\mathbf{x}_{rij}\|^2+Q}.$$

Note that $\psi(\|\mathbf{x}_{rij}\|)$ is strictly increasing and bounded by $0\leq\psi(\|\mathbf{x}_{rij}\|)<\psi_{\max}=Pr^2/Q$ for $\|\mathbf{x}_{rij}\|<r$.

Let $\mathbf{L}(\mathbf{x}_r)=\left[l_{ij}(\mathbf{x}_r)\right]$ be an $N_r\times N_r$ weighted Laplacian matrix of the tree network of the remote robots, where the (i,j)-th element $l_{ij}(\mathbf{x}_r)$ is given by

$$l_{ij}(\mathbf{x}_r)=\begin{cases}-\frac{2P(r^2+Q)}{(r^2-\|\mathbf{x}_{rij}\|^2+Q)^2}, & j\neq i \text{ and } j\in\mathcal{N}_i,\\ 0, & j\neq i \text{ and } j\notin\mathcal{N}_i,\\ -\sum_{k\neq i}l_{ik}(\mathbf{x}_r), & j=i.\end{cases}$$

The notation $\mathbf{L}(\mathbf{x}_r)$ of the weighted Laplacian matrix indicates its dependency on the remote robot positions $\mathbf{x}_r=\left(\mathbf{x}_{r1}^\mathsf{T},\cdots,\mathbf{x}_{rN_r}^\mathsf{T}\right)^\mathsf{T}$ because $l_{ij}(\mathbf{x}_r)=l_{ji}(\mathbf{x}_r)$ depends on the distance $\|\mathbf{x}_{rij}\|$ between a pair of adjacent remote robots $(i,j)\in\mathcal{E}$. Let $\mathbf{l}_i(\mathbf{x}_r)$ be the i-th column of $\mathbf{L}(\mathbf{x}_r)$. It follows then that $\boldsymbol{\theta}_{ri}=\left[\mathbf{l}_i^\mathsf{T}(\mathbf{x}_r)\otimes\mathbf{I}_n\right]\mathbf{x}_r$ for $i=1,\cdots,N_r$.

The sliding variables $\mathbf{s}_i$ in (4.3) for all remote robots can be reorganized into

$$\Pi_1:\quad\dot{\mathbf{x}}_r=-\sigma\left[\mathbf{L}(\mathbf{x}_r)\otimes\mathbf{I}_n\right]\mathbf{x}_r+\mathbf{s}-\eta\mathbf{u}_{lr},\tag{4.4}$$

where $\mathbf{L}^\mathsf{T}(\mathbf{x}_r)=\mathbf{L}(\mathbf{x}_r)$, and $\mathbf{s}-\eta\mathbf{u}_{lr}$ is the input to the dynamical system Π_1 in Figure 4.1(a), with $\mathbf{s}=\left(\mathbf{s}_1^\mathsf{T},\cdots,\mathbf{s}_{N_r}^\mathsf{T}\right)^\mathsf{T}$ and $\mathbf{u}_{lr}=\left(\boldsymbol{\theta}_{lr1}^\mathsf{T},\cdots,\boldsymbol{\theta}_{lrN_l}^\mathsf{T},\mathbf{0}^\mathsf{T}\right)^\mathsf{T}$. They also convert the remote robot dynamics (4.2) into

$$\mathbf{M}_{ri}(\mathbf{x}_{ri})\dot{\mathbf{s}}_i+\mathbf{C}_{ri}(\mathbf{x}_{ri},\dot{\mathbf{x}}_{ri})\mathbf{s}_i=\sigma\boldsymbol{\Delta}_{rri}+\eta\boldsymbol{\Delta}_{lri}+\mathbf{f}_{ri},\tag{4.5}$$

where the mismatched dynamics resulting from the inter-remote robot and local robot-remote robot couplings are $\boldsymbol{\Delta}_{rri}=\mathbf{M}_{ri}(\mathbf{x}_{ri})\dot{\boldsymbol{\theta}}_{ri}+\mathbf{C}_{ri}(\mathbf{x}_{ri},\dot{\mathbf{x}}_{ri})\boldsymbol{\theta}_{ri}$ and $\boldsymbol{\Delta}_{lri}=\mathbf{M}_{ri}(\mathbf{x}_{ri})\dot{\boldsymbol{\theta}}_{lri}+\mathbf{C}_{ri}(\mathbf{x}_{ri},\dot{\mathbf{x}}_{ri})\boldsymbol{\theta}_{lri}$ if $i=1,\cdots,N_l$, and $\boldsymbol{\Delta}_{lri}=\mathbf{0}$ otherwise, respectively.

Let the controllers of the remote robots $i = 1, \cdots, N_r$ be

$$\mathbf{f}_{ri} = -K_{ri}(t)\mathbf{s}_i - D_{ri}\dot{\mathbf{x}}_{ri}, \tag{4.6}$$

where the gains $D_{ri} > 0$ and $K_{ri}(t)$ are scalars to be determined. After stacking the mismatched dynamics $\boldsymbol{\Delta}_{rri}$ and $\boldsymbol{\Delta}_{lri}$ of all remote robots into

$$\boldsymbol{\Delta}_r = \left(\sigma\boldsymbol{\Delta}_{rr1}^{\mathsf{T}} + \eta\boldsymbol{\Delta}_{lr1}^{\mathsf{T}}, \cdots, \sigma\boldsymbol{\Delta}_{rrN_r}^{\mathsf{T}} + \eta\boldsymbol{\Delta}_{lrN_r}^{\mathsf{T}}\right)^{\mathsf{T}}, \tag{4.7}$$

and combining their inertia and Christoffel matrices into $\mathbf{M}_r(\mathbf{x}_r) = \mathrm{Diag}\{\mathbf{M}_{ri}(\mathbf{x}_{ri})\}$ and $\mathbf{C}_r(\mathbf{x}_r, \dot{\mathbf{x}}_r) = \mathrm{Diag}\{\mathbf{C}_{ri}(\mathbf{x}_{ri}, \dot{\mathbf{x}}_{ri})\}$, the remote robot dynamics (4.5) under the control (4.6) become

$$\Pi_2: \quad \mathbf{M}_r(\mathbf{x}_r)\dot{\mathbf{s}} + \mathbf{C}_r(\mathbf{x}_r, \dot{\mathbf{x}}_r)\mathbf{s} = \boldsymbol{\Delta}_r - \mathbf{K}_r(t)\mathbf{s} - \mathbf{D}_r\dot{\mathbf{x}}_r \tag{4.8}$$

with $\mathbf{K}_r(t) = \mathrm{Diag}\{K_{ri}(t)\mathbf{I}_n\}$ and $\mathbf{D}_r = \mathrm{Diag}\{D_{ri}\mathbf{I}_n\}$. The dynamical system Π_2 has the state $\mathbf{s}$, the dynamic feedback $-\mathbf{K}_r(t)\mathbf{s}$, the input $-\mathbf{D}_r\dot{\mathbf{x}}_r$ and is perturbed by $\boldsymbol{\Delta}_r$, see Figure 4.1(b).

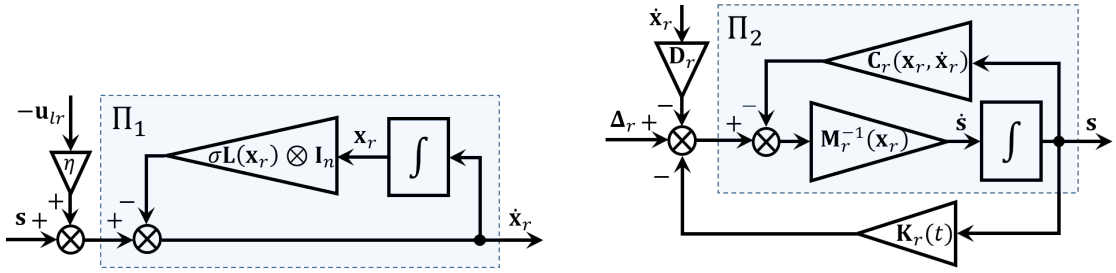

(a) The input-output diagram of Π_1. (b) The input-output diagram of Π_2.

Figure 4.1: The input-output diagrams of the systems Π_1 in (4.4) and Π_2 in (4.8).

Therefore, the sliding variables $\mathbf{s}_i$ in (4.3) restructure the remote multi-robot system (4.2) under the control of (4.6) into a negative feedback interconnection Π_3 of Π_1 in (4.4) and Π_2 in (4.8): the output $\mathbf{s}$ of Π_2 is the input to Π_1, and the output $\dot{\mathbf{x}}_r$ of Π_1 is negatively fed back to Π_2. As shown in Figure 4.2(a), the feedback interconnected system Π_3 has two inputs: (i) $-\mathbf{u}_{lr}$, from the couplings between the local robots and the remote multi-robot system; and (ii) $\boldsymbol{\Delta}_r$, the uncertainty in the reshaped dynamics of the remote multi-robot system.

The force feedback to every user $i = 1, \cdots, N_l$ is obtained by connecting their

local robot i to their associated leader remote robot i via

$$\mathbf{f}_{li} = \boldsymbol{\theta}_{lri} - D_{li}\dot{\mathbf{x}}_{li} \tag{4.9}$$

with $D_{li} > 0$. With $\mathbf{M}_l(\mathbf{x}_l) = \text{Diag}\{\mathbf{M}_{li}(\mathbf{x}_{li})\}$ and $\mathbf{C}_l(\mathbf{x}_l, \dot{\mathbf{x}}_l) = \text{Diag}\{\mathbf{C}_{li}(\mathbf{x}_{li}, \dot{\mathbf{x}}_{li})\}$, all local robots (4.1) under the control of (4.9) form

$$\Pi_4 : \quad \mathbf{M}_l(\mathbf{x}_l)\ddot{\mathbf{x}}_l + \mathbf{C}_l(\mathbf{x}_l, \dot{\mathbf{x}}_l)\dot{\mathbf{x}}_l = \mathbf{f}_h + \mathbb{I}\mathbf{u}_{lr} - \mathbf{D}_l\dot{\mathbf{x}}_l, \tag{4.10}$$

where $\mathbf{x}_l = \left(\mathbf{x}_{l1}^\mathsf{T}, \cdots, \mathbf{x}_{lN_l}^\mathsf{T}\right)^\mathsf{T}$ and $\mathbf{f}_h = \left(\mathbf{f}_{h1}^\mathsf{T}, \cdots, \mathbf{f}_{hN_l}^\mathsf{T}\right)^\mathsf{T}$ group the positions and user forces of all local robots, and $\mathbb{I} = \left[\mathbf{I}_{N_l}\ \mathbf{0}_{N_l \times (N_r - N_l)}\right] \otimes \mathbf{I}_n$ and $\mathbf{D}_l = \text{Diag}\{D_{li}\mathbf{I}_n\}$. As seen in Figure 4.2(b), the dynamical system Π_4 has: two inputs, $\mathbf{f}_h$ from all users and $\mathbf{u}_{lr}$ from all couplings between the local robots and the remote multi-robot system; and one output, $\dot{\mathbf{x}}_l$.

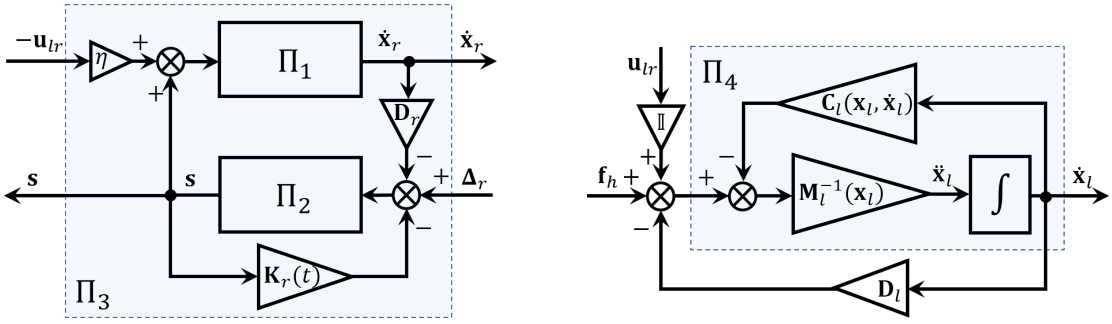

(a) The input-output diagram of Π_3.

(b) The input-output diagram of Π_4.

Figure 4.2: The input-output diagrams: (a) of the remote multi-robot system Π_3 (the feedback interconnection of Π_1 and Π_2); and (b) of the local robots Π_4.

4.1.1.2 Connectivity Maintenance

This section shows that, with no prerequisite for the closed-loop passivity, the connectivity of the remote multi-robot system can be preserved by selecting appropriate gains for the designed system Π_3. Maintaining the tree network $\mathcal{G}(t)$ of the remote robots is equivalent to rendering the edge set $\mathcal{E}(t)$ invariant. Therefore, the proof shows how to choose gains to shape the energy production of Π_3 to guarantee that all remote robots that are initially adjacent remain adjacent throughout time, i.e., $\|\mathbf{x}_{rij}(t)\| < r$, $\forall (i,j) \in \mathcal{E}(0)$ and $\forall t \geq 0$.

Because Π_3 is a negative feedback interconnection of Π_1 and Π_2, see Figure 4.2(a),

its energy production depends on the energy productions of Π_1 and Π_2. Define the storage function of the system Π_1 by

$$V_1 = \frac{\sigma}{2}\sum_{i=1}^{N_r}\sum_{j\in\mathcal{N}_i}\psi(\|\mathbf{x}_{rij}\|). \tag{4.11}$$

After stacking all $\boldsymbol{\theta}_{ri}$, $i = 1, \cdots, N_r$ into $\boldsymbol{\theta}_r$ by $\boldsymbol{\theta}_r = (\boldsymbol{\theta}_{r1}^\mathsf{T}, \cdots, \boldsymbol{\theta}_{rN_r}^\mathsf{T})^\mathsf{T} = [\mathbf{L}(\mathbf{x}_r)\otimes\mathbf{I}_n]\mathbf{x}_r$, the time derivative of V_1 along the dynamics (4.4) of Π_1 is

$$\begin{aligned}\dot{V}_1 =&\sigma\sum_{i=1}^{N_r}\sum_{j\in\mathcal{N}_i}\dot{\mathbf{x}}_{ri}^\mathsf{T}\nabla_i\psi(\|\mathbf{x}_{rij}\|) = \sigma\sum_{i=1}^{N_r}\dot{\mathbf{x}}_{ri}^\mathsf{T}\boldsymbol{\theta}_{ri} = \sigma\dot{\mathbf{x}}_r^\mathsf{T}\boldsymbol{\theta}_r = \sigma\dot{\mathbf{x}}_r^\mathsf{T}\big[\mathbf{L}(\mathbf{x}_r)\otimes\mathbf{I}_n\big]\mathbf{x}_r\\ =&\dot{\mathbf{x}}_r^\mathsf{T}\big(\mathbf{s}-\eta\mathbf{u}_{lr}-\dot{\mathbf{x}}_r\big) = \dot{\mathbf{x}}_r^\mathsf{T}\mathbf{s}-\eta\dot{\mathbf{x}}_r^\mathsf{T}\mathbf{u}_{lr}-\dot{\mathbf{x}}_r^\mathsf{T}\dot{\mathbf{x}}_r,\end{aligned} \tag{4.12}$$

which implies that the dynamical system Π_1 is output strictly passive with the input $\mathbf{s}-\eta\mathbf{u}_{lr}$ and the output $\dot{\mathbf{x}}_r$.

Further, let the storage function of Π_2 be the following anisotropic scaling of its kinetic energy:

$$V_2 = \frac{1}{2}\sum_{i=1}^{N_r}\frac{1}{D_{ri}}\mathbf{s}_i^\mathsf{T}\mathbf{M}_{ri}(\mathbf{x}_{ri})\mathbf{s}_i. \tag{4.13}$$

After using Property 1.2, the time derivative of V_2 along the dynamics (4.8) of Π_2 is

$$\begin{aligned}\dot{V}_2 =&\sum_{i=1}^{N_r}\frac{1}{D_{ri}}\mathbf{s}_i^\mathsf{T}\big[\sigma\boldsymbol{\Delta}_{rri}+\eta\boldsymbol{\Delta}_{lri}-K_{ri}(t)\mathbf{s}_i-D_{ri}\dot{\mathbf{x}}_{ri}\big]\\ =&\mathbf{s}^\mathsf{T}\mathbf{D}_r^{-1}\boldsymbol{\Delta}_r-\mathbf{s}^\mathsf{T}\dot{\mathbf{x}}_r-\mathbf{s}^\mathsf{T}\mathbf{D}_r^{-1}\mathbf{K}_r(t)\mathbf{s},\end{aligned} \tag{4.14}$$

which implies that the dynamical system Π_2 is output strictly passive with the input $\boldsymbol{\Delta}_r-\mathbf{D}_r\dot{\mathbf{x}}_r$ and the output $\mathbf{s}$.

Then, the storage function of the system Π_3 is defined by

$$V_3 = V_1 + V_2, \tag{4.15}$$

which, by (4.12) and (4.14), varies according to

$$\dot{V}_3 = \mathbf{s}^\mathsf{T}\mathbf{D}_r^{-1}\boldsymbol{\Delta}_r-\eta\dot{\mathbf{x}}_r^\mathsf{T}\mathbf{u}_{lr}-\dot{\mathbf{x}}_r^\mathsf{T}\dot{\mathbf{x}}_r-\mathbf{s}^\mathsf{T}\mathbf{D}_r^{-1}\mathbf{K}_r(t)\mathbf{s}, \tag{4.16}$$

where the zero sum of $\dot{\mathbf{x}}_r^\mathsf{T}\mathbf{s}$ in $\dot{V}_1$ and $-\mathbf{s}^\mathsf{T}\dot{\mathbf{x}}_r$ in $\dot{V}_2$ proves that the negative feedback

interconnection of Π_1 and Π_2 (see Figure 4.2(a)) is power-preserving. Equation (4.16) implies that Π_3 is output strictly passive with the input $\big(-\mathbf{u}_{lr}^{\mathsf{T}}, \boldsymbol{\Delta}_r^{\mathsf{T}}\big)^{\mathsf{T}}$ and the output $\big(\dot{\mathbf{x}}_r^{\mathsf{T}}, \mathbf{s}^{\mathsf{T}}\big)^{\mathsf{T}}$.

Proposition 4.1. *Under Assumption 4.4 and given any $\Delta > 0$, choose Q and P by $[r^2-(N_r-1)(r-\epsilon)^2]Q+[r^2-(r-\epsilon)^2]r^2 > 0$ and $[r^2-(r-\epsilon)^2+Q]Pr^2-(N_r-1)(r-\epsilon)^2PQ > [r^2-(r-\epsilon)^2+Q]Q\Delta$. It ensures then that $V_1(0)+\Delta < \sigma Pr^2/Q = \sigma\psi_{\max}$.*

Proof. Assumption 4.4 and the definition of $\psi(\|\mathbf{x}_{rij}\|)$ imply that $V_1(0) < \sigma P(N_r - 1)(r-\epsilon)^2/[r^2-(r-\epsilon)^2+Q]$, where $N_r - 1$ is the number of links in $\mathcal{G}(0)$. Let $\omega = \sigma P/([r^2-(r-\epsilon)^2+Q]\,Q) > 0$. It follows then that $\sigma\psi_{\max} - V_1(0) \geq \sigma Pr^2/Q - \sigma P(N_r-1)(r-\epsilon)^2/[r^2-(r-\epsilon)^2+Q] = \omega[r^2\,(r^2-(r-\epsilon)^2+Q) - (N_r-1)(r-\epsilon)^2Q] = \omega\big([r^2-(N_r-1)(r-\epsilon)^2]\,Q+[r^2-(r-\epsilon)^2]\,r^2\big) > 0$ can be ensured by selecting $Q > 0$ as required. Afterthat, choosing $P > 0$ as required can make $V_1(0)+\Delta < \sigma\psi_{\max}$. ■

Proposition 4.2. *Under Assumption 4.4 and given any $\Delta > 0$, select Q and P as required in Proposition 4.1. At any time $t \geq 0$, if $V_1(\tau) \leq V_1(0)+\Delta$, $\forall\tau \in [0,t]$, then $\|\mathbf{x}_{ij}(t)\| < r$ for every $(i,j) \in \mathcal{E}(0)$.*

Proof. By Proposition 4.1, $V_1(\tau) \leq V_1(0)+\Delta$ implies that $V_1(\tau) < \sigma\psi_{\max}$, $\forall\tau \in [0,t]$. Assumption 4.4 and the property of $\psi(\|\mathbf{x}_{rij}\|)$ further lead to $0 \leq \psi(\|\mathbf{x}_{ij}(0)\|) < \psi_{\max}$, $\forall(i,j) \in \mathcal{E}(0)$. Suppose that, at time t, the link (i,j) has among all links in $\mathcal{E}(0)$ the maximal length $\|\mathbf{x}_{ij}(t)\| = r$. Then, $\psi(\|\mathbf{x}_{ij}(t)\|) = \psi_{\max}$ and $0 \leq \psi(\|\mathbf{x}_{lm}(t)\|) \leq \psi_{\max}$ for any other $(l,m) \in \mathcal{E}(0)$ because $\|\mathbf{x}_{lm}(t)\| \leq r$ and $\psi(\cdot)$ is continuous, positive definite and strictly increasing on $[0,r]$. Hence, $V_1(t) = \sigma\psi(\|\mathbf{x}_{ij}(t)\|) + \sigma\sum_{(l,m)\in\overline{\mathcal{E}}(0)}\psi(\|\mathbf{x}_{lm}(t)\|) \geq \sigma\psi_{\max}$, where $\overline{\mathcal{E}}(0) = \mathcal{E}(0) - \{(i,j)\}$, which contradicts $V_1(\tau) \leq V_1(0)+\Delta < \sigma\psi_{\max}$. Thus, $\|\mathbf{x}_{ij}(t)\| < r$ for every $(i,j) \in \mathcal{E}(0)$ ■

For connectivity maintenance, V_3 should also be upper-bounded by $\sigma\psi_{\max}$ (by the above two propositions). As shown in the following, V_3 can be limited appropriately by controlling the excess of output passivity of Π_3.

Let $\widetilde{\mathbf{x}}_r = \big[\mathbf{B}^{\mathsf{T}} \otimes \mathbf{I}_n\big]\,\mathbf{x}_r$ and define a diagonal matrix $\mathbf{W}(\mathbf{x}_r)$ whose diagonal collects the weights $l_{ij}(\mathbf{x}_r)$ of $N_r - 1$ edges $(i,j) \in \mathcal{E}$ in the tree network of the remote robots. Thereafter, the edge Laplacian $\mathbf{L}_e$ serves to bound V_1 by

$$V_1 \leq \frac{\sigma k_r}{4\lambda_L}\mathbf{x}_r^{\mathsf{T}}\left[\mathbf{L}^{\mathsf{T}}(\mathbf{x}_r)\mathbf{L}(\mathbf{x}_r) \otimes \mathbf{I}_n\right]\mathbf{x}_r, \tag{4.17}$$

where $k_r = (r^2+Q)/P$, refer to Appendix B for detailed derivations of (4.17). The dynamics in (4.4) and further algebraic manipulations yield $\sigma^2 \mathbf{x}_r^\mathsf{T}[\mathbf{L}^\mathsf{T}(\mathbf{x}_r)\mathbf{L}(\mathbf{x}_r)\otimes \mathbf{I}_n]\mathbf{x}_r = (\mathbf{s}-\eta\mathbf{u}_{lr}-\dot{\mathbf{x}}_r)^\mathsf{T}(\mathbf{s}-\eta\mathbf{u}_{lr}-\dot{\mathbf{x}}_r) \leq 4\dot{\mathbf{x}}_r^\mathsf{T}\dot{\mathbf{x}}_r + 4\mathbf{s}^\mathsf{T}\mathbf{s} + 2\eta^2\mathbf{u}_{lr}^\mathsf{T}\mathbf{u}_{lr}$, and V_3 can thus be linked to the output passivity indices of Π_3 by

$$V_3 \leq \frac{k_r}{2\sigma\lambda_L}\big(2\dot{\mathbf{x}}_r^\mathsf{T}\dot{\mathbf{x}}_r + 2\mathbf{s}^\mathsf{T}\mathbf{s} + \eta^2\mathbf{u}_{lr}^\mathsf{T}\mathbf{u}_{lr}\big) + \frac{1}{2}\mathbf{s}^\mathsf{T}\mathbf{D}_r^{-1}\mathbf{\Lambda}_r\mathbf{s}, \tag{4.18}$$

where $\mathbf{\Lambda}_r = \text{Diag}\{\lambda_{ri}\mathbf{I}_n\}$ with $\lambda_{ri}\mathbf{I}_n \succeq \mathbf{M}_{ri}(\mathbf{x}_{ri})$ for every remote robot $i = 1, \cdots, N_r$.

Similarly, the power supplied to Π_3 via the port $\big(-\mathbf{u}_{lr}, \dot{\mathbf{x}}_r\big)$ can be measured by

$$-4\eta\dot{\mathbf{x}}_r^\mathsf{T}\mathbf{u}_{lr} \leq \dot{\mathbf{x}}_r^\mathsf{T}\dot{\mathbf{x}}_r + 4\eta^2\mathbf{u}_{lr}^\mathsf{T}\mathbf{u}_{lr}. \tag{4.19}$$

The power injected into Π_3 by the mismatched dynamics $\mathbf{\Delta}_r$ resulting from the state transformation (4.5) is upper-bounded in Appendix C by

$$\mathbf{s}^\mathsf{T}\mathbf{D}_r^{-1}\mathbf{\Delta}_r \leq \mathbf{1}_{N_r n}^\mathsf{T}\mathbf{D}_r^{-1}\big[\eta\mathbb{I}^\mathsf{T}\mathbb{I} + \sigma(3\mathbf{D}+2\mathbf{A})\otimes\mathbf{I}_n\big]\dot{\mathbf{x}}_r^2 + \mathbf{s}^\mathsf{T}\mathbf{D}_r^{-1}\mathbf{\Gamma}_1^c(t)\mathbf{s} + \eta^2\bar{\mathbf{f}}_h^\mathsf{T}\mathbb{I}\mathbf{D}_r^{-1}\mathbb{I}^\mathsf{T}\bar{\mathbf{f}}_h, \tag{4.20}$$

where $\mathbf{\Gamma}_1^c(t) = \eta\mathbb{I}^\mathsf{T}\mathbf{\Gamma}_{lr}^c(t)\mathbb{I} + \sigma\mathbf{\Gamma}_{rr}(t)$, with $\mathbf{\Gamma}_{lr}^c(t)$ a function of the position and velocity differences between the leader remote robots and their associated local robots, and $\mathbf{\Gamma}_{rr}(t)$ a function of the displacements between the remote robots. Note that the i-th main diagonal blocks of both $\mathbf{\Gamma}_{lr}^c(t)$ and $\mathbf{\Gamma}_{rr}(t)$ require solely 1-hop exchanges of the remote robots' states for all $i = 1, \cdots, N_r$.

Following Appendix D, Equations (4.16)-(4.20) together bound the power production of Π_3 by

$$\dot{V}_3 \leq \frac{\eta^2}{8}\bar{\mathbf{f}}_h^\mathsf{T}\mathbb{I}\left(9\mathbf{I}_{N_r n} + 8\mathbf{D}_r^{-1}\right)\mathbb{I}^\mathsf{T}\bar{\mathbf{f}}_h - \frac{\sigma\lambda_L}{4k_r}V_3 - \frac{1}{2}\mathbf{1}_{N_r n}^\mathsf{T}\mathbf{D}_r^{-1}\mathbf{D}_{cr}\dot{\mathbf{x}}_r^2 - \mathbf{s}^\mathsf{T}\mathbf{D}_r^{-1}\mathbf{K}_{cr}(t)\mathbf{s}, \tag{4.21}$$

after using $\mathbf{u}_{lr}^\mathsf{T}\mathbf{u}_{lr} \leq \bar{\mathbf{f}}_h^\mathsf{T}\mathbb{I}\mathbb{I}^\mathsf{T}\bar{\mathbf{f}}_h$, where $\mathbf{D}_{cr} = \mathbf{D}_r - 2\eta\mathbb{I}^\mathsf{T}\mathbb{I} - 2\sigma\big(3\mathbf{D}+2\mathbf{A}\big)\otimes\mathbf{I}_n$ and $\mathbf{K}_{cr}(t) = \mathbf{K}_r(t) - \left(\sigma\lambda_L\mathbf{\Lambda}_r + 2k_r\mathbf{D}_r\right)/(8k_r) - \mathbf{\Gamma}_1^c(t)$. The bound on $\dot{V}_3$ in (4.21) indicates that the maximum rate of energy injection into Π_3 is determined by $\bar{\mathbf{f}}_h$, while the excess/shortage of output passivity of Π_3 depends on V_3, $\dot{\mathbf{x}}_r$ and $\mathbf{s}$. The following lemma defines the level of passivity of Π_3 that guarantees the connectivity of the remote multi-robot system.

Lemma 4.1. *For the remote multi-robot system* (4.2) *under the control of* (4.6)*, select* D_{ri} *and update* $K_{ri}(t)$ *to guarantee that* $\mathbf{D}_r^{-1}\mathbf{D}_{cr}\mathbf{1}_{N_r n} \geq \mathbf{0}$ *and* $\mathbf{K}_{cr}(t) \succeq \mathbf{0}$ *and*

such that

$$V_3(0) + \frac{k_r \eta^2}{2\sigma\lambda_L} \overline{\mathbf{f}}_h^{\mathsf{T}} \mathbb{I}\big(9\mathbf{I}_{N_r n} + 8\mathbf{D}_r^{-1}\big)\mathbb{I}^{\mathsf{T}} \overline{\mathbf{f}}_h < \sigma\psi_{\max}. \tag{4.22}$$

Then, the tree network of the remote robots remains invariant, $\mathcal{E}(t) = \mathcal{E}(0), \forall t \geq 0$.

Proof. The conditions that $\mathbf{D}_r^{-1}\mathbf{D}_{cr}\mathbf{1}_{N_r n} \geq \mathbf{0}$ and $\mathbf{K}_{cr}(t) \succeq \mathbf{0}$ lead to

$$\dot{V}_3 \leq -\frac{\sigma\lambda_L}{4k_r} V_3 + \frac{\eta^2}{8} \overline{\mathbf{f}}_h^{\mathsf{T}} \mathbb{I}\big(9\mathbf{I}_{N_r n} + 8\mathbf{D}_r^{-1}\big)\mathbb{I}^{\mathsf{T}} \overline{\mathbf{f}}_h.$$

Then, applying Grönwall's inequality to it yields

$$V_1(t) \leq V_3(t) \leq \frac{k_r \eta^2}{2\sigma\lambda_L} \overline{\mathbf{f}}_h^{\mathsf{T}} \mathbb{I}\big(9\mathbf{I}_{N_r n} + 8\mathbf{D}_r^{-1}\big)\mathbb{I}^{\mathsf{T}} \overline{\mathbf{f}}_h + V_3(0) \cdot \exp\left(-\frac{\sigma\lambda_L t}{4k_r}\right) < \sigma\psi_{\max},$$

and the tree network of the remote robots is positively invariant by Proposition 4.2. ■

The above proof of connectivity maintenance is by induction on time. Together with $V_2 \geq 0$, Proposition 4.2 gives a sufficient condition for preserving the tree network: $V_3(t) < \sigma\psi_{\max}$ for every $t \geq 0$. Given that $V_3(0) < \sigma\psi_{\max}$ by (4.22), it suffices to prove that $V_3(t) < \sigma\psi_{\max}$ if $V_3(\tau) < \sigma\psi_{\max}$ for all $\tau \in [0, t)$. The assumption that $V_3(\tau) < \sigma\psi_{\max}$ for all $\tau \in [0, t)$, namely, that the edge set $\mathcal{E}$ is invariant during the time interval $[0, t)$, precludes two logical paradoxes in the proof of $V_3(t) < \sigma\psi_{\max}$: (i) that the controller (4.6) of every remote robot i can employ the information of all its initial neighbours $j \in \mathcal{N}_i$ in the tree network; and (ii) that $\|\mathbf{x}_{rij}\| < r$ for every pair of initially adjacent remote robots $(i, j) \in \mathcal{E}(0)$.

All conditions in Lemma 4.1 are feasible by Assumptions 4.3 and 4.4, refer to Appendix E. The assumed tree communication network of the teleoperated multi-robot system leads to (4.17) through $\mathbf{L}_e \succeq \lambda_L \mathbf{I}_{N_r}$. It then contributes to bounding $\dot{V}_3$ by V_3 in (4.21), and thus to connectivity maintenance in Lemma 4.1. Because a spanning tree is fundamental for every connected network, the proposed control paves the way for global connectivity maintenance with switching spanning trees.

The design of the system Π_3 is motivated by the equivalence between maintaining the tree network connectivity of the remote multi-robot system and rendering the associated edge set $\mathcal{E}(t)$ invariant. The potentials $\psi(\|\mathbf{x}_{rij}\|)$ of all initial inter-remote robot links $(i, j) \in \mathcal{E}(0)$ convert the problem of rendering $\mathcal{E}(t)$ invariant into the problem of upper bounding the energy V_3 by $\sigma\psi_{\max}$. Then, the condition (4.22) implies that the connectivity of the remote multi-robot system (indexed by V_3) depends

both on the initial energy $V_3(0)$ of Π_3 and on the energy injected into Π_3 by the local robot-remote robot interconnections $-\mathbf{u}_{lr}$ (with the bounds $\overline{\mathbf{f}}_h$). By (4.15), the dependence on $V_3(0)$ of (4.22) constrains the initial velocities $\dot{\mathbf{x}}_{ri}(0)$ of, and the initial distances $\|\mathbf{x}_{rij}(0)\|$ between, the remote robots. The impact of the local robot-remote robot couplings can be tuned by η^2/σ in (E.2). In the light of (4.4), increasing σ strengthens inter-remote robot connections, and reducing η attenuates the perturbing effect of $-\mathbf{u}_{lr}$. Together, the ratio η^2/σ regulates $\overline{\alpha}$ and, with it, the energy injected into Π_3 by the local robot-remote robot couplings as per (E.2).

The uncertainty $\mathbf{\Delta}_r$ in the dynamics (4.8) of all remote robots, which changes with the their states, is an input to the system Π_3, whose power injection is upper-bounded by (4.20). Because $\mathbf{\Gamma}^c_{lr}(t)$ and $\mathbf{\Gamma}_{rr}(t)$ are time-varying, the condition $\mathbf{K}_{cr}(t) \succeq \mathbf{0}$ imposes that $\mathbf{K}_r(t)$ be updated dynamically. Nevertheless, the update of $\mathbf{K}_r(t)$ is distributed in the sense of implementation because all remote robot controls rely exclusively on 1-hop communications. By the definitions of $\mathbf{\Gamma}_{rr}(t)$ and $\mathbf{\Gamma}^c_{lr}(t)$ in Appendix B, each follower i needs only the positions of its neighbours $j \in \mathcal{N}_i$ in the tree network, and each leader needs the positions of its neighbouring remote robots and the position and velocity of its associated local robot.

In summary, the storage function V_3 can be upper-bounded so as to guarantee the tree network connectivity of the remote multi-robot system. Because $-\mathbf{u}_{lr}$ is an exogenous input to the system Π_3, the power which it injects into Π_3 needs to be measured and compensated by an excess of output passivity of Π_1. A particular challenge is that $-\mathbf{u}_{lr}$ depends on the distances between the leader remote robots and their associated local robots. Dynamically updated damping could dissipate the energy injected into Π_3 via the port $(-\mathbf{u}_{lr}, \dot{\mathbf{x}}_r)$, but the power-preserving interconnection of Π_1 and Π_2 (see in Figure 4.2(a)) prohibits such an update. Therefore, the proposed controller saturates the local robot-remote robot couplings $\boldsymbol{\theta}_{lri}$ to $\overline{\mathbf{f}}_{hi}$ in (4.3). This coupling saturation limits the power injected into Π_3 through the port $(-\mathbf{u}_{lr}, \dot{\mathbf{x}}_r)$ as in (4.19) and further in (4.21), and permits to upper bound the energy V_3 of Π_3 to guarantee the connectivity of the remote multi-robot system with constant damping injection as in Lemma 4.1.

4.1.1.3 Closed-Loop Passivity

This section develops a dynamic feedback passivation strategy for multi-user teleoperation of a remote multi-robot system with connectivity maintained as above. The

energy behaviours of the local robots and local robot-remote robot couplings guide the proposed modulation of inter-remote robot couplings and of local damping injection at the remote robots.

Let the storage Π_4 in (4.10) of the local robots be quantified by the following weighted sum of kinetic energies:

$$V_4 = \frac{\eta}{2}\dot{\mathbf{x}}_l^{\mathsf{T}}\mathbf{M}_l(\mathbf{x}_l)\dot{\mathbf{x}}_l. \tag{4.23}$$

The time derivative of V_4 along the local robot dynamics (4.10),

$$\dot{V}_4 = \eta\dot{\mathbf{x}}_l^{\mathsf{T}}\mathbf{f}_h + \eta\dot{\mathbf{x}}_l^{\mathsf{T}}\mathbb{I}\mathbf{u}_{lr} - \eta\dot{\mathbf{x}}_l^{\mathsf{T}}\mathbf{D}_l\dot{\mathbf{x}}_l, \tag{4.24}$$

shows that Π_4 is output strictly passive with respect to the input $\mathbf{f}_h + \mathbb{I}\mathbf{u}_{lr}$ and the output $\dot{\mathbf{x}}_l$, see Figure 4.2(b).

The controllers (4.9) and (4.6) interconnect the local and remote robots via the inputs $-\eta\mathbf{u}_{lr}$ to Π_1 in (4.4) and $\mathbb{I}\mathbf{u}_{lr}$ to Π_4 in (4.10). Modelling them as a two-port coupling network Π_5 with the power ports $(\dot{\mathbf{x}}_r, \mathbf{u}_{lr})$ and $(\mathbb{I}^{\mathsf{T}}\dot{\mathbf{x}}_l, -\mathbf{u}_{lr})$, see Figure 4.3, the energy of Π_5 can be quantified by

$$V_5 = \eta\sum_{i=1}^{N_l}\int_{\mathbf{0}}^{\mathbf{x}_{lri}} \tanh\left(K_{lri}\boldsymbol{\delta}\right)^{\mathsf{T}}\overline{\mathbf{F}}_{hi}d\boldsymbol{\delta}, \tag{4.25}$$

which is a positive definite function of $\left(\mathbf{x}_{lr1}^{\mathsf{T}}, \cdots, \mathbf{x}_{lrN_l}^{\mathsf{T}}\right)^{\mathsf{T}}$ as $\tanh(\cdot)$ is strictly increasing and odd. The derivative of V_5,

$$\begin{aligned}\dot{V}_5 =& \eta\sum_{i=1}^{N_l}\tanh\left[K_{lri}(\mathbf{x}_{li}-\mathbf{x}_{ri})\right]^{\mathsf{T}}\overline{\mathbf{F}}_{hi}\left(\dot{\mathbf{x}}_{li}-\dot{\mathbf{x}}_{ri}\right) = \eta\sum_{i=1}^{N_l}\boldsymbol{\theta}_{lri}^{\mathsf{T}}\left(\dot{\mathbf{x}}_{ri}-\dot{\mathbf{x}}_{li}\right)\\ =& \eta\left(\boldsymbol{\theta}_{lr1}^{\mathsf{T}}, \cdots, \boldsymbol{\theta}_{lrN_l}^{\mathsf{T}}, \mathbf{0}^{\mathsf{T}}\right)\dot{\mathbf{x}}_r - \eta\left(\boldsymbol{\theta}_{lr1}^{\mathsf{T}}, \cdots, \boldsymbol{\theta}_{lrN_l}^{\mathsf{T}}, \mathbf{0}^{\mathsf{T}}\right)\mathbb{I}^{\mathsf{T}}\dot{\mathbf{x}}_l = \eta\mathbf{u}_{lr}^{\mathsf{T}}\dot{\mathbf{x}}_r - \eta\mathbf{u}_{lr}^{\mathsf{T}}\mathbb{I}^{\mathsf{T}}\dot{\mathbf{x}}_l\end{aligned} \tag{4.26}$$

shows that the two-port network Π_5 is passive (lossless) with respect to the inputs $\left(\dot{\mathbf{x}}_r^{\mathsf{T}}\ \dot{\mathbf{x}}_l^{\mathsf{T}}\mathbb{I}\right)^{\mathsf{T}}$ and the outputs $\left(\mathbf{u}_{lr}^{\mathsf{T}}\ -\mathbf{u}_{lr}^{\mathsf{T}}\right)^{\mathsf{T}}$.

Then, the two-port network obtained by interconnecting Π_3, Π_4 and Π_5 in Figure 4.3 models the multi-local robot-remote multi-robot system teleoperator. Its power port $\left(\mathbf{f}_h, \dot{\mathbf{x}}_l\right)$ is for the physical interaction, and hence for the energy exchange, with human users. Given Assumption 4.1, multi-user teleoperation of the remote multi-robot system will be rendered stable by making the teleoperator passive with

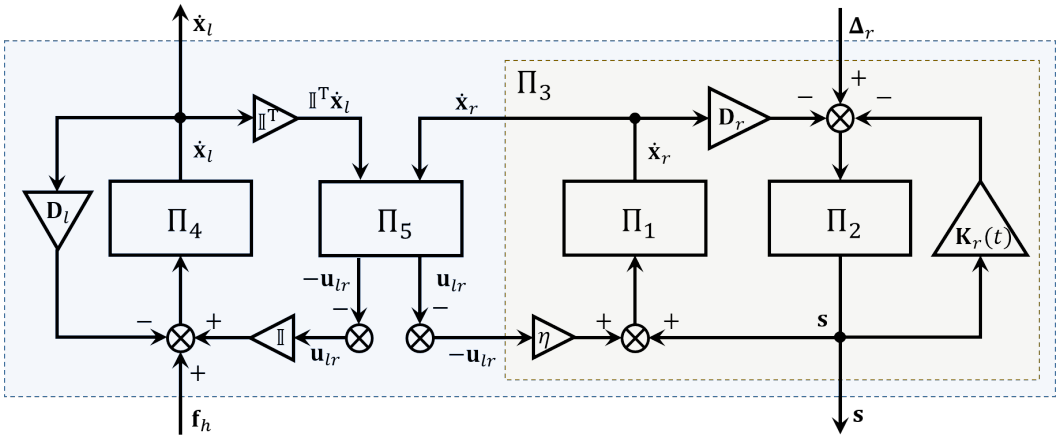

Figure 4.3: A schematic representation of the internal power interconnections of the closed-loop bilateral teleoperator with multiple local and remote robots.

respect to $\left(\mathbf{f}_h, \dot{\mathbf{x}}_l\right)$. To this end, the energy potentially injected by $\boldsymbol{\Delta}_r$ will be dissipated by feedback passivation.

Let the storage function of the teleoperator be

$$V = (V_1 + V_2) + V_4 + V_5 = V_3 + V_4 + V_5, \tag{4.27}$$

where V_i-s are the storage functions of the networks Π_i, $i = 1, \cdots, 5$. By adding (4.16), (4.24) and (4.26), its time derivative becomes

$$\dot{V} = \eta\dot{\mathbf{x}}_l^\mathsf{T}\mathbf{f}_h + \mathbf{s}^\mathsf{T}\mathbf{D}_r^{-1}\boldsymbol{\Delta}_r - \eta\dot{\mathbf{x}}_l^\mathsf{T}\mathbf{D}_l\dot{\mathbf{x}}_l - \dot{\mathbf{x}}_r^\mathsf{T}\dot{\mathbf{x}}_r - \mathbf{s}^\mathsf{T}\mathbf{D}_r^{-1}\mathbf{K}_r(t)\mathbf{s}, \tag{4.28}$$

where $-\eta\dot{\mathbf{x}}_r^\mathsf{T}\mathbf{u}_{lr} + \eta\dot{\mathbf{x}}_l^\mathsf{T}\mathbb{I}\mathbf{u}_{lr} + \eta\mathbf{u}_{lr}^\mathsf{T}\dot{\mathbf{x}}_r - \eta\mathbf{u}_{lr}^\mathsf{T}\mathbb{I}^\mathsf{T}\dot{\mathbf{x}}_l = 0$ confirms that the interconnection of Π_1 and Π_4 through Π_5 is power-preserving. Further, $\dot{V}$ demonstrates that the overall teleoperator is output strictly passive with the inputs $\mathbf{f}_h$ and $\boldsymbol{\Delta}_r$ and the outputs $\dot{\mathbf{x}}_l$, $\dot{\mathbf{x}}_r$ and $\mathbf{s}$, with the output passivity index determined by the control gains $\mathbf{D}_l$, $\mathbf{D}_r$ and $\mathbf{K}_r(t)$.

However, the energy injected by the uncertainty $\boldsymbol{\Delta}_r$ may be unbounded. Because $\boldsymbol{\Delta}_r$ in (4.7) is a function of the states of the teleoeprator, the possible lack of passivity induced by $\boldsymbol{\Delta}_r$ can be approximated by (see Appendix F)

$$\mathbf{s}^\mathsf{T}\mathbf{D}_r^{-1}\boldsymbol{\Delta}_r \leq \eta\dot{\mathbf{x}}_l^\mathsf{T}\mathbb{D}_r\dot{\mathbf{x}}_l + \mathbf{1}_{N_r n}^\mathsf{T}\mathbf{D}_r^{-1}\mathbf{R}\dot{\mathbf{x}}_r^2 + \mathbf{s}^\mathsf{T}\mathbf{D}_r^{-1}\boldsymbol{\Gamma}_1^p(t)\mathbf{s}, \tag{4.29}$$

where $\mathbb{D}_r = \mathbb{I}\mathbf{D}_r^{-1}\mathbb{I}^\mathsf{T}$, $\mathbf{R} = 2\eta\mathbb{I}^\mathsf{T}\mathbb{I} + \sigma\left(3\mathbf{D} + 2\mathbf{A}\right) \otimes \mathbf{I}_n$, and $\boldsymbol{\Gamma}_1^p(t) = \eta\mathbb{I}^\mathsf{T}\boldsymbol{\Gamma}_{lr}^p(t)\mathbb{I} + \sigma\boldsymbol{\Gamma}_{rr}(t)$

a function of the states of the teleoperator that entails dynamic feedback passivation. The inequality (4.29) suggests to rectify the potentially detrimental perturbation $\boldsymbol{\Delta}_r$ through the surplus of output passivity. Using (4.29), the supply rate (4.28) can be further bounded by

$$\dot{V} \leq \eta \dot{\mathbf{x}}_l^{\mathsf{T}} \mathbf{f}_h - \dot{\mathbf{x}}_l^{\mathsf{T}} \widehat{\mathbf{D}}_{pl} \dot{\mathbf{x}}_l - \mathbf{1}_{N_r n}^{\mathsf{T}} \widehat{\mathbf{D}}_{pr} \dot{\mathbf{x}}_r^2 - \mathbf{s}^{\mathsf{T}} \widehat{\mathbf{K}}_{pr}(t) \mathbf{s}, \tag{4.30}$$

where $\widehat{\mathbf{D}}_{pl} = \eta \left(\mathbf{D}_l - \mathbb{D}_r \right)$ and $\widehat{\mathbf{D}}_{pr} = \mathbf{D}_r^{-1} \big(\mathbf{D}_r - \mathbf{R} \big)$ are constant, and $\widehat{\mathbf{K}}_{pr}(t) = \mathbf{D}_r^{-1} \big[\mathbf{K}_r(t) - \boldsymbol{\Gamma}_1^p(t) \big]$ is state-dependent. Therefore, the dynamic feedback can make the teleoperator passive. The following lemma explicitly formulates the selection and update of control gains.

Lemma 4.2. *Consider the teleoperator with multiple local* (4.1) *and remote* (4.2) *robots under the control of* (4.9) *and* (4.6)*. Let D_{li} and D_{ri} be set and $K_{ri}(t)$ be updated to obey all conditions in Lemma 4.1 and to make $\widehat{\mathbf{D}}_{pl} \succeq \mathbf{0}$, $\widehat{\mathbf{D}}_{pr} \mathbf{1}_{N_r n} \geq \mathbf{0}$ and $\widehat{\mathbf{K}}_{pr}(t) \succeq \mathbf{0}$. Then, the teleoperator is passive with respect to the power port $\big(\mathbf{f}_h, \dot{\mathbf{x}}_l \big)$. Further, if $\widehat{\mathbf{D}}_{pl} \succ \mathbf{0}$, $\widehat{\mathbf{D}}_{pr} \mathbf{1}_{N_r n} > \mathbf{0}$ and $\widehat{\mathbf{K}}_{pr}(t) \succ \mathbf{0}$, then $\dot{\mathbf{x}}_l$, $\dot{\mathbf{x}}_r$ and $\mathbf{s}$ are square integrable.*

Proof. The conditions in Lemma 4.1 guarantee the tree connectivity of the remote robot network. Then, if $\widehat{\mathbf{D}}_{pl} \succeq \mathbf{0}$, $\widehat{\mathbf{D}}_{pr} \mathbf{1}_{N_r n} \geq \mathbf{0}$ and $\widehat{\mathbf{K}}_{pr}(t) \succeq \mathbf{0}$, the passivity of the teleoperator can be directly concluded from (4.30). Further, if $\widehat{\mathbf{D}}_{pl} \succ \mathbf{0}$, $\widehat{\mathbf{D}}_{pr} \mathbf{1}_{N_r n} > \mathbf{0}$ and $\widehat{\mathbf{K}}_{pr}(t) \succ \mathbf{0}$, then there exists $k > 0$ such that $\dot{V} \leq \eta \dot{\mathbf{x}}_l^{\mathsf{T}} \mathbf{f}_h - k \big(\dot{\mathbf{x}}_l^{\mathsf{T}} \dot{\mathbf{x}}_l + \dot{\mathbf{x}}_r^{\mathsf{T}} \dot{\mathbf{x}}_r + \mathbf{s}^{\mathsf{T}} \mathbf{s} \big)$. The time integration of $\dot{V}$ then leads to $k \int_0^t \| \dot{\mathbf{x}}_l(\tau) \|^2 d\tau + k \int_0^t \| \dot{\mathbf{x}}_r(\tau) \|^2 d\tau + k \int_0^t \| \mathbf{s}(\tau) \|^2 d\tau \leq V(0) - V(t) + \eta \int_0^t \dot{\mathbf{x}}_l^{\mathsf{T}}(\tau) \mathbf{f}_h(\tau) d\tau$, and, together with $V(t) \geq 0$ and Assumption 4.1, proves that $\dot{\mathbf{x}}_l$, $\dot{\mathbf{x}}_r$ and $\mathbf{s}$ are square integrable. ■

The multi-local robot-remote multi-robot system teleoperator is a networked robotic system in physical interaction with its multiple human operators via the power-preserving ports $\big(\mathbf{f}_{hi}, \dot{\mathbf{x}}_{li} \big)$. Since power-preserving interconnections of passive components yield passive systems, this chapter assumes passive human operators and passivates the teleoperator to guarantee stable multi-user teleoperation of a remote multi-robot system with tree connectivity.

To the teleoperator, the user forces $\mathbf{f}_{hi}$ are inputs that are transmitted to the remote multi-robot system through couplings of the leader remote robots to the local robots. In return, the teleoperator feeds haptic cues back to human users through couplings of the local robots to the leader remote robots. Those haptic cues may

convey unwanted fluctuations of the remote multi-robot system. More importantly, improper inter-remote robot couplings may amplify unfavourable motion deviations at the local robots and jeopardize the safety of the system [180].

To eliminate the reflection-induced instability, this section renders the teleoperator passive. It designs a feedback passivation strategy that modulates the couplings and damping injection throughout the teleoperator based on inter-robot distances and velocities. Intuitively, the remote multi-robot system collectively behaves like a deformable multinodal object interacting with multiple local robots: the local robots are linked to their associated leader remote robots by the saturated Proportional ($\boldsymbol{\theta}_{lri}$) plus damping ($-D_{li}\dot{\mathbf{x}}_{li}$) control (4.9), while the remote multi-robot system adaptively tracks the local robots using the dynamic controllers (4.6). Typically, $\eta K_{ri}(t) \neq 1$ and the local robot-remote robot couplings are time-varying and asymmetric. Further, the control inputs $-\sigma K_{ri}(t)\boldsymbol{\theta}_{ri}$ in $\mathbf{f}_{ri}$ to the remote multi-robot system imply that inter-remote robot couplings are also dynamically adjusted based on the distances between the remote robots. Nonetheless, the gain selection in Lemma 4.2 provably renders the teleoperator passive with respect to its power port $\left(\mathbf{f}_h, \dot{\mathbf{x}}_l\right)$.

This chapter considers multi-user teleoperation of a multi-robot system in free motion without the environment forces $\mathbf{f}_{ei}$ in (4.2). Because the teleoperator exchanges energy only with users via the power ports $(\mathbf{f}_{hi}, \dot{\mathbf{x}}_{li})$, Assumption 4.1 and Lemma 4.2 guarantee its closed-loop stability. The stable teleoperation of a multi-robot system in interaction with its environment remains a challenge. Early research preserves the local [50] and global [52] connectivity of the multi-robot system with inter-robot couplings derived from unbounded potentials. Those couplings grow infinite when inter-robot distances approach the communication radius. Therefore, unbounded potential-based designs can become numerically unstable and are sensitive to noise in the practical implementation. Instead, this chapter embeds the gradient of a bounded potential into the sliding surfaces $\mathbf{s}_i$ and converts the multi-robot system dynamics (4.2) into (4.5) to circumvent numerical instability, but cannot guarantee passive interactions between the remote multi-robot system and environments. Future research can investigate how to update coupling and damping gains of the remote multi-robot system to render the teleoperator passive with respect to the power ports $(\mathbf{f}_{ei}, \dot{\mathbf{x}}_{ri})$.

It is not trivial to adapt the passive regulation of the interaction of a multi-robot system with external entities in [47, 48] to connectivity maintenance via bounded potentials. Section 4.1.1.2 shows that inter-remote robot couplings preserve the con-

nectivity of the remote robot network by limiting its energy to a certain threshold. During physical interaction, a passive environment can inject an unknown amount of energy into the remote multi-robot system, thwarting the quantification of an energy threshold for connectivity maintenance. A viable solution is: (i) to prescribe a maximum energy to be stored in the remote multi-robot system; (ii) to monitor the global power injection; and (iii) to adjust the energy dissipation of the multi-robot system appropriately. To this end, the tank-based energy monitoring technique and the dynamically scaled interconnection method in [47, 48] can be employed to extend our design to address physical interactions between the remote multi-robot system and environments.

4.1.2 Teleoperation With Delays

A multi-local robot-remote multi-robot system teleoperator can have time-varying delays in both the local robot-remote robot and inter-remote robot communications. In a first step towards overcoming delay-induced challenges, this section extends the feedback passivation strategy in Section 4.1.1 to cope with time delays in the local robot-remote robot communications.

4.1.2.1 Control as Interconnection

In Section 4.1.1, the sliding variables $\mathbf{s}_i$ designed in (4.3) split the remote multi-robot system dynamics (4.2) into two dynamics Π_1 and Π_2 that are negatively feedback interconnected. The resulting dynamics Π_3 are consistently perturbed by the uncertainty $\boldsymbol{\Delta}_r$, in which $\boldsymbol{\Delta}_{lri}$ is injected by the local robot-remote robot couplings $\boldsymbol{\theta}_{lri}$. To preserve the tree connectivity of the remote robots and ensure the passivity of bilateral teleoperation, the control gains $\mathbf{K}_r(t)$ of the leader remote robots are updated as in Lemma 4.1 and Lemma 4.2, using the transmitted positions and velocities of the local robots. The time-varying communication delays between the local and leader remote robots may thwart the adaptation of $\mathbf{K}_r(t)$. Hereafter, the harmful effect of delays is overcome by insulating $\boldsymbol{\Delta}_r$ from the local side with appropriate local robot-remote robot interconnections.

Endow every leader remote robot i with an auxiliary variable $\boldsymbol{\xi}_i$ that evolves with

$$\dot{\boldsymbol{\xi}}_i = K_{lci}(\mathbf{x}_{lid} - \boldsymbol{\xi}_i) + \boldsymbol{\theta}_{cri}, \tag{4.31}$$

where $i = 1, \cdots, N_l$, $K_{lci} > 0$, $\mathbf{x}_{lid} = \mathbf{x}_{li}(t - T_{li}(t))$ is the position of the local robot i delayed by $T_{li}(t)$, and $\boldsymbol{\theta}_{cri} = \overline{\mathbf{F}}_{hi} \cdot \tanh\left[K_{cri}(\mathbf{x}_{ri} - \boldsymbol{\xi}_i)\right]$ with $K_{cri} > 0$. Further, reconstruct the sliding variable $\mathbf{s}_i$ of each leader remote robot $i = 1, \cdots, N_l$ by

$$\mathbf{s}_i = \dot{\mathbf{x}}_{ri} + \sigma\boldsymbol{\theta}_{ri} + \eta\boldsymbol{\theta}_{cri}, \tag{4.32}$$

and rearrange the dynamics (4.2) of all remote robots into

$$\mathbf{M}_{ri}(\mathbf{x}_{ri})\dot{\mathbf{s}}_i + \mathbf{C}_{ri}(\mathbf{x}_{ri}, \dot{\mathbf{x}}_{ri})\mathbf{s}_i = \sigma\boldsymbol{\Delta}_{rri} + \eta\boldsymbol{\Delta}_{cri} + \mathbf{f}_{ri}, \tag{4.33}$$

where $i = 1, \cdots, N_r$, $\boldsymbol{\Delta}_{rri}$ are given in (4.5), and $\boldsymbol{\Delta}_{cri} = \mathbf{M}_{ri}(\mathbf{x}_{ri})\dot{\boldsymbol{\theta}}_{cri} + \mathbf{C}_{ri}(\mathbf{x}_{ri}, \dot{\mathbf{x}}_{ri})\boldsymbol{\theta}_{cri}$ for $i = 1, \cdots, N_l$, and $\boldsymbol{\Delta}_{cri} = \mathbf{0}$ otherwise. Then, as in Section 4.1.1.1, the remote multi-robot system dynamics $\widehat{\Pi}_3$ with the control (4.6) can be cast into a feedback interconnection of

$$\widehat{\Pi}_1: \quad \dot{\mathbf{x}}_r = -\sigma\left[\mathbf{L}(\mathbf{x}_r) \otimes \mathbf{I}_n\right]\mathbf{x}_r + \mathbf{s} - \eta\mathbf{u}_{cr} \tag{4.34}$$

and the transformed remote multi-robot system dynamics,

$$\widehat{\Pi}_2: \quad \mathbf{M}_r(\mathbf{x}_r)\dot{\mathbf{s}} + \mathbf{C}_r(\mathbf{x}_r, \dot{\mathbf{x}}_r)\mathbf{s} = \widehat{\boldsymbol{\Delta}}_r - \mathbf{K}_r(t)\mathbf{s} - \mathbf{D}_r\dot{\mathbf{x}}_r, \tag{4.35}$$

where $\mathbf{u}_{cr} = \left(\boldsymbol{\theta}_{cr1}^{\mathsf{T}}, \cdots, \boldsymbol{\theta}_{crN_l}^{\mathsf{T}}, \mathbf{0}^{\mathsf{T}}\right)^{\mathsf{T}}$ and $\widehat{\boldsymbol{\Delta}}_r = \left(\sigma\boldsymbol{\Delta}_{rr1}^{\mathsf{T}} + \eta\boldsymbol{\Delta}_{cr1}^{\mathsf{T}}, \cdots, \sigma\boldsymbol{\Delta}_{rrN_r}^{\mathsf{T}} + \eta\boldsymbol{\Delta}_{crN_r}^{\mathsf{T}}\right)^{\mathsf{T}}$, see Figure 4.4(a).

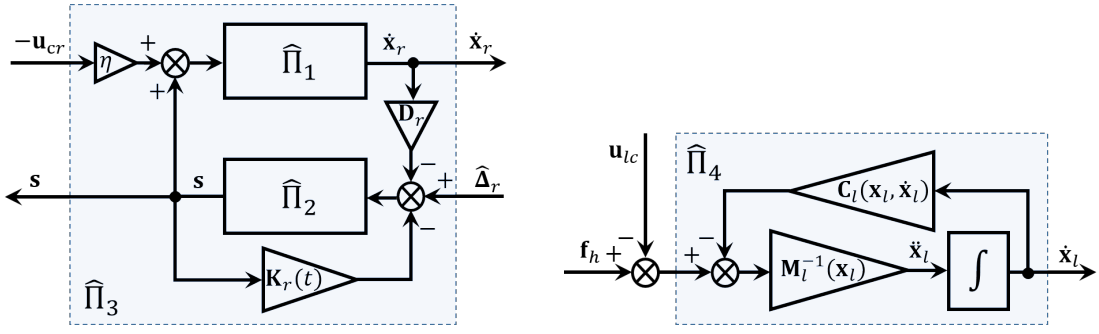

(a) The input-output diagram of $\widehat{\Pi}_3$. (b) The input-output diagram of $\widehat{\Pi}_4$.

Figure 4.4: The input-output diagrams: (a) of the remote multi-robot system $\widehat{\Pi}_3$ (the feedback interconnection of $\widehat{\Pi}_1$ and $\widehat{\Pi}_2$); and (b) of the local robots $\widehat{\Pi}_4$.

The force feedback is rendered to every operator i by connecting their local robot

to an associated leader remote robot i via

$$\mathbf{f}_{li} = K_{lci}(\boldsymbol{\xi}_{id} - \mathbf{x}_{li}) - D_{li}\dot{\mathbf{x}}_{li}, \tag{4.36}$$

where $\boldsymbol{\xi}_{id} = \boldsymbol{\xi}_i(t - T_{ri}(t))$ arrives at the local robot i at time t with a delay $T_{ri}(t)$. Then, the local robot dynamics $\widehat{\Pi}_4$ become

$$\widehat{\Pi}_4 : \quad \mathbf{M}_l(\mathbf{x}_l)\ddot{\mathbf{x}}_l + \mathbf{C}_l(\mathbf{x}_l, \dot{\mathbf{x}}_l)\dot{\mathbf{x}}_l = \mathbf{f}_h - \mathbf{u}_{lc}, \tag{4.37}$$

where the input $\mathbf{u}_{lc} = \mathbf{D}_l\dot{\mathbf{x}}_l - \mathbf{u}_{lcd}$ with $\mathbf{u}_{lcd} = \mathbf{K}_{lc}\,(\boldsymbol{\xi}_d - \mathbf{x}_l)$, $\mathbf{K}_{lc} = \mathrm{Diag}\big\{K_{lci}\mathbf{I}_n\big\}$ and $\boldsymbol{\xi}_d = \big(\boldsymbol{\xi}_{1d}^{\mathsf{T}}, \cdots, \boldsymbol{\xi}_{N_l d}^{\mathsf{T}}\big)^{\mathsf{T}}$. Unlike Figure 4.2(b), Figure 4.4(b) depicts the damping injection $-\mathbf{D}_l\dot{\mathbf{x}}_l$ as an input to the local robot dynamics $\widehat{\Pi}_4$. This treatment of the injected damping is key to passivating the time-delay local robot-remote robot interconnections hereafter.

Let $\boldsymbol{\xi} = \big(\boldsymbol{\xi}_1^{\mathsf{T}}, \cdots, \boldsymbol{\xi}_{N_l}^{\mathsf{T}}\big)^{\mathsf{T}}$ and group the dynamics (4.31) of the auxiliary variables $\boldsymbol{\xi}_i$ into

$$\dot{\boldsymbol{\xi}} = \mathbf{u}_{ldc} + \mathbb{I}\mathbf{u}_{cr}, \tag{4.38}$$

where $\mathbf{u}_{ldc} = \mathbf{K}_{lc}\,(\mathbf{x}_{ld} - \boldsymbol{\xi})$ with the time-delay positions $\mathbf{x}_{ld} = \big(\mathbf{x}_{l1d}^{\mathsf{T}}, \cdots, \mathbf{x}_{lN_l d}^{\mathsf{T}}\big)^{\mathsf{T}}$ of the local robots. The teleoperator can then be modelled as in Figure 4.5, where the shaded region groups the dynamics $\widehat{\Pi}_c$ of the time-delay local robot-remote robot interconnections. Note that $\widehat{\Pi}_c$ includes the damping injection $-\mathbf{D}_l\dot{\mathbf{x}}_l$ at the local side and the auxiliary dynamics (4.40) at the remote multi-robot system side, to facilitate the passivation of those interconnections in this section. Note also that $\widehat{\Pi}_5$ and $\widehat{\Pi}_6$ possess integrator-type dynamics: $\widehat{\Pi}_5$ is a nonlinear single integrator with the inputs $\big[\dot{\mathbf{x}}_r\ (\mathbb{I}^{\mathsf{T}}\dot{\boldsymbol{\xi}})\big]$ and the outputs $[\mathbf{u}_{cr}\ \ -\mathbf{u}_{cr}]$, as shown in Figure 4.6(a); in contrast, $\widehat{\Pi}_6$ has the inputs $\big[\dot{\mathbf{x}}_l\ \dot{\boldsymbol{\xi}}\big]$ and the outputs $[-\mathbf{u}_{lcd}\ \ -\mathbf{u}_{ldc}]$ and includes, besides a linear single integrator, the uncertain dynamics $\boldsymbol{\Delta}_{lc} = \big(\boldsymbol{\xi}^{\mathsf{T}} - \boldsymbol{\xi}_d^{\mathsf{T}},\ \mathbf{x}_l^{\mathsf{T}} - \mathbf{x}_{ld}^{\mathsf{T}}\big)^{\mathsf{T}}$ induced by time-varying delays, see Figure 4.6(b).

Grouping $\widehat{\Pi}_3$ and $\widehat{\Pi}_4$ into a physical component and $\widehat{\Pi}_5$ and $\widehat{\Pi}_6$ into a cyber component permits to reorganize the teleoperator in Figure 4.5 as in Figure 4.7. The physical component therein is a block diagonalization of the dynamics $\widehat{\Pi}_4$ and $\widehat{\Pi}_3$ and has two input-output pairs: $([\mathbf{f}_h\ \widehat{\boldsymbol{\Delta}}_r], [\dot{\mathbf{x}}_l\ \mathbf{s}])$ and $(-[\mathbf{u}_{lc}\ \mathbf{u}_{cr}], [\dot{\mathbf{x}}_l\ \dot{\mathbf{x}}_r])$. The first pair of the inputs $\big[\mathbf{f}_h\ \widehat{\boldsymbol{\Delta}}_r\big]$ and the outputs $\big[\dot{\mathbf{x}}_l\ \mathbf{s}\big]$ comprises: the power port $\big(\mathbf{f}_h, \dot{\mathbf{x}}_l\big)$ reserved for the physical interaction, and hence for the exchange of energy, with users; and the power port $\big(\widehat{\boldsymbol{\Delta}}_r, \mathbf{s}\big)$ to be damped by internal feedback passivation for

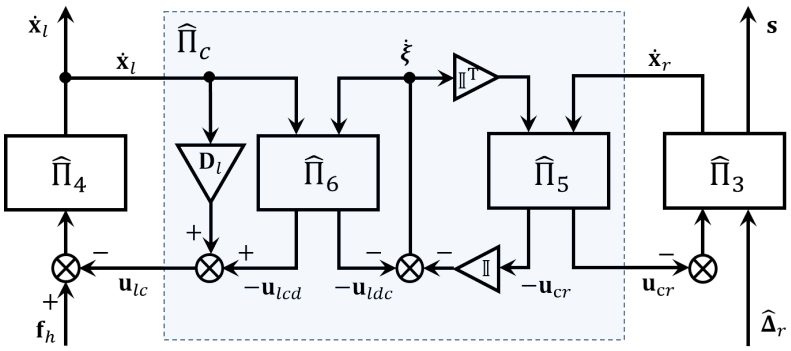

Figure 4.5: The input-output dynamic interconnections of the teleoperator with time-delay communications between the local and remote robots.

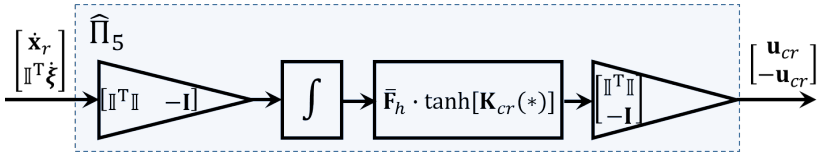

(a) The subsystem $\widehat{\Pi}_5$ is a nonlinear single integrator.

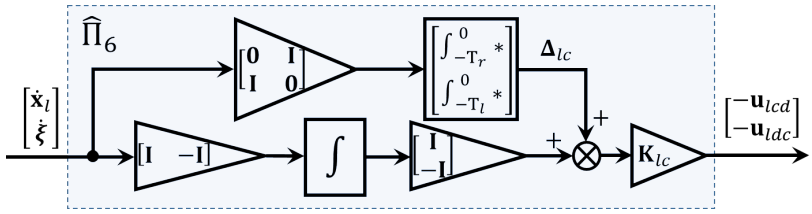

(b) The subsystem $\widehat{\Pi}_6$ combines a linear integrator with the delay-induced uncertain dynamics $\boldsymbol{\Delta}_{lc}$.

Figure 4.6: The subsystems $\widehat{\Pi}_5$ and $\widehat{\Pi}_6$ of $\widehat{\Pi}_c$ (the system of time-delay local robot-remote robot couplings) in Figure 4.5.

connectivity maintenance, and by external energy dissipation for closed-loop passivity. The second pair of the inputs $-[\mathbf{u}_{lc}\ \mathbf{u}_{cr}]$ and the outputs $[\dot{\mathbf{x}}_l\ \dot{\mathbf{x}}_r]$ is the power-preserving interconnection with the cyber component $\widehat{\Pi}_c$.

The cyber component $\widehat{\Pi}_c$ of the teleoperator consists of a block diagonalization of the dynamics $\widehat{\Pi}_5$ and $\widehat{\Pi}_6$. It couples the local and remote sides, and comprises the delay-induced uncertain dynamics $\boldsymbol{\Delta}_{lc}$ in $\widehat{\Pi}_6$. The feedforward damping injection at the local side and the feedback auxiliary dynamics $\dot{\boldsymbol{\xi}}$ at the remote multi-robot system side render the cyber component passive. Note the "control as interconnection" paradigm of the proposed strategy: a power-preserving interconnection of a non-passive physical component with a passive cyber component.

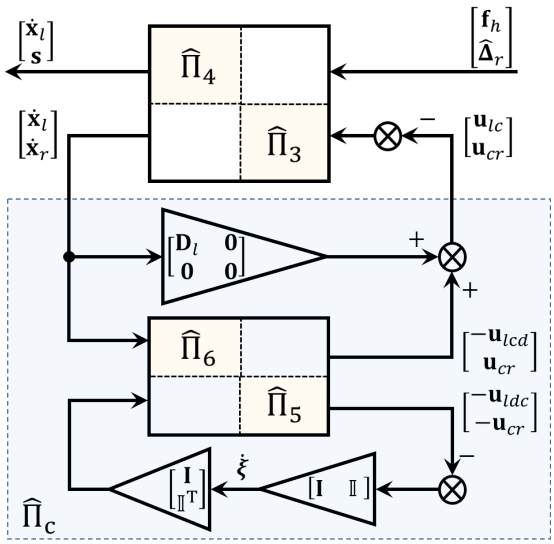

Figure 4.7: The controlled teleoperator as a power-conserving interconnection of a non-passive physical component with a passive cyber component.

4.1.2.2 Connectivity and Passivity

Similar to Section 4.1.1, this section first maintains the tree connectivity of the remote multi-robot system without assuming a passive teleoperator. It then renders passive a teleoperator whose remote multi-robot system is connected.

At the remote multi-robot system side, $\widehat{\Pi}_3$ is a feedback interconnection of $\widehat{\Pi}_1$ and $\widehat{\Pi}_2$. In turn, $\widehat{\Pi}_1$ and $\widehat{\Pi}_2$ are analogous to Π_1 and Π_2. Then, V_3 in (4.15) can measure the energy of $\widehat{\Pi}_3$. Its derivative along the dynamics (4.34) and (4.35) is

$$\begin{aligned}\dot{V}_3 =&\sigma\dot{\mathbf{x}}_r^{\mathsf{T}}\big[\mathbf{L}(\mathbf{x}_r)\otimes\mathbf{I}_n\big]\mathbf{x}_r+\sum_{i=1}^{N_r}\frac{1}{D_{ri}}\mathbf{s}_i^{\mathsf{T}}\big[\sigma\boldsymbol{\Delta}_{rri}+\eta\boldsymbol{\Delta}_{cri}-K_{ri}(t)\mathbf{s}_i-D_{ri}\dot{\mathbf{x}}_{ri}\big]\\ =&\dot{\mathbf{x}}_r^{\mathsf{T}}\big(\mathbf{s}-\eta\mathbf{u}_{cr}-\dot{\mathbf{x}}_r\big)+\mathbf{s}^{\mathsf{T}}\mathbf{D}_r^{-1}\widehat{\boldsymbol{\Delta}}_r-\mathbf{s}^{\mathsf{T}}\mathbf{D}_r^{-1}\mathbf{K}_r(t)\mathbf{s}-\mathbf{s}^{\mathsf{T}}\dot{\mathbf{x}}_r\\ =&\mathbf{s}^{\mathsf{T}}\mathbf{D}_r^{-1}\widehat{\boldsymbol{\Delta}}_r-\eta\dot{\mathbf{x}}_r^{\mathsf{T}}\mathbf{u}_{cr}-\dot{\mathbf{x}}_r^{\mathsf{T}}\dot{\mathbf{x}}_r-\mathbf{s}^{\mathsf{T}}\mathbf{D}_r^{-1}\mathbf{K}_r(t)\mathbf{s}.\end{aligned}\tag{4.39}$$

Appendix G shows that $\widehat{\boldsymbol{\Delta}}_r$ injects power bounded by

$$\mathbf{s}^{\mathsf{T}}\mathbf{D}_r^{-1}\widehat{\boldsymbol{\Delta}}_r\leq\mathbf{1}_{Nrn}^{\mathsf{T}}\mathbf{D}_r^{-1}\big[\eta\mathbb{I}^{\mathsf{T}}\mathbb{I}+\sigma(3\mathbf{D}+2\mathbf{A})\otimes\mathbf{I}_n\big]\dot{\mathbf{x}}_r^2+\mathbf{s}^{\mathsf{T}}\mathbf{D}_r^{-1}\boldsymbol{\Gamma}_2^c(t)\mathbf{s}+\eta^2\bar{\mathbf{f}}_h^{\mathsf{T}}\mathbb{I}\mathbf{D}_r^{-1}\mathbb{I}^{\mathsf{T}}\bar{\mathbf{f}}_h,\tag{4.40}$$

with $\boldsymbol{\Gamma}_2^c(t)=\eta\mathbb{I}^{\mathsf{T}}\boldsymbol{\Gamma}_{cr}^c(t)\mathbb{I}+\sigma\boldsymbol{\Gamma}_{rr}(t)$, and the remote multi-robot system $\widehat{\Pi}_3$ extracts the maximum power,

$$-4\eta\dot{\mathbf{x}}_r^{\mathsf{T}}\mathbf{u}_{cr}\leq\dot{\mathbf{x}}_r^{\mathsf{T}}\dot{\mathbf{x}}_r+4\eta^2\mathbf{u}_{cr}^{\mathsf{T}}\mathbf{u}_{cr},\tag{4.41}$$

from the local robot-remote robot couplings $\widehat{\Pi}_c$. Similar to (4.18), the input $-\mathbf{u}_{cr}$ and the outputs $\dot{\mathbf{x}}_r$ and $\mathbf{s}$ of the remote multi-robot system determine an upper bound on the energy V_3 of $\widehat{\Pi}_3$ as follows

$$V_3 \leq \frac{k_r}{2\sigma\lambda_L}\left(2\dot{\mathbf{x}}_r^{\mathsf{T}}\dot{\mathbf{x}}_r + 2\mathbf{s}^{\mathsf{T}}\mathbf{s} + \eta^2\mathbf{u}_{cr}^{\mathsf{T}}\mathbf{u}_{cr}\right) + \frac{1}{2}\mathbf{s}^{\mathsf{T}}\mathbf{D}_r^{-1}\mathbf{\Lambda}_r\mathbf{s}. \tag{4.42}$$

From Appendix H, Equations (4.40)-(4.42) then result in the upper bound on $\dot{V}_3$ in (4.39) by

$$\dot{V}_3 \leq \frac{\eta^2}{8}\bar{\mathbf{f}}_h^{\mathsf{T}}\mathbb{I}\left(9\mathbf{I}_{N_r n} + 8\mathbf{D}_r^{-1}\right)\mathbb{I}^{\mathsf{T}}\bar{\mathbf{f}}_h - \frac{\sigma\lambda_L}{4k_r}V_3 - \frac{1}{2}\mathbf{1}_{N_r n}^{\mathsf{T}}\mathbf{D}_r^{-1}\widehat{\mathbf{D}}_{cr}\dot{\mathbf{x}}_r^2 - \mathbf{s}^{\mathsf{T}}\mathbf{D}_r^{-1}\widehat{\mathbf{K}}_{cr}(t)\mathbf{s}, \tag{4.43}$$

where $\mathbf{u}_{cr}^{\mathsf{T}}\mathbf{u}_{cr} \leq \bar{\mathbf{f}}_h^{\mathsf{T}}\mathbb{I}\mathbb{I}^{\mathsf{T}}\bar{\mathbf{f}}_h$ has been used, $\widehat{\mathbf{D}}_{cr} = \mathbf{D}_r - 2\eta\mathbb{I}^{\mathsf{T}}\mathbb{I} - 2\sigma(3\mathbf{D} + 2\mathbf{A}) \otimes \mathbf{I}_n$, and $\widehat{\mathbf{K}}_{cr}(t) = \mathbf{K}_r(t) - (\sigma\lambda_L\mathbf{\Lambda}_r + 2k_r\mathbf{D}_r)/(8k_r) - \mathbf{\Gamma}_2^c(t)$.

The strong similarity between (4.43) and (4.21) is expected as $\widehat{\Pi}_1$ and $\widehat{\Pi}_2$ have the same input-output properties and feedback interconnection in $\widehat{\Pi}_3$ as Π_1 and Π_2 have in Π_3. With the inputs $[-\mathbf{u}_{lr}\ \ \mathbf{\Delta}_r]$ to Π_3 replaced by the inputs $[-\mathbf{u}_{cr}\ \ \widehat{\mathbf{\Delta}}_r]$ to $\widehat{\Pi}_3$, the control gains $\mathbf{K}_r(t)$ of the leader remote robots need to be updated online to make $\widehat{\mathbf{K}}_{cr}(t)$ rather than $\mathbf{K}_{cr}(t)$ positive semi-definite, and thus to preserve the tree network of the remote robots, in the presence of time-delay communications between the local and remote robots. More specifically, the auxiliary dynamics (4.38) at the remote robots eliminate the need for the quantities of the local robots when updating $\mathbf{K}_r(t)$ to maintain connectivity.

The following lemma summarizes the conditions for preserving the tree connectivity of the remote multi-robot system with time-delay communications to local robots.

Lemma 4.3. *Consider the remote multi-robot system* (4.2) *under the control* (4.6). *Let the auxiliary variables* $\boldsymbol{\xi}_i$ *have the dynamics* (4.31) *and the sliding variables* $\mathbf{s}_i$ *be redefined in* (4.32) *for all leader remote robots. Also, select* D_{ri} *and update* $K_{ri}(t)$ *to make* $\mathbf{D}_r^{-1}\widehat{\mathbf{D}}_{cr}\mathbf{1}_{N_r n} \geq \mathbf{0}$ *and* $\widehat{\mathbf{K}}_{cr}(t) \succeq \mathbf{0}$ *and to satisfy* (4.22). *Then, the tree communication network of the remote multi-robot system is invariant, i.e.,* $\mathcal{E}(t) = \mathcal{E}(0)$, $\forall t \geq 0$.

Proof. The proof is similar to the proof of Lemma 4.1 and is omitted. ■

Consider the teleoperator with dynamics recast as in Figure 4.7 and with the tree connectivity of the remote robots preserved as in Lemma 4.3. Its passivity can be

inferred from the passivity of its physical (the local and remote robots, or the plant) and cyber (the local robot-remote robot couplings plus the local robot damping, or the dynamic controller $\widehat{\Pi}_c$) components.

Let V_4 in (4.23) be the storage function of the local robots $\widehat{\Pi}_4$, and

$$\widehat{V}_p = V_3 + V_4 \tag{4.44}$$

be the energy of the physical component. By Appendix I, the uncertain dynamics $\widehat{\boldsymbol{\Delta}}_r$ may cause a shortage of passivity of physical component:

$$\mathbf{s}^{\mathsf{T}}\mathbf{D}_r^{-1}\widehat{\boldsymbol{\Delta}}_r \leq \eta\dot{\boldsymbol{\xi}}^{\mathsf{T}}\mathbb{D}_r\dot{\boldsymbol{\xi}} + \mathbf{1}_{N_r n}^{\mathsf{T}}\mathbf{D}_r^{-1}\mathbf{R}\dot{\mathbf{x}}_r^2 + \mathbf{s}^{\mathsf{T}}\mathbf{D}_r^{-1}\boldsymbol{\Gamma}_2^p(t)\mathbf{s} \tag{4.45}$$

with $\mathbb{D}_r$ and $\mathbf{R}$ defined in (4.29) and $\boldsymbol{\Gamma}_2^p(t) = \eta\mathbb{I}^{\mathsf{T}}\boldsymbol{\Gamma}_{cr}^p(t)\mathbb{I} + \sigma\boldsymbol{\Gamma}_{rr}(t)$. Then, (4.39), (4.45) and the derivative of V_4 along (4.37) lead to

$$\dot{\widehat{V}}_p \leq \eta\dot{\mathbf{x}}_l^{\mathsf{T}}\mathbf{f}_h - \eta\left(\dot{\mathbf{x}}_l^{\mathsf{T}}\ \dot{\mathbf{x}}_r^{\mathsf{T}}\right)\left(\mathbf{u}_{lc}^{\mathsf{T}}\ \mathbf{u}_{cr}^{\mathsf{T}}\right)^{\mathsf{T}} + \eta\dot{\boldsymbol{\xi}}^{\mathsf{T}}\mathbb{D}_r\dot{\boldsymbol{\xi}} - \mathbf{1}_{N_r n}^{\mathsf{T}}\overline{\mathbf{D}}_{pr}\dot{\mathbf{x}}_r^2 - \mathbf{s}^{\mathsf{T}}\overline{\mathbf{K}}_{pr}(t)\mathbf{s}, \tag{4.46}$$

for $\overline{\mathbf{D}}_{pr} = \mathbf{D}_r^{-1}\big(\mathbf{D}_r - \mathbf{R}\big)$ and $\overline{\mathbf{K}}_{pr}(t) = \mathbf{D}_r^{-1}\big[\mathbf{K}_r(t) - \boldsymbol{\Gamma}_2^p(t)\big]$.

By (4.46), the physical component exchanges energy with users via the port $\big(\mathbf{f}_h, \dot{\mathbf{x}}_l\big)$, and with the cyber component $\widehat{\Pi}_c$ via the port $(-[\mathbf{u}_{lc}\ \mathbf{u}_{cr}], [\dot{\mathbf{x}}_l\ \dot{\mathbf{x}}_r])$. Given that the feedback passivation control $-\mathbf{K}_r(t)\mathbf{s} - \mathbf{D}_r\dot{\mathbf{x}}_r$ can dissipate only part of the energy potentially injected into $\widehat{\Pi}_3$ through the power port $\big(\widehat{\boldsymbol{\Delta}}_r, \mathbf{s}\big)$, the controller $\widehat{\Pi}_c$ will be designed to extract sufficient power by $\eta\dot{\boldsymbol{\xi}}^{\mathsf{T}}\mathbb{D}_r\dot{\boldsymbol{\xi}}$ in (4.46) to make the teleoperator passive. Namely, the excess passivity of the cyber component $\widehat{\Pi}_c$ will be designed to compensate the potential lack of passivity of the physical component (the plant). Nonetheless, time-varying delays in communications between the local and remote multi-robot system sides can lead to the uncertainty $\boldsymbol{\Delta}_{lc}$ in $\widehat{\Pi}_6$ and, hence, to a non-passive composition of $\widehat{\Pi}_5$ and $\widehat{\Pi}_6$. The potential shortage of controller passivity caused by delays will be tackled by the damping in feedforward at the local robots and by the auxiliary dynamics $\dot{\boldsymbol{\xi}}$ in feedback at the remote robots.

To evaluate the passivity of the composition of $\widehat{\Pi}_5$ and $\widehat{\Pi}_6$, first quantify the energy of the nonlinear single integrator $\widehat{\Pi}_5$ by

$$\widehat{V}_5 = \eta\sum_{i=1}^{N_l}\int_{\mathbf{0}}^{\mathbf{x}_{ri}-\boldsymbol{\xi}_i}\tanh\left(K_{cri}\boldsymbol{\delta}_i\right)^{\mathsf{T}}\overline{\mathbf{F}}_{hi}d\boldsymbol{\delta}_i, \tag{4.47}$$

which is positive definite in $\mathbf{x}_{ri} - \boldsymbol{\xi}_i$ since $\tanh(\cdot)$ is strictly increasing and odd. By $\mathbf{u}_{cr}$ in (4.34), the derivative of $\widehat{V}_5$ is

$$\begin{aligned}\dot{\widehat{V}}_5 =&\eta \sum_{i=1}^{N_l} \tanh\left[K_{cri}(\mathbf{x}_{ri} - \boldsymbol{\xi}_i)\right]^{\mathsf{T}} \overline{\mathbf{F}}_{hi}\big(\dot{\mathbf{x}}_{ri} - \dot{\boldsymbol{\xi}}_i\big) = \eta \sum_{i=1}^{N_l} \boldsymbol{\theta}_{cri}^{\mathsf{T}}\big(\dot{\mathbf{x}}_{ri} - \dot{\boldsymbol{\xi}}\big) \\ =&\eta\left(\boldsymbol{\theta}_{cr1}^{\mathsf{T}}, \cdots, \boldsymbol{\theta}_{crN_l}^{\mathsf{T}}, \mathbf{0}^{\mathsf{T}}\right)\dot{\mathbf{x}}_r - \eta\left(\boldsymbol{\theta}_{cr1}^{\mathsf{T}}, \cdots, \boldsymbol{\theta}_{crN_l}^{\mathsf{T}}, \mathbf{0}^{\mathsf{T}}\right)\mathbb{I}^{\mathsf{T}}\dot{\boldsymbol{\xi}} = \eta \mathbf{u}_{cr}^{\mathsf{T}}\big(\dot{\mathbf{x}}_r - \mathbb{I}^{\mathsf{T}}\dot{\boldsymbol{\xi}}\big),\end{aligned} \tag{4.48}$$

and indicates that $\widehat{\Pi}_5$ in Figure 4.6(a) is passive (lossless) with respect to the inputs $[\dot{\mathbf{x}}_r \ \mathbb{I}^{\mathsf{T}}\dot{\boldsymbol{\xi}}]$ and the outputs $[\mathbf{u}_{cr} \ -\mathbf{u}_{cr}]$. Second, measure the storage of the linear integrator $\widehat{\Pi}_6$ with the delay-induced uncertainty $\boldsymbol{\Delta}_{lc}$ by

$$\widehat{V}_6 = \frac{\eta}{2}(\mathbf{x}_l - \boldsymbol{\xi})^{\mathsf{T}}\mathbf{K}_{lc}(\mathbf{x}_l - \boldsymbol{\xi}), \tag{4.49}$$

of which the time derivative is

$$\begin{aligned}\dot{\widehat{V}}_6 =&\eta\big(\dot{\mathbf{x}}_l - \dot{\boldsymbol{\xi}}\big)^{\mathsf{T}}\mathbf{K}_{lc}(\mathbf{x}_l - \boldsymbol{\xi}) = \eta\dot{\mathbf{x}}_l^{\mathsf{T}}\mathbf{K}_{lc}(\mathbf{x}_l - \boldsymbol{\xi}) + \eta\dot{\boldsymbol{\xi}}^{\mathsf{T}}\mathbf{K}_{lc}(\boldsymbol{\xi} - \mathbf{x}_l) \\ =&\eta\dot{\mathbf{x}}_l^{\mathsf{T}}\mathbf{K}_{lc}(\mathbf{x}_l - \boldsymbol{\xi}_d + \boldsymbol{\xi}_d - \boldsymbol{\xi}) + \eta\dot{\boldsymbol{\xi}}^{\mathsf{T}}\mathbf{K}_{lc}(\boldsymbol{\xi} - \mathbf{x}_{ld} + \mathbf{x}_{ld} - \mathbf{x}_l) \\ =&-\eta\dot{\mathbf{x}}_l^{\mathsf{T}}\mathbf{K}_{lc}(\boldsymbol{\xi}_d - \mathbf{x}_l) - \eta\dot{\boldsymbol{\xi}}^{\mathsf{T}}\mathbf{K}_{lc}(\mathbf{x}_{ld} - \boldsymbol{\xi}) - \eta\dot{\mathbf{x}}_l^{\mathsf{T}}\mathbf{K}_{lc}(\boldsymbol{\xi} - \boldsymbol{\xi}_d) - \eta\dot{\boldsymbol{\xi}}^{\mathsf{T}}\mathbf{K}_{lc}(\mathbf{x}_l - \mathbf{x}_{ld}) \\ =&-\eta\dot{\mathbf{x}}_l^{\mathsf{T}}\mathbf{u}_{lcd} - \eta\dot{\boldsymbol{\xi}}^{\mathsf{T}}\mathbf{u}_{ldc} - \eta\dot{\mathbf{x}}_l^{\mathsf{T}}\mathbf{K}_{lc}(\boldsymbol{\xi} - \boldsymbol{\xi}_d) - \eta\dot{\boldsymbol{\xi}}^{\mathsf{T}}\mathbf{K}_{lc}(\mathbf{x}_l - \mathbf{x}_{ld}) \\ =&-\eta\left(\mathbf{u}_{lcd}^{\mathsf{T}} \ \mathbf{u}_{ldc}^{\mathsf{T}}\right)\left(\dot{\mathbf{x}}_l^{\mathsf{T}} \ \dot{\boldsymbol{\xi}}^{\mathsf{T}}\right)^{\mathsf{T}} - \eta\big(\dot{\mathbf{x}}_l^{\mathsf{T}} \ \dot{\boldsymbol{\xi}}^{\mathsf{T}}\big)\big(\mathbf{I}_2 \otimes \mathbf{K}_{lc}\big)\boldsymbol{\Delta}_{lc}.\end{aligned} \tag{4.50}$$

Then, the energy stored in the interconnections between the local and leader remote robots (the composition of $\widehat{\Pi}_5$ and $\widehat{\Pi}_6$) is

$$\widehat{V}_c = \widehat{V}_5 + \widehat{V}_6, \tag{4.51}$$

and summing (4.48) and (4.50) leads to its time derivative as follows

$$\begin{aligned}\dot{\widehat{V}}_c =&\eta\big(\mathbf{u}_{cr}^{\mathsf{T}} \ -\mathbf{u}_{cr}^{\mathsf{T}}\big)\big(\dot{\mathbf{x}}_r^{\mathsf{T}} \ (\mathbb{I}^{\mathsf{T}}\dot{\boldsymbol{\xi}})^{\mathsf{T}}\big)^{\mathsf{T}} - \eta\big(\mathbf{u}_{lcd}^{\mathsf{T}} \ \mathbf{u}_{ldc}^{\mathsf{T}}\big)\big(\dot{\mathbf{x}}_l^{\mathsf{T}} \ \dot{\boldsymbol{\xi}}^{\mathsf{T}}\big)^{\mathsf{T}} - \eta\big(\dot{\mathbf{x}}_l^{\mathsf{T}} \ \dot{\boldsymbol{\xi}}^{\mathsf{T}}\big)\big(\mathbf{I}_2 \otimes \mathbf{K}_{lc}\big)\boldsymbol{\Delta}_{lc} \\ =&\eta\big(-\mathbf{u}_{lcd}^{\mathsf{T}} \ \mathbf{u}_{cr}^{\mathsf{T}}\big)\big(\dot{\mathbf{x}}_l^{\mathsf{T}} \ \dot{\mathbf{x}}_r^{\mathsf{T}}\big)^{\mathsf{T}} - \eta\big(\mathbf{u}_{ldc}^{\mathsf{T}} \ \mathbf{u}_{cr}^{\mathsf{T}}\big)\big[\mathbf{I}_{N_l n} \ \mathbb{I}\big]^{\mathsf{T}}\dot{\boldsymbol{\xi}} - \eta\big(\dot{\mathbf{x}}_l^{\mathsf{T}} \ \dot{\boldsymbol{\xi}}^{\mathsf{T}}\big)\big(\mathbf{I}_2 \otimes \mathbf{K}_{lc}\big)\boldsymbol{\Delta}_{lc}.\end{aligned}$$

In $\dot{\widehat{V}}_c$, the potential lack of passivity $-\eta\big(\dot{\mathbf{x}}_l^{\mathsf{T}} \ \dot{\boldsymbol{\xi}}^{\mathsf{T}}\big)\big(\mathbf{I}_2 \otimes \mathbf{K}_{lc}\big)\boldsymbol{\Delta}_{lc}$ resulting from the delay-induced uncertain dynamics $\boldsymbol{\Delta}_{lc}$ depends on the input $\dot{\mathbf{x}}_l$ and on the auxiliary dynamics $\dot{\boldsymbol{\xi}}$. Lemma 1 in [84] inspires the following passivation strategy: include the damping $-\mathbf{D}_l\dot{\mathbf{x}}_l$ of local robots as a feedforward loop in $\widehat{\Pi}_c$ to convert the output $-\mathbf{u}_{lcd}$

into $\mathbf{u}_{lc}$ to compensate for the shortage of passivity linked to $\dot{\mathbf{x}}_l$; add a feedback loop inside $\widehat{\Pi}_c$ to connect the outputs $[-\mathbf{u}_{ldc} \ -\mathbf{u}_{cr}]$ to the inputs $[\dot{\boldsymbol{\xi}} \ \mathbb{I}^{\mathsf{T}}\dot{\boldsymbol{\xi}}]$ by the adaptation of $\boldsymbol{\xi}$ in (4.38); and inject adequate dissipation in $\widehat{\Pi}_c$ to balance the lack of passivity of both the cyber component (the local robot-remote robot couplings) and the physical component (the local and remote robots). Thus, the gist in this section is a feedforward-feedback passivation strategy that transforms the local robot-remote robot couplings into a dynamical controller $\widehat{\Pi}_c$ that is interconnected with the physical component and regulates the passivity margin of the teleoperator.

More specifically, the feedforward loop by $\mathbf{u}_{lc} = \mathbf{D}_l\dot{\mathbf{x}}_l - \mathbf{u}_{lcd}$ in (4.37) and the feedback loop by $\dot{\boldsymbol{\xi}} = \mathbf{u}_{ldc} + \mathbb{I}\mathbf{u}_{cr}$ in (4.38) jointly convert $\dot{\widehat{V}}_c$ into

$$\begin{aligned}\dot{\widehat{V}}_c =&\eta\big(\mathbf{u}_{lc}^{\mathsf{T}} - \dot{\mathbf{x}}_l^{\mathsf{T}}\mathbf{D}_l^{\mathsf{T}} \ \mathbf{u}_{cr}^{\mathsf{T}}\big)\big(\dot{\mathbf{x}}_l^{\mathsf{T}} \ \dot{\mathbf{x}}_r^{\mathsf{T}}\big)^{\mathsf{T}} - \eta\big(\mathbf{u}_{ldc}^{\mathsf{T}} + \mathbf{u}_{cr}^{\mathsf{T}}\mathbb{I}^{\mathsf{T}}\big)\dot{\boldsymbol{\xi}} - \eta\big(\dot{\mathbf{x}}_l^{\mathsf{T}} \ \dot{\boldsymbol{\xi}}^{\mathsf{T}}\big)\big(\mathbf{I}_2 \otimes \mathbf{K}_{lc}\big)\boldsymbol{\Delta}_{lc}\\ =&\eta\big(\mathbf{u}_{lc}^{\mathsf{T}} \ \mathbf{u}_{cr}^{\mathsf{T}}\big)\big(\dot{\mathbf{x}}_l^{\mathsf{T}} \ \dot{\mathbf{x}}_r^{\mathsf{T}}\big)^{\mathsf{T}} - \eta\dot{\mathbf{x}}_l^{\mathsf{T}}\mathbf{D}_l\dot{\mathbf{x}}_l - \eta\dot{\boldsymbol{\xi}}^{\mathsf{T}}\dot{\boldsymbol{\xi}} - \eta\big(\dot{\mathbf{x}}_l^{\mathsf{T}} \ \dot{\boldsymbol{\xi}}^{\mathsf{T}}\big)\big(\mathbf{I}_2 \otimes \mathbf{K}_{lc}\big)\boldsymbol{\Delta}_{lc},\end{aligned}$$

from which it follows that

$$\begin{aligned}\widehat{V}_c(t) =&\widehat{V}_c(0) + \eta\int_0^t \big(\mathbf{u}_{lc}^{\mathsf{T}}(\tau) \ \mathbf{u}_{cr}^{\mathsf{T}}(\tau)\big)\big(\dot{\mathbf{x}}_l^{\mathsf{T}}(\tau) \ \dot{\mathbf{x}}_r^{\mathsf{T}}(\tau)\big)^{\mathsf{T}}d\tau - \eta\int_0^t \dot{\mathbf{x}}_l^{\mathsf{T}}(\tau)\mathbf{D}_l\dot{\mathbf{x}}_l(\tau)d\tau\\ &- \eta\int_0^t \dot{\boldsymbol{\xi}}^{\mathsf{T}}(\tau)\dot{\boldsymbol{\xi}}(\tau)d\tau - \eta\int_0^t \big(\dot{\mathbf{x}}_l^{\mathsf{T}}(\tau) \ \dot{\boldsymbol{\xi}}^{\mathsf{T}}(\tau)\big)\big(\mathbf{I}_2 \otimes \mathbf{K}_{lc}\big)\boldsymbol{\Delta}_{lc}(\tau)d\tau\\ \leq&\widehat{V}_c(0) + \eta\int_0^t \big(\mathbf{u}_{lc}^{\mathsf{T}}(\tau) \ \mathbf{u}_{cr}^{\mathsf{T}}(\tau)\big)\big(\dot{\mathbf{x}}_l^{\mathsf{T}}(\tau) \ \dot{\mathbf{x}}_r^{\mathsf{T}}(\tau)\big)^{\mathsf{T}}d\tau - \eta\sum_{i=1}^{N_l} D_{li}\int_0^t \big\|\dot{\mathbf{x}}_{li}(\tau)\big\|^2 d\tau\\ &+ \frac{\eta}{2}\int_0^t \big\|\dot{\boldsymbol{\xi}}(\tau)\big\|^2 d\tau - \eta\int_0^t \big\|\dot{\boldsymbol{\xi}}(\tau)\big\|^2 d\tau + \eta\sum_{i=1}^{N_l} K_{lci}^2\left(\overline{T}_{li}^2 + \overline{T}_{ri}^2\right)\int_0^t \big\|\dot{\mathbf{x}}_{li}(\tau)\big\|^2 d\tau\\ \leq&\widehat{V}_c(0) + \eta\int_0^t \big(\mathbf{u}_{lc}^{\mathsf{T}}(\tau) \ \mathbf{u}_{cr}^{\mathsf{T}}(\tau)\big)\big(\dot{\mathbf{x}}_l^{\mathsf{T}}(\tau) \ \dot{\mathbf{x}}_r^{\mathsf{T}}(\tau)\big)^{\mathsf{T}}d\tau\\ &- \widehat{D}_{pl}\int_0^t \|\dot{\mathbf{x}}_l(\tau)\|^2 d\tau - \frac{\eta}{2}\int_0^t \big\|\dot{\boldsymbol{\xi}}(\tau)\big\|^2 d\tau,\end{aligned} \tag{4.52}$$

by Lemma 1 in [84], where $\widehat{D}_{pl} = \eta \min\limits_{i=1,\cdots,N_l}\big\{D_{li} - K_{lci}^2\big(\overline{T}_{li}^2 + \overline{T}_{ri}^2\big)\big\}$. By (4.52), the dynamical controller $\widehat{\Pi}_c$ is passive with respect to the inputs $[\dot{\mathbf{x}}_l \ \dot{\mathbf{x}}_r]$ and the new outputs $[\mathbf{u}_{lc} \ \mathbf{u}_{cr}]$, with the excess of passivity controlled by the feedforward and feedback loops.

Then, interconnecting the passive dynamical controller $\widehat{\Pi}_c$ with the non-passive physical component as shown in Figure 4.7 can lead to a passive time-delay teleoperator. Specifically, after adding the time integration of $\dot{\widehat{V}}_p$ in (4.46) and $\widehat{V}_c$ in (4.52),

the energy stored in the teleoperator,

$$\widehat{V} = (V_3 + V_4) + \left(\widehat{V}_5 + \widehat{V}_6\right) = \widehat{V}_p + \widehat{V}_c, \tag{4.53}$$

can be bounded by

$$\begin{aligned} \widehat{V}(t) \leq & \widehat{V}(0) + \eta \int_0^t \dot{\mathbf{x}}_l^{\mathsf{T}}(\tau)\mathbf{f}_h(\tau)d\tau - \widehat{D}_\xi \int_0^t \left\|\dot{\boldsymbol{\xi}}(\tau)\right\|^2 d\tau \\ & - \widehat{K}_{pr} \int_0^t \|\mathbf{s}(\tau)\|^2 d\tau - \sum_{i=l,r} \widehat{D}_{pi} \int_0^t \|\dot{\mathbf{x}}_i(\tau)\|^2 d\tau, \end{aligned} \tag{4.54}$$

where $\overline{\mathbf{K}}_{pr}(t) \succeq \widehat{K}_{pr}\mathbf{I}_{N_r n}$, $\overline{\mathbf{D}}_{pr} \succeq \widehat{D}_{pr}\mathbf{I}_{N_r n}$ and $\eta\mathbf{I}_{N_l n}/2 - \eta\mathbb{D}_r \succeq \widehat{D}_\xi \mathbf{I}_{N_l n}$. The zero sum of the time integrals of the duality product of $[\dot{\mathbf{x}}_l \ \dot{\mathbf{x}}_r]$ and $[\mathbf{u}_{lc} \ \mathbf{u}_{cr}]$ confirms that the physical component of the teleoperator and the dynamical controller $\widehat{\Pi}_c$ in Figure 4.7 are interconnected in a power-preserving way. In doing so, the dynamical controller $\widehat{\Pi}_c$ can extract the excess of energy from the physical component through their interconnection, and the feedback loop formed by $\dot{\boldsymbol{\xi}}$ inside $\widehat{\Pi}_c$ can dissipate it to keep the overall teleoperator passive.

The following lemma provides the conditions on control gains that guarantee the passivity of the teleoperator.

Lemma 4.4. *Consider the teleoperator with multiple local* (4.1) *and remote* (4.2) *robots under the control of* (4.36) *and* (4.6)*. Let the auxiliary variables* $\boldsymbol{\xi}_i$ *have the dynamics* (4.31) *and the sliding variables* $\mathbf{s}_i$ *be redefined in* (4.32) *for all leader remote robots. Under the conditions in Lemma 4.3, set* D_{li} *and* D_{ri} *and update all* $K_{ri}(t)$ *such that* $\widehat{D}_{pl}$*,* $\widehat{D}_{pr}$*,* $\widehat{K}_{pr}$ *and* $\widehat{D}_\xi$ *in* (4.54) *are nonnegative. Then, the teleoperator is passive with respect to the power port* $\left(\mathbf{f}_h, \dot{\mathbf{x}}_l\right)$*. Further, if* $\widehat{D}_{pl}$*,* $\widehat{D}_{pr}$*,* $\widehat{K}_{pr}$ *and* $\widehat{D}_\xi$ *are positive, then* $\dot{\mathbf{x}}_l$*,* $\dot{\mathbf{x}}_r$*,* $\mathbf{s}$ *and* $\dot{\boldsymbol{\xi}}$ *are square integrable.*

Proof. The proof is similar to the proof of Lemma 4.2 and is omitted. ■

From an energy perspective, the feedforward damping at the local robots, $-\mathbf{D}_l\dot{\mathbf{x}}_l$ in $\widehat{\Pi}_c$ in Figure 4.7, dissipates both the energy of the physical component and the energy accumulated due to the delay-induced uncertainty $\boldsymbol{\Delta}_{lc}$. The feedback auxiliary dynamics $\dot{\boldsymbol{\xi}}$ split each coupling between a local and a leader remote robot into a series of two springs, and dissipate part of the energy of one spring as they transfer the rest to the other spring. The dissipation injected by (4.38) alleviates the destabilizing effect of $\boldsymbol{\Delta}_{lc}$ in (4.52) and of $\widehat{\boldsymbol{\Delta}}_r$ in (4.54). Equation (4.52) also shows that the

dynamics (4.38) can dissipate and transfer energy only when the energies stored in the two springs are unbalanced, i.e., $\dot{\boldsymbol{\xi}} \neq \mathbf{0}$. Balancing the two springs is not equivalent to depleting them of energy. Thence, as will be proven in Theorem 4.1, the synchronization of the local and remote robots would still rely on their damping to deplete them of energy.

The damping injection in $\mathbf{f}_{li}$ and $\mathbf{f}_{ri}$ can exacerbate the "phantom forces" perceived by users without correspondence to any remote interaction [73]. These forces oppose users' motions and increase their effort when tele-driving the remote multi-robot system, especially for substantial communication delays. They slow down and fatigue human operators. For smaller delays, lower damping could reduce the "phantom forces" and mitigate the deterioration of performance [181]. Yet, the extra damping injection can haptically cue human users about the velocities of remote robots through their elastic couplings, and is critical for safe teleoperation of the remote multi-robot system by novice users.

4.1.3 Steady-State Performance

This section evaluates the steady-state performance of time-delay multi-user teleoperation of a remote multi-robot system under the proposed connectivity-preserving passivation control, in two cases: (i) Theorem 4.1 confirms the position synchronization and accurate force feedback when passive users manipulate the teleoperator; and (ii) Theorem 4.2 specifies the spatial distribution of the remote multi-robot system based on the locations of the local robots held stationary by users.

Theorem 4.1. *Consider the teleoperator with multiple local* (4.1) *and remote* (4.2) *robots under the control of* (4.36) *and* (4.6). *Define the auxiliary variables* $\boldsymbol{\xi}_i$ *by* (4.31) *and the sliding variables* $\mathbf{s}_i$ *by* (4.32) *for all leader remote robots. Under the conditions in Lemma 4.3, let* $\widehat{D}_{pl}$, $\widehat{D}_{pr}$, $\widehat{K}_{pr}$ *and* $\widehat{D}_{\xi}$ *in* (4.54) *be positive. Then:*

1. *All local and remote robots become stationary at infinite time:* $\dot{\mathbf{x}}_{li}(t) \to \mathbf{0}$ *and* $\dot{\mathbf{x}}_{rj}(t) \to \mathbf{0}$ *as* $t \to +\infty$ *for all* $i = 1, \cdots, N_l$ *and all* $j = 1, \cdots, N_r$.

2. *The force feedback to every user approaches the sum of all other user forces:* $\mathbf{f}_{li}(t) \to \sum_{j \neq i} \mathbf{f}_{hj}(t)$ *as* $t \to +\infty$ *for all* $i = 1, \cdots, N_l$.

3. *If no users operate their local robots, the positions of all robots converge asymptotically:* $\mathbf{x}_{li}(t) - \mathbf{x}_{rj}(t) \to \mathbf{0}$ *as* $t \to +\infty$ *for all* $i = 1, \cdots, N_l$ *and all* $j = 1, \cdots, N_r$.

Proof. The conditions in Lemma 4.3 guarantee connectivity preservation for the tree network of the remote robots. Given Assumption 4.1, positive $\widehat{D}_{pl}$, $\widehat{D}_{pr}$, $\widehat{K}_{pr}$ and $\widehat{D}_{\xi}$ lead to $\{\dot{\mathbf{x}}_l, \dot{\mathbf{x}}_r, \mathbf{s}, \dot{\boldsymbol{\xi}}\} \in \mathcal{L}_2$ by Lemma 4.4. Further, (4.44), (4.51), (4.53) and (4.54) together indicate that V_3, V_4, $\widehat{V}_5$ and $\widehat{V}_6$ are upper-bounded. By (E.1) and (4.13), finite V_3 in (4.15) ensures finite $\big[\mathbf{L}(\mathbf{x}_r) \otimes \mathbf{I}_n\big]\mathbf{x}_r$ and $\mathbf{s}$. Similarly, $\dot{\mathbf{x}}_l$ is finite because V_4 in (4.23) is upper bounded. Finite $\widehat{V}_5$ in (4.47) and $\widehat{V}_6$ in (4.49) guarantee that $\mathbb{I}\mathbf{x}_r - \boldsymbol{\xi}$ and $\mathbf{x}_l - \boldsymbol{\xi}$ are bounded, respectively. Then, using (4.34) and (4.38), it follows that $\{\dot{\mathbf{x}}_l, \dot{\mathbf{x}}_r, \mathbf{s}, \dot{\boldsymbol{\xi}}\} \in \mathcal{L}_\infty \cap \mathcal{L}_2$ and thus that $\{\dot{\mathbf{x}}_l(t), \dot{\mathbf{x}}_r(t), \mathbf{s}(t), \dot{\boldsymbol{\xi}}(t)\} \to \mathbf{0}$ as $t \to +\infty$.

Given Assumptions 4.2 and 4.5, the time derivative of (4.37) leads to bounded $\ddot{\mathbf{x}}_l$. Then, by Barbalat's lemma, $\dot{\mathbf{x}}_l(t) \to \mathbf{0}$ implies that $\ddot{\mathbf{x}}_l(t) \to \mathbf{0}$. Further, $\dot{\mathbf{x}}_l(t) \to \mathbf{0}$ and $\dot{\boldsymbol{\xi}}(t) \to \mathbf{0}$ make $\mathbf{u}_{lc}(t) \to -\mathbf{u}_{lcd}(t) \to \mathbf{u}_{ldc}(t)$. Then, Equations (4.37)-(4.38) lead to $\mathbf{u}_{lc}(t) + \mathbb{I}\mathbf{u}_{cr}(t) \to \mathbf{0}$ as $t \to +\infty$. From $\big(\mathbf{1}_{N_r} \otimes \mathbf{I}_n\big)^{\mathsf{T}}\mathbf{u}_{cr} = \big[\big(\mathbf{1}_{N_l}^{\mathsf{T}}\ \mathbf{1}_{N_r-N_l}^{\mathsf{T}}\big) \otimes \mathbf{I}_n\big]\mathbf{u}_{cr} = \big[\big(\mathbf{1}_{N_l}^{\mathsf{T}}\ \mathbf{0}_{N_r-N_l}^{\mathsf{T}}\big) \otimes \mathbf{I}_n\big]\mathbf{u}_{cr} = \big(\mathbf{1}_{N_l} \otimes \mathbf{I}_n\big)^{\mathsf{T}}\mathbb{I}\mathbf{u}_{cr}$, it follows that

$$\begin{aligned} &\lim_{t\to+\infty} \eta\big(\mathbf{1}_{N_r} \otimes \mathbf{I}_n\big)^{\mathsf{T}}\mathbf{u}_{cr}(t) + \eta\big(\mathbf{1}_{N_l} \otimes \mathbf{I}_n\big)^{\mathsf{T}}\mathbf{u}_{lc}(t) \\ =&\lim_{t\to+\infty} \eta\big(\mathbf{1}_{N_l} \otimes \mathbf{I}_n\big)^{\mathsf{T}}\big[\mathbb{I}\mathbf{u}_{cr}(t) + \mathbf{u}_{lc}(t)\big] = \mathbf{0}. \end{aligned} \tag{4.55}$$

Further, $\dot{\mathbf{x}}_r(t) \to \mathbf{0}$, $\mathbf{s}(t) \to \mathbf{0}$ and (4.34) imply that $\eta\mathbf{u}_{cr}(t) \to -\sigma\big[\mathbf{L}(\mathbf{x}_r(t)) \otimes \mathbf{I}_n\big]\mathbf{x}_r(t)$. From $\eta\sum_{i=1}^{N_l}\mathbf{f}_{li} = \sigma\big[\mathbf{1}_{N_r}^{\mathsf{T}}\mathbf{L}(\mathbf{x}_r) \otimes \mathbf{I}_n\big]\mathbf{x}_r - \eta\big(\mathbf{1}_{N_l} \otimes \mathbf{I}_n\big)^{\mathsf{T}}\mathbf{u}_{lc} = \sigma\big(\mathbf{1}_{N_r} \otimes \mathbf{I}_n\big)^{\mathsf{T}}\big[\mathbf{L}(\mathbf{x}_r) \otimes \mathbf{I}_n\big]\mathbf{x}_r - \eta\big(\mathbf{1}_{N_l} \otimes \mathbf{I}_n\big)^{\mathsf{T}}\mathbf{u}_{lc}$, it follows that

$$\begin{aligned} &\lim_{t\to+\infty} \eta\big(\mathbf{1}_{N_r} \otimes \mathbf{I}_n\big)^{\mathsf{T}}\mathbf{u}_{cr}(t) + \eta\big(\mathbf{1}_{N_l} \otimes \mathbf{I}_n\big)^{\mathsf{T}}\mathbf{u}_{lc}(t) \\ =&-\lim_{t\to+\infty} \sigma\big(\mathbf{1}_{N_r} \otimes \mathbf{I}_n\big)^{\mathsf{T}}\big[\mathbf{L}(\mathbf{x}_r(t)) \otimes \mathbf{I}_n\big]\mathbf{x}_r(t) + \lim_{t\to+\infty} \eta\big(\mathbf{1}_{N_l} \otimes \mathbf{I}_n\big)^{\mathsf{T}}\mathbf{u}_{lc}(t) \\ =&-\lim_{t\to+\infty} \eta\sum_{i=1}^{N_l}\mathbf{f}_{li}(t). \end{aligned} \tag{4.56}$$

Together, Equations (4.55)-(4.56) lead to $\lim_{t\to+\infty}\sum_{i=1}^{N_l}\mathbf{f}_{li}(t) = \mathbf{0}$. From $\dot{\mathbf{x}}_{li}(t) \to \mathbf{0}$ and $\ddot{\mathbf{x}}_{li}(0) \to \mathbf{0}$ and the local robot dynamics (4.1), it follows that $-\mathbf{f}_{li}(t) \to \mathbf{f}_{hi}(t)$ as $t \to +\infty$ for all $i = 1, \cdots, N_l$. Thence, force feedback is achieved in the steady state, $\mathbf{f}_{li}(t) \to \sum_{j\neq i}\mathbf{f}_{hj}(t)$ as $t \to +\infty$.

When no users operate their local robots, namely $\mathbf{f}_{hi} = \mathbf{0}$ for all $i = 1, \cdots, N_l$, then $\dot{\mathbf{x}}_l(t) \to \mathbf{0}$ and $\ddot{\mathbf{x}}_l \to \mathbf{0}$ and (4.37) imply that $\mathbf{u}_{lcd}(t) \to \mathbf{0}$. Also, $\dot{\boldsymbol{\xi}}(t) \to \mathbf{0}$ and (4.38) lead to $\mathbf{u}_{ldc}(t) + \mathbb{I}\mathbf{u}_{cr}(t) \to \mathbf{0}$ as $t \to +\infty$. Together, $\dot{\mathbf{x}}_l(t) \to \mathbf{0}$ and $\dot{\boldsymbol{\xi}}(t) \to \mathbf{0}$ yield $\mathbf{x}_l(t) \to \boldsymbol{\xi}(t) \to \mathbb{I}\mathbf{x}_r(t)$. Then, $\mathbf{u}_{cr}$ in (4.34) implies that $\mathbf{u}_{cr}(t) \to \mathbf{0}$ and thus that

$[\mathbf{L}(\mathbf{x}_r(t)) \otimes \mathbf{I}_n]\,\mathbf{x}_r(t) \to \mathbf{0}$ by $\dot{\mathbf{x}}_r(t) \to \mathbf{0}$ and $\mathbf{s}(t) \to \mathbf{0}$. The preserved tree network of the remote robots then ensures the convergence of their positions: $\mathbf{x}_{ri}(t) - \mathbf{x}_{rj}(t) \to \mathbf{0}$ for all $i, j = 1, \cdots, N_r$. Together with $\mathbf{x}_l(t) \to \mathbb{I}\mathbf{x}_r(t)$, it implies the synchronization of all robots: $\mathbf{x}_{li}(t) - \mathbf{x}_{rj}(t) \to \mathbf{0}$ as $t \to +\infty, \forall i = 1, \cdots, N_l$ and $\forall j = 1, \cdots, N_r$. ■

For the freely moving multi-robot system (4.2), Theorem 4.1 shows that, in the multi-user teleoperation context, the steady-state force feedback to each human user is the aggregation of all other user forces. This property permits users to haptically perceive the intentions of their peers in applications like the cooperative tele-deployment of a robotic sensor network. During the transient phase, the local robot-remote robot interconnections also convey to users the dynamics of their associated leader remote robots. Because the leader remote robots are coupled to other remote robots, human users can feel the dynamics of the entire multi-robot system together with other user-applied forces. An analysis to relate the force feedback to the states of the teleoperator and a control method to shape the feedback are intriguing and challenging problems [54]. An initial passivity-constrained optimization [47] dynamically scales the viscoelastic interconnections of a leader remote robot with its neighbours, but requires the leader robot to estimate all interaction forces between the remote multi-robot system and environments and to broadcast the optimal scaling factors to all its neighbours.

The proof of the steady-state force feedback in Theorem 4.1 leverages the assumption of an undirected communication network of the remote robots in (4.56). More precisely, the bidirectional inter-remote robot information exchanges enable intra-multi-robot system couplings that permit each user to perceive the sum of all other user-applied forces in the steady state. If intra-multi-robot system communications are directed, not all user-applied forces can be transferred to other users across the multi-robot system network due to the lack of a directed transmission path. Instead, human users would feel the dynamics of some remote robots to which their local robots are connected during teleoperation.

Theorem 4.1 evaluates the position synchronization and force feedback performance of the teleoperator in the steady state. Theorem 4.2 resolves the spatial distribution of the remote multi-robot system in the steady state using the locations of the local robots.

Theorem 4.2. *Consider the multi-local robot-remote multi-robot system teleoperator controlled as in Theorem 4.1. Let all users hold their local robots immobile,* $\dot{\mathbf{x}}_{li}(t) = \mathbf{0}$

and $\mathbf{x}_{li}(t) = \mathbf{x}_{li}^*$ *for all* $i = 1, \cdots, N_l$ *and all* $t \geq 0$. *Then, all remote robots converge asymptotically to the convex hull spanned by all local robots, namely,* $\dot{\mathbf{x}}_{ri}(t) \to \mathbf{0}$ *and* $\mathbf{x}_{ri}(t) \to \mathbf{x}_{ri}^* \in \mathcal{C}_h$ *with the convex hull* $\mathcal{C}_h$ *defined by*

$$\mathcal{C}_h = \left\{ \sum_{j=1}^{N_l} \lambda_j \mathbf{x}_{lj}^* \,\middle|\, \lambda_j \geq 0 \text{ and } \sum_{j=1}^{N_l} \lambda_j = 1 \right\}.$$

Proof. When all human users hold their local robots fixed, $\dot{\mathbf{x}}_l(t) = \mathbf{0}$ for all $t \geq 0$ and they inject no energy into the teleoperator, which itself is passive with the proposed controller. Theorem 4.1 then leads to $\{\dot{\mathbf{x}}_r, \mathbf{s}, \dot{\boldsymbol{\xi}}\} \in \mathcal{L}_\infty \cap \mathcal{L}_2$, and further to $\dot{\mathbf{x}}_r(t) \to \mathbf{0}$, $\mathbf{s}(t) \to \mathbf{0}$ and $\dot{\boldsymbol{\xi}}(t) \to \mathbf{0}$ as $t \to +\infty$.

Define $\widehat{\mathbf{K}}(t) = \mathrm{Diag}\{\widehat{\mathbf{K}}_{cri}(t)\}$ with $\widehat{\mathbf{K}}_{cri}(t)$ given by $\widehat{\mathbf{K}}_{cri}(t)\big(\mathbf{x}_{ri} - \boldsymbol{\xi}_i\big) = \overline{\mathbf{F}}_{hi} \cdot \tanh\big[K_{cri}\big(\mathbf{x}_{ri} - \boldsymbol{\xi}_i\big)\big]$ for $i = 1, \cdots, N_l$. Note that $\widehat{\mathbf{K}}(t)$ is diagonal and uniformly positive definite, i.e., $\widehat{\mathbf{K}}(t) \succ \epsilon \mathbf{I}_{N_l n}$ for some $\epsilon > 0$ as $\mathbf{x}_{ri} - \boldsymbol{\xi}_i$ are bounded. Let $\mathbb{L}(t) = \mathbf{L}(\mathbf{x}_r(t)) \otimes \mathbf{I}_n$. Then, $\mathbf{u}_{cr}$ becomes $\mathbf{u}_{cr} = \mathbb{I}^\mathsf{T}\widehat{\mathbf{K}}(t)\big(\mathbb{I}\mathbf{x}_r - \boldsymbol{\xi}\big)$, the steady-state dynamics of $\widehat{\Pi}_1$ in (4.34) become

$$\begin{aligned}\lim_{t\to+\infty} \dot{\mathbf{x}}_r(t) &= \lim_{t\to+\infty} \mathbf{s}(0) - \lim_{t\to+\infty} \sigma\big[\mathbf{L}(\mathbf{x}_r(t)) \otimes \mathbf{I}_n\big]\mathbf{x}_r(t) - \lim_{t\to+\infty} \eta\mathbb{I}^\mathsf{T}\widehat{\mathbf{K}}(t)\big[\mathbb{I}\mathbf{x}_r(t) - \boldsymbol{\xi}(t)\big] \\ &= -\lim_{t\to+\infty} \big[\eta\mathbb{I}^\mathsf{T}\widehat{\mathbf{K}}(t)\mathbb{I} + \sigma\mathbb{L}(t)\big]\mathbf{x}_r(t) + \lim_{t\to+\infty} \eta\mathbb{I}^\mathsf{T}\widehat{\mathbf{K}}(t)\boldsymbol{\xi}(t) = \mathbf{0},\end{aligned}$$

and the steady-state dynamics of $\boldsymbol{\xi}$ in (4.38) become

$$\begin{aligned}\lim_{t\to+\infty} \dot{\boldsymbol{\xi}}(t) &= \lim_{t\to+\infty} \mathbf{K}_{lc}\big[\mathbf{x}_l^* - \boldsymbol{\xi}(t)\big] + \lim_{t\to+\infty} \mathbb{I}\mathbb{I}^\mathsf{T}\widehat{\mathbf{K}}(t)\big[\mathbb{I}\mathbf{x}_r(t) - \boldsymbol{\xi}(t)\big] \\ &= -\lim_{t\to+\infty} \big[\mathbf{K}_{lc} + \mathbb{I}\mathbb{I}^\mathsf{T}\widehat{\mathbf{K}}(t)\big]\boldsymbol{\xi}(t) + \lim_{t\to+\infty} \mathbb{I}\mathbb{I}^\mathsf{T}\widehat{\mathbf{K}}(t)\mathbb{I}\mathbf{x}_r(t) + \mathbf{K}_{lc}\mathbf{x}_l^* = \mathbf{0}.\end{aligned}$$

Stack the two steady-state dynamics $\dot{\mathbf{x}}_r$ and $\dot{\boldsymbol{\xi}}$ by

$$\begin{bmatrix} \mathbf{K}_{lc}\mathbf{x}_l^* \\ \mathbf{0} \end{bmatrix} - \lim_{t\to+\infty} \begin{bmatrix} \mathbf{K}_{lc} + \mathbb{I}\mathbb{I}^\mathsf{T}\widehat{\mathbf{K}}(t) & -\mathbb{I}\mathbb{I}^\mathsf{T}\widehat{\mathbf{K}}(t)\mathbb{I} \\ -\eta\mathbb{I}^\mathsf{T}\widehat{\mathbf{K}}(t) & \eta\mathbb{I}^\mathsf{T}\widehat{\mathbf{K}}(t)\mathbb{I} + \sigma\mathbb{L}(t) \end{bmatrix} \begin{bmatrix} \boldsymbol{\xi}(t) \\ \mathbf{x}_r(t) \end{bmatrix} = \lim_{t\to+\infty} \begin{bmatrix} \dot{\boldsymbol{\xi}}(t) \\ \dot{\mathbf{x}}_r(t) \end{bmatrix} = \begin{bmatrix} \mathbf{0} \\ \mathbf{0} \end{bmatrix}.$$

Using $\mathbb{I}\mathbb{I}^\mathsf{T} = \mathbf{I}_{N_l n}$, the two steady-state dynamics $\dot{\mathbf{x}}_r$ and $\dot{\boldsymbol{\xi}}$, can be rewritten as

$$-\lim_{t\to+\infty} \widehat{\mathbf{L}}(t) \begin{bmatrix} \boldsymbol{\xi}(t) \\ \frac{1}{\sqrt{\eta}}\mathbf{x}_r(t) \end{bmatrix} + \begin{bmatrix} \mathbf{K}_{lc}\mathbf{x}_l^* \\ \mathbf{0} \end{bmatrix} = \lim_{t\to+\infty} \begin{bmatrix} \dot{\boldsymbol{\xi}}(t) \\ \frac{1}{\sqrt{\eta}}\dot{\mathbf{x}}_r(t) \end{bmatrix} = \begin{bmatrix} \mathbf{0} \\ \mathbf{0} \end{bmatrix}, \tag{4.57}$$

where $\widehat{\mathbf{L}}(t)$ is given by

$$\begin{aligned}\widehat{\mathbf{L}}(t) &= \begin{bmatrix} \mathbf{K}_{lc} + \widehat{\mathbf{K}}(t) & -\sqrt{\eta}\widehat{\mathbf{K}}(t)\mathbb{I} \\ -\sqrt{\eta}\mathbb{I}^{\mathsf{T}}\widehat{\mathbf{K}}(t) & \eta\mathbb{I}^{\mathsf{T}}\widehat{\mathbf{K}}(t)\mathbb{I} + \sigma\mathbb{L}(t) \end{bmatrix} \\ &= \begin{bmatrix} \mathbf{I}_{N_l n} \\ -\sqrt{\eta}\mathbb{I}^{\mathsf{T}} \end{bmatrix} \widehat{\mathbf{K}}(t) \begin{bmatrix} \mathbf{I}_{N_l n} & -\sqrt{\eta}\mathbb{I} \end{bmatrix} + \begin{bmatrix} \mathbf{K}_{lc} & \mathbf{0} \\ \mathbf{0} & \sigma\mathbb{L}(t) \end{bmatrix},\end{aligned}$$

and is clearly uniformly positive semi-definite.

The proof that $\widehat{\mathbf{L}}(t) \succ \mathbf{0}$ is by contradiction. Suppose that $\widehat{\mathbf{L}}(t)$ has a non-trivial null space. Then, there exists a nonzero vector $\mathbf{v} = \begin{pmatrix} \mathbf{v}_1^{\mathsf{T}} & \mathbf{v}_2^{\mathsf{T}} \end{pmatrix}^{\mathsf{T}}$ such that $\mathbf{v}^{\mathsf{T}}\widehat{\mathbf{L}}(t)\mathbf{v} = \big(\mathbf{v}_1^{\mathsf{T}} - \sqrt{\eta}\mathbf{v}_2^{\mathsf{T}}\mathbb{I}^{\mathsf{T}}\big)\widehat{\mathbf{K}}(t)\big(\mathbf{v}_1 - \sqrt{\eta}\mathbb{I}\mathbf{v}_2\big) + \mathbf{v}_1^{\mathsf{T}}\mathbf{K}_{lc}\mathbf{v}_1 + \sigma\mathbf{v}_2^{\mathsf{T}}\mathbb{L}(t)\mathbf{v}_2 = 0$. Because $\mathbf{K}_{lc} \succ \mathbf{0}$, $\widehat{\mathbf{K}}(t) \succ \mathbf{0}$ and $\mathbb{L}(t)$ is a weighted Laplacian matrix, $\mathbf{v}^{\mathsf{T}}\widehat{\mathbf{L}}(t)\mathbf{v} = 0$ requires that $\mathbf{v}_1 = \mathbf{0}$, $\mathbf{v}_2 = \mu\mathbf{1}_{N_r n}$ and $\mathbf{v}_1 = \sqrt{\eta}\mathbb{I}\mathbf{v}_2$ for some integer μ. By the definition of $\mathbb{I}$, this is possible only if $\mu = 0$ and thus $\mathbf{v} = \mathbf{0}$, which contradicts the hypothesis that $\widehat{\mathbf{L}}(t)$ has a non-trivial null space.

Being a nonsingular M-matrix, $\widehat{\mathbf{L}}(t)$ has thence a nonnegative inverse $\widehat{\mathbf{L}}^{-1}(t)$. It follows then that

$$\mathbf{H}(t) = \begin{bmatrix} \mathbf{I}_{N_l n} & \mathbf{0} \\ \mathbf{0} & \sqrt{\eta}\mathbf{I}_{N_r n} \end{bmatrix} \widehat{\mathbf{L}}^{-1}(t) \begin{bmatrix} \mathbf{K}_{lc} \\ \mathbf{0} \end{bmatrix}$$

is also nonnegative. Nevertheless, $\mathbf{H}(t)$ depends on the states of the teleoperator because $\mathbb{L}(t)$ and $\widehat{\mathbf{K}}(t)$ in $\widehat{\mathbf{L}}(t)$ are state-dependent. The spatial distribution of all remote robots can be derived by post- and pre-multiplying $\widehat{\mathbf{L}}(t)$ as follows

$$\begin{aligned}\mathbf{1} &= \begin{bmatrix} \mathbf{I}_{N_l n} & \mathbf{0} \\ \mathbf{0} & \sqrt{\eta}\mathbf{I}_{N_r n} \end{bmatrix} \widehat{\mathbf{L}}^{-1}(t)\widehat{\mathbf{L}}(t) \begin{bmatrix} \mathbf{1}_{N_l n} \\ \frac{1}{\sqrt{\eta}}\mathbf{1}_{N_r n} \end{bmatrix} \\ &= \begin{bmatrix} \mathbf{I}_{N_l n} & \mathbf{0} \\ \mathbf{0} & \sqrt{\eta}\mathbf{I}_{N_r n} \end{bmatrix} \widehat{\mathbf{L}}^{-1}(t) \begin{bmatrix} \mathbf{K}_{lc} \\ \mathbf{0} \end{bmatrix} \mathbf{1}_{N_l n} = \mathbf{H}(t)\mathbf{1}_{N_l n},\end{aligned}$$

which implies that every row of $\mathbf{H}(t)$ sums to 1. As a result, the steady-state locations of all remote robots can be derived by solving (4.57) as follows

$$\lim_{t\to+\infty} \begin{bmatrix} \mathbf{I}_{N_l n} & \mathbf{0} \\ \mathbf{0} & \sqrt{\eta}\mathbf{I}_{N_r n} \end{bmatrix} \widehat{\mathbf{L}}^{-1}(t) \begin{bmatrix} \mathbf{K}_{lc}\mathbf{x}_l^* \\ \mathbf{0} \end{bmatrix} - \lim_{t\to+\infty} \begin{bmatrix} \mathbf{I}_{N_l n} & \mathbf{0} \\ \mathbf{0} & \sqrt{\eta}\mathbf{I}_{N_r n} \end{bmatrix} \widehat{\mathbf{L}}^{-1}(t)\widehat{\mathbf{L}}(t) \begin{bmatrix} \boldsymbol{\xi}(t) \\ \frac{1}{\sqrt{\eta}}\mathbf{x}_r(t) \end{bmatrix}$$

$$= \lim_{t\to+\infty} \mathbf{H}(t)\mathbf{x}_l^* - \lim_{t\to+\infty} \begin{bmatrix} \boldsymbol{\xi}(t) \\ \mathbf{x}_r(t) \end{bmatrix} = \begin{bmatrix} \mathbf{0} \\ \mathbf{0} \end{bmatrix}.$$

Although $\mathbf{H}(t)$ is state-dependent, the sum of each of its rows is invariably 1. Thus, all remote robots approach the convex hull $\mathcal{C}_h$ formed by all local robots asymptotically. ■

Theorem 4.2 formulates the problem in the context of multi-user teleoperation of a robotic network. Containment control through teleoperation can be advantageous because it permits the dynamic re-deployment of a robotic network based on the physical interactions among multiple users. For example, in the spatio-temporal sampling, the assignment of a robotic sensor network could be determined interactively through haptic negotiations among its human operators instead of being fixed or pre-programmed. The connectivity and passivity analyses in Sections 4.1.1 and 4.1.2 guarantee the safety of the physical interaction with the robotic system. Furthermore, the force feedback and position synchronization, guaranteed in Theorem 4.1, enable all human users to perceive the intentions of other users and to impose their decisions on the robotic network. Lastly, Theorem 4.2 clarifies the active role that operators play in altering the spatial layout of the remote multi-robot system.

4.2 Experimental Results

This section compares the proposed connectivity-preserving passivation strategy to P+d control [174] through experiments[1] on a teleoperation platform with 4 local and 10 remote robots. Experimental results substantiate that both controls can stabilize the time-delay multi-user teleoperation of a remote multi-robot system. However, P+d control may fail to preserve the connectivity of the multi-robot system and, thus, to support the multi-user collaboration when deploying the remote robots. In contrast, the proposed control maintains all intra-multi-robot system connections regardless how fast user commands change and, thus, enables all users to participate in the containment control of the multi-robot system.

As shown in Figure 4.8, the experimental platform contains 4 Geomagic Touch local robots (L1-L4) and a remote multi-robot system with 10 Novint Falcon remote robots (R1-R10). The coloured lines show the time-delay communications between

[1] `https://youtu.be/9Rss6ImyvFs`

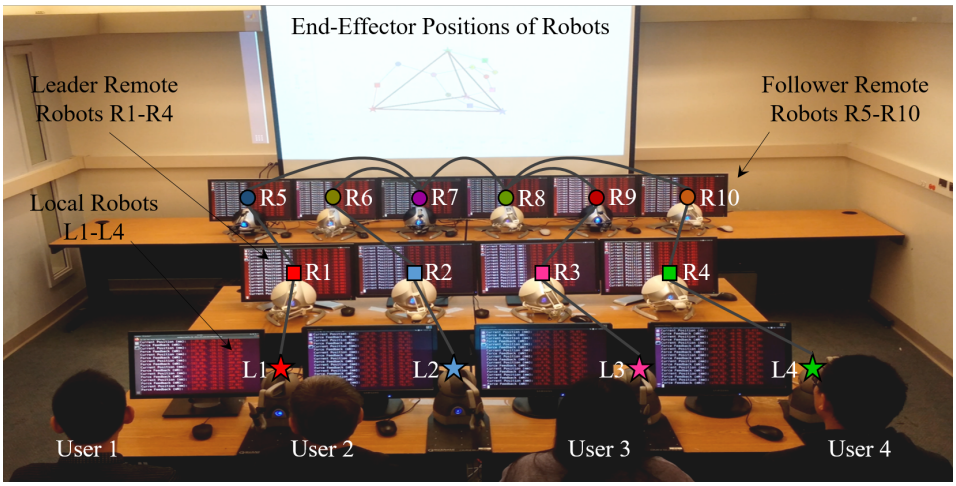

Figure 4.8: The experimental setup for multi-user teleoperation of a distributed multi-robot system with proximity-limited communications.

the local and remote robots. The dark grey lines indicate the proximity-limited communications between the remote robots. Each robot is controlled locally via USB 2.0 by a C++ program running on a unique dedicated Ubuntu machine at 1 kHz. Every C++ programs can get the position measurements of, and impose the control forces on, the end-effectors of robots in their local East, North, Up Cartesian coordinate systems by calling standard haptic APIs: the OpenHaptics® toolkit for the local robots and the CHAI3D[2] SDK for the remote robots. These programs can further compute the end-effector velocities of robots from their position measurements using second-order low-pass filters with a cut-off frequency of 100 Hz. All machines connect to a 16-port network switch, the NETGEAR® GS316, and further to the Internet through Insignia™ CAT-6 ethernet cables. They run the Robot Operating System (ROS) to send/read the position signals to/from other robots at an approximate rate of 50 Hz. Because the local control loops of all robots run at a higher frequency (1 kHz) than the ROS interface (50 Hz), all robot positions are delayed by up to 40 ms when received by, and employed in the control of, their neighbours.

Controlling the local Geomagic Touch and the remote Novint Falcon robots is challenging because they are all haptic devices with limited performance. The inexact gravity compensation and the inherent dry friction severely limit their motion accuracy. Moreover, the damping injection through control can lead to instability because of velocity estimation errors. The experiments address these practical chal-

[2] `https://www.chai3d.org`

lenges by: abstracting all local robots by point proxies with mass 10 g and all remote robots by point proxies with mass 100 g; coupling all local robots to their proxies for bilateral teleoperation; controlling all remote robots to track their proxies; and tuning control gains that connect robots to their proxies so as to permit to assume that these proxies adequately represent physical robot dynamics and to carry out the experimental comparison in the virtual layer (proxies). Additionally, the positions of all virtual proxies are projected on a screen, see Figure 4.8.

As shown in Section 4.1, the proposed control inherits the position synchronization and force feedback capabilities of P+d control, and also preserves all proximity-constrained communications between the remote robots. The two experiments herein validate all results in Section 4.1 using the following 7 steps.

A. **Autonomous Mode**

1. Regulate all local (L1-L4) and remote (R1-R10) robots to their initial positions depicted in Figure 4.9.
2. Activate the controllers of the remote robots and keep the local robots at their initial positions.
3. Activate the controllers of the local robots without applying any user forces to the local robots.

T. **Teleoperation Mode**

4. The user 1 repetitively strains and relaxes the coupling between the local robot L1 and the remote robot R1.
5. All users cooperatively change the spatial distribution of the remote multi-robot system.
6. The user 1 yanks and releases their local robot L1 regardless of the connectivity of the remote multi-robot system.
7. All users move their local robots close to their original positions.

In the autonomous mode: Step 1 initializes the states (positions and velocities) of all robots to guarantee Assumptions 4.3 and 4.4; Step 2 evaluates the containment control in Theorem 4.2; and Step 3 investigates the autonomous synchronization of the remote multi-robot system in Theorem 4.1. In the subsequent teleoperation mode, four operators use their local robots to teleoperate the remote multi-robot system:

Step 4 tests the steady-state force feedback in Theorem 4.1; Step 5 verifies that the robust synchronization in Theorem 4.1 enables users to collectively tele-guide the remote multi-robot system; Step 6 compares multi-robot system connectivity preservation under the proposed and under P+d control; and Step 7 demonstrates the need to preserve the multi-robot system connectivity during teleoperation.

In the comparison in Step 6, the users 2-4 keep their local robots L2-L4 in a fixed triangle at the top right corner of the workspace, while the user 1 repeatedly yanks their local robot L1 from near the fixed triangle to the bottom left corner of the workspace, to endanger the connectivity of the remote robot network. The average acceleration of L1, $\Xi = 4d/t^2$ with d its travel distance and t its travel time, provides an empiric aggressiveness metric for the motions of the user 1. Table 4.1 reports the aggressiveness, Ξ, of all user trials in Step 6 for both experiments.

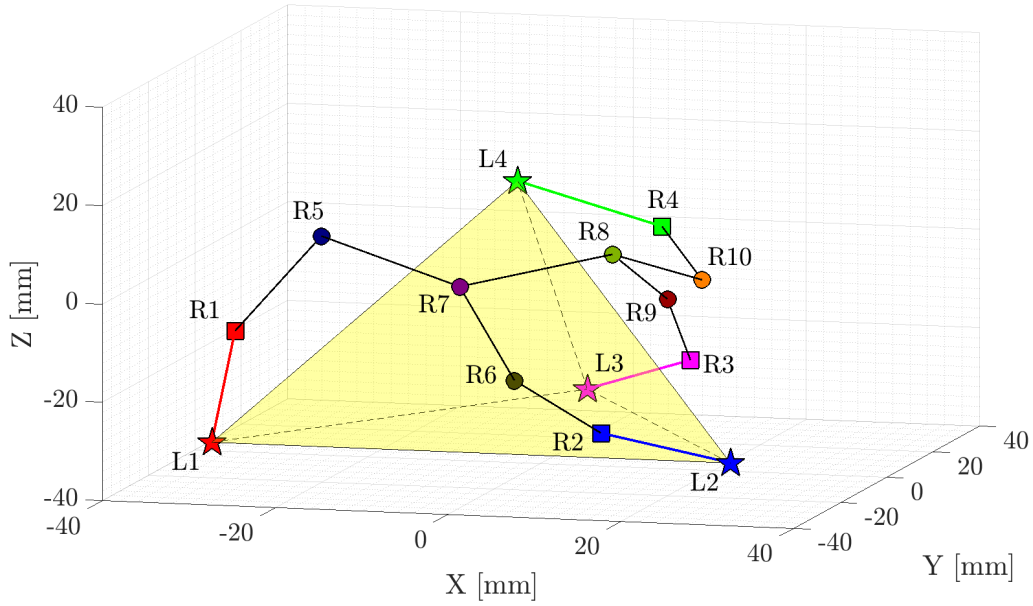

Figure 4.9: The initial positions of all robots and their communication links.

Due to their limited workspaces, the communication radius of all Novint Falcon robots in the remote multi-robot system is set to $r = 30$ mm, see Figure 4.9. In addition to the masses of the virtual proxies, the injected damping impacts the quality of user experience during teleoperation. On the one hand, sufficient damping stabilizes the system and suppresses unwanted robot vibrations. On the other hand, too much damping demands increased user effort and tires the operator. For both experiments, the damping gains $D_* = 1$ for all robots are first selected heuristically, to support high-quality user experience. Then, the Proportional control gains $P_* = 1500$ are tuned

for tight but stable multi-robot system synchronization. Trial and error indicates that P+d control cannot maintain the multi-robot system connected when the user 1 applies forces larger than 3 N while other users keep their local robots stationary. Therefore, the couplings between the local robots and their proxies, and between the proxies of the local and leader remote robots, are saturated by $\overline{\mathbf{f}}_{hi} = (5, 5, 5)^{\mathsf{T}}$ N. Lastly, the gains of the proposed control are chosen by $P = 1$, $Q = 0.01$, $\sigma = 50$, $\eta = 1$ and $K_* = 1000$ for connectivity-preserving teleoperation.

Table 4.1: The aggressiveness of the user 1' actions during Step 6 of the teleoperation.

Controller	**Aggressiveness Metric Ξ**				
P+d Control	0.11	0.14	0.17	0.10	0.16
	0.61	1.78	0.13	0.13	1.75
The Proposed Control	0.11	0.11	0.39	0.11	0.17
	0.18	1.79	1.85	1.83	1.89
	0.14	0.23	0.58	0.24	0.33
	1.91	1.93	2.26	1.95	0.12
	0.15	0.16			

The remaining of this section contrasts the connectivity-preserving synchronization performance of P+d control and of the proposed control in Figures 4.10 and 4.12. Because both control approaches equally enable all users to teleoperate the remote multi-robot system, Figures 4.11 and 4.13 depict the control force $\mathbf{f}_{l1}$ of the local robot L1 and the sum $\mathbf{f}_{h234} = \mathbf{f}_{h2} + \mathbf{f}_{h3} + \mathbf{f}_{h4}$ of the forces applied by the users 2-4 to illustrate the force feedback performance. Because all local robots lack force measurement, the user forces $\mathbf{f}_{hi}$ are approximated by the coupling forces between the local robots and their proxies.

4.2.1 Teleoperation Under P+d Control

Figure 4.10 presents the experimental 4-user teleoperation of the 10-robot remote multi-robot system under P+d control during various steps of the experimental procedure. Figure 4.10(a) plots the paths of all remote robots (R1-R10) in Step 2, from their initial positions (markers with dashed edges) at $t = 35$ s to their final positions (markers with solid edges) inside the convex hull spanned by all local robots (L1-L4) at $t = 42$ s. It illustrates that P+d control is a suitable containment strategy given a connected multi-robot system. Figures 4.10(b)-4.10(c) depict all robot positions at

two time instants when the user 1 strains at $t = 58$ s, and then restores at $t = 60$ s, the coupling between the local robot L1 and the leader remote robot R1 in Step 4. They confirm that the remote multi-robot system behaves as an elastic body that deforms as a result of its interactions with four users. Figure 4.10(d) shows the paths of all robots from $t = 77$ s to $t = 88$ s in Step 5, when four users move their local robots to carry the connected multi-robot system to another area. All arrows on the paths indicate the movement directions. Once the multi-robot system has reached the new area, the user 1 recommences to strain the coupling between the robots L1 and R1, this time with larger and faster motions. Figure 4.10(e) shows that a sudden motion of the user 1, with $\Xi = 1.78$, accelerates the remote robot R1 so much that its neighbour R5 cannot follow it sufficiently fast. As a result, at $t = 107$ s in Step 6, their inter-distance grows larger than their communication range r and their communication link breaks (the dashed line in Figure 4.10(e)), disconnecting R1 from the multi-robot system. Figure 4.10(f) displays the retraction of all local robots close to their original positions from $t = 134$ s to $t = 138$ s in Step 7. Note that, because the remote robot R1 is detached from the multi-robot system in this step, the user 1 has no control over the motion of the multi-robot system, only over the motion of R1. In practice, it may be undesirable that any user loses their ability to tele-guide the remote multi-robot system.

In Step 6, the user 1 yanks their local robot L1 10 times, from $t = 89$ s to $t = 130$ s in the experimental video, to examine the multi-robot system connectivity under P+d control. Table 4.1 lists the aggressiveness Ξ of all user 1's motions in chronological order, from left to right and from up to down. In the experiment, the multi-robot system remains connected for the user motions with $\Xi \leq 0.61$; and it disconnects for Ξ increasing to 1.75 and 1.78 (Figure 4.10(e)).

Figure 4.11 plots the force feedback $\mathbf{f}_{l1} = \left(f_{l1}^x, f_{l1}^y, f_{l1}^z\right)^\mathsf{T}$ to the user 1 and the sum $\mathbf{f}_{h234} = \left(f_{h234}^x, f_{h234}^y, f_{h234}^z\right)^\mathsf{T}$ of other user-applied forces. In each subplot, the areas coloured light yellow, pink, green and blue indicate the teleoperation steps 4-7, and the 7 dots indicate the force values that correspond to the system states at $t = 58$ s, $t = 60$ s, $t = 77$ s, $t = 88$ s, $t = 107$ s, $t = 134$ s and $t = 138$ s in Figure 4.10. As the local robot L1 moves to its position in Figure 4.10(b) guided by its user and then moves to its position in Figure 4.10(c) when released by its user, the force feedback f_{l1}^z approaches -5 N and then drops to near 0 N in the yellow area in Figure 4.11. In Step 5, all users cooperatively move the multi-robot system as shown in Figure 4.10(d) and reduce the volume of the tetrahedron they span. Hence,

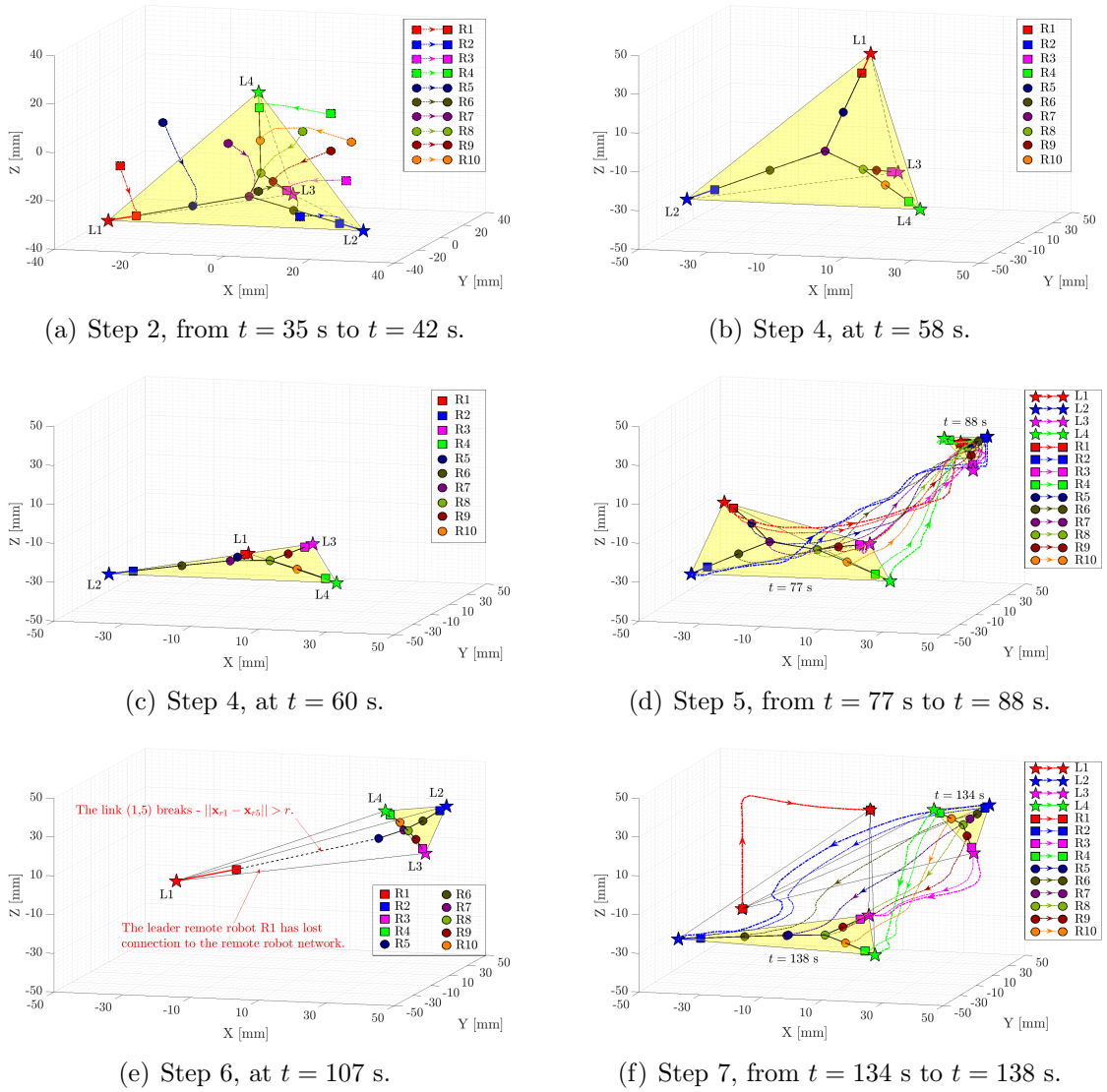

(a) Step 2, from $t = 35$ s to $t = 42$ s.

(b) Step 4, at $t = 58$ s.

(c) Step 4, at $t = 60$ s.

(d) Step 5, from $t = 77$ s to $t = 88$ s.

(e) Step 6, at $t = 107$ s.

(f) Step 7, from $t = 134$ s to $t = 138$ s.

Figure 4.10: The experimental 4-user teleoperation of a 10-robot remote multi-robot system under P+d control.

the force feedback $\mathbf{f}_{l1}$ to the user 1 becomes approximately zero in the pink area in Figure 4.11. Then the user 1 yanks their local robot L1 and f_{l1}^x and f_{l1}^z reach their upper bound 5 N repeatedly in the green area of Figure 4.11, until the communication link $(1, 5)$ breaks the 7-th time, see Figure 4.10(e). While the link $(1, 5)$ is broken, the robots L1 and R1 are synchronized and detached from other robots, and the force feedback $\mathbf{f}_{l1}$ becomes $\mathbf{0}$. Later, the user 1 reconnects the robots R1 and R5 and yanks L1 repeatedly again, breaking the link $(1, 5)$ the third time. When all users slowly move their local robots close to their initial locations in Figure 4.10(f), the detached

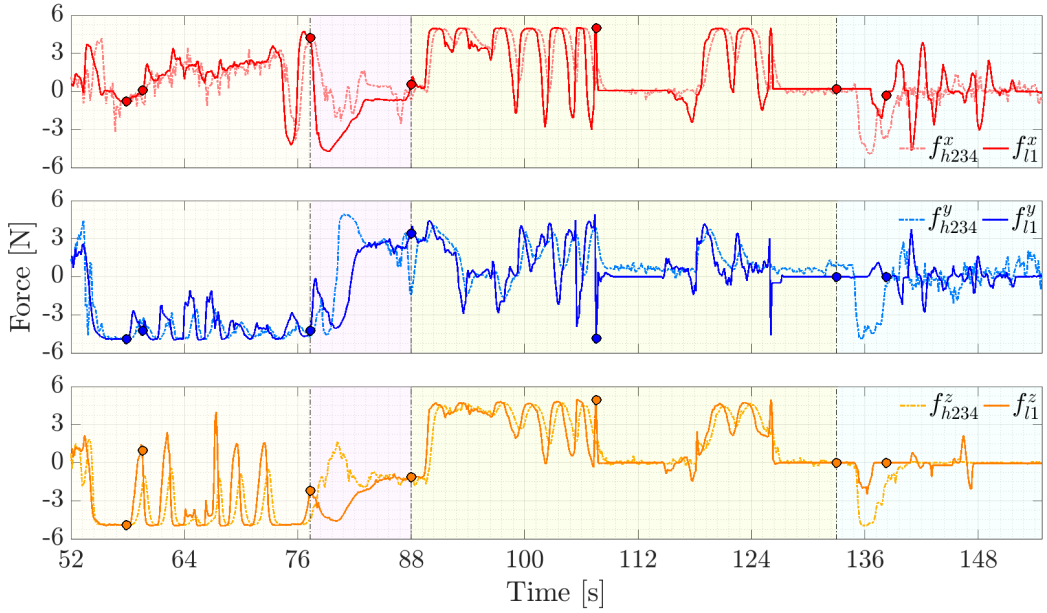

Figure 4.11: The control force $\mathbf{f}_{l1}$ of the local robot L1 and the sum $\mathbf{f}_{h234}$ of the forces of the users 2-4 during teleoperation under P+d control.

L1-R1 robot pair conveys almost no force feedback to the user 1. From $t = 138$ s to $t = 150$ s, the user 1 wiggles L1 quickly to make R1 lag far behind L1, and they can feel a stronger force feedback due to the dynamics of R1. Figure 4.11 shows that P+d control can display to the user 1 the sum of other user forces when the multi-robot system is connected, especially when the L1-R1 coupling is stretched. When the link $(1, 5)$ is broken and the multi-robot system is disconnected, the force feedback $\mathbf{f}_{l1}$ no longer conveys $\mathbf{f}_{h234}$, see their pronounced discrepancy after $t = 139$ s in Figure 4.11.

In summary, P+d control: (i) stabilizes teleoperation and achieves containment control of a connected multi-robot system while conveying the sum of other user forces to each operator; (ii) but cannot preserve the connectivity of the multi-robot system if an operator's commands are too aggressive. As illustrated by the experiment above, the aggressive user cannot teleoperate the disconnected multi-robot system or feel the forces of other users. The following section verifies experimentally that the proposed connectivity-preserving passivation strategy can overcome this limitation of P+d control.

4.2.2 Teleoperation Under The Proposed Control

Figure 4.12 presents the experimental 4-user teleoperation of the 10-robot remote multi-robot system under the control proposed in this chapter. The experiment is similar to the one in the previous section (because the users strive to repeat their telemanipulations), but some results are different. In Figure 4.12(a), the teleoperated multi-robot system is more compact and the couplings between the leader remote robots R1-R4 and their associated local robots L1-L4 are weaker than in Figure 4.10(a). This result validates that the developed controller can maintain the remote multi-robot system more tightly interconnected than P+d control thanks to its connectivity-preserving characteristic. Figures 4.12(b)-4.12(c) depict two teleoperator configurations when the user 1 strains at $t = 195$ s and relaxes at $t = 196$ s the connection between their local robot L1 and the leader remote robot R1 in Step 4. They prove that the remote multi-robot system behaves analogously under the proposed control and under P+d control: it deforms when the user 1 stretches it in Figure 4.12(b) and regains its configuration when the user force disappears in Figure 4.12(c). Figure 4.12(d) shows that the remote multi-robot system is more compact and stays farther away from the boundary of the convex hull spanned by the local robots L1-L4 from $t = 208$ s to $t = 217$ s when all users cooperatively transport it to another region in Step 5. This feature can make the proposed passivation controller preferable to P+d control in applications that require the remote multi-robot system to cohesively navigate through confined spaces: the users can enforce safety constraints using their local devices; and the proposed control can maintain the remote robots close to each other and a safe distance away from those constraints. Figure 4.12(e) validates the key feature of the proposed controller: its ability to preserve the initial connectivity of the remote multi-robot system even when the user 1 moves their local robot L1 suddenly with $\Xi = 1.93$ and over large distance at $t = 255$ s. Step 6 in the experiment demonstrates that the proposed control maintains all intra-multi-robot system connections when the user 1 threatens them by saturating the L1-R1 coupling (the red line): the control of the leader remote robots prioritizes their proximity-constrained connections to other remote robots over their connections to their local robots, which occur over the Internet and are not limited by distance. Favouring connectivity preservation, the proposed passivation controller also preserves the role of all users in the collaborative delivery of the remote multi-robot system and in adjusting its spatial distribution after $t = 271$ s, see Figure 4.12(f).

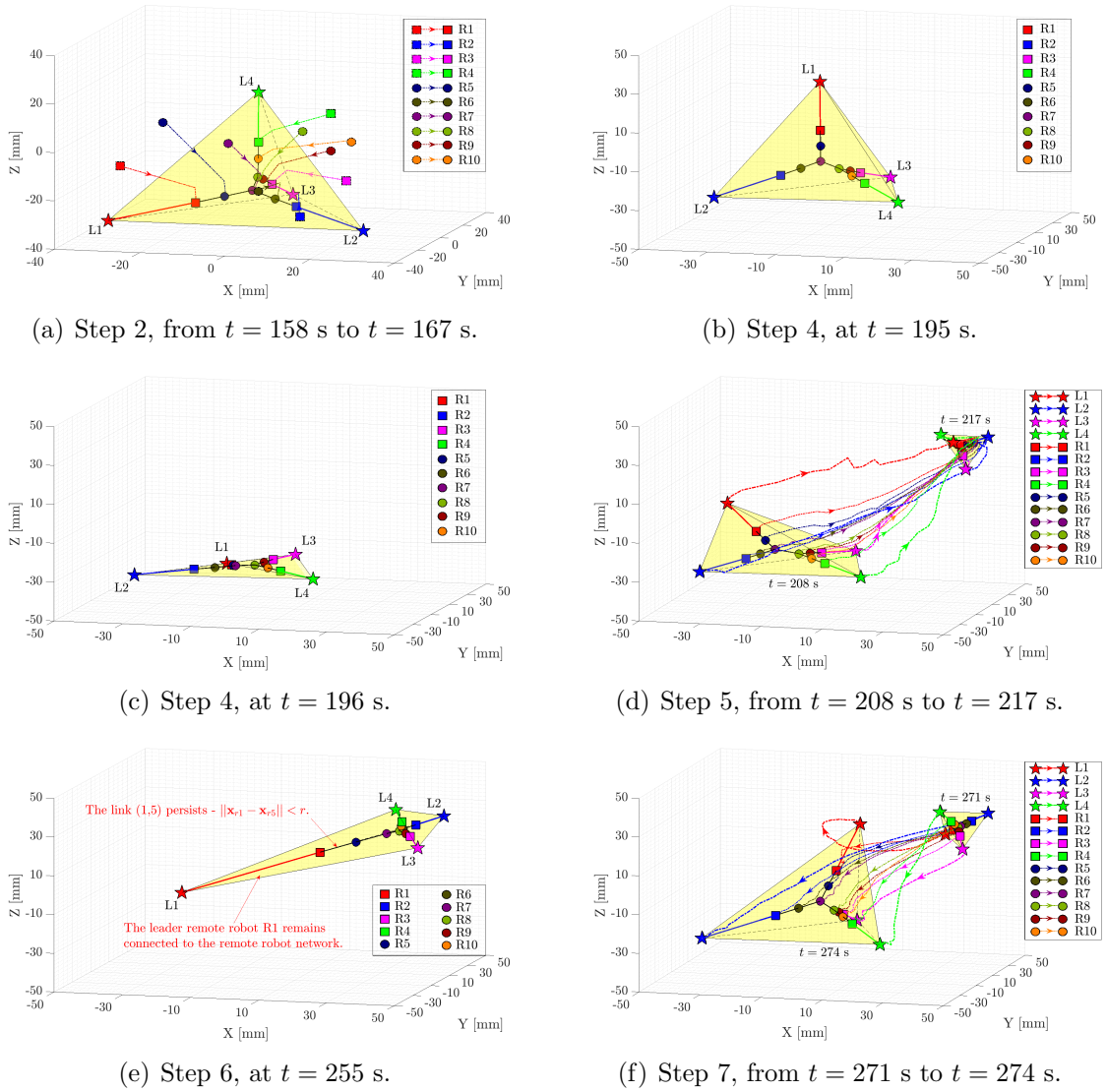

(a) Step 2, from $t = 158$ s to $t = 167$ s.

(b) Step 4, at $t = 195$ s.

(c) Step 4, at $t = 196$ s.

(d) Step 5, from $t = 208$ s to $t = 217$ s.

(e) Step 6, at $t = 255$ s.

(f) Step 7, from $t = 271$ s to $t = 274$ s.

Figure 4.12: The experimental 4-user teleoperation of a 10-robot remote multi-robot system under the proposed feedforward-feedback passivation control.

To verify that the proposed feedforward-feedback passivation controller preserves the tree connectivity of the remote multi-robot system, the user 1 yanks their local robot L1 repeatedly in Step 6 of the experiment, from $t = 217$ s to $t = 270$ s. Table 4.1 lists the aggressiveness Ξ of the user 1's motions in chronological order, from left to right and from up to down. The 7th to the 10th and the 16th to the 19th motions all have $\Xi \geq 1.78$, namely they are more rapid and sudden than the motions of the user 1 in Section 4.2.1. Nevertheless, they cannot break any communication links of the remote multi-robot system. In practical teleoperation, such aggressive manipulations

may arise due to human errors and need to be handled by the teleoperation controller.

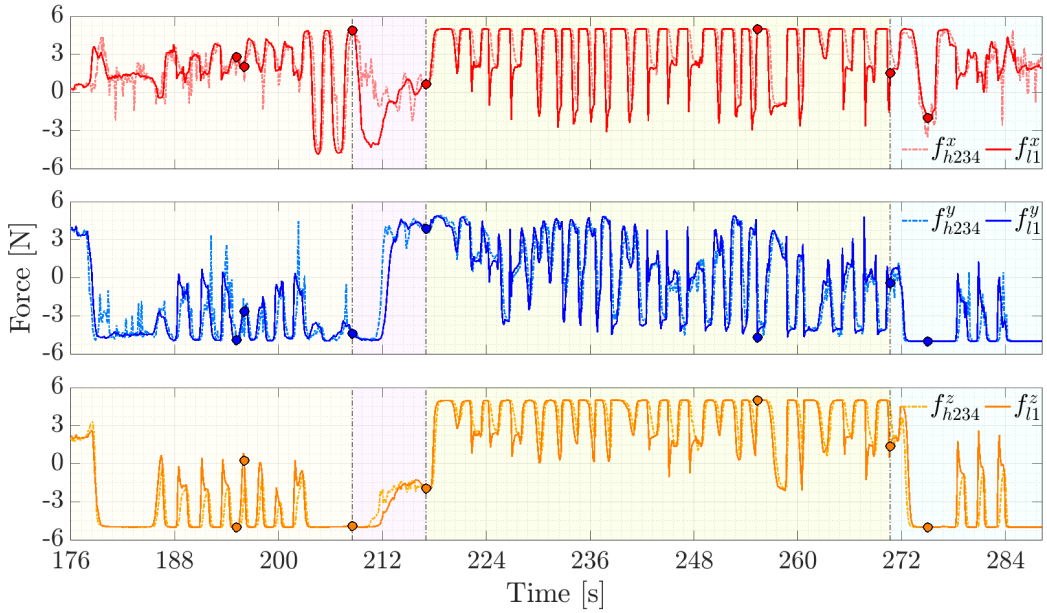

Figure 4.13: The control force $\mathbf{f}_{l1}$ of the local robot L1 and the sum $\mathbf{f}_{h234}$ of the forces of the users 2-4 during teleoperation under the proposed feedforward-feedback passivation control.

Figure 4.13 depicts the the force feedback $\mathbf{f}_{l1}$ to the user 1 and the sum $\mathbf{f}_{h234}$ of other user-applied forces. As in Figure 4.11, the four coloured areas correspond to the teleoperation steps 4-7, and the 7 dots indicate the forces that correspond to the system states in Figure 4.12. In Step 4, the user 1 lifts their local robot L1 nine times from $t = 178$ s to $t = 205$ s. For example, during the motion of L1 from its position in Figure 4.12(b) to its position in Figure 4.12(c), the force feedback f^z_{l1} changes from -5 N to about 0 N in Figure 4.13 to convey to the user 1 the distance of R1 from L1. Then the multi-robot system moves from $t = 208$ s to $t = 217$ s in Figure 4.12(d) and the volume of their spanned tetrahedron decreases, leading to almost zero feedback forces f^x_{l1} and f^z_{l1} in the pink area of Figure 4.13. In Step 6, repeated aggressive actions of the user 1 lead to the frequent saturation of the force feedback in the green area of Figure 4.13. This figure shows that, at $t = 255$ s, the system state in Figure 4.12(e) feeds back to the user 1 a force $\mathbf{f}_{l1} = \big(5, -4.5, 5\big)^{\mathsf{T}}$ N nearly proportional to the displacement of R1 from L1. After guiding the multi-robot system to the position in Figure 4.12(f), the user 1 releases and forces their robot L1 to the bottom and top of its workspace three more times between $t = 277$ s and $t = 285$ s. The force profile is similar to that in Step 4 and implies that the

multi-robot system remains elastic. Notably, the strong agreement of $\mathbf{f}_{l1}$ and $\mathbf{f}_{h234}$ throughout the teleoperation validates that the user 1 accurately perceives other user forces in the steady state, and other user forces plus the dynamics of the teleoperator during the transient phases.

The experiment confirms that the proposed feedforward-feedback passivation controller has force feedback performance similar to P+d control, but can preserve the connectivity of the remote multi-robot system in the presence of aggressive user actions.

4.3 Conclusion

This chapter has developed a control strategy for bilateral multi-user teleoperation of a remote multi-robot system that guarantees both the tree connectivity of the multi-robot system and the passivity of the teleoperator. In contrast to existing results, the proposed strategy designs intra-multi-robot system couplings based on a bounded potential. This design facilitates future extensions to systems with additional constraints, such as time-delay communications between, and bounded actuation of, the remote robots. The new strategy strictly limits the energy stored in the remote multi-robot system, and thus its passivity level, to a certain upper bound. To this end, a sliding variable at each remote robot decomposes the teleoperator into an interconnection of several subsystems. The input-output properties of those subsystems inspire a dynamic feedback strategy that passivates delay-free teleoperation. Then, a reframing of the overall teleoperator by the "control as interconnection" paradigm leads to a novel feedforward-feedback strategy that passivates time-delay teleoperation. The rigorous proofs claim the performance of the proposed connectivity-preserving passivation strategy in terms of position synchronization, force feedback and containment control in the steady state. An experimental comparison with P+d control validates the proposed design empirically.

Chapter 5

Distributed Multi-Robot Teleoperation With Winners-Take-All Authority Dispatch

In this chapter, we transfer the authority sharing concept from hand-by-hand haptic training to multi-user teleoperation of a multi-robot system. The new setting features a unique and arduous challenge: the remote robot network needs to automatically dispatch a dominance factor to every leader remote robot in a distributed manner in response to users' requests. Specifically, we particularize a WTA principle that permits only winners to tele-drive the remote robot group. Based on the Oja's rule for PCA [182], this chapter firstly devises a dynamic network to achieve WTA authority dispatch and justifies its power by the conjunction of set invariance and a dedicated quotient function. Yet, it is not trivial to synthesize the design with passivity-based teleoperation control schemes. For this reason, this chapter then reformulates a constrained quadratic programming with a rigorous effectiveness proof, searches the unique minimizer by a distributed primal-dual method at an exponential convergence rate, interconnects the WTA algorithm with physical robot dynamics in a power-preserving way, and analyses passive teleoperation performance with multiple storage functions. Two comparative experiments have also corroborated that the proposed control with WTA authority dispatch outperforms P+d control [174] with no authority dispatch in terms of teleoperation versatility.

5.1 Preliminaries

We consider a distributed multi-robot teleoperation system that consists of $N_l \geq 1$ local robots and a group of $N_r \geq N_l$ remote robots. The underlying communication network of the remote robot group is assumed to be a tree. In the remote robot team: the first N_l robots are leaders that can communicate with their associated local robots; and the remaining $N_r - N_l$ robots are followers that can exchange information only with their neighbours within the group.

5.1.1 System Dynamics

The EL dynamics of the local robots $i = 1, \cdots, N_l$ are

$$\mathbf{M}_{li}(\mathbf{x}_{li})\ddot{\mathbf{x}}_{li} + \mathbf{C}_{li}(\mathbf{x}_{li}, \dot{\mathbf{x}}_{li})\dot{\mathbf{x}}_{li} = \mathbf{f}_{li} + \mathbf{f}_{hi}, \tag{5.1}$$

and of the remote robots $i = 1, \cdots, N_r$ be

$$\mathbf{M}_{ri}(\mathbf{x}_{ri})\ddot{\mathbf{x}}_{ri} + \mathbf{C}_{ri}(\mathbf{x}_{ri}, \dot{\mathbf{x}}_{ri})\dot{\mathbf{x}}_{ri} = \mathbf{f}_{ri}, \tag{5.2}$$

where the subscripts li and ri indicate the local and remote robot quantities, respectively. In particular, in the subscript ri, $i = 1, \cdots, N_l$ and $i = N_l+1, \cdots, N_r$ indicate the leader and follower remote robots, respectively. The control forces are $\mathbf{f}_{li}$ for the local robot $i = 1, \cdots, N_l$, and $\mathbf{f}_{ri}$ for the remote robot $i = 1, \cdots, N_r$. Lastly, $\mathbf{f}_{hi}$ is the force applied by the human user i to their local robot i.

Assumption 5.1. *The human users are passive, i.e.,* $\int_0^t \dot{\mathbf{x}}_{li}^{\mathsf{T}}(\tau)\mathbf{f}_{hi}(\tau)d\tau < +\infty$, *for any* $i = 1, \cdots, N_l$ *and* $t \geq 0$.

For ease of presentation, assume that each local robot i communicates with a single leader remote robot i, $i = 1, \cdots, N_l$. The force feedback to the user i is computed by

$$\mathbf{f}_{li} = P_{lr}(\mathbf{x}_{ri} - \mathbf{x}_{li}) - D_l\dot{\mathbf{x}}_{li}, \tag{5.3}$$

with $i = 1, \cdots, N_l$, and P_{lr} and D_l positive constants. For team coordination and teleoperation, the remote robots $i = N_l + 1, \cdots, N_r$ are controlled by

$$\mathbf{f}_{ri} = -\sum_{j \in \mathcal{N}_i} P_{ij}(\mathbf{x}_{ri} - \mathbf{x}_{rj}) - D_r\dot{\mathbf{x}}_{ri}, \tag{5.4}$$

where the subscript $j \in \mathcal{N}_i$ indexes the remote robots j in the set $\mathcal{N}_i$ of neighbours of the remote robot i, and $P_{ij} = P_{ji}$ and D_r are positive constants. The leader remote robots $i = 1, \cdots, N_l$ are controlled by

$$\mathbf{f}_{ri} = \omega_i P_{lr}(\mathbf{x}_{li} - \mathbf{x}_{ri}) - \sum_{j \in \mathcal{N}_i} P_{ij}(\mathbf{x}_{ri} - \mathbf{x}_{rj}) - D_r \dot{\mathbf{x}}_{ri} - \mathbf{K}_{ri}(t) \cdot \mathrm{Sign}(\dot{\mathbf{x}}_{ri}), \tag{5.5}$$

where the scalar authority factor ω_i is to be designed in Section 5.2, the positive semi-definite matrix $\mathbf{K}_{ri}(t)$ is to be determined in Section 5.3, dependent on the states of robots and thus on time, and $\mathrm{Sign}(\dot{\mathbf{x}}_{ri})$ takes the sign of $\dot{\mathbf{x}}_{ri}$ component-wisely.

The control forces $\mathbf{f}_{li}$ of the local robots $i = 1, \cdots, N_l$ feed $P_{lr}(\mathbf{x}_{ri} - \mathbf{x}_{li})$ back to the users i, informing them about $\mathbf{x}_{ri} - \mathbf{x}_{li}$, the displacement between their local robot i and the leader remote robot i. The control forces $\mathbf{f}_{ri}$ of the remote robots $i = 1, \cdots, N_r$ robustly coordinate all remote robots through the diffusive couplings $-\sum_{j \in \mathcal{N}_i} P_{ij}(\mathbf{x}_{ri} - \mathbf{x}_{rj})$ and the damping injection $-D_r \dot{\mathbf{x}}_{ri}$. Notably, the force $P_{lr}(\mathbf{x}_{li} - \mathbf{x}_{ri})$ that connects the leader remote robot i to its associated local robot i is dynamically scaled by the allocated authority factor $\omega_i \in [0, 1]$. Thus, different users have different impact on tele-driving the group of remote robots. Because the time-varying authority factors ω_i break the symmetry of the local robot-leader remote robot couplings, making them non power-preserving, the additional damping $-\mathbf{K}_{ri}(t) \cdot \mathrm{Sign}(\dot{\mathbf{x}}_{ri})$ is introduced at the leader remote robots to passivate the overall teleoperator.

5.1.2 Winners Take All

The key objective of this chapter is to design a distributed algorithm to dispatch the authority factors $\omega_i \in [0, 1]$ to all leader remote robots $i = 1, \cdots, N_l$ during teleoperation. Consider a team of remote robots for sampling and data collection in an uncertain environment, and several human users at different locations and with different levels of demand for teleoperating the remote robots. The users convey their demands by sending the bids u_i, $i = 1, \cdots, N_l$, to the leader remote robots. Let larger bids indicate stronger demand. After the leader remote robots collect all user bids, the network must compare them and distribute appropriate teleoperation authority to all users by adapting the authority factors ω_i of the leader remote robots in real time. Because the forces $P_{lr}(\mathbf{x}_{li} - \mathbf{x}_{ri})$ applied by the local robots on their associated leader remote robots are scaled by the authority factors ω_i, see Equation (5.5), the

higher bids u_i must lead to the larger authority factors ω_i to indeed grant users higher teleoperation control authority over the group of remote robots.

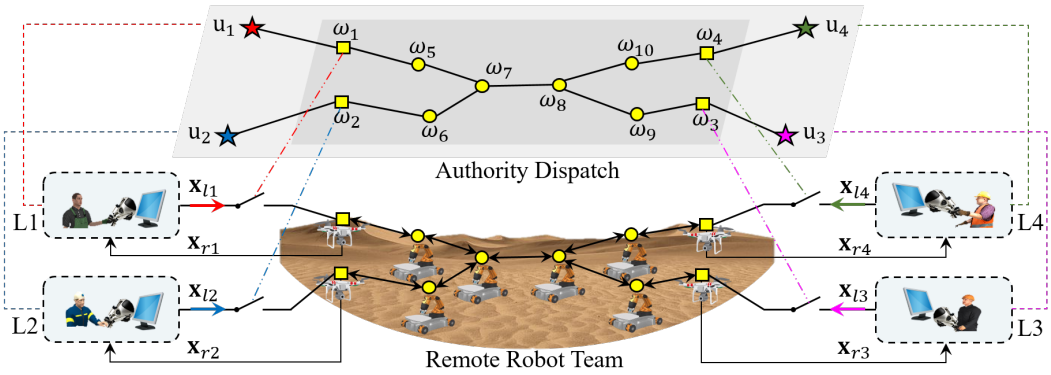

Figure 5.1: A distributed multi-robot teleoperation system with $N_l = 4$ local robots and $N_r = 10$ remote robots.

To make the problem mathematically tractable, let $\epsilon > 0$ be the prescribed resolution of the authority dispatch algorithm for the remote robot network, and let $\mathcal{U} = \{b_1, \cdots, b_m\}$ be a set of candidate user bids, with $b_1 \geq \epsilon$ and $b_i - b_{i-1} \geq \epsilon$ for $i = 2, \cdots, m$. Over distributed communications, let the remote robots $i = 1, \cdots, N_r$ be endowed with an authority factor ω_i and receive a bid u_i as follows.

B1 The leader remote robots receive piecewise constant bids $u_i(t) = u_i(t_k) \in \mathcal{U}$, $i = 1, \cdots, N_l$, from their local robots for time $t \in [t_k, t_{k+1})$, where $k = 1, 2, 3, \cdots$ is the switching signal of the bidding process.

B2 All follower remote robots receive constant bids $u_i(t) = b_0 \geq 0$, $i = N_l + 1, \cdots, N_r$, for all time $t \geq 0$.

If human operators submit higher (lower) bids to the robot network when they observe more (less) urgent circumstances, the WTA authority dispatch network should behave as follows.

O1 If all user bids $u_i(t)$, $i \in \mathcal{S}_w = \{1, \cdots, N_l\}$, are equal, the algorithm distributes the same authority factor $\omega_i(t) = 1/N_l$ to all leader remote robots as $t \to +\infty$.

O2 If some user bids $u_i(t)$, $i \in \mathcal{S}_w \subsetneq \{1, \cdots, N_l\}$, are equal and higher than all other user bids $u_j(t)$, $j \in \mathcal{S}_l = \{1, \cdots, N_l\} - \mathcal{S}_w$, the algorithm distributes an authority factor $\omega_i(t) = 1/|\mathcal{S}_w|$ to the leader remote robots $i \in \mathcal{S}_w$, and a factor $\omega_j(t) = 0$ to the remaining leader remote robots $j \in \mathcal{S}_l$, as $t \to +\infty$.

The control force $\mathbf{f}_{ri}$ of the remote robot i indicates that the teleoperation authority of the user i vanishes as the distributed authority factor $\omega_i(t) \to 0$ and recovers as $\omega_i(t) \to 1$. As shown in the following sections and illustrated in Figure 5.1, the above WTA authority dispatch network enables all winning users to interactively adjust the spatial layout of the remote robots within the convex hull spanned by their local robots.

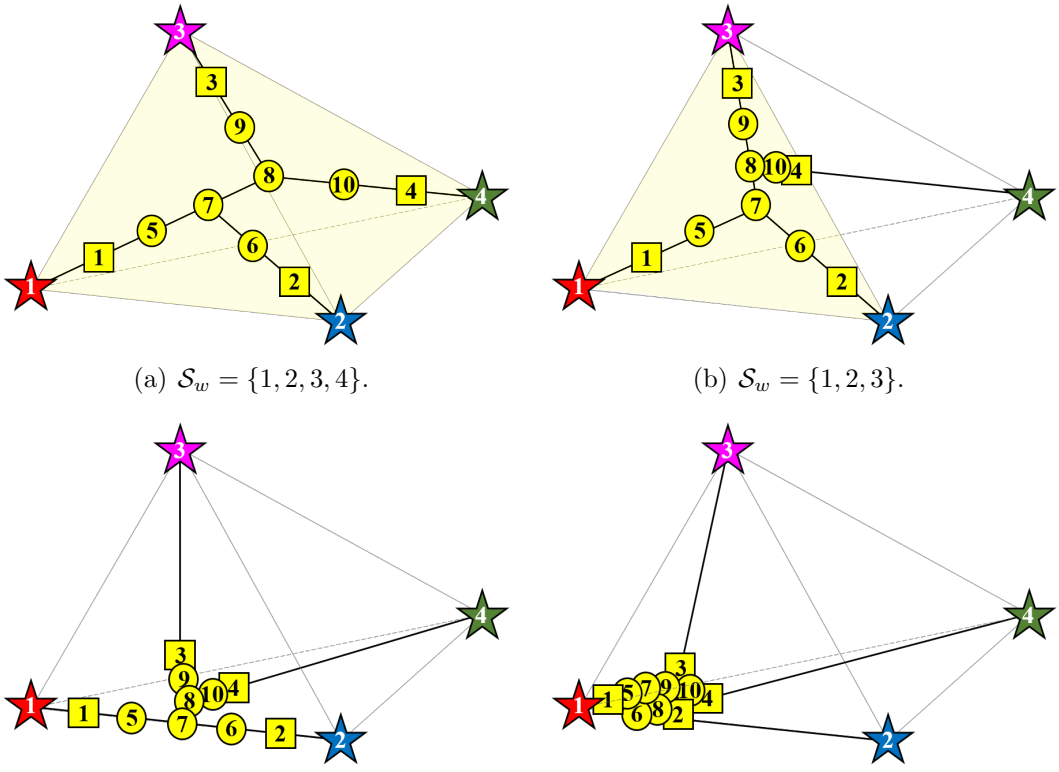

(a) $\mathcal{S}_w = \{1, 2, 3, 4\}$. (b) $\mathcal{S}_w = \{1, 2, 3\}$.

(c) $\mathcal{S}_w = \{1, 2\}$. (d) $\mathcal{S}_w = \{1\}$.

Figure 5.2: The steady-state spatial layout of a tree network of 10 remote robots teleoperated by 4 human users, for different sets of winners.

5.2 Distributed Authority Dispatch

This section designs two distributed WTA authority dispatch algorithms with exponential convergence. The first algorithm is derived from the Oja's rule for PCA but lacks passivity for feedback interconnection with physical robot dynamics. The second algorithm is developed by solving a constrained quadratic programming via primal-dual dynamics, of which the equilibrium-independent passivity favours passive

teleoperation in Section 5.3.

Throughout this section, let $\boldsymbol{\omega} = (\omega_1, \cdots, \omega_{N_r})^\mathsf{T}$ collect the authority factors of all remote robots, and $\mathbf{u}_{tk} = \big(u_1(t_k), \cdots, u_{N_r}(t_k)\big)^\mathsf{T}$ be the vector of all bids received by the remote robot network, during the time period $[t_k, t_{k+1})$.

5.2.1 Principal Component Analysis

This subsection introduces a WTA algorithm derived from the Oja's rule for PCA, in which the default bids received by the follower remote robots are particularly set to $b_0 = b_1$. Let the authority variable ω_i of each remote robot i evolve with

$$\dot{\omega}_i = \sigma\big[u_i(t_k)\omega_i - N_r\eta_i\omega_i\big], \tag{5.6a}$$

$$\eta_i = \alpha_i + u_i(t_k)\omega_i^2, \tag{5.6b}$$

$$\dot{\alpha}_i = \sum_{j\in\mathcal{N}_i} g_{ij}(t)(\eta_j - \eta_i) + \sum_{j\in\mathcal{N}_i} h_{ij}(t)\cdot\operatorname{sign}(\eta_j - \eta_i), \tag{5.6c}$$

where $i = 1, \cdots, N_r$, $\sigma > 0$, and $g_{ij}(t) = g_{ji}(t)$ and $h_{ij}(t) = h_{ji}(t)$ are to be designed. The dynamics of the overall decision-making layer can be synthesized into

$$\dot{\boldsymbol{\omega}} = \sigma\big[\mathbf{u}_{tk}\circ\boldsymbol{\omega} - N_r\boldsymbol{\eta}\circ\boldsymbol{\omega}\big], \tag{5.7a}$$

$$\boldsymbol{\eta} = \boldsymbol{\alpha} + \mathbf{u}_{tk}\circ\boldsymbol{\omega}^2, \tag{5.7b}$$

$$\dot{\boldsymbol{\alpha}} = -\mathbf{L}(t)\boldsymbol{\eta} - \mathbf{B}\mathbf{H}(t)\cdot\operatorname{sign}(\mathbf{B}^\mathsf{T}\boldsymbol{\eta}), \tag{5.7c}$$

where $\mathbf{L}(t) = \mathbf{B}\mathbf{G}(t)\mathbf{B}^\mathsf{T}$ with $\mathbf{G}(t) = \operatorname{diag}\{g_{ij}(t)\}$ and $\mathbf{H}(t) = \operatorname{diag}\{h_{ij}(t)\}$.

In (5.7b), $\boldsymbol{\eta}$ is dynamically updated to estimate $\mathbf{u}_{tk}^\mathsf{T}\boldsymbol{\omega}^2\mathbf{1}/N_r$. By (5.7), the error of estimation,

$$\boldsymbol{\delta} = \boldsymbol{\eta} - \mathbf{u}_{tk}^\mathsf{T}\boldsymbol{\omega}^2\frac{\mathbf{1}}{N_r}, \tag{5.8}$$

evolves according to

$$\begin{aligned}
\dot{\boldsymbol{\delta}} =& -\mathbf{L}(t)\boldsymbol{\eta} - \mathbf{B}\mathbf{H}(t)\cdot\operatorname{sign}(\mathbf{B}^\mathsf{T}\boldsymbol{\eta}) + 2\mathbf{u}_{tk}\circ\boldsymbol{\omega}\circ\dot{\boldsymbol{\omega}} - 2\mathbf{u}_{tk}^\mathsf{T}(\boldsymbol{\omega}\circ\dot{\boldsymbol{\omega}})\frac{\mathbf{1}}{N_r}\\
=& -\mathbf{L}(t)\boldsymbol{\eta} - \mathbf{B}\mathbf{H}(t)\cdot\operatorname{sign}(\mathbf{B}^\mathsf{T}\boldsymbol{\eta}) + 2\mathbf{L}_c(\mathbf{u}_{tk}\circ\boldsymbol{\omega}\circ\dot{\boldsymbol{\omega}})\\
=& -\mathbf{L}(t)\left(\boldsymbol{\delta} + \mathbf{u}_{tk}^\mathsf{T}\boldsymbol{\omega}^2\frac{\mathbf{1}}{N_r}\right) - \mathbf{B}\mathbf{H}(t)\cdot\operatorname{sign}\left[\mathbf{B}^\mathsf{T}\left(\boldsymbol{\delta} + \mathbf{u}_{tk}^\mathsf{T}\boldsymbol{\omega}^2\frac{\mathbf{1}}{N_r}\right)\right]\\
&+ 2\sigma\mathbf{L}_c\left[\mathbf{u}_{tk}\circ\boldsymbol{\omega}^2\circ(\mathbf{u}_{tk} - N_r\boldsymbol{\eta})\right]\\
=& -\mathbf{L}(t)\boldsymbol{\delta} - \mathbf{B}\mathbf{H}(t)\cdot\operatorname{sign}(\mathbf{B}^\mathsf{T}\boldsymbol{\delta}) + 2\sigma\mathbf{L}_c\left[\mathbf{u}_{tk}\circ\boldsymbol{\omega}^2\circ(\mathbf{u}_{tk} - N_r\boldsymbol{\eta})\right]
\end{aligned} \tag{5.9}$$

where $\mathbf{L}_c = \mathbf{I} - \mathbf{1}\mathbf{1}^\mathsf{T}/N_r$ is a Laplacian matrix of a complete graph of order N_r.

Let $\overline{\delta} = \mathbf{1}^\mathsf{T}\boldsymbol{\delta}$ be the sum of estimation errors. It follows then that:

Proposition 5.1. *If $\boldsymbol{\alpha}(0) = \mathbf{0}$, then $\overline{\delta}(t) = 0$ and thus $\mathbf{L}_c\boldsymbol{\delta}(t) = \boldsymbol{\delta}(t)$ for all $t \geq 0$.*

Proof. Firstly, $\boldsymbol{\alpha}(0) = \mathbf{0}$ leads to

$$\begin{aligned}\overline{\delta}(0) =&\mathbf{1}^\mathsf{T}\boldsymbol{\delta}(0) = \mathbf{1}^\mathsf{T}\big[\boldsymbol{\eta}(0) - \mathbf{u}_{tk}^\mathsf{T}(0)\boldsymbol{\omega}^2(0)\mathbf{1}\big] = \mathbf{1}^\mathsf{T}\boldsymbol{\eta}(0) - N_r\mathbf{u}_{tk}^\mathsf{T}(0)\boldsymbol{\omega}^2(0)\\ =&\mathbf{1}^\mathsf{T}\big[\boldsymbol{\alpha}(0) + N_r\mathbf{u}_{tk}(0)\circ\boldsymbol{\omega}^2(0)\big] - N_r\mathbf{u}_{tk}^\mathsf{T}(0)\boldsymbol{\omega}^2(0) = 0.\end{aligned}$$

Then, $\overline{\delta}$ is invariant by validating its derivative as follows

$$\dot{\overline{\delta}} =\mathbf{1}^\mathsf{T}\dot{\boldsymbol{\delta}} = -\mathbf{1}^\mathsf{T}\mathbf{L}(t)\boldsymbol{\delta} - \mathbf{1}^\mathsf{T}\mathbf{B}\mathbf{H}(t)\cdot\operatorname{sign}(\mathbf{B}^\mathsf{T}\boldsymbol{\delta}) + 2\mathbf{1}^\mathsf{T}\mathbf{L}_c(\mathbf{u}\circ\boldsymbol{\omega}\circ\dot{\boldsymbol{\omega}}) = 0.$$

Hence, $\overline{\delta}(t) = \overline{\delta}(0) = 0$ for any $t \geq 0$. Further, with $\mathbf{L}_c = \mathbf{I} - \mathbf{1}\mathbf{1}^\mathsf{T}/N_r$, it follows from $\overline{\delta}(t) = \mathbf{1}^\mathsf{T}\boldsymbol{\delta}(t) = 0$ that $\mathbf{L}_c\boldsymbol{\delta}(t) = \boldsymbol{\delta}(t)$. ■

The Lyapunov candidate constructed to study the convergence of the WTA authority dispatch algorithm (5.6) is

$$V = V_1 + \kappa V_2 = \frac{1}{4}(\boldsymbol{\omega}^\mathsf{T}\boldsymbol{\omega} - 1)^2 + \frac{\kappa}{2}\boldsymbol{\delta}^\mathsf{T}\boldsymbol{\delta}, \tag{5.10}$$

where $\epsilon > 0$ will be determined, $V_1 = (\boldsymbol{\omega}^\mathsf{T}\boldsymbol{\omega} - 1)^2/4$ measures the deviation from 1 of the decision variables $\boldsymbol{\omega}$, and $V_2 = \boldsymbol{\delta}^\mathsf{T}\boldsymbol{\delta}/2$ quantifies the impact of the estimation error $\boldsymbol{\delta}$. Along Equations (5.7)-(5.9), the derivative of V_1 becomes

$$\begin{aligned}\dot{V}_1 =&(\boldsymbol{\omega}^\mathsf{T}\boldsymbol{\omega} - 1)\boldsymbol{\omega}^\mathsf{T}\dot{\boldsymbol{\omega}} = \sigma(\boldsymbol{\omega}^\mathsf{T}\boldsymbol{\omega} - 1)\boldsymbol{\omega}^\mathsf{T}\big[\mathbf{u}_{tk}\circ\boldsymbol{\omega} - N_r\boldsymbol{\eta}\circ\boldsymbol{\omega}\big]\\ =&\sigma(\boldsymbol{\omega}^\mathsf{T}\boldsymbol{\omega} - 1)\boldsymbol{\omega}^\mathsf{T}\left[\mathbf{u}_{tk}\circ\boldsymbol{\omega} - N_r\left(\boldsymbol{\delta} + \mathbf{u}_{tk}^\mathsf{T}\boldsymbol{\omega}^2\frac{\mathbf{1}}{N_r}\right)\circ\boldsymbol{\omega}\right]\\ =&\sigma(\boldsymbol{\omega}^\mathsf{T}\boldsymbol{\omega} - 1)(\mathbf{u}_{tk}^\mathsf{T}\boldsymbol{\omega}^2 - N_r\boldsymbol{\omega}^\mathsf{T}(\boldsymbol{\delta}\circ\boldsymbol{\omega}) - \mathbf{u}_{tk}^\mathsf{T}\boldsymbol{\omega}^2\boldsymbol{\omega}^\mathsf{T}\boldsymbol{\omega})\\ =&-\sigma\mathbf{u}_{tk}^\mathsf{T}\boldsymbol{\omega}^2(\boldsymbol{\omega}^\mathsf{T}\boldsymbol{\omega} - 1)^2 - \sigma N_r(\boldsymbol{\omega}^\mathsf{T}\boldsymbol{\omega} - 1)\boldsymbol{\delta}^\mathsf{T}\boldsymbol{\omega}^2\\ \leq&-\sigma\mathbf{u}_{tk}^\mathsf{T}\boldsymbol{\omega}^2(\boldsymbol{\omega}^\mathsf{T}\boldsymbol{\omega} - 1)^2 + \frac{\sigma}{2}\mathbf{u}_{tk}^\mathsf{T}\boldsymbol{\omega}^2(\boldsymbol{\omega}^\mathsf{T}\boldsymbol{\omega} - 1)^2 + \frac{\sigma}{2}N_r^2(\boldsymbol{\delta}\circ\boldsymbol{\omega})^\mathsf{T}\mathbf{U}_{tk}^{-1}(\boldsymbol{\delta}\circ\boldsymbol{\omega})\\ =&-\frac{\sigma}{2}\mathbf{u}_{tk}^\mathsf{T}\boldsymbol{\omega}^2(\boldsymbol{\omega}^\mathsf{T}\boldsymbol{\omega} - 1)^2 + \frac{\sigma}{2}N_r^2\boldsymbol{\delta}^\mathsf{T}\boldsymbol{\Omega}\mathbf{U}_{tk}^{-1}\boldsymbol{\Omega}\boldsymbol{\delta},\end{aligned}$$

where $\mathbf{U}_{tk}^{-1}$ with $\mathbf{U}_{tk} = \operatorname{diag}\{\mathbf{u}_{tk}\}$ is well-defined because $u_i(t_k) \geq b_1 > 0$ for every

$i = 1, \cdots, N_r$. Similarly, the derivative of V_2 is

$$\begin{aligned}
\dot{V}_2 =& -\boldsymbol{\delta}^{\mathsf{T}}\mathbf{L}(t)\boldsymbol{\delta} - \boldsymbol{\delta}^{\mathsf{T}}\mathbf{B}\mathbf{H}(t)\cdot\operatorname{sign}(\mathbf{B}^{\mathsf{T}}\boldsymbol{\delta}) + 2\sigma\boldsymbol{\delta}^{\mathsf{T}}\mathbf{L}_c\left[\mathbf{u}_{tk}\circ\boldsymbol{\omega}^2\circ(\mathbf{u}_{tk} - N_r\boldsymbol{\eta})\right] \\
=& -\boldsymbol{\delta}^{\mathsf{T}}\mathbf{L}(t)\boldsymbol{\delta} - \boldsymbol{\delta}^{\mathsf{T}}\mathbf{B}\mathbf{H}(t)\cdot\operatorname{sign}(\mathbf{B}^{\mathsf{T}}\boldsymbol{\delta}) \\
&+ 2\sigma\boldsymbol{\delta}^{\mathsf{T}}\mathbf{L}_c\left[\mathbf{u}_{tk}^2\circ\boldsymbol{\omega}^2 - N_r\mathbf{u}_{tk}\circ\boldsymbol{\omega}^2\circ\left(\boldsymbol{\delta} + \mathbf{u}_{tk}^{\mathsf{T}}\boldsymbol{\omega}^2\frac{\mathbf{1}}{N_r}\right)\right] \\
=& -\boldsymbol{\delta}^{\mathsf{T}}\mathbf{L}(t)\boldsymbol{\delta} - \boldsymbol{\delta}^{\mathsf{T}}\mathbf{B}\mathbf{H}(t)\cdot\operatorname{sign}(\mathbf{B}^{\mathsf{T}}\boldsymbol{\delta}) \\
&+ 2\sigma\boldsymbol{\delta}^{\mathsf{T}}\mathbf{L}_c\left[\mathbf{u}_{tk}^2\circ\boldsymbol{\omega}^2 - (\mathbf{u}_{tk}^{\mathsf{T}}\boldsymbol{\omega}^2)\mathbf{u}_{tk}\circ\boldsymbol{\omega}^2\right] - 2\sigma N_r\boldsymbol{\delta}^{\mathsf{T}}\mathbf{L}_c(\mathbf{u}_{tk}\circ\boldsymbol{\omega}^2\circ\boldsymbol{\delta}) \\
=& -\boldsymbol{\delta}^{\mathsf{T}}\mathbf{L}(t)\boldsymbol{\delta} - \boldsymbol{\delta}^{\mathsf{T}}\mathbf{B}\mathbf{H}(t)\cdot\operatorname{sign}(\mathbf{B}^{\mathsf{T}}\boldsymbol{\delta}) \\
&+ 2\sigma\boldsymbol{\delta}^{\mathsf{T}}\left(\mathbf{u}_{tk}\circ\boldsymbol{\omega}\circ\left[(\mathbf{I} - \boldsymbol{\omega}\boldsymbol{\omega}^{\mathsf{T}})(\mathbf{u}_{tk}\circ\boldsymbol{\omega})\right]\right) - 2\sigma N_r\boldsymbol{\delta}^{\mathsf{T}}\boldsymbol{\Omega}\mathbf{U}_{tk}\boldsymbol{\Omega}\boldsymbol{\delta}
\end{aligned}$$

where $\mathbf{L}_c\boldsymbol{\delta} = \boldsymbol{\delta}$ in Proposition 5.1 has been applied, and $\boldsymbol{\Omega} = \operatorname{diag}\{\boldsymbol{\omega}\}$.

Because $\mathbf{L}_c$ can be decomposed by a positive semi-definite $\mathbf{T}$ into $\mathbf{L}_c = \mathbf{B}\mathbf{T}\mathbf{B}^{\mathsf{T}}$, let $\boldsymbol{\upsilon} = (\upsilon_1, \cdots, \upsilon_{N_r-1})^{\mathsf{T}}$ with υ_i the maximum absolute value of all elements in the i-th row of $\mathbf{T}\mathbf{B}^{\mathsf{T}}$, and let $\boldsymbol{\Upsilon} = \operatorname{diag}\{\boldsymbol{\upsilon}\} \succeq \mathbf{0}$ and $\widetilde{\boldsymbol{\delta}} = \mathbf{B}^{\mathsf{T}}\boldsymbol{\delta}$. From Appendix J, the error of estimation $\boldsymbol{\delta}$ admits that

$$\begin{aligned}
&2\sigma\boldsymbol{\delta}^{\mathsf{T}}\left(\mathbf{u}_{tk}\circ\boldsymbol{\omega}\circ\left[(\mathbf{I} - \boldsymbol{\omega}\boldsymbol{\omega}^{\mathsf{T}})(\mathbf{u}_{tk}\circ\boldsymbol{\omega})\right]\right) \\
\leq& \frac{\sigma}{4\kappa}(1 - \boldsymbol{\omega}^{\mathsf{T}}\boldsymbol{\omega})^2\mathbf{u}_{tk}^{\mathsf{T}}\boldsymbol{\omega}^2 + \sigma N_r(b_m - b_1)\left|\widetilde{\boldsymbol{\delta}}\right|^{\mathsf{T}}\boldsymbol{\Upsilon}|\mathbf{B}|^{\mathsf{T}}\boldsymbol{\eta} \\
&+ \sigma N_r(b_m - b_1)\widetilde{\boldsymbol{\delta}}^{\mathsf{T}}\boldsymbol{\Upsilon}^2\widetilde{\boldsymbol{\delta}} + \sigma\boldsymbol{\delta}^{\mathsf{T}}\left[4\kappa b_m^2\boldsymbol{\Omega}\mathbf{U}_{tk}\boldsymbol{\Omega} + N_r(b_m - b_1)|\mathbf{B}||\mathbf{B}|^{\mathsf{T}}\right]\boldsymbol{\delta}.
\end{aligned} \tag{5.11}$$

For every pair of adjacent remote robots $(i, j) \in \mathcal{E}$, design $h_{ij}(t)$ by

$$h_{ij}(t) = \sigma N_r(b_m - b_1)\upsilon_k(\eta_i + \eta_j), \tag{5.12}$$

where the k-th column of $\mathbf{B}$ associates with the communication link (i, j) between the remote robots i and j, and update $g_{ij}(t)$ by

$$\begin{aligned}
g_{ij}(t) =& \sigma N_r\left(\frac{N_r^2}{4\kappa b_1^2} - \frac{3}{4}N_r + 2\kappa b_m^2\right)\left[(\eta_i + \eta_j)\upsilon_k^2 + K_c(N_r - 1)(\eta_i - \eta_j)^2 + K_c\upsilon^2\right] \\
&+ \frac{1}{\kappa}\sigma N_r(4N_r - 3)(b_m - b_1)\upsilon_k^2
\end{aligned} \tag{5.13}$$

where K_c is the maximum singular value of $\mathbf{T}\mathbf{B}^{\mathsf{T}}\mathbf{B}\mathbf{T}$. Because the selection of $h_{ij}(t)$

in (5.12) for every $(i,j) \in \mathcal{E}$ makes

$$\begin{aligned}
&- \boldsymbol{\delta}^{\mathsf{T}}\mathbf{B}\mathbf{H}(t) \cdot \operatorname{sign}(\mathbf{B}^{\mathsf{T}}\boldsymbol{\delta}) + \sigma N_r(b_m - b_1) \left|\widetilde{\boldsymbol{\delta}}\right|^{\mathsf{T}} \boldsymbol{\Upsilon}|\mathbf{B}|^{\mathsf{T}}\boldsymbol{\eta} \\
=& - \widetilde{\boldsymbol{\delta}}^{\mathsf{T}}\mathbf{H}(t) \cdot \operatorname{sign}(\widetilde{\boldsymbol{\delta}}) + \sigma N_r(b_m - b_1) \left|\widetilde{\boldsymbol{\delta}}\right|^{\mathsf{T}} \boldsymbol{\Upsilon}|\mathbf{B}|^{\mathsf{T}}\boldsymbol{\eta} \\
=& - \sum_{(i,j)\in\mathcal{E}} h_{ij}(t)|\delta_i - \delta_j| + \sigma N_r(b_m - b_1) \sum_{(i,j)\in\mathcal{E}} |\delta_i - \delta_j|\upsilon_k(\eta_i + \eta_j) = 0,
\end{aligned}$$

combining $\dot{V}_1$ and $\dot{V}_2$ and using (5.11)-(5.13) lead to the time derivative of V by

$$\begin{aligned}
\dot{V} \leq& - \frac{\sigma}{4}\mathbf{u}_{tk}^{\mathsf{T}}\boldsymbol{\omega}^2(\boldsymbol{\omega}^{\mathsf{T}}\boldsymbol{\omega} - 1)^2 + \frac{\sigma}{2}N_r^2\boldsymbol{\delta}^{\mathsf{T}}\boldsymbol{\Omega}\mathbf{U}_{tk}^{-1}\boldsymbol{\Omega}\boldsymbol{\delta} - \kappa\boldsymbol{\delta}^{\mathsf{T}}\mathbf{L}(t)\boldsymbol{\delta} + \sigma\kappa N_r(b_m - b_1)\widetilde{\boldsymbol{\delta}}^{\mathsf{T}}\boldsymbol{\Upsilon}^2\widetilde{\boldsymbol{\delta}} \\
&+ \sigma\kappa\boldsymbol{\delta}^{\mathsf{T}}\left[4\kappa b_m^2\boldsymbol{\Omega}\mathbf{U}_{tk}\boldsymbol{\Omega} + N_r(b_m - b_1)|\mathbf{B}||\mathbf{B}|^{\mathsf{T}}\right]\boldsymbol{\delta} - 2\sigma\kappa N_r\boldsymbol{\delta}^{\mathsf{T}}\boldsymbol{\Omega}\mathbf{U}_{tk}\boldsymbol{\Omega}\boldsymbol{\delta} \\
=& - \frac{\sigma}{4}\mathbf{u}_{tk}^{\mathsf{T}}\boldsymbol{\omega}^2(\boldsymbol{\omega}^{\mathsf{T}}\boldsymbol{\omega} - 1)^2 - \frac{\sigma\kappa}{2}\boldsymbol{\delta}^{\mathsf{T}}\boldsymbol{\delta}\mathbf{u}_{tk}^{\mathsf{T}}\boldsymbol{\omega}^2 \\
&+ \boldsymbol{\delta}^{\mathsf{T}}\left[\sigma\boldsymbol{\Lambda}(t) - \kappa\mathbf{L}(t)\right]\boldsymbol{\delta} + \sigma\kappa N_r(b_m - b_1)\widetilde{\boldsymbol{\delta}}^{\mathsf{T}}\boldsymbol{\Upsilon}^2\widetilde{\boldsymbol{\delta}}
\end{aligned}$$

where $(\sigma\kappa/2)\boldsymbol{\delta}^{\mathsf{T}}\boldsymbol{\delta}\mathbf{u}_{tk}^{\mathsf{T}}\boldsymbol{\omega}^2$ has been added and subtracted in the above with

$$\boldsymbol{\Lambda}(t) = \frac{\kappa}{2}\mathbf{u}_{tk}^{\mathsf{T}}\boldsymbol{\omega}^2\mathbf{I} + \frac{1}{2}N_r^2\boldsymbol{\Omega}\mathbf{U}_{tk}^{-1}\boldsymbol{\Omega} + \kappa\left[(4\kappa b_m^2 - 2N_r)\boldsymbol{\Omega}\mathbf{U}_{tk}\boldsymbol{\Omega} + N_r(b_m - b_1)|\mathbf{B}||\mathbf{B}|^{\mathsf{T}}\right].$$

From Appendix K, we have also that

$$\boldsymbol{\delta}^{\mathsf{T}}\boldsymbol{\Lambda}(t)\boldsymbol{\delta} \leq \widetilde{\boldsymbol{\delta}}^{\mathsf{T}}\boldsymbol{\Gamma}(t)\widetilde{\boldsymbol{\delta}}, \tag{5.14}$$

where $\boldsymbol{\Gamma}(t)$ is given by

$$\begin{aligned}
\boldsymbol{\Gamma}(t) =& 4N_r(N_r - 1)(b_m - b_1)\boldsymbol{\Upsilon}^2 + N_r\left(\frac{N_r^2}{4b_1^2} - \frac{3}{4}\kappa N_r + 2\kappa^2 b_m^2\right) \\
&\cdot \left[\boldsymbol{\Upsilon} \cdot \operatorname{diag}\{|\mathbf{B}|^{\mathsf{T}}\boldsymbol{\eta}\} \cdot \boldsymbol{\Upsilon} + K_c(N_r - 1) \cdot \operatorname{diag}\left\{\left(\mathbf{B}^{\mathsf{T}}\boldsymbol{\eta}\right)^2\right\} + K_c\boldsymbol{\Upsilon}^4\right]
\end{aligned}$$

With $\boldsymbol{\delta}^{\mathsf{T}}\mathbf{L}(t)\boldsymbol{\delta} = \widetilde{\boldsymbol{\delta}}^{\mathsf{T}}\mathbf{G}(t)\widetilde{\boldsymbol{\delta}}$, it further upper-bounds $\dot{V}$ by

$$\begin{aligned}
\dot{V} \leq& - \frac{\sigma}{4}(\boldsymbol{\omega}^{\mathsf{T}}\boldsymbol{\omega} - 1)^2\mathbf{u}_{tk}^{\mathsf{T}}\boldsymbol{\omega}^2 - \frac{\sigma\kappa}{2}\boldsymbol{\delta}^{\mathsf{T}}\boldsymbol{\delta}\mathbf{u}_{tk}^{\mathsf{T}}\boldsymbol{\omega}^2 \\
&+ \widetilde{\boldsymbol{\delta}}^{\mathsf{T}}\left[\sigma\boldsymbol{\Gamma}(t) - \kappa\mathbf{G}(t) + \sigma\kappa N_r(b_m - b_1)\boldsymbol{\Upsilon}^2\right]\widetilde{\boldsymbol{\delta}}.
\end{aligned}$$

Choosing $w_{ij}(t)$ by (5.13) for every $(i,j) \in \mathcal{E}$ makes $\sigma\boldsymbol{\Gamma}(t) - \kappa\mathbf{G}(t) + \sigma\kappa N_r(b_m -$

$b_1)\boldsymbol{\Upsilon}^2 = \mathbf{0}$ and converts thus the derivative of V into

$$\dot{V} \leq -\mu(t)V, \tag{5.15}$$

where $\mu(t) = \sigma \mathbf{u}^\mathsf{T}\boldsymbol{\omega}^2$. By Grönwall's inequality, the time integration of (5.15) from $t_k \geq 0$ to $t \geq t_k$ yields

$$V(t) \leq \exp\left(-\int_{t_k}^{t} \mu(\theta)d\theta\right) \cdot V(t_k). \tag{5.16}$$

The following lemma is key to proving the convergence of the WTA althority dispatch algorithm (5.6) in Theorem 5.1.

Lemma 5.1. *Let the dynamics* (5.6) *of the authority variables* ω_i *start with* $\omega_i(t_k) = 1/\sqrt{N_r}$ *and* $\alpha_i(t_k) = 0, \forall i = 1, \cdots, N_r$. *Then, the dynamic modulations* (5.12)-(5.13) *of* $h_{ij}(t)$ *and* $g_{ij}(t)$ *guarantee that:*

1. *The authority variables* $\boldsymbol{\omega}$ *and the estimating error variables* $\boldsymbol{\delta}$ *stay in an invariant set,*

$$\mathcal{S}_I = \left\{(\boldsymbol{\omega}, \boldsymbol{\delta}) \in \mathbb{R}^{N_r} \times \mathbb{R}^{N_r} \;\middle|\; \left(\|\boldsymbol{\omega}\|^2 - 1\right)^2 + 2\kappa\|\boldsymbol{\delta}\|^2 \leq 2\kappa b_m^2/N_r^2\right\}.$$

2. *If* κ *is selected by* $\kappa \leq N_r^2(1-\rho^2)^2/(2b_m^2)$ *with* $0 < \rho < 1$, *then the variables* $\boldsymbol{\omega}$ *and* $\boldsymbol{\delta}$ *exponentially converge to an attractive set,*

$$\mathcal{S}_A = \left\{(\boldsymbol{\omega}, \boldsymbol{\delta}) \in \mathbb{R}^{N_r} \times \mathbb{R}^{N_r} \;\middle|\; (\|\boldsymbol{\omega}\|^2 - 1)^2 + 2\kappa\|\boldsymbol{\delta}\|^2 = 0\right\},$$

and the rate of convergence is $\sigma\rho b_1$.

Proof. 1. The definition of V in (5.10) and the conclusion (5.16) together lead to $(\|\boldsymbol{\omega}\|^2 - 1)^2 + 2\kappa\|\boldsymbol{\delta}\|^2 \leq 4V(t_k)$. Further, the initializations $\omega_i(t_k) = 1/\sqrt{N_r}$ and $\alpha_i(t_k) = 0$ guarantee that $2N_r^2 V(t_k) = \kappa \mathbf{u}_{tk}^\mathsf{T}\mathbf{L}_c\mathbf{L}_c\mathbf{u}_{tk} \leq \kappa b_m^2$, because 0 and 1 are the eigenvalues of $\mathbf{L}_c$. Therefore, $\boldsymbol{\omega}$ and $\boldsymbol{\delta}$ are bounded within $\mathcal{S}_I$.

2. The invariant set $\mathcal{I}$ indicates that $\|\boldsymbol{\omega}\|^2 \geq 1 - \sqrt{2\kappa}b_m/N_r$. Selecting κ as required then guarantees that $\|\boldsymbol{\omega}\|^2 \geq \rho$ and thus $\mu(t) \geq \sigma\rho b_1$ for all time. It follows that $(\|\boldsymbol{\omega}\|^2 - 1)^2 + 2\kappa\|\boldsymbol{\delta}\|^2 \leq 4\exp[-\sigma\rho b_1(t - t_k)] \cdot V(t_k)$, which proves the exponential convergence to the attractive set $\mathcal{S}_A$. ■

The following theorem summarizes the convergence of the proposed WTA authority dispatch algorithm (5.6).

Theorem 5.1. *Let the distributed WTA authority dispatch algorithm* (5.6) *be initialized by* $\omega_i(t_k) = 1/\sqrt{N_r}$ *and* $\alpha_i(t_k) = 0$ *for* $i = 1, \cdots, N_r$. *Further, choose* $\sigma > 0$ *heuristically, select* κ *as in Lemma 5.1, and update the gains* $h_{ij}(t)$ *by* (5.12) *and* $g_{ij}(t)$ *by* (5.13) *for all* $(i,j) \in \mathcal{E}$. *If the user* w *is the only winner, then the authority variables of the leader remote robot* w *and of all other robots asymptotically converge to* 1 *and* 0, *respectively, i.e.,* $\omega_w(t) \to 1$ *and* $\omega_l(t) \to 0$ *for all* $l \neq w$.

Proof. The selection of κ in Lemma 5.1 ensures that $2\|\boldsymbol{\delta}\| \leq \sqrt{2V(t_k)/\kappa}\cdot\exp[-\sigma\rho b_1(t-t_k)]$. The evolution of all authority variables $\boldsymbol{\omega}$ is studied using the quotient function:

$$E = \sum_{l\neq w} \frac{\omega_l}{\omega_w}, \tag{5.17}$$

where $l, w \in \{1, \cdots, N_r\}$ with $l \neq w$ are defined in the theorem. By (5.6a), ω_w and all ω_l-s are positive for all time as they start from $1/\sqrt{N_r}$. Further, because $\boldsymbol{\omega}$ is bounded by $\mathcal{S}_I$, E becomes zero if and only if $\omega_l = 0$ for all $l \neq w$. Then, the derivative of E along the WTA authority dispatch dynamics (5.6) is

$$\begin{aligned}
\dot{E} =& \sum_{l\neq w} \frac{\sigma[u_l(t_k)\omega_l - N_r\eta_l\omega_l]\omega_w - \sigma[u_w(t_k)\omega_w - N_r\eta_w\omega_w]\omega_l}{\omega_w^2} \\
=& \sum_{l\neq w} \left(\sigma[u_l(t_k) - u_w(t_k)]\frac{\omega_l}{\omega_w} + \sigma N_r(\eta_w - \eta_l)\frac{\omega_l}{\omega_w} \right) \\
=& \sigma \sum_{l\neq w} \left([u_l(t_k) - u_w(t_k)]\frac{\omega_l}{\omega_w} + N_r(\delta_w - \delta_l)\frac{\omega_l}{\omega_w} \right) \\
\leq& -\sigma\left(\epsilon - 2N_r\|\boldsymbol{\delta}\|\right)\sum_{l\neq w}\frac{\omega_l}{\omega_w} \leq \left[-\sigma\epsilon + \sigma\sqrt{2V(t_k)/\kappa}\cdot\exp(-\sigma\rho b_1 t)\right] E.
\end{aligned} \tag{5.18}$$

Then, the time integration of $\dot{E}$ from t_k to t gives that, as $t \to +\infty$,

$$\begin{aligned}
E(t) \leq& \exp\left[-\sigma\epsilon(t-t_k) + \sigma\sqrt{2V(t_k)/\kappa}\int_{t_k}^{t}\exp(-\sigma\rho b_1\theta)d\theta \right] E(t_k) \\
\leq& \exp\left[-\sigma\epsilon(t-t_k) + \sqrt{2V(t_k)/\kappa}/(\rho b_1)\exp(-\sigma\rho b_1 t_0) \right] E(t_k) \to 0,
\end{aligned}$$

which, together with $E(t) \geq 0$, ensures that $E(t)$ converges to zero exponentially. By $\mathcal{S}_I$ in Lemma 5.1, $\boldsymbol{\omega}$ is bounded, and thus $E(t) \to 0$ indicates that $\omega_l(t) \to 0$ for

every $l \neq w$. Because $\boldsymbol{\omega}$ exponentially converges to $\mathcal{S}_A$, $\omega_i(t) \to 0$ exponentially for all $i \neq k$ further means that $\omega_w(t) \to 1$ exponentially. The proof is complete. ■

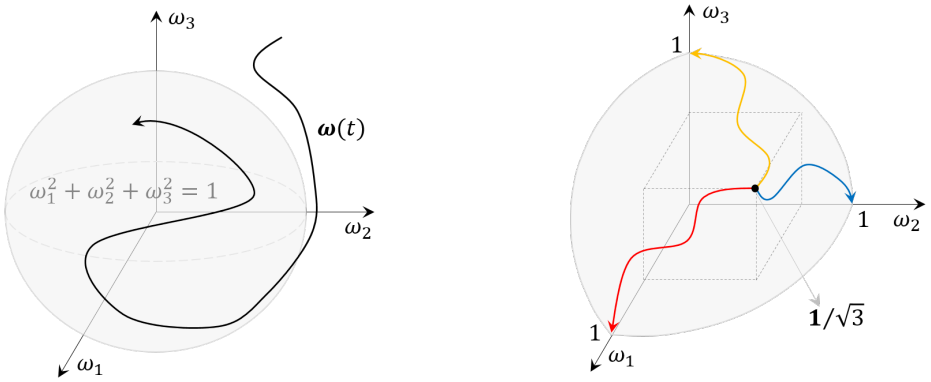

(a) The authority variables $\boldsymbol{\omega}$ exponentially converge to $\|\boldsymbol{\omega}\| = 1$.

(b) The authority factors ω_w and ω_l exponentially converge to 1 and 0, respectively.

Figure 5.3: The exponential convergence of the WTA authority dispatch algorithm (5.6) is proven by the conjunction of (a) the function V in (5.10) and (b) the function E in (5.17).

The exponential convergence of the WTA authority dispatch algorithm (5.6) is proven by the conjunction of the functions V in (5.10) and E in (5.17). An example with $N_l = N_r = 3$ is provided in Figure 5.3 for interpretation. In Lemma 5.1, the evolution of V in (5.15) implies that the variables $\boldsymbol{\omega}$ and $\boldsymbol{\delta}$ are properly bounded within $\mathcal{S}_I$, and are exponentially convergent to $\mathcal{S}_A$, see Figure 5.3(a). On this basis, in Theorem 5.1, the evolution of E in (5.18) indicates further that only ω_w and ω_l exponentially approach 1 and 0, respectively, see Figure 5.3(b). As a result, every leader remote robot $i = 1, \cdots, N_l$ can detect if it is communicating with the winner's local robot by evaluating its own authority variable ω_i: yes if $\omega_i(t) \to 1$; and no if $\omega_i(t) \to 0$. Nevertheless, the passivity of (5.6) is unclear by studying the functions V and E in the above, which prohibits its power-preserving interconnection with physical robot dynamics and thus the closed-loop implementation of a passive teleoperator. For this reason, the following section derives a passive WTA authority dispatch algorithm from a constrained quadratic programming formulation.

5.2.2 Constrained Quadratic Programming

Let the default bids received by the follower remote robots be $b_0 = 0$. As proven in Lemma 5.2, this subsection formulates the following constrained quadratic program to accomplish WTA authority dispatch:

$$\begin{aligned} \underset{\boldsymbol{\omega}\in\mathbb{R}^{N_r}}{\text{minimize}} \quad & f(\boldsymbol{\omega}) = \frac{\epsilon}{2}\boldsymbol{\omega}^{\mathsf{T}}\boldsymbol{\omega} - \boldsymbol{\omega}^{\mathsf{T}}\mathbf{u}_{tk}, && \text{(5.19a)} \\ \text{subject to} \quad & \mathbf{1}^{\mathsf{T}}\boldsymbol{\omega} = 1, && \text{(5.19b)} \\ & \mathbf{0} \leq \boldsymbol{\omega} \leq \mathbf{1}, && \text{(5.19c)} \end{aligned}$$

where $\epsilon > 0$ is the resolution of the user bids.

Lemma 5.2. *The minimizer* $\boldsymbol{\omega}^* = \left(\omega_1^*, \cdots, \omega_{N_r}^*\right)^{\mathsf{T}}$ *of the convex program* (5.19) *allocates an authority factor* ω_i^* *to each leader remote robot* $i = 1, \cdots, N_l$ *that fulfills the objectives O1 and O2.*

Proof. The first step derives a transformation of (5.19) for the subsequent search for its minimizer $\boldsymbol{\omega}^*$ through the first-order optimality condition. Because $u_i(t_k) \geq \epsilon$ and $u_j(t_k) = 0$ for $i = 1, \cdots, N_l$ and $j = N_l + 1, \cdots, N_r$, there exists a maximal set $\mathcal{S}_w \subseteq \{1, \cdots, N_l\}$, $\mathcal{S}_w \neq \emptyset$, such that: $u_i(t_k) = u_j(t_k)$ for any $i, j \in \mathcal{S}_w$, and $u_i(t_k) - u_j(t_k) \geq \epsilon$ for any $i \in \mathcal{S}_w$ and $j \notin \mathcal{S}_w$. After selecting $l \notin \mathcal{S}_w$ arbitrarily, define $\widehat{\boldsymbol{\omega}}$ and $\widehat{\mathbf{u}}_{tk}$ by deleting ω_l and $u_l(t_k)$ from $\boldsymbol{\omega}$ and $\mathbf{u}_{tk}$, respectively, to convert (5.19b) into $\omega_l = 1 - \widehat{\boldsymbol{\omega}}^{\mathsf{T}}\mathbf{1}$ and then (5.19a) into

$$f(\boldsymbol{\omega}) = \frac{\epsilon}{2}\widehat{\boldsymbol{\omega}}^{\mathsf{T}}\left(\mathbf{I} + \mathbf{1}\mathbf{1}^{\mathsf{T}}\right)\widehat{\boldsymbol{\omega}} - \widehat{\boldsymbol{\omega}}^{\mathsf{T}}\left[\widehat{\mathbf{u}}_{tk} - u_l(t_k)\mathbf{1} + \epsilon\mathbf{1}\right] + \delta,$$

where $\delta = \epsilon/2 - u_l(t_k)$. Dropping the constant δ, (5.19) becomes:

$$\begin{aligned} \underset{\widehat{\boldsymbol{\omega}}\in\mathbb{R}^{N_r-1}}{\text{minimize}} \quad & \widehat{f}(\widehat{\boldsymbol{\omega}}) = \frac{\epsilon}{2}\widehat{\boldsymbol{\omega}}^{\mathsf{T}}\left(\mathbf{I} + \mathbf{1}\mathbf{1}^{\mathsf{T}}\right)\widehat{\boldsymbol{\omega}} - \widehat{\boldsymbol{\omega}}^{\mathsf{T}}\left[\widehat{\mathbf{u}}_{tk} - u_l(t_k)\mathbf{1} + \epsilon\mathbf{1}\right], && \text{(5.20a)} \\ \text{subject to} \quad & \mathbf{0} \leq \widehat{\boldsymbol{\omega}} \leq \mathbf{1}, && \text{(5.20b)} \\ & 0 \leq \mathbf{1}^{\mathsf{T}}\widehat{\boldsymbol{\omega}} \leq 1, && \text{(5.20c)} \end{aligned}$$

where (5.20c) is by $0 \leq \omega_l \leq 1$ in (5.19c). Because the quadratic program (5.20) satisfies Slater's condition, $\widehat{\boldsymbol{\omega}}^*$ minimizes (5.20) iff

$$\mathbf{0} \in \nabla\widehat{f}(\widehat{\boldsymbol{\omega}}^*) + \mathcal{N}_{\widehat{\mathcal{C}}}(\widehat{\boldsymbol{\omega}}^*) = \epsilon\left(\mathbf{I} + \mathbf{1}\mathbf{1}^{\mathsf{T}}\right)\widehat{\boldsymbol{\omega}}^* - \left[\widehat{\mathbf{u}}_{tk} - u_l(t_k)\mathbf{1} + \epsilon\mathbf{1}\right] + \mathcal{N}_{\widehat{\mathcal{C}}}(\widehat{\boldsymbol{\omega}}^*), \quad \text{(5.21)}$$

where $\mathcal{N}_{\widehat{\mathcal{C}}}(\widehat{\boldsymbol{\omega}}^*)$ is the normal cone of $\widehat{\mathcal{C}}$ at $\widehat{\boldsymbol{\omega}}^*$ with

$$\widehat{\mathcal{C}} = \Big\{ \widehat{\boldsymbol{\omega}} \in \mathbb{R}^{N_r-1} \Big| \ \mathbf{0} \leq \widehat{\boldsymbol{\omega}} \leq \mathbf{1}, \text{ and } 0 \leq \mathbf{1}^\mathsf{T} \widehat{\boldsymbol{\omega}} \leq 1 \Big\}.$$

The second step uses contradiction to show that the minimizer $\widehat{\boldsymbol{\omega}}^*$ of (5.20) satisfies $\mathbf{1}^\mathsf{T}\widehat{\boldsymbol{\omega}}^* = 1$. Suppose that $\mathbf{1}^\mathsf{T}\widehat{\boldsymbol{\omega}}^* < 1$. Then, (5.20b) indicates that $\widehat{\omega}_i^* < 1 \ \forall i = 1, \cdots, N_r - 1$, where $\widehat{\omega}_i^*$ is the i-th element of $\widehat{\boldsymbol{\omega}}^*$. Hence, $\mathbf{n}^* \leq \mathbf{0}$ for any normal vector $\mathbf{n}^* \in \mathcal{N}_{\widehat{\mathcal{C}}}(\widehat{\boldsymbol{\omega}}^*)$. The first-order optimality condition (5.21) leads to

$$\epsilon\big(\mathbf{I} + \mathbf{1}\mathbf{1}^\mathsf{T}\big)\widehat{\boldsymbol{\omega}}^* = [\widehat{\mathbf{u}}_{tk} - u_l(t_k)\mathbf{1} + \epsilon\mathbf{1}] - \mathbf{n}^* \geq \widehat{\mathbf{u}}_{tk} - u_l(t_k)\mathbf{1} + \epsilon\mathbf{1}$$

for some $\mathbf{n}^* \in \mathcal{N}_{\widehat{C}}(\widehat{\boldsymbol{\omega}}^*)$, and the assumption $\mathbf{1}^\mathsf{T}\widehat{\boldsymbol{\omega}}^* < 1$ yields

$$\epsilon\widehat{\boldsymbol{\omega}}^* \geq \widehat{\mathbf{u}}_{tk} - u_l(t_k)\mathbf{1} + \epsilon\mathbf{1} - \epsilon\mathbf{1}\mathbf{1}^\mathsf{T}\widehat{\boldsymbol{\omega}}^* > \widehat{\mathbf{u}}_{tk} - u_l(t_k)\mathbf{1},$$

and further that $\epsilon\omega_i^* > u_i(t_k) - u_l(t_k) \ \forall i \neq l$. From $l \notin \mathcal{S}_w$, it follows that $u_i(t_k) - u_l(t_k) \geq \epsilon \ \forall i \in \mathcal{S}_w$, and further that $\omega_i^* > 1 \ \forall i \in \mathcal{S}_w$, which contradicts (5.20b). Thus, $\mathbf{1}^\mathsf{T}\widehat{\boldsymbol{\omega}}^* = 1$.

The last step shows that $\omega_i^* = 1/|\mathcal{S}_w| \ \forall i \in \mathcal{S}_w$. Following the second step, selecting $l \notin \mathcal{S}_w$ in sequence implies that $\omega_i^* = 1 - \mathbf{1}^\mathsf{T}\widehat{\boldsymbol{\omega}}^* = 0$ for all $i \notin \mathcal{S}_w$ and thus $\sum_{i\in\mathcal{S}_w} \omega_i^* = 1$. It then simplifies the minimization problem (5.19) by

$$\begin{aligned}
\underset{\boldsymbol{\omega}_w \in \mathbb{R}^{|\mathcal{S}_w|}}{\text{minimize}} \quad & f_w(\boldsymbol{\omega}_w) = \frac{\epsilon}{2}\boldsymbol{\omega}_w^\mathsf{T}\boldsymbol{\omega}_w - \boldsymbol{\omega}_w^\mathsf{T}\mathbf{u}_{w,tk}, && \text{(5.22a)} \\
\text{subject to} \quad & \mathbf{1}^\mathsf{T}\boldsymbol{\omega}_w = 1, && \text{(5.22b)} \\
& \mathbf{0} \leq \boldsymbol{\omega}_w \leq \mathbf{1}, && \text{(5.22c)}
\end{aligned}$$

where $\boldsymbol{\omega}_w$ and $\mathbf{u}_{w,tk}$ are defined by removing all ω_l and $u_l(t_k)$ with $l \notin \mathcal{S}_w$ from $\boldsymbol{\omega}$ and $\mathbf{u}_{tk}$. Hence, $\mathbf{u}_{w,tk} = b\mathbf{1}$ for some $b \in \mathcal{U}$. Again, the problem (5.22) is strictly convex and satisfies Slater's condition. Using the first-order optimality condition, $\boldsymbol{\omega}_w^*$ is the minimizer of (5.22) iff

$$\mathbf{0} \in \nabla f_w(\boldsymbol{\omega}_w^*) + \mathcal{N}_{\mathcal{C}_w}(\boldsymbol{\omega}_w^*), \tag{5.23}$$

where $\mathcal{N}_{\mathcal{C}_w}(\boldsymbol{\omega}_w^*)$ is the normal cone of the set $\mathcal{C}_w$ at $\boldsymbol{\omega}_w^*$ with

$$\mathcal{C}_w = \Big\{ \boldsymbol{\omega}_w \in \mathbb{R}^{|\mathcal{S}_w|} \Big| \ \mathbf{1}^\mathsf{T}\boldsymbol{\omega}_w = 1, \text{ and } \mathbf{0} \leq \boldsymbol{\omega}_w \leq \mathbf{1} \Big\}.$$

Let $\boldsymbol{\omega}_w^* = 1/|\mathcal{S}_w|$. Then, for any $\boldsymbol{\omega}_w \in \mathcal{C}_w$,

$$\begin{aligned}&\left[\nabla f_w(\boldsymbol{\omega}_w^*)\right]^{\mathsf{T}}(\boldsymbol{\omega}_w - \boldsymbol{\omega}_w^*) = (\epsilon\boldsymbol{\omega}_w^* - \mathbf{u}_{w,tk})^{\mathsf{T}}(\boldsymbol{\omega}_w - \boldsymbol{\omega}_w^*)\\ &= \left(\frac{\epsilon}{|\mathcal{S}_w|} - b\right)\mathbf{1}^{\mathsf{T}}\left(\boldsymbol{\omega}_w - \frac{\mathbf{1}}{|\mathcal{S}_w|}\right) = 0,\end{aligned}$$

which means that $-\nabla f_w(\boldsymbol{\omega}_w^*) \in \mathcal{N}_{\mathcal{C}_w}(\boldsymbol{\omega}_w^*)$. That is, $\boldsymbol{\omega}_w^* = 1/|\mathcal{S}_w|$ satisfies the condition (5.23) and is therefore the minimizer of (5.22). As a result, $\omega_i^* = 1/|\mathcal{S}_w|$ and $\omega_j^* = 0$ for every $i \in \mathcal{S}_w$ and $j \notin \mathcal{S}_w$. The proof is completed. ■

The optimization-based formulation (5.19) for WTA authority dispatch is inspired by the WTA neural network [138]. Lemma 5.2 asserts that the solution of (5.19) deploys equitable authority factors $\omega_i^* = 1/|\mathcal{S}_w|$ $i \in \mathcal{S}_w$ to all leader remote robots receiving the highest user bids. The succeeding extensions of [138] focus on centralized implementations and are not applicable to multi-user teleoperation of distributed multi-robot systems. Compared to the asymptotically convergent distributed WTA neural dynamics [140, 141, 143], this chapter transforms (5.19) into a nonsmooth optimization which it solves with a new, exponentially convergent, distributed gradient algorithm that acts as a dynamic controller to passivate the teleoperator.

In the constrained convex minimization (5.19), the cost function $f(\boldsymbol{\omega})$ in (5.19a) is separable in the sense that it sums $(\epsilon/2)\omega_i^2 - \omega_i u_i(t_k)$ with $i = 1, \cdots, N_r$, and the box constraints $0 \leq \omega_i \leq 1$ in (5.19c) are local. However, the equality constraint (5.19b) involves the authority factors ω_i assigned to all remote robots. For distributed implementation, let an auxiliary variable $\boldsymbol{\upsilon} \in \mathbb{R}^{N_r-1}$ augment (5.19) as follows

$$\underset{(\boldsymbol{\omega},\boldsymbol{\upsilon})\in\mathbb{R}^{N_r}\times\mathbb{R}^{N_r-1}}{\text{minimize}} \quad f(\boldsymbol{\omega},\boldsymbol{\upsilon}) = \frac{\epsilon}{2}\boldsymbol{\omega}^{\mathsf{T}}\boldsymbol{\omega} - \boldsymbol{\omega}^{\mathsf{T}}\mathbf{u}_{tk} + \frac{\kappa}{2}\left\|\boldsymbol{\omega} + \mathbf{B}\boldsymbol{\upsilon} - \frac{\mathbf{1}}{N_r}\right\|^2, \tag{5.24a}$$

$$\text{subject to} \quad \boldsymbol{\omega} + \mathbf{B}\boldsymbol{\upsilon} - \frac{\mathbf{1}}{N_r} = \mathbf{0}, \tag{5.24b}$$

$$\mathbf{0} \leq \boldsymbol{\omega} \leq \mathbf{1}, \tag{5.24c}$$

where $\kappa > 0$ and $\mathbf{B}$ is the incidence matrix associated with the tree communication network of the remote robots.

Let $\mathbf{L}_e = \mathbf{B}^{\mathsf{T}}\mathbf{B}$ be the edge Laplacian matrix of the tree robot network. The following lemma establishes the equivalence between the problems (5.19) and (5.24).

Lemma 5.3. *Let the network of the remote robots have a tree topology. Then, the augmented optimization problem* (5.24) *is convex with the objective function* $f(\boldsymbol{\omega}, \boldsymbol{\upsilon})$ *strongly convex. Further,* $\boldsymbol{\omega}^*$ *is the unique minimizer of* (5.19) *iff* $(\boldsymbol{\omega}^*, -\mathbf{L}_e^{-1}\mathbf{B}^\mathsf{T}\boldsymbol{\omega}^*)$ *is the unique minimizer of* (5.24).

Proof. The equality constraint (5.24b) is affine and the inequality constraints (5.24c) are linear, the proof thus starts by showing that $f(\boldsymbol{\omega}, \boldsymbol{\upsilon})$ is strongly convex with respect to $(\boldsymbol{\omega}, \boldsymbol{\upsilon})$. Using $\mathbf{B}^\mathsf{T}\mathbf{1} = \mathbf{0}$, $f(\boldsymbol{\omega}, \boldsymbol{\upsilon})$ can be rearranged into

$$f(\boldsymbol{\omega}, \boldsymbol{\upsilon}) = \frac{1}{2}\begin{bmatrix}\boldsymbol{\omega}\\ \boldsymbol{\upsilon}\end{bmatrix}^\mathsf{T}\mathbf{H}\begin{bmatrix}\boldsymbol{\omega}\\ \boldsymbol{\upsilon}\end{bmatrix} - \begin{bmatrix}\boldsymbol{\omega}\\ \boldsymbol{\upsilon}\end{bmatrix}^\mathsf{T}\begin{bmatrix}\mathbf{u}_{tk} + \frac{\kappa}{N_r}\mathbf{1}\\ \mathbf{0}\end{bmatrix} + \frac{\kappa}{2N_r}$$

which is quadratic in $(\boldsymbol{\omega}, \boldsymbol{\upsilon})$ with

$$\mathbf{H} = \begin{bmatrix}(\epsilon+\kappa)\mathbf{I} & \kappa\mathbf{B}\\ \kappa\mathbf{B}^\mathsf{T} & \kappa\mathbf{L}_e\end{bmatrix}.$$

Owing to the tree topology of the network of the remote robots, $\kappa\mathbf{L}_e \succ \mathbf{0}$ and the Schur complement of $(\epsilon+\kappa)\mathbf{I} \succ \mathbf{0}$ in $\mathbf{H}$ is

$$\kappa\mathbf{L}_e - \kappa\mathbf{B}^\mathsf{T}\cdot(\epsilon+\kappa)^{-1}\mathbf{I}\cdot\kappa\mathbf{B} = \kappa\mathbf{L}_e - \frac{\kappa^2}{\epsilon+\kappa}\mathbf{B}^\mathsf{T}\mathbf{B} = \kappa\mathbf{L}_e - \frac{\kappa^2}{\epsilon+\kappa}\mathbf{L}_e = \frac{\kappa\epsilon}{\epsilon+\kappa}\mathbf{L}_e \succ \mathbf{0}.$$

Namely, $\mathbf{H} \succ \mathbf{0}$ and thus $f(\boldsymbol{\omega}, \boldsymbol{\upsilon})$ is strongly convex in $(\boldsymbol{\omega}, \boldsymbol{\upsilon})$.

Because both $f(\boldsymbol{\omega})$ and $f(\boldsymbol{\omega}, \boldsymbol{\upsilon})$ are strongly convex, the minimizers of both the problems (5.19) and (5.24) are unique. Further, the problem (5.24) is equivalent to

$$\begin{aligned}
\underset{(\boldsymbol{\omega},\boldsymbol{\upsilon})\in\mathbb{R}^{N_r}\times\mathbb{R}^{N_r-1}}{\text{minimize}} \quad & f(\boldsymbol{\omega}) = \frac{\epsilon}{2}\boldsymbol{\omega}^\mathsf{T}\boldsymbol{\omega} - \boldsymbol{\omega}^\mathsf{T}\mathbf{u}_{tk},, && \text{(5.25a)}\\
\text{subject to} \quad & \boldsymbol{\omega} + \mathbf{B}\boldsymbol{\upsilon} - \frac{\mathbf{1}}{N_r} = \mathbf{0}, && \text{(5.25b)}\\
& \mathbf{0} \le \boldsymbol{\omega} \le \mathbf{1}, && \text{(5.25c)}
\end{aligned}$$

by simplifying $f(\boldsymbol{\omega}, \boldsymbol{\upsilon})$ with (5.24b). It remains to prove that the constraint (5.25b) is true iff $\boldsymbol{\upsilon} = -\mathbf{L}_e^{-1}\mathbf{B}^\mathsf{T}\boldsymbol{\omega}$ and (5.19b) holds. If (5.25b) is true, then

$$\begin{aligned}
\mathbf{L}_e^{-1}\mathbf{B}^\mathsf{T}\left(\boldsymbol{\omega} + \mathbf{B}\boldsymbol{\upsilon} - \frac{\mathbf{1}}{N_r}\right) &= \mathbf{L}_e^{-1}\mathbf{B}^\mathsf{T}\boldsymbol{\omega} + \boldsymbol{\upsilon} = \mathbf{0},\\
\left(\boldsymbol{\omega} + \mathbf{B}\boldsymbol{\upsilon} - \frac{\mathbf{1}}{N_r}\right)^\mathsf{T}\mathbf{1} &= \boldsymbol{\omega}^\mathsf{T}\mathbf{1} - 1 = 0,
\end{aligned}$$

and thus $\boldsymbol{\upsilon} = -\mathbf{L}_e^{-1}\mathbf{B}^\mathsf{T}\boldsymbol{\omega}$ and $\boldsymbol{\omega}^\mathsf{T}\mathbf{1} = 1$. Now let $\boldsymbol{\upsilon} = -\mathbf{L}_e^{-1}\mathbf{B}^\mathsf{T}\boldsymbol{\omega}$ and (5.19b) be true. Using (5.19b), together with $\mathbf{B}^\mathsf{T}\mathbf{1} = \mathbf{0}$, $\mathrm{rank}(\mathbf{B}) = N_r - 1$ and $\mathrm{rank}(\mathbf{1}) = 1$, $\boldsymbol{\omega}$ can be written as

$$\boldsymbol{\omega} = \frac{\mathbf{1}}{N_r} - \mathbf{B}\widehat{\boldsymbol{\upsilon}}, \quad \forall \widehat{\boldsymbol{\upsilon}} \in \mathbb{R}^{N_r-1},$$

and, in conjunction with $\boldsymbol{\upsilon} = -\mathbf{L}_e^{-1}\mathbf{B}^\mathsf{T}\boldsymbol{\omega}$, yields

$$\boldsymbol{\upsilon} = -\mathbf{L}_e^{-1}\mathbf{B}^\mathsf{T}\left(\frac{\mathbf{1}}{N_r} - \mathbf{B}\widehat{\boldsymbol{\upsilon}}\right) = \mathbf{L}_e^{-1}\mathbf{B}^\mathsf{T}\mathbf{B}\widehat{\boldsymbol{\upsilon}} = \widehat{\boldsymbol{\upsilon}}.$$

Thus, the condition (5.25b) is true by the two equations above. ■

The encoding of the equality constraint (5.24b) into the cost function $f(\boldsymbol{\omega})$ makes the augmented objective function $f(\boldsymbol{\omega}, \boldsymbol{\upsilon})$ strongly convex with respect to the extended optimization variable $(\boldsymbol{\omega}, \boldsymbol{\upsilon})$. The benefit in Lemma 5.3 is instrumental to the upcoming proof of the exponential convergence of the proposed distributed WTA algorithm. Yet, because the coexistence of the equality (5.24b) and inequality (5.24c) constraints thwart the exponential convergence of conventional primal-dual algorithms, this paper eliminates the equality constraint (5.24b) through the nonsmooth penalty function:

$$\underset{(\boldsymbol{\omega},\boldsymbol{\upsilon})\in\mathbb{R}^{N_r}\times\mathbb{R}^{N_r-1}}{\text{minimize}} \quad f_\gamma(\boldsymbol{\omega}, \boldsymbol{\upsilon}) = f(\boldsymbol{\omega}, \boldsymbol{\upsilon}) + \gamma\mathbf{1}^\mathsf{T}\left|\boldsymbol{\omega} + \mathbf{B}\boldsymbol{\upsilon} - \frac{\mathbf{1}}{N_r}\right|, \tag{5.26a}$$

$$\text{subject to} \quad \mathbf{0} \leq \boldsymbol{\omega} \leq \mathbf{1}, \tag{5.26b}$$

where $\gamma > 0$ is determined using Proposition 5.2 (whose proof is obtained following the derivations in [183, Chapter 4.3.1]) and Lemma 5.4 below.

Proposition 5.2. *Let $\boldsymbol{\lambda}^* = (\lambda_1^*, \cdots, \lambda_{N_r}^*)^\mathsf{T}$ be a vector of multipliers associated with the equality constraint* (5.24b)*. Then, the problems* (5.24) *and* (5.26) *have the same solution if $\gamma > \max\limits_{i=1,\cdots,N_r} |\lambda_i^*|$.*

Lemma 5.4. *Let $(\boldsymbol{\omega}^*, \boldsymbol{\upsilon}^*)$ be the unique minimizer of the problem* (5.24)*. The vector of multipliers associated with the equality constraint* (5.24b) *is $\boldsymbol{\lambda}^* = \lambda^*\mathbf{1}$ with $|\lambda^*| \leq b_m - \epsilon/N_l$.*

Proof. Let the partial derivatives of $f(\boldsymbol{\omega}, \boldsymbol{\upsilon})$ with respect to $\boldsymbol{\omega}$ and $\boldsymbol{\upsilon}$ at $(\boldsymbol{\omega}^*, \boldsymbol{\upsilon}^*)$

respectively be

$$\nabla_{\boldsymbol{\omega}} f(\boldsymbol{\omega}^*, \boldsymbol{\upsilon}^*) = \epsilon\boldsymbol{\omega}^* - \mathbf{u}_{tk} + \kappa\left(\boldsymbol{\omega}^* + \mathbf{B}\boldsymbol{\upsilon}^* - \frac{\mathbf{1}}{N_r}\right),$$
$$\nabla_{\boldsymbol{\upsilon}} f(\boldsymbol{\omega}^*, \boldsymbol{\upsilon}^*) = \kappa\mathbf{B}^{\mathsf{T}}\left(\boldsymbol{\omega}^* + \mathbf{B}\boldsymbol{\upsilon}^* - \frac{\mathbf{1}}{N_r}\right).$$

By the Karush-Kuhn-Tucker (KKT) conditions for the unique solution $(\boldsymbol{\omega}^*, \boldsymbol{\upsilon}^*)$ of the program (5.24), there exist Lagrangian multipliers $\boldsymbol{\mu}_-^* = (\mu_{1-}^*, \cdots, \mu_{N_r-}^*)^{\mathsf{T}}$ and $\boldsymbol{\mu}_+^* = (\mu_{1+}^*, \cdots, \mu_{N_r+}^*)^{\mathsf{T}}$ associated to the box constraint (5.24c) such that

$$\nabla_{\boldsymbol{\omega}} f(\boldsymbol{\omega}^*, \boldsymbol{\upsilon}^*) + \boldsymbol{\lambda}^* - \boldsymbol{\mu}_-^* + \boldsymbol{\mu}_+^* = \mathbf{0}, \tag{5.27a}$$
$$\nabla_{\upsilon} f(\boldsymbol{\omega}^*, \boldsymbol{\upsilon}^*) + \mathbf{B}^{\mathsf{T}}\boldsymbol{\lambda}^* = \mathbf{0}, \tag{5.27b}$$
$$\boldsymbol{\omega}^* + \mathbf{B}\boldsymbol{\upsilon}^* - \frac{\mathbf{1}}{N_r} = \mathbf{0}, \tag{5.27c}$$
$$\boldsymbol{\mu}_-^* \geq \mathbf{0}, \quad \boldsymbol{\omega}^* \geq \mathbf{0}, \quad \boldsymbol{\omega}^{*\mathsf{T}}\boldsymbol{\mu}_-^* = 0, \tag{5.27d}$$
$$\boldsymbol{\mu}_+^* \geq \mathbf{0}, \quad \boldsymbol{\omega}^* \leq \mathbf{1}, \quad (\boldsymbol{\omega}^* - \mathbf{1})^{\mathsf{T}}\boldsymbol{\mu}_+^* = 0. \tag{5.27e}$$

Then (5.27c) can simplify (5.27a) and (5.27b) by $\boldsymbol{\lambda}^* = -\epsilon\boldsymbol{\omega}^* + \mathbf{u}_{tk} + \boldsymbol{\mu}_-^* - \boldsymbol{\mu}_+^*$ and by $\mathbf{B}^{\mathsf{T}}\boldsymbol{\lambda}^* = \mathbf{0}$, respectively. Given that $\emptyset \neq \mathcal{S}_w \subseteq \{1, \cdots, N_l\}$ and $\omega_l^* = 0\ \forall l \notin \mathcal{S}_w$ (see the proof of Lemma 5.2), there exists $h \in \mathcal{S}_w$ with $u_h(t_k) \geq b_1$ such that $\omega_h^* \geq \frac{1}{N_l}$. If $\omega_h^* = 1$, then $\mu_{h-}^* = 0$ by (5.27d) and $\lambda_h^* = -\epsilon + u_h(t_k) - \mu_{h+}^*$. If $\omega_h^* < 1$, then $\mu_{h-}^* = \mu_{h+}^* = 0$ and $\lambda_h^* = -\epsilon\omega_h^* + u_h(t_k)$. Because $\omega_l^* = 0$, (5.27e) leads to $\mu_{l+}^* = 0$, and hence $\lambda_l^* = u_l(t_k) + \mu_{l-}^* \geq 0$. Then $\mathbf{B}^{\mathsf{T}}\boldsymbol{\lambda}^* = \mathbf{0}$ yields $\lambda_i^* = \lambda_h^* = \lambda_l^* \geq 0\ \forall i = 1, \cdots, N_r$. Hence, λ_h^* is bounded by

$$|\lambda_h^*| = \begin{cases} |-\epsilon + u_h(t_k) - \mu_{h+}^*| \leq b_m - \epsilon, & \text{if } \omega_h^* = 1, \\ |-\epsilon\omega_h^* + u_h(t_k)| \leq b_m - \epsilon/N_l, & \text{if } \omega_h^* < 1, \end{cases}$$

and $|\lambda_i^*| \leq b_m - \epsilon/N_l\ \forall i = 1, \cdots, N_r$. ■

The proof of Lemma 5.4 tailors that of Lemma 5.1 in [144] to match the problem (5.26) with the problem (5.24). For the vector $\boldsymbol{\lambda}$ of multipliers associated to the equality constraint (5.24b), Lemma 5.4 first establishes that $\boldsymbol{\lambda}^*$ is spanned by $\mathbf{1}$, and then finds an explicit upper bound of $\boldsymbol{\lambda}^*$ to facilitate the algorithm design. Together, Proposition 5.2 and Lemma 5.4 recast the distributed WTA authority dispatch problem as the nonsmooth program (5.26) and permit to develop a projected

gradient algorithm to solve the problem:

$$k_\omega \dot{\boldsymbol{\omega}} \in \mathrm{Proj}_{\mathcal{C}^b_{\boldsymbol{\omega}}}\big[\boldsymbol{\omega}, -\nabla_{\boldsymbol{\omega}} f_\gamma(\boldsymbol{\omega}, \boldsymbol{\upsilon}) + \mathbf{f}\big], \tag{5.28a}$$

$$k_\eta \dot{\boldsymbol{\upsilon}} \in -\nabla_{\boldsymbol{\upsilon}} f_\gamma(\boldsymbol{\omega}, \boldsymbol{\upsilon}), \tag{5.28b}$$

where k_ω and k_η are positive constants, $\mathcal{C}^b_{\boldsymbol{\omega}} = \big\{\boldsymbol{\omega} \in \mathbb{R}^{N_r} \big| \ \mathbf{0} \leq \boldsymbol{\omega} \leq \mathbf{1}\big\}$ is the set of box constraints, $\mathbf{f} = (f_1, \cdots, f_{N_r})^\mathsf{T}$ is an input reserved to couple the authority dispatch algorithm with the network of the remote robots, and $\nabla_{\boldsymbol{\omega}} f_\gamma(\boldsymbol{\omega}, \boldsymbol{\upsilon})$ and $\nabla_{\boldsymbol{\upsilon}} f_\gamma(\boldsymbol{\omega}, \boldsymbol{\upsilon})$ are the subdifferentials of $f_\gamma(\boldsymbol{\omega}, \boldsymbol{\upsilon})$ with respect to $\boldsymbol{\omega}$ and $\boldsymbol{\upsilon}$, respectively,

$$\begin{aligned}
\nabla_{\boldsymbol{\omega}} f_\gamma(\boldsymbol{\omega}, \boldsymbol{\upsilon}) =& \epsilon\boldsymbol{\omega} - \mathbf{u}_{tk} + \kappa\left(\boldsymbol{\omega} + \mathbf{B}\boldsymbol{\upsilon} - \frac{\mathbf{1}}{N_r}\right) + \gamma \cdot \mathrm{sign}\left(\boldsymbol{\omega} + \mathbf{B}\boldsymbol{\upsilon} - \frac{\mathbf{1}}{N_r}\right), \\
\nabla_{\boldsymbol{\upsilon}} f_\gamma(\boldsymbol{\omega}, \boldsymbol{\upsilon}) =& \kappa\mathbf{B}^\mathsf{T}\left(\boldsymbol{\omega} + \mathbf{B}\boldsymbol{\upsilon} - \frac{\mathbf{1}}{N_r}\right) + \gamma\mathbf{B}^\mathsf{T} \cdot \mathrm{sign}\left(\boldsymbol{\omega} + \mathbf{B}\boldsymbol{\upsilon} - \frac{\mathbf{1}}{N_r}\right).
\end{aligned}$$

Let $\boldsymbol{\eta} = (\eta_1, \cdots, \eta_{N_r})^\mathsf{T} = \mathbf{B}\boldsymbol{\upsilon}$. Then, $\mathbf{B}^\mathsf{T}\mathbf{1} = \mathbf{0}$ and $\mathbf{L} = \mathbf{B}\mathbf{B}^\mathsf{T}$ refine (5.28) into the projected gradient algorithm

$$k_\omega \dot{\boldsymbol{\omega}} \in \mathrm{Proj}_{\mathcal{C}^b_{\boldsymbol{\omega}}}\big[\boldsymbol{\omega}, -\nabla_{\boldsymbol{\omega}} f_\gamma(\boldsymbol{\omega}, \boldsymbol{\upsilon}) + \mathbf{f}\big], \tag{5.29a}$$

$$k_\eta \dot{\boldsymbol{\upsilon}} \in -\nabla_{\boldsymbol{\upsilon}} f_\gamma(\boldsymbol{\omega}, \boldsymbol{\upsilon}), \tag{5.29b}$$

whose distributed implementation is obtained by using the box constraint set $\mathcal{C}^b_{\boldsymbol{\omega}}$:

$$k_\omega \dot{\omega}_i \in \mathrm{Proj}_{[0,1]}\big[\omega_i, -(\epsilon+\kappa)\omega_i - \kappa\eta_i + f_i + u_i(t_k) + \kappa/N_r - \gamma \cdot \mathrm{sign}\,(\alpha_i)\,\big], \tag{5.30a}$$

$$k_\eta \dot{\eta}_i \in \sum_{j\in\mathcal{N}_i} \kappa\big[(\omega_j - \omega_i) + (\eta_j - \eta_i)\big] + \sum_{j\in\mathcal{N}_i} \gamma\big[\mathrm{sign}\,(\alpha_j) - \mathrm{sign}\,(\alpha_i)\,\big], \tag{5.30b}$$

where $\alpha_i = \omega_i + \eta_i - 1/N_r$ for every remote robot $i = 1, \cdots, N_r$. A beneficial property of (5.29) needed in the upcoming analysis is the following:

Proposition 5.3. *Let* (5.29) *start with* $\boldsymbol{\omega}(0) \in \mathcal{C}^b_{\boldsymbol{\omega}}$ *and* $\mathbf{1}^\mathsf{T}\boldsymbol{\eta}(0) = 0$. *Then,* $\boldsymbol{\omega}(t) \in \mathcal{C}^b_{\boldsymbol{\omega}}$ *and* $\mathbf{1}^\mathsf{T}\boldsymbol{\eta}(t) = 0$ *for all time* $t \geq 0$.

Proof. Because $\boldsymbol{\omega} \in \mathrm{int}(\mathcal{C}^b_{\boldsymbol{\omega}}) \subsetneq \mathcal{C}^b_{\boldsymbol{\omega}}$ if $\mathcal{N}_{\mathcal{C}^b_{\boldsymbol{\omega}}}(\boldsymbol{\omega}) = \{\mathbf{0}\}$ and $\boldsymbol{\omega} \in \partial\mathcal{C}^b_{\boldsymbol{\omega}}$ if $\mathcal{N}_{\mathcal{C}^b_{\boldsymbol{\omega}}}(\boldsymbol{\omega}) \neq \{\mathbf{0}\}$, a sufficient condition for $\boldsymbol{\omega}(t) \in \mathcal{C}^b_{\boldsymbol{\omega}}$ is that $\mathbf{n}^\mathsf{T}\dot{\boldsymbol{\omega}} \leq 0$ for $\mathbf{n} \in \mathcal{N}^*_{\mathcal{C}^b_{\boldsymbol{\omega}}}(\boldsymbol{\omega}) \neq \{\mathbf{0}\}$. Then given any $\mathbf{g} \in \mathbb{R}^{N_r}$, it has that $\mathbf{n}^\mathsf{T}\mathrm{Proj}_{\mathcal{C}^b_{\boldsymbol{\omega}}}(\boldsymbol{\omega}, \mathbf{g}) = 0$ if $\mathbf{g} = \mathbf{0}$; $\mathbf{n}_* = \mathbf{g}/\|\mathbf{g}\|$, $\mathrm{Proj}_{\mathcal{C}^b_{\boldsymbol{\omega}}}(\boldsymbol{\omega}, \mathbf{g}) = (\mathbf{I} - \mathbf{n}_*\mathbf{n}_*^\mathsf{T})\mathbf{g} = \mathbf{0}$ and thus $\mathbf{n}^\mathsf{T}\mathrm{Proj}_{\mathcal{C}^b_{\boldsymbol{\omega}}}(\boldsymbol{\omega}, \mathbf{g}) = 0$ if $\mathbf{0} \neq \mathbf{g} \in \mathcal{N}_{\mathcal{C}^b_{\boldsymbol{\omega}}}(\boldsymbol{\omega})$; and $\mathbf{n}_* = \mathbf{0}$, $\mathrm{Proj}_{\mathcal{C}^b_{\boldsymbol{\omega}}}(\boldsymbol{\omega}, \mathbf{g}) = (\mathbf{I} - \mathbf{n}_*\mathbf{n}_*^\mathsf{T})\mathbf{g} = \mathbf{g}$, and thus $\mathbf{n}^\mathsf{T}\mathrm{Proj}_{\mathcal{C}^b_{\boldsymbol{\omega}}}(\boldsymbol{\omega}, \mathbf{g}) \leq 0$ if

$\mathbf{0} \neq \mathbf{g} \notin \mathcal{N}_{\mathcal{C}_{\boldsymbol{\omega}}^b}(\boldsymbol{\omega})$. Then (5.29a) leads to $k_\omega \mathbf{n}^\mathsf{T} \dot{\boldsymbol{\omega}} \leq 0$ for $\mathbf{n} \in \mathcal{N}^*_{\mathcal{C}_{\boldsymbol{\omega}}^b}(\boldsymbol{\omega}) \neq \{\mathbf{0}\}$, and further to $\boldsymbol{\omega}(t) \in \mathcal{C}_{\boldsymbol{\omega}}^b \ \forall t \geq 0$. Thereafter, pre-multiplying (5.29b) by $\mathbf{1}^\mathsf{T}$ yields $k_\eta \mathbf{1}^\mathsf{T} \dot{\boldsymbol{\eta}} \in -\kappa \mathbf{1}^\mathsf{T}\mathbf{L}(\boldsymbol{\omega} + \boldsymbol{\eta}) - \gamma \mathbf{1}^\mathsf{T}\mathbf{L} \cdot \operatorname{sign}(\boldsymbol{\omega} + \boldsymbol{\eta} - \mathbf{1}/N_r) = \{0\}$, which together with $\mathbf{1}^\mathsf{T}\boldsymbol{\eta}(0) = 0$ implies that $\mathbf{1}^\mathsf{T}\boldsymbol{\eta}(t) = 0 \ \forall t \geq 0$. ■

Before verifying the distributed WTA authority dispatch strategy, the following lemma explicitly characterizes an equilibrium of the algorithm (5.29) using the minimizer of (5.26).

Lemma 5.5. *If $(\boldsymbol{\omega}^*, \boldsymbol{\upsilon}^*)$ is the unique minimizer of* (5.26) *with $\mathbf{f} = \mathbf{0}$, then $(\overline{\boldsymbol{\omega}}, \overline{\boldsymbol{\eta}}) = (\boldsymbol{\omega}^*, \mathbf{B}\boldsymbol{\upsilon}^*)$ is an equilibrium of the dynamics* (5.29)*, namely,*

$$k_\omega \dot{\overline{\boldsymbol{\omega}}} = \mathbf{0} \in \operatorname{Proj}_{\mathcal{C}_{\boldsymbol{\omega}}^b}\left[\overline{\boldsymbol{\omega}}, -(\epsilon+\kappa)\overline{\boldsymbol{\omega}} - \kappa\overline{\boldsymbol{\eta}} + \mathbf{u}_{tk} + \frac{\kappa}{N_r}\mathbf{1} - \gamma \cdot \operatorname{sign}\left(\overline{\boldsymbol{\omega}} + \overline{\boldsymbol{\eta}} - \frac{\mathbf{1}}{N_r}\right)\right], \tag{5.31a}$$

$$k_\eta \dot{\overline{\boldsymbol{\eta}}} = \mathbf{0} \in -\kappa\mathbf{L}(\overline{\boldsymbol{\omega}} + \overline{\boldsymbol{\eta}}) - \gamma\mathbf{L} \cdot \operatorname{sign}\left(\overline{\boldsymbol{\omega}} + \overline{\boldsymbol{\eta}} - \frac{\mathbf{1}}{N_r}\right). \tag{5.31b}$$

Proof. The KKT conditions of (5.26) are

$$\begin{aligned}
\mathbf{0} \in& (\epsilon+\kappa)\boldsymbol{\omega}^* + \kappa\mathbf{B}\boldsymbol{\upsilon}^* - \mathbf{u}_{tk} - \frac{\kappa}{N_r}\mathbf{1} + \gamma \cdot \operatorname{sign}\left(\boldsymbol{\omega}^* + \mathbf{B}\boldsymbol{\upsilon}^* - \frac{\mathbf{1}}{N_r}\right) + \mathcal{N}_{\mathcal{C}_{\boldsymbol{\omega}}^b}(\boldsymbol{\omega}^*), \\
\mathbf{0} \in& \kappa\mathbf{B}^\mathsf{T}\left(\boldsymbol{\omega}^* + \mathbf{B}\boldsymbol{\upsilon}^* - \frac{\mathbf{1}}{N_r}\right) + \gamma\mathbf{B}^\mathsf{T} \cdot \operatorname{sign}\left(\boldsymbol{\omega}^* + \mathbf{B}\boldsymbol{\upsilon}^* - \frac{\mathbf{1}}{N_r}\right).
\end{aligned}$$

Then, there exists $\overline{\mathbf{n}} \in \mathcal{N}_{\mathcal{C}_{\boldsymbol{\omega}}^b}(\overline{\boldsymbol{\omega}})$ such that

$$\overline{\mathbf{n}} \in -(\epsilon+\kappa)\overline{\boldsymbol{\omega}} - \kappa\overline{\boldsymbol{\eta}} + \mathbf{u}_{tk} + \frac{\kappa}{N_r}\mathbf{1} - \gamma \cdot \operatorname{sign}\left(\overline{\boldsymbol{\omega}} + \overline{\boldsymbol{\eta}} - \frac{\mathbf{1}}{N_r}\right), \tag{5.32a}$$

$$\mathbf{0} \in -\kappa\mathbf{L}(\overline{\boldsymbol{\omega}} + \overline{\boldsymbol{\eta}}) - \gamma\mathbf{L} \cdot \operatorname{sign}\left(\overline{\boldsymbol{\omega}} + \overline{\boldsymbol{\eta}} - \frac{\mathbf{1}}{N_r}\right), \tag{5.32b}$$

and (5.31b) follows from (5.32b).

To show that (5.32a) implies (5.31a), note that (5.31a) holds if there exists

$$\mathbf{g} \in -(\epsilon+\kappa)\overline{\boldsymbol{\omega}} - \kappa\overline{\boldsymbol{\eta}} + \mathbf{u}_{tk} + \frac{\kappa}{N_r}\mathbf{1} - \gamma \cdot \operatorname{sign}\left(\overline{\boldsymbol{\omega}} + \overline{\boldsymbol{\eta}} - \frac{\mathbf{1}}{N_r}\right) \tag{5.33}$$

that satisfies $\mathbf{0} = \operatorname{Proj}_{\mathcal{C}_{\boldsymbol{\omega}}^b}(\overline{\boldsymbol{\omega}}, \mathbf{g})$. Equation (5.31a) holds if $\operatorname{Proj}_{\mathcal{C}_{\boldsymbol{\omega}}^b}(\overline{\boldsymbol{\omega}}, \mathbf{g}) = \mathbf{g} = \mathbf{0}$ when $\mathcal{N}_{\mathcal{C}_{\boldsymbol{\omega}}^b}(\overline{\boldsymbol{\omega}}) = \{\mathbf{0}\}$, and if $\operatorname{Proj}_{\mathcal{C}_{\boldsymbol{\omega}}^b}(\overline{\boldsymbol{\omega}}, \mathbf{g}) = \mathbf{g} - \mathbf{n}_*\mathbf{n}_*^\mathsf{T}\mathbf{g} = \mathbf{0}$ with $\mathbf{n}_*^\mathsf{T}\mathbf{g} \geq 0$ and $\mathbf{n}_* \in \mathcal{N}_{\mathcal{C}_{\boldsymbol{\omega}}^b}(\overline{\boldsymbol{\omega}})$

when $\mathcal{N}_{\mathcal{C}_{\boldsymbol{\omega}}^b}(\overline{\boldsymbol{\omega}}) \neq \{\mathbf{0}\}$. In other words, (5.31a) is satisfied if there exists $\mathbf{g}$ in (5.33) such that $\mathbf{g} \in \mathcal{N}_{\mathcal{C}_{\boldsymbol{\omega}}^b}(\overline{\boldsymbol{\omega}})$. Hence, (5.32a) implies (5.32a).

It then follows that $(\overline{\boldsymbol{\omega}}, \overline{\boldsymbol{\eta}}) = (\boldsymbol{\omega}^*, \mathbf{B}\boldsymbol{\upsilon}^*)$ obeys (5.31) and is an equilibrium of the dynamics (5.29). ■

Let the deviations of $\boldsymbol{\omega}$ and $\boldsymbol{\eta}$ from their equilibria $\overline{\boldsymbol{\omega}}$ and $\overline{\boldsymbol{\eta}}$ be $\widetilde{\boldsymbol{\omega}} = \boldsymbol{\omega} - \overline{\boldsymbol{\omega}}$ and $\widetilde{\boldsymbol{\eta}} = \boldsymbol{\eta} - \overline{\boldsymbol{\eta}}$, respectively. The efficacy of the algorithm (5.29) for solving the problem (5.26) can be verified with Lemma 5.5 by

$$k_\omega \dot{\widetilde{\boldsymbol{\omega}}} \in \mathrm{Proj}_{\mathcal{C}_{\boldsymbol{\omega}}^b}\big[\boldsymbol{\omega}, \mathbf{g}(\boldsymbol{\omega}, \boldsymbol{\eta})\big] \ominus \mathrm{Proj}_{\mathcal{C}_{\boldsymbol{\omega}}^b}\big[\overline{\boldsymbol{\omega}}, \overline{\mathbf{g}}(\overline{\boldsymbol{\omega}}, \overline{\boldsymbol{\eta}})\big], \tag{5.34a}$$

$$k_\eta \dot{\widetilde{\boldsymbol{\eta}}} \in -\kappa \mathbf{L}(\widetilde{\boldsymbol{\omega}} + \widetilde{\boldsymbol{\eta}}) - \gamma \mathbf{L}\mathbf{h}(\boldsymbol{\omega}, \boldsymbol{\eta}, \overline{\boldsymbol{\omega}}, \overline{\boldsymbol{\eta}}), \tag{5.34b}$$

with $\ominus$ the Minkowski difference of two subdifferentials, and

$$\begin{aligned}
\mathbf{g}(\boldsymbol{\omega}, \boldsymbol{\eta}) =& -(\epsilon + \kappa)\boldsymbol{\omega} - \kappa\boldsymbol{\eta} + \mathbf{f} + \mathbf{u}_{tk} + \frac{\kappa}{N_r}\mathbf{1} - \gamma \cdot \mathrm{sign}\left(\boldsymbol{\omega} + \boldsymbol{\eta} - \frac{\mathbf{1}}{N_r}\right), \\
\overline{\mathbf{g}}(\overline{\boldsymbol{\omega}}, \overline{\boldsymbol{\eta}}) =& -(\epsilon + \kappa)\overline{\boldsymbol{\omega}} - \kappa\overline{\boldsymbol{\eta}} + \mathbf{u}_{tk} + \frac{\kappa}{N_r}\mathbf{1} - \gamma \cdot \mathrm{sign}\left(\overline{\boldsymbol{\omega}} + \overline{\boldsymbol{\eta}} - \frac{\mathbf{1}}{N_r}\right), \\
\mathbf{h}(\boldsymbol{\omega}, \boldsymbol{\eta}, \overline{\boldsymbol{\omega}}, \overline{\boldsymbol{\eta}}) =& \mathrm{sign}\left(\boldsymbol{\omega} + \boldsymbol{\eta} - \frac{\mathbf{1}}{N_r}\right) \ominus \mathrm{sign}\left(\overline{\boldsymbol{\omega}} + \overline{\boldsymbol{\eta}} - \frac{\mathbf{1}}{N_r}\right).
\end{aligned}$$

Adding and deleting $\mathbf{g}(\boldsymbol{\omega}, \boldsymbol{\eta}) - \overline{\mathbf{g}}(\overline{\boldsymbol{\omega}}, \overline{\boldsymbol{\eta}})$ in (5.34a) transforms (5.34) to

$$\begin{aligned}
k_\omega \dot{\widetilde{\boldsymbol{\omega}}} \in& \Big(\mathrm{Proj}_{\mathcal{C}_{\boldsymbol{\omega}}^b}\big[\boldsymbol{\omega}, \mathbf{g}(\boldsymbol{\omega}, \boldsymbol{\eta})\big] - \mathbf{g}(\boldsymbol{\omega}, \boldsymbol{\eta})\Big) \ominus \Big(\mathrm{Proj}_{\mathcal{C}_{\boldsymbol{\omega}}^b}\big[\overline{\boldsymbol{\omega}}, \overline{\mathbf{g}}(\overline{\boldsymbol{\omega}}, \overline{\boldsymbol{\eta}})\big] - \overline{\mathbf{g}}(\overline{\boldsymbol{\omega}}, \overline{\boldsymbol{\eta}})\Big) \\
& - (\epsilon + \kappa)\widetilde{\boldsymbol{\omega}} - \kappa\widetilde{\boldsymbol{\eta}} + \mathbf{f} - \gamma \mathbf{h}(\boldsymbol{\omega}, \boldsymbol{\eta}, \overline{\boldsymbol{\omega}}, \overline{\boldsymbol{\eta}}),
\end{aligned} \tag{5.35a}$$

$$k_\eta \dot{\widetilde{\boldsymbol{\eta}}} \in -\kappa \mathbf{L}(\widetilde{\boldsymbol{\omega}} + \widetilde{\boldsymbol{\eta}}) - \gamma \mathbf{L}\mathbf{h}(\boldsymbol{\omega}, \boldsymbol{\eta}, \overline{\boldsymbol{\omega}}, \overline{\boldsymbol{\eta}}). \tag{5.35b}$$

Now let a storage function for the WTA authority dispatch dynamics (5.29) be

$$V_{ad} = \frac{k_\omega}{2}\widetilde{\boldsymbol{\omega}}^\mathsf{T}\widetilde{\boldsymbol{\omega}} + \frac{k_\eta}{2}\widetilde{\boldsymbol{\eta}}^\mathsf{T}\mathbf{L}^\dagger\widetilde{\boldsymbol{\eta}}, \tag{5.36}$$

where $\mathbf{L}^\dagger$ is the positive semi-definite generalized inverse of the Laplacian matrix $\mathbf{L}$ and obeys $\mathbf{L}\mathbf{L}^\dagger = \mathbf{L}^\dagger\mathbf{L} = \mathbf{I} - \mathbf{1}\mathbf{1}^\mathsf{T}/N_r$.

By initializing the algorithm (5.29b) by $\mathbf{1}^\mathsf{T}\boldsymbol{\eta}(0) = 0$, Proposition 5.3 guarantees that $\mathbf{1}^\mathsf{T}\boldsymbol{\eta}(t) = 0$ and hence that $\mathbf{1}^\mathsf{T}\widetilde{\boldsymbol{\eta}}(t) = 0\ \forall t \geq 0$. Then, V_{ad} varies along the error

dynamics (5.35) with

$$\begin{aligned}\dot{V}_{ad} \in &- (\epsilon+\kappa)\widetilde{\boldsymbol{\omega}}^{\mathsf{T}}\widetilde{\boldsymbol{\omega}} - \kappa\widetilde{\boldsymbol{\omega}}^{\mathsf{T}}\widetilde{\boldsymbol{\eta}} + \widetilde{\boldsymbol{\omega}}^{\mathsf{T}}\mathbf{f} - \kappa\widetilde{\boldsymbol{\eta}}^{\mathsf{T}}\widetilde{\boldsymbol{\omega}} - \kappa\widetilde{\boldsymbol{\eta}}^{\mathsf{T}}\widetilde{\boldsymbol{\eta}} - \gamma\big(\widetilde{\boldsymbol{\omega}}+\widetilde{\boldsymbol{\eta}}\big)^{\mathsf{T}}\mathbf{h}(\boldsymbol{\omega},\boldsymbol{\eta},\overline{\boldsymbol{\omega}},\overline{\boldsymbol{\eta}}) \\ &+ \widetilde{\boldsymbol{\omega}}^{\mathsf{T}}\Big[\big(\mathrm{Proj}_{\mathcal{C}^b_{\boldsymbol{\omega}}}\big[\boldsymbol{\omega},\mathbf{g}(\boldsymbol{\omega},\boldsymbol{\eta})\big] - \mathbf{g}(\boldsymbol{\omega},\boldsymbol{\eta})\big) \ominus \big(\mathrm{Proj}_{\mathcal{C}^b_{\boldsymbol{\omega}}}\big[\overline{\boldsymbol{\omega}},\overline{\mathbf{g}}(\overline{\boldsymbol{\omega}},\overline{\boldsymbol{\eta}})\big] - \overline{\mathbf{g}}(\overline{\boldsymbol{\omega}},\overline{\boldsymbol{\eta}})\big)\Big].\end{aligned}$$

The last two steps needed for the exponential convergence and passivity of (5.29) are the following two properties of the projection operator $\mathrm{Proj}_{\mathcal{C}^b_{\boldsymbol{\omega}}}(\cdot,\cdot)$ and the subdifferential $\mathrm{sign}(\cdot)$.

Proposition 5.4. *If $\overline{\boldsymbol{\omega}} \in \mathcal{C}^b_{\boldsymbol{\omega}}$ and* (5.29a) *starts with $\boldsymbol{\omega}(0) \in \mathcal{C}^b_{\boldsymbol{\omega}}$, then*

$$\widetilde{\boldsymbol{\omega}}^{\mathsf{T}}\Big[\big(\mathrm{Proj}_{\mathcal{C}^b_{\boldsymbol{\omega}}}\big[\boldsymbol{\omega},\mathbf{g}(\boldsymbol{\omega},\boldsymbol{\eta})\big] - \mathbf{g}(\boldsymbol{\omega},\boldsymbol{\eta})\big) \ominus \big(\mathrm{Proj}_{\mathcal{C}^b_{\boldsymbol{\omega}}}\big[\overline{\boldsymbol{\omega}},\overline{\mathbf{g}}(\overline{\boldsymbol{\omega}},\overline{\boldsymbol{\eta}})\big] - \overline{\mathbf{g}}(\overline{\boldsymbol{\omega}},\overline{\boldsymbol{\eta}})\big)\Big] \leq 0.$$

Proof. Proposition 5.3 implies that $\boldsymbol{\omega}(t) \in \mathcal{C}^b_{\boldsymbol{\omega}}\ \forall t \geq 0$. And also, $\mathrm{Proj}_{\mathcal{C}^b_{\boldsymbol{\omega}}}\big[\boldsymbol{\omega},\mathbf{g}(\boldsymbol{\omega},\boldsymbol{\eta})\big] = (\mathbf{I}-\mathbf{n}_*\mathbf{n}_*^{\mathsf{T}})\mathbf{g}(\boldsymbol{\omega},\boldsymbol{\eta})$ and $\mathrm{Proj}_{\mathcal{C}^b_{\boldsymbol{\omega}}}\big[\overline{\boldsymbol{\omega}},\overline{\mathbf{g}}(\overline{\boldsymbol{\omega}},\overline{\boldsymbol{\eta}})\big] = (\mathbf{I}-\overline{\mathbf{n}}_*\overline{\mathbf{n}}_*^{\mathsf{T}})\overline{\mathbf{g}}(\overline{\boldsymbol{\omega}},\overline{\boldsymbol{\eta}})$, where

$$\mathbf{n}_* = \arg\max_{\mathbf{n}\in\mathcal{N}_{\mathcal{C}^b_{\boldsymbol{\omega}}}(\boldsymbol{\omega})} \mathbf{n}^{\mathsf{T}}\mathbf{g}(\boldsymbol{\omega},\boldsymbol{\eta}), \text{ and } \overline{\mathbf{n}}_* = \arg\max_{\overline{\mathbf{n}}\in\mathcal{N}_{\mathcal{C}^b_{\boldsymbol{\omega}}}(\overline{\boldsymbol{\omega}})} \overline{\mathbf{n}}^{\mathsf{T}}\overline{\mathbf{g}}(\overline{\boldsymbol{\omega}},\overline{\boldsymbol{\eta}}).$$

Moreover, $\boldsymbol{\omega} \in \mathcal{C}^b_{\boldsymbol{\omega}}$ and $\overline{\boldsymbol{\omega}} \in \mathcal{C}^b_{\boldsymbol{\omega}}$ lead to $\mathbf{n}_*^{\mathsf{T}}\mathbf{g}(\boldsymbol{\omega},\boldsymbol{\eta}) \geq 0$ and $\overline{\mathbf{n}}_*^{\mathsf{T}}\overline{\mathbf{g}}(\overline{\boldsymbol{\omega}},\overline{\boldsymbol{\eta}}) \geq 0$, and thus

$$\begin{aligned}&\widetilde{\boldsymbol{\omega}}^{\mathsf{T}}\Big[\big(\mathrm{Proj}_{\mathcal{C}^b_{\boldsymbol{\omega}}}\big[\boldsymbol{\omega},\mathbf{g}(\boldsymbol{\omega},\boldsymbol{\eta})\big] - \mathbf{g}(\boldsymbol{\omega},\boldsymbol{\eta})\big) \ominus \big(\mathrm{Proj}_{\mathcal{C}^b_{\boldsymbol{\omega}}}\big[\overline{\boldsymbol{\omega}},\overline{\mathbf{g}}(\overline{\boldsymbol{\omega}},\overline{\boldsymbol{\eta}})\big] - \overline{\mathbf{g}}(\overline{\boldsymbol{\omega}},\overline{\boldsymbol{\eta}})\big)\Big] \\ =&\widetilde{\boldsymbol{\omega}}^{\mathsf{T}}\left[\big(\mathbf{I}-\mathbf{n}_*\mathbf{n}_*^{\mathsf{T}}\big)\mathbf{g}(\boldsymbol{\omega},\boldsymbol{\eta}) - \mathbf{g}(\boldsymbol{\omega},\boldsymbol{\eta})\right] \ominus \widetilde{\boldsymbol{\omega}}^{\mathsf{T}}\left[\big(\mathbf{I}-\overline{\mathbf{n}}_*\overline{\mathbf{n}}_*^{\mathsf{T}}\big)\overline{\mathbf{g}}(\overline{\boldsymbol{\omega}},\overline{\boldsymbol{\eta}}) - \overline{\mathbf{g}}(\overline{\boldsymbol{\omega}},\overline{\boldsymbol{\eta}})\right] \\ =&\Big(-\left[(\boldsymbol{\omega}-\overline{\boldsymbol{\omega}})^{\mathsf{T}}\mathbf{n}_*\right]\left[\mathbf{n}_*^{\mathsf{T}}\mathbf{g}(\boldsymbol{\omega},\boldsymbol{\eta})\right]\Big) \ominus \Big(-\left[(\boldsymbol{\omega}-\overline{\boldsymbol{\omega}})^{\mathsf{T}}\overline{\mathbf{n}}_*\right]\left[\overline{\mathbf{n}}_*^{\mathsf{T}}\overline{\mathbf{g}}(\overline{\boldsymbol{\omega}},\overline{\boldsymbol{\eta}})\right]\Big) \leq 0,\end{aligned}$$

given that $(\boldsymbol{\omega}-\overline{\boldsymbol{\omega}})^{\mathsf{T}}\mathbf{n}_* \geq 0$ and $(\boldsymbol{\omega}-\overline{\boldsymbol{\omega}})^{\mathsf{T}}\overline{\mathbf{n}}_* \leq 0$. ■

Proposition 5.5. *The inequality $S = \big(\widetilde{\boldsymbol{\omega}}+\widetilde{\boldsymbol{\eta}}\big)^{\mathsf{T}}\mathbf{h}(\boldsymbol{\omega},\boldsymbol{\eta},\overline{\boldsymbol{\omega}},\overline{\boldsymbol{\eta}}) \geq 0$ holds for all pairs of $(\boldsymbol{\omega},\boldsymbol{\eta})$ and $(\overline{\boldsymbol{\omega}},\overline{\boldsymbol{\eta}})$.*

Proof. The proof is by enumeration and is omitted. ■

Together, Proposition 5.4 and Proposition 5.5 bound $\dot{V}_{ad}$ by

$$\dot{V}_{ad} \leq -\begin{bmatrix}\widetilde{\boldsymbol{\omega}}\\ \widetilde{\boldsymbol{\eta}}\end{bmatrix}^{\mathsf{T}}\begin{bmatrix}(\epsilon+\kappa)\mathbf{I} & \kappa\mathbf{I}\\ \kappa\mathbf{I} & \kappa\mathbf{I}\end{bmatrix}\begin{bmatrix}\widetilde{\boldsymbol{\omega}}\\ \widetilde{\boldsymbol{\eta}}\end{bmatrix} + \begin{bmatrix}\widetilde{\boldsymbol{\omega}}\\ \widetilde{\boldsymbol{\eta}}\end{bmatrix}^{\mathsf{T}}\begin{bmatrix}\mathbf{f}\\ \mathbf{0}\end{bmatrix}, \tag{5.37}$$

thus (5.29) is output strictly passive with the input $(\mathbf{f}^{\mathsf{T}},\mathbf{0}^{\mathsf{T}})^{\mathsf{T}}$ and the output $(\widetilde{\boldsymbol{\omega}}^{\mathsf{T}},\widetilde{\boldsymbol{\eta}}^{\mathsf{T}})^{\mathsf{T}}$.

Moreover, the following lemma proves that (5.29) is exponentially convergent, unlike the algorithms in [140, 141] which are asymptotically convergent.

Lemma 5.6. *With no input, i.e.,* $\mathbf{f} = \mathbf{0}$*, the state* $\boldsymbol{\omega}$ *of the dynamical system* (5.29) *converges exponentially to the minimizer* $\boldsymbol{\omega}^*$ *of the problem* (5.26)*.*

Proof. The definition of V_{ad} (5.36) implies that

$$V_{ad} \leq \min\left(\frac{k_\omega}{2}, \frac{k_\eta}{2\lambda_L}\right) \cdot \left(\widetilde{\boldsymbol{\omega}}^\mathsf{T}\widetilde{\boldsymbol{\omega}} + \widetilde{\boldsymbol{\eta}}^\mathsf{T}\widetilde{\boldsymbol{\eta}}\right)$$

where λ_L is the second smallest eigenvalue of $\mathbf{L}$. From (5.37), when $\mathbf{f} = \mathbf{0}$, $\dot{V}_{ad}$ can be further upper-bounded by

$$\dot{V}_{ad} \leq -\frac{2\kappa + \epsilon - \sqrt{4\kappa^2 + \epsilon^2}}{2}\left(\widetilde{\boldsymbol{\omega}}^\mathsf{T}\widetilde{\boldsymbol{\omega}} + \widetilde{\boldsymbol{\eta}}^\mathsf{T}\widetilde{\boldsymbol{\eta}}\right).$$

Together, the two inequalities above lead to $\dot{V}_{ad} \leq -\rho V_{ad}$ and further to $V_{ad}(t) \leq \exp(-\rho t) \cdot V_{ad}(0)$ by Grönwall's inequality, where the rate of decay is

$$\rho = \frac{2\kappa + \epsilon - \sqrt{4\kappa^2 + \epsilon^2}}{2} \max\left(\frac{2}{k_\omega}, \frac{2\lambda_L}{k_\eta}\right).$$

Because $V_{ad} \geq k_\omega \widetilde{\boldsymbol{\omega}}^\mathsf{T}\widetilde{\boldsymbol{\omega}}/2$, it follows that $\widetilde{\boldsymbol{\omega}}$ reduces to zero, and hence the state variable $\boldsymbol{\omega}$ of (5.29) converges exponentially to the minimizer $\boldsymbol{\omega}^*$ of (5.26). ■

5.3 Passive Feedback Interconnection

This section interconnects the WTA algorithm (5.30) in feedback with the physical robots (5.1)-(5.2), and designs the dynamic gains $\mathbf{K}_{ri}(t)$ in (5.5) and the reserved inputs f_i in (5.30) to make the closed-loop teleoperator passive. The gains $\mathbf{K}_{ri}(t)$ regulate the connections of the remote robot network (5.2) to the local robots (5.1) and the damping injected into the leaders of (5.2) based on the authority factors dispatched by the algorithm. The inputs f_i adapt the evolution rate of the algorithm in search for the minimizer of (5.26) based on the states of robots.

Recall that the equilibrium $\boldsymbol{\omega}^*$ of the authority dispatch dynamics (5.29) varies with the set $\mathcal{S}_w$ of winners. For a remote robot network teleoperated by N_l users, the dynamics (5.29) have $P = 2^{N_l} - 1$ different attractors $\mathcal{A}^*_{\boldsymbol{\omega}} = \{\boldsymbol{\omega}^*_{\mathcal{P}_1}, \cdots, \boldsymbol{\omega}^*_{\mathcal{P}_P}\}$, where $\mathcal{P}_p$ with $p = 1, \cdots, P$ indexes all equilibria of (5.29). For example, if $N_l = 3$, there are:

$P = 7$ possible S_w-s - $\mathcal{S}_w^{\mathcal{P}_1} = \{1\}$, $\mathcal{S}_w^{\mathcal{P}_2} = \{2\}$, $\mathcal{S}_w^{\mathcal{P}_3} = \{3\}$, $\mathcal{S}_w^{\mathcal{P}_4} = \{1,2\}$, $\mathcal{S}_w^{\mathcal{P}_5} = \{1,3\}$, $\mathcal{S}_w^{\mathcal{P}_5} = \{2,3\}$ and $\mathcal{S}_w^{\mathcal{P}_7} = \{1,2,3\}$; and $P = 7$ corresponding equilibria - $\boldsymbol{\omega}^*_{\mathcal{P}_1} = \left(1,0,0,\mathbf{0}^\mathsf{T}\right)^\mathsf{T}$, $\boldsymbol{\omega}^*_{\mathcal{P}_2} = \left(0,1,0,\mathbf{0}^\mathsf{T}\right)^\mathsf{T}$, $\boldsymbol{\omega}^*_{\mathcal{P}_3} = \left(0,0,1,\mathbf{0}^\mathsf{T}\right)^\mathsf{T}$, $\boldsymbol{\omega}^*_{\mathcal{P}_4} = \left(1/2,1/2,0,\mathbf{0}^\mathsf{T}\right)^\mathsf{T}$, $\boldsymbol{\omega}^*_{\mathcal{P}_5} = \left(1/2,0,1/2,\mathbf{0}^\mathsf{T}\right)^\mathsf{T}$, $\boldsymbol{\omega}^*_{\mathcal{P}_6} = \left(0,1/2,1/2,\mathbf{0}^\mathsf{T}\right)^\mathsf{T}$, and $\boldsymbol{\omega}^*_{\mathcal{P}_7} = \left(1/3,1/3,1/3,\mathbf{0}^\mathsf{T}\right)^\mathsf{T}$, with $\mathbf{0}$ an $(N_r - N_l)$-dimensional vector.

Given the one-to-one correspondence between $\boldsymbol{\omega}^*_{\mathcal{P}_p}$ and $\mathcal{S}_w^{\mathcal{P}_p}$, the teleoperator with online WTA authority dispatch has P associated behaviours: each vector $\boldsymbol{\omega}^*_{\mathcal{P}_p}$ of distributed authority factors drives the network of the remote robots to the convex hull spanned by the winning local robots $\mathcal{S}_w^{\mathcal{P}_p}$, see Figure 5.2. Then, the teleoperator with dynamic authority dispatch is a switched system with time-dependent switching events. As in Section 5.2.2, t_k with $k = 0,1,2,\cdots$ and $t_0 = 0$ is the sequence of switching times caused by the changes in the set $\mathcal{S}_w(t)$ of winners. Namely, $\mathcal{S}_w(t)$ is invariant during every time interval $t \in [t_k, t_{k+1})$ and changes at every switching instant t_k. The switching signal of the teleoperator is a piecewise constant function of time $\sigma : [0,+\infty) \mapsto \mathcal{P} = \{\mathcal{P}_1,\cdots,\mathcal{P}_P\}$. Correspondingly, the mode of the closed-loop teleoperator with $\mathcal{S}_w(t) = \mathcal{S}_w^{\mathcal{P}_p}$ is the $\mathcal{P}_p$-subsystem. Without loss of generality, the following analysis takes the switching signal and the set of winners as $\sigma(t) = \mathcal{P}_h$ and $\mathcal{S}_w(t) = \mathcal{S}_w^{\mathcal{P}_h}$ with $h \in \{1,\cdots,P\}$ during $t \in [t_k, t_{k+1})$ with $k \in \{0,1,2,\cdots\}$. Thus, the $\mathcal{P}_h$-subsystem is active, and all $\mathcal{P}_l$-subsystems with $l \neq h$ are inactive. The definition of passivity below, adapted from [184], helps investigate the system.

Definition 5.1. *The multi-robot teleoperator* (5.1)-(5.2) *with online WTA authority dispatch* (5.29) *and switching signals $\sigma(t)$, $t \geq 0$, is passive with respect to the power ports $(\mathbf{f}_{hi}, \dot{\mathbf{x}}_{li})$, $i = 1,\cdots,N_l$, if there exist positive definite continuous storage functions $V_{\mathcal{P}_p}$, $p = 1,\cdots,P$, and locally integrable cross-supply rates $S^{\mathcal{P}_h}_{\mathcal{P}_l}(t)$ with $\sigma(t) = h$ and $l \neq h$ during $[t_k, t_{k+1})$, $k = 0,1,2,\cdots$, such that*

$$V_{\mathcal{P}_h}(t) - V_{\mathcal{P}_h}(s) + \sum_{i=1}^{N_l} \int_s^t \delta \dot{\mathbf{x}}_{li}^\mathsf{T}(\tau) \dot{\mathbf{x}}_{li}(\tau) d\tau$$
$$+ \sum_{i=1}^{N_r} \int_s^t \delta \dot{\mathbf{x}}_{ri}^\mathsf{T}(\tau) \dot{\mathbf{x}}_{ri}(\tau) d\tau \leq \sum_{i=1}^{N_l} \int_s^t \omega^*_{i,\mathcal{P}_h} \mathbf{f}_{hi}^\mathsf{T}(\tau) \dot{\mathbf{x}}_{li}(\tau) d\tau$$

for some $\delta \geq 0$ with $\omega^*_{i,\mathcal{P}_h}$ the i-th element of $\boldsymbol{\omega}^*_{\mathcal{P}_h}$, and

$$V_{\mathcal{P}_l}(t) - V_{\mathcal{P}_l}(s) \leq \int_s^t S^{\mathcal{P}_h}_{\mathcal{P}_l}(\tau) d\tau$$

with $S_{\mathcal{P}_l}^{\mathcal{P}_h} \in \mathcal{L}_1$*, where* $t_k \leq s \leq t < t_{k+1}$*. Further, the teleoperator is output strictly passive if* $\delta > 0$*.*

Let $\mathbf{x}_l = \left(\mathbf{x}_{l1}^{\mathsf{T}}, \cdots, \mathbf{x}_{lN_l}^{\mathsf{T}}\right)^{\mathsf{T}}$ and $\mathbf{x}_r = \left(\mathbf{x}_{r1}^{\mathsf{T}}, \cdots, \mathbf{x}_{rN_r}^{\mathsf{T}}\right)^{\mathsf{T}}$ collect the local (5.1) and remote (5.2) robot dynamics into

$$\mathbf{M}_l(\mathbf{x}_l)\ddot{\mathbf{x}}_l + \mathbf{C}_l(\mathbf{x}_l, \dot{\mathbf{x}}_l)\dot{\mathbf{x}}_l = \mathbf{f}_l + \mathbf{f}_h, \tag{5.38a}$$

$$\mathbf{M}_r(\mathbf{x}_r)\ddot{\mathbf{x}}_r + \mathbf{C}_r(\mathbf{x}_r, \dot{\mathbf{x}}_r)\dot{\mathbf{x}}_r = \mathbf{f}_r, \tag{5.38b}$$

where $\mathbf{M}_*(\mathbf{x}_*) = \mathrm{Diag}\{\mathbf{M}_{*i}(\mathbf{x}_{*i})\}$ and $\mathbf{C}_*(\mathbf{x}_*, \dot{\mathbf{x}}_*) = \mathrm{Diag}\{\mathbf{C}_{*i}(\mathbf{x}_{*i}, \dot{\mathbf{x}}_{*i})\}$ are block diagonal matrices with $* = l, r$, and $\mathbf{f}_h = \left(\mathbf{f}_{h1}^{\mathsf{T}}, \cdots, \mathbf{f}_{hN_l}^{\mathsf{T}}\right)^{\mathsf{T}}$. The control inputs are

$$\mathbf{f}_l = P_{lr}(\mathbb{I}\mathbf{x}_r - \mathbf{x}_l) - D_l\dot{\mathbf{x}}_l, \tag{5.39a}$$

$$\mathbf{f}_r = P_{lr}\mathbf{\Omega}\mathbb{I}^{\mathsf{T}}(\mathbf{x}_l - \mathbb{I}\mathbf{x}_r) - \left(\mathbf{L}_p \otimes \mathbf{I}_n\right)\mathbf{x}_r - D_r\dot{\mathbf{x}}_r - \mathbb{I}^{\mathsf{T}}\mathbf{K}_r(t)\mathbb{I} \cdot \mathrm{Sign}(\dot{\mathbf{x}}_r), \tag{5.39b}$$

where $\mathbb{I} = \left[\mathbf{I}_{N_l}\ \mathbf{0}_{N_l \times (N_r - N_l)}\right] \otimes \mathbf{I}_n$, $\mathbf{\Omega} = \mathrm{diag}\{\boldsymbol{\omega}\} \otimes \mathbf{I}_n$, $\mathbf{K}_r(t) = \mathrm{Diag}\{\mathbf{K}_{ri}(t)\}$, and $\mathbf{L}_p$ is a weighted Laplacian matrix whose (i,j)-th element is $l_{ij}^p = 0$ if $j \neq i$ and $j \notin \mathcal{N}_i$, $l_{ij}^p = -P_{ij}$ if $j \neq i$ and $j \in \mathcal{N}_i$, and $l_{ij}^p = -\sum_{k \neq i} l_{ik}^p$ if $j = i$.

As the equilibrium $\boldsymbol{\omega}^*$ of the WTA authority dispatch algorithm (5.29) changes with $\mathcal{S}_w$, and a unique pair $(\overline{\boldsymbol{\omega}}_{\mathcal{P}_p} = \boldsymbol{\omega}_{\mathcal{P}_p}^*, \overline{\boldsymbol{\eta}}_{\mathcal{P}_p})$ corresponds to each $\mathcal{P}_p$-subsystem, the storage function

$$V_{\mathcal{P}_p} = V_{ad}^{\mathcal{P}_p} + V_l^{\mathcal{P}_p} + V_r + V_{lr}^{\mathcal{P}_p} + V_{rr}, \tag{5.40}$$

which serves to investigate the energy behaviour of each $\mathcal{P}_p$-subsystem, $p = 1, \cdots, P$, is defined as follows:

$$V_{ad}^{\mathcal{P}_p} = \frac{k_\omega}{2}\widetilde{\boldsymbol{\omega}}_{\mathcal{P}_p}^{\mathsf{T}}\widetilde{\boldsymbol{\omega}}_{\mathcal{P}_p} + \frac{k_\eta}{2}\widetilde{\boldsymbol{\eta}}_{\mathcal{P}_p}^{\mathsf{T}}\mathbf{L}^{\dagger}\widetilde{\boldsymbol{\eta}}_{\mathcal{P}_p}$$

is the energy V_{ad} in (5.36) of the WTA authority dispatch network (5.29) for the $\mathcal{P}_p$-subsystem with the set of winners $\mathcal{S}_w = \mathcal{S}_w^{\mathcal{P}_p}$;

$$V_l^{\mathcal{P}_p} = \frac{1}{2}\dot{\mathbf{x}}_l^{\mathsf{T}}\left(\mathbb{I}\mathbf{\Omega}_{\mathcal{P}_p}^{*\frac{1}{2}}\mathbb{I}^{\mathsf{T}}\right)\mathbf{M}_l(\mathbf{x}_l)\left(\mathbb{I}\mathbf{\Omega}_{\mathcal{P}_p}^{*\frac{1}{2}}\mathbb{I}^{\mathsf{T}}\right)\dot{\mathbf{x}}_l$$

is the kinetic energy of the winning local robots (5.38a), with $\mathbf{\Omega}_{\mathcal{P}_p}^{*\frac{1}{2}}$ the component-wise

square root of $\boldsymbol{\Omega}^*_{\mathcal{P}_p} = \text{diag}\{\boldsymbol{\omega}^*_{\mathcal{P}_p}\} \otimes \mathbf{I}_n$;

$$V_r = \frac{1}{2}\dot{\mathbf{x}}_r^\mathsf{T}\mathbf{M}_r(\mathbf{x}_r)\dot{\mathbf{x}}_r,$$

is the kinetic energy of all remote robots (5.38b);

$$V_{lr}^{\mathcal{P}_p} = \frac{P_{lr}}{2}\big(\mathbf{x}_l - \mathbb{I}\mathbf{x}_r\big)^\mathsf{T}\mathbb{I}\boldsymbol{\Omega}^*_{\mathcal{P}_p}\mathbb{I}^\mathsf{T}\big(\mathbf{x}_l - \mathbb{I}\mathbf{x}_r\big),$$

is the potential energy of the connections of all winning local robots to their associated leader remote robots; and

$$V_{rr} = \frac{1}{2}\mathbf{x}_r^\mathsf{T}\big(\mathbf{L}_p \otimes \mathbf{I}_n\big)\mathbf{x}_r.$$

is the potential energy of all inter-remote robot connections.

Along the dynamics (5.38a) and (5.39a), $V_l^{\mathcal{P}_p}$ and V_r vary with

$$\begin{aligned}
\dot{V}_l^{\mathcal{P}_p} =& \dot{\mathbf{x}}_l^\mathsf{T}\big(\mathbb{I}\boldsymbol{\Omega}^*_{\mathcal{P}_p}\mathbb{I}^\mathsf{T}\big)\big[P_{lr}(\mathbb{I}\mathbf{x}_r - \mathbf{x}_l) - D_l\dot{\mathbf{x}}_l + \mathbf{f}_h\big],\\
\dot{V}_r =& P_{lr}\dot{\mathbf{x}}_r^\mathsf{T}\boldsymbol{\Omega}\mathbb{I}^\mathsf{T}(\mathbf{x}_l - \mathbb{I}\mathbf{x}_r) - \dot{\mathbf{x}}_r^\mathsf{T}\big(\mathbf{L}_p \otimes \mathbf{I}_n\big)\mathbf{x}_r - D_r\dot{\mathbf{x}}_r^\mathsf{T}\dot{\mathbf{x}}_r - \dot{\mathbf{x}}_r^\mathsf{T}\mathbb{I}^\mathsf{T}\mathbf{K}_r(t)\mathbb{I}\cdot\text{Sign}(\dot{\mathbf{x}}_r).
\end{aligned}$$

Further, $\mathbb{I}^\mathsf{T}\mathbb{I} = \text{Diag}\{\mathbf{I}_{N_l}, \mathbf{0}_{(N_r-N_l)\times(N_r-N_l)}\} \otimes \mathbf{I}_n$ and $\boldsymbol{\Omega}^*_{\mathcal{P}_p} = \text{diag}\{\boldsymbol{\omega}^*_{\mathcal{P}_p}\} \otimes \mathbf{I}_n$ with the i-th entry of $\boldsymbol{\omega}^*_{\mathcal{P}_p}$ being $\omega^*_{i,\mathcal{P}_p} = 0$ for $i = N_l+1, \cdots, N_r$, lead to $\mathbb{I}^\mathsf{T}\mathbb{I}\boldsymbol{\Omega}^*_{\mathcal{P}_p} = \boldsymbol{\Omega}^*_{\mathcal{P}_p}$ and to

$$\dot{V}_{lr}^{\mathcal{P}_p} = -P_{lr}\dot{\mathbf{x}}_l^\mathsf{T}\mathbb{I}\boldsymbol{\Omega}^*_{\mathcal{P}_p}\mathbb{I}^\mathsf{T}(\mathbb{I}\mathbf{x}_r - \mathbf{x}_l) - P_{lr}\dot{\mathbf{x}}_r^\mathsf{T}\boldsymbol{\Omega}^*_{\mathcal{P}_p}\mathbb{I}^\mathsf{T}(\mathbf{x}_l - \mathbb{I}\mathbf{x}_r).$$

After summing $\dot{V}_{ad}^{\mathcal{P}_p}$, $\dot{V}_l^{\mathcal{P}_p}$, $\dot{V}_r$, $\dot{V}_{lr}^{\mathcal{P}_p}$ and

$$\dot{V}_{rr} = \dot{\mathbf{x}}_r^\mathsf{T}\big(\mathbf{L}_p \otimes \mathbf{I}_n\big)\mathbf{x}_r$$

the power balance of the $\mathcal{P}_p$-subsystem becomes

$$\begin{aligned}
\dot{V}_{\mathcal{P}_p} \leq& \dot{V}_{ad}^{\mathcal{P}_p} + \dot{\mathbf{x}}_l^\mathsf{T}\big(\mathbb{I}\boldsymbol{\Omega}^*_{\mathcal{P}_p}\mathbb{I}^\mathsf{T}\big)\mathbf{f}_h + P_{lr}\dot{\mathbf{x}}_r^\mathsf{T}\big(\boldsymbol{\Omega} - \boldsymbol{\Omega}^*_{\mathcal{P}_p}\big)\mathbb{I}^\mathsf{T}(\mathbf{x}_l - \mathbb{I}\mathbf{x}_r)\\
&- D_l\dot{\mathbf{x}}_l^\mathsf{T}\big(\mathbb{I}\boldsymbol{\Omega}^*_{\mathcal{P}_p}\mathbb{I}^\mathsf{T}\big)\dot{\mathbf{x}}_l - D_r\dot{\mathbf{x}}_r^\mathsf{T}\dot{\mathbf{x}}_r - \dot{\mathbf{x}}_r^\mathsf{T}\mathbb{I}^\mathsf{T}\mathbf{K}_r(t)\mathbb{I}\cdot\text{Sign}(\dot{\mathbf{x}}_r),
\end{aligned} \tag{5.41}$$

where $-\dot{\mathbf{x}}_r^\mathsf{T}\big(\mathbf{L}_p \otimes \mathbf{I}_n\big)\mathbf{x}_r + \dot{\mathbf{x}}_r^\mathsf{T}\big(\mathbf{L}_p \otimes \mathbf{I}_n\big)\mathbf{x}_r = 0$ results from the power-preserving interconnections between the remote robots.

By Definition 5.1, passive teleoperation constrains how the energies of the active $\mathcal{P}_h$-subsystem and all inactive $\mathcal{P}_l$-subsystems evolve during each time inter-

val $[t_k, t_{k+1})$. Therefore, the increases in their energies must be examined next.

For the active $\mathcal{P}_h$-subsystem, the sign-indefinite term $\Delta = P_{lr}\dot{\mathbf{x}}_r^{\mathsf{T}}\big(\mathbf{\Omega} - \mathbf{\Omega}^*_{\mathcal{P}_h}\big)\mathbb{I}^{\mathsf{T}}(\mathbf{x}_l - \mathbb{I}\mathbf{x}_r) = P_{lr}\sum_{i=1}^{N_l}\widetilde{\omega}_{i,\mathcal{P}_h}\dot{\mathbf{x}}_{ri}^{\mathsf{T}}(\mathbf{x}_{li} - \mathbf{x}_{ri})$ in the power balance inequality (5.41) indicates that $\widetilde{\boldsymbol{\omega}}_{\mathcal{P}_h}$, which arises from the transient phase of the authority dispatch dynamics (5.29), compromises the conservation of power in the couplings between the local and leader remote robots. Opportunely, by (5.37), the energy $V_{ad}^{\mathcal{P}_h}$ of the WTA authority dispatch network of the active $\mathcal{P}_h$-subsystem changes according to

$$\dot{V}_{ad}^{\mathcal{P}_h} \leq -\kappa\widetilde{\boldsymbol{\omega}}_{\mathcal{P}_h}^{\mathsf{T}}\widetilde{\boldsymbol{\omega}}_{\mathcal{P}_h} + \widetilde{\boldsymbol{\omega}}_{\mathcal{P}_h}^{\mathsf{T}}\mathbf{f},$$

where $\mathbf{f} = (f_1, \cdots, f_{N_r})^{\mathsf{T}}$ is reserved to couple the WTA algorithm to the underlying robot dynamics. Let f_i be

$$f_i = \begin{cases} P_{lr}\dot{\mathbf{x}}_{ri}^{\mathsf{T}}(\mathbf{x}_{ri} - \mathbf{x}_{li}) & \text{for } i = 1, \cdots, N_l, \\ 0 & \text{for } i = N_l + 1, \cdots, N_r. \end{cases} \tag{5.42}$$

Because $-\dot{\mathbf{x}}_r^{\mathsf{T}}\mathbb{I}^{\mathsf{T}}\mathbf{K}_r(t)\mathbb{I}\cdot\mathrm{Sign}(\dot{\mathbf{x}}_r) \leq 0$, the time integration of $\dot{V}_{\mathcal{P}_p}$ in (5.41) for $p = h$ from s to t leads to

$$\begin{aligned} &V_{\mathcal{P}_h}(t) - V_{\mathcal{P}_h}(s) + \sum_{i=1}^{N_l}\int_s^t \omega^*_{i,\mathcal{P}_h} D_l\dot{\mathbf{x}}_{li}^{\mathsf{T}}(\tau)\dot{\mathbf{x}}_{li}(\tau)d\tau + \sum_{i=1}^{N_r}\int_s^t D_r\dot{\mathbf{x}}_{ri}^{\mathsf{T}}(\tau)\dot{\mathbf{x}}_{ri}(\tau)d\tau \\ \leq &\sum_{i=1}^{N_l}\int_s^t \omega^*_{i,\mathcal{P}_h}\dot{\mathbf{x}}_{li}^{\mathsf{T}}(\tau)\mathbf{f}_{hi}(\tau)d\tau - \sum_{i=1}^{N_l}\int_s^t \kappa\widetilde{\omega}^2_{i,\mathcal{P}_h}(\tau)d\tau, \end{aligned} \tag{5.43}$$

where $\widetilde{\omega}_{i,\mathcal{P}_h}$ is the i-th component of $\widetilde{\boldsymbol{\omega}}_{\mathcal{P}_h}$ for $i = 1, \cdots, N_l$.

The energy balance inequality (5.43) shows that $\mathbf{f}$ designed in (5.42) shapes the energy behaviour of the active $\mathcal{P}_h$-subsystem to meet the first condition of passive teleoperation in Definition 5.1. Algebraically, $\mathbf{f}$ cancels the sign-indefinite term Δ in (5.41). From a control standpoint, $\mathbf{f}$ connects the output of the robot dynamics (5.1)-(5.2) to the input of the WTA authority dispatch algorithm (5.29). As a result, the WTA dynamics can extract the sign-indefinite energy Δ from the physical robots and dissipate it by appropriately adapting its evolution. In addition, the excess of passivity due to $\widetilde{\omega}_{i,\mathcal{P}_h}$, $\dot{\mathbf{x}}_{li}$ and $\dot{\mathbf{x}}_{ri}$ in (5.43) is key in the upcoming steady-state performance analysis of the teleoperation system.

For every inactive $\mathcal{P}_l$-subsystem, the energy $V_{ad}^{\mathcal{P}_l}$ of the WTA authority dispatch

network is bounded by

$$V_{ad}^{\mathcal{P}_l} = \frac{k_\omega}{2}\big(\widetilde{\boldsymbol{\omega}}_{\mathcal{P}_h} + \widetilde{\boldsymbol{\omega}}_{hl}\big)^{\mathsf{T}}\big(\widetilde{\boldsymbol{\omega}}_{\mathcal{P}_h} + \widetilde{\boldsymbol{\omega}}_{hl}\big) + \frac{k_\eta}{2}\big(\widetilde{\boldsymbol{\eta}}_{\mathcal{P}_h} + \widetilde{\boldsymbol{\eta}}_{hl}\big)^{\mathsf{T}}\mathbf{L}^{\dagger}\big(\widetilde{\boldsymbol{\eta}}_{\mathcal{P}_h} + \widetilde{\boldsymbol{\eta}}_{hl}\big) < +\infty$$

because $\widetilde{\boldsymbol{\omega}}_{\mathcal{P}_h}$, $\widetilde{\boldsymbol{\eta}}_{\mathcal{P}_h}$, $\widetilde{\boldsymbol{\omega}}_{hl} = \boldsymbol{\omega}^*_{\mathcal{P}_h} - \boldsymbol{\omega}^*_{\mathcal{P}_l}$ and $\widetilde{\boldsymbol{\eta}}_{hl} = \overline{\boldsymbol{\eta}}_{\mathcal{P}_h} - \overline{\boldsymbol{\eta}}_{\mathcal{P}_l}$ all are bounded by the analysis in Section 5.2.2. It follows from $0 \leq \omega_i \leq 1$ and $\omega^*_{i,\mathcal{P}_l} \in \{0, 1/|\mathcal{S}_w|, 1\}$ that

$$\dot{\mathbf{x}}_r^{\mathsf{T}}\widetilde{\boldsymbol{\Omega}}_{\mathcal{P}_l}\mathbb{I}^{\mathsf{T}}(\mathbf{x}_l - \mathbb{I}\mathbf{x}_r) = \sum_{i=1}^{N_l}\max(\omega_i, 1-\omega_i)|\dot{\mathbf{x}}_{ri}|^{\mathsf{T}}|\mathbf{x}_{li} - \mathbf{x}_{ri}|,$$

where $\widetilde{\boldsymbol{\Omega}}_{\mathcal{P}_l} = \boldsymbol{\Omega} - \boldsymbol{\Omega}^*_{\mathcal{P}_l}$. Hence, letting the control $\mathbf{f}_{ri}$ of every leader remote robot $i = 1, \cdots, N_l$ adapt with

$$\mathbf{K}_{ri}(t) = P_{lr} \cdot \max(\omega_i, 1-\omega_i) \cdot \mathrm{diag}\{|\mathbf{x}_{li} - \mathbf{x}_{ri}|\} \tag{5.44}$$

constrains the energy increase of the inactive $\mathcal{P}_l$-subsystem according to

$$\begin{aligned} &V_{\mathcal{P}_l}(t) - V_{\mathcal{P}_l}(s) + D_l\sum_{i=1}^{N_l}\omega^*_{i,\mathcal{P}_l}\int_s^t \dot{\mathbf{x}}_{li}^{\mathsf{T}}(\tau)\dot{\mathbf{x}}_{li}(\tau)d\tau + D_r\sum_{i=1}^{N_r}\int_s^t \dot{\mathbf{x}}_{ri}^{\mathsf{T}}(\tau)\dot{\mathbf{x}}_{ri}(\tau)d\tau \\ \leq &V_{ad}^{\mathcal{P}_l}(t) - V_{ad}^{\mathcal{P}_l}(s) + \sum_{i=1}^{N_l}\omega^*_{i,\mathcal{P}_l}\int_s^t \dot{\mathbf{x}}_{li}^{\mathsf{T}}(\tau)\mathbf{f}_{hi}(\tau)d\tau. \end{aligned} \tag{5.45}$$

Assumption 5.1 together with bounded $V_{as}^{\mathcal{P}_l}$ ultimately ensure that the energy balance inequality (5.45) of every inactive $\mathcal{P}_l$-subsystem complies with the second condition of passive teleoperation in Definition 5.1.

For a switched system: the energies $V_{\mathcal{P}_p}$ of all its $\mathcal{P}_p$-subsystems are functions of the same system state variables; the energy behaviours of all subsystems, both active and inactive, contribute to the energy behaviour of the system; and the active $\mathcal{P}_h$-subsystem can inject energy into the inactive $\mathcal{P}_l$-subsystem, as characterized by the cross-supply rate $S^{\mathcal{P}_h}_{\mathcal{P}_l}$ in Definition 5.1. Therefore, limiting only the energy growth of the active subsystem by the winners-injected energy as in (5.43) is insufficient for passive teleoperation with dynamic WTA authority dispatch. Additional damping must be injected into the leader remote robots via (5.44) to constrain the energy stored by every inactive $\mathcal{P}_l$-subsystem by (5.45).

The design (5.42) of f_i together with the adaptation of $\mathbf{K}_{ri}(t)$ (5.44) connect the physical robots (5.1)-(5.2) in feedback with the WAT algorithm (5.30) to make the

teleoperator passive with performance guaranteed in the following theorem.

Theorem 5.2. *Let a teleoperator with N_l local robots* (5.1) *and a tree network of N_r remote robots* (5.2) *apply force feedback to users, coordinate the remote robots and enable teleoperation via the controllers* (5.3), (5.4) *and* (5.5), *respectively.*

Design a bidding mechanism B1-B2 for users to send requests to the remote robots, and associate the authority factors ω_i and the auxiliary variables η_i that start with $\omega_i(0) \in [0,1]$ and $\eta_i(0) = 0$ and evolve with (5.30) *to all remote robots.*

Design the inputs f_i to (5.30) *by* (5.42) *and adapt the damping of all leader remote robots by* (5.44). *Then, the teleoperator is passive with the following properties.*

1. *The velocities of all robots are of class $\mathcal{L}_2 \cap \mathcal{L}_\infty$ and approach zero at infinite time, i.e., $\{\dot{\mathbf{x}}_{li}, \dot{\mathbf{x}}_{rj}\} \in \mathcal{L}_2 \cap \mathcal{L}_\infty$ and $\{\dot{\mathbf{x}}_{li}(t), \dot{\mathbf{x}}_{rj}(t)\} \to \mathbf{0}$ as $t \to +\infty$ $\forall i = 1, \cdots, N_l$ and $j = 1, \cdots, N_r$.*

2. *The authority factors distributed to the remote robots fulfill the WTA objectives O1 and O2 if the set of winners $\mathcal{S}_w$ is invariant.*

3. *The network of the remote robots moves towards the convex hull spanned by the winning local robots, i.e., $\mathbf{x}_{rj}(t) \to \mathbf{x}^*_{rj} \in \mathcal{C}_{\mathbf{x}_r}$ as $t \to +\infty$, where*

$$\mathcal{C}_{\mathbf{x}_r} = \left\{ \sum_{i \in \mathcal{S}_w} \lambda_i \mathbf{x}_{li} \,\middle|\, \lambda_i \geq 0 \text{ and } \sum_{i \in \mathcal{S}_w} \lambda_i = 1 \right\}.$$

4. *The force feedback to each winning user $i \in \mathcal{S}_w$ converges to the sum of forces applied by all other winning users $j \in \mathcal{S}_w - \{i\}$, i.e., $\mathbf{f}_{li}(t) \to \sum_{j \in \mathcal{S}_w - \{i\}} \mathbf{f}_{hj}(t)$ as $t \to +\infty$, while the force feedback to all other users $k \notin \mathcal{S}_w$ converges to a scaled approximate average displacement of the winners' local robots from their local robots, i.e., $\mathbf{f}_{lk}(t) \to P_{lr}[\mathbf{x}_{rk}(t) - \mathbf{x}_{lk}(t)] \approx \sum_{i \in \mathcal{S}_w} P_{lr}[\mathbf{x}_{li}(t) - \mathbf{x}_{lk}(t)]/|\mathcal{S}_w|$ as $t \to +\infty$.*

5. *The positions of all robots are synchronized when all user forces vanish, i.e., $\mathbf{x}_{li}(t) - \mathbf{x}_{rj}(t) \to \mathbf{0}$ $\forall i = 1, \cdots, N_l$ and $j = 1, \cdots, N_r$ as $t \to +\infty$ if $\mathbf{f}_{hi}(t) = 0$ $\forall t \geq 0$.*

Proof. By Definition 5.1, the energy balance inequalities of the active $\mathcal{P}_h$-subsystem, (5.43), and every inactive $\mathcal{P}_l$-subsystem (5.45) indicate a passive teleoperator.

1. Each $V_{\mathcal{P}_p}$ in (5.40), $p = 1, \cdots, P$, is bounded by (5.43) and (5.45). Thus, $\dot{\mathbf{x}}_l$ and $\dot{\mathbf{x}}_r$ are of class $\mathcal{L}_\infty$. Further, positive D_l and D_r in (5.43) and (5.45) imply that $\dot{\mathbf{x}}_l$ and $\dot{\mathbf{x}}_r$ are of class $\mathcal{L}_2$. With bounded $\ddot{\mathbf{x}}_l$ and $\ddot{\mathbf{x}}_r$ in (5.38), Barbalats' lemma leads to $\{\dot{\mathbf{x}}_l(t), \dot{\mathbf{x}}_r(t)\} \to \mathbf{0}$ as $t \to +\infty$.

2. Given an invariant set $\mathcal{S}_w$ of winners, the equilibrium $\boldsymbol{\omega}^*$ of (5.29) remains invariant. Because all $V_{\mathcal{P}_p}$ are bounded, all displacements $\mathbf{x}_{ri} - \mathbf{x}_{li}$ of the leader remote robots i from their associated local robots i are bounded. Then, $\dot{\mathbf{x}}_r(t) \to \mathbf{0}$ and (5.42) imply that $\mathbf{f}(t) \to \mathbf{0}$. As in the proof of Lemma 5.6, (5.37) implies that the authority dispatch network (5.29) is exponentially ISS with the input $\mathbf{f}$ and the state $\widetilde{\boldsymbol{\omega}}$. Hence, $\mathbf{f}(t) \to \mathbf{0}$ implies that $\widetilde{\boldsymbol{\omega}}(t) \to \mathbf{0}$ as $t \to +\infty$ and, by Lemma 5.2, that the WTA election objectives O1 and O2 are acheived.

3. Because $\dot{\mathbf{f}}_h$ is bounded, the time derivatives of (5.38) imply that $\dddot{\mathbf{x}}_l$ and $\dddot{\mathbf{x}}_r$ are bounded. The boundedness of $\dddot{\mathbf{x}}_l$ and $\dddot{\mathbf{x}}_r$, together with $\{\dot{\mathbf{x}}_l, \dot{\mathbf{x}}_r\} \to \mathbf{0}$ and Barbalat's lemma, leads to $\{\ddot{\mathbf{x}}_l(t), \ddot{\mathbf{x}}_r(t)\} \to \mathbf{0}$ as $t \to +\infty$ and thus, to $\mathbf{f}_r \to \mathbf{0}$ in (5.38b). Then (5.39b) implies that $P_{lr}\boldsymbol{\Omega}(t)\mathbb{I}^\mathsf{T}\mathbf{x}_l(t) - \big[P_{lr}\boldsymbol{\Omega}(t)\mathbb{I}^\mathsf{T}\mathbb{I} + \big(\mathbf{L}_p \otimes \mathbf{I}_n\big)\big]\mathbf{x}_r(t) \to \mathbf{0}$ as $t \to +\infty$, and, by $\boldsymbol{\omega}(t) \to \boldsymbol{\Omega}^*$, that $P_{lr}\boldsymbol{\Omega}^*\mathbb{I}^\mathsf{T}\mathbf{x}_l(t) - \big[P_{lr}\boldsymbol{\Omega}^*\mathbb{I}^\mathsf{T}\mathbb{I} + \big(\mathbf{L}_p \otimes \mathbf{I}_n\big)\big]\mathbf{x}_r(t) \to \mathbf{0}$. Because $\boldsymbol{\Omega}^* = \mathrm{diag}\{\boldsymbol{\omega}^*\} \otimes \mathbf{I}_n \succeq \mathbf{0}$ is diagonal with $\mathbf{1}^\mathsf{T}\boldsymbol{\Omega}^*\mathbf{1} = 1$ by Lemma 5.2, it and $\mathbf{L}_p \succeq \mathbf{0}$ make $\widehat{\mathbf{L}}_p = P_{lr}\boldsymbol{\Omega}^*\mathbb{I}^\mathsf{T}\mathbb{I} + \big(\mathbf{L}_p \otimes \mathbf{I}_n\big) = P_{lr}\boldsymbol{\Omega}^* + \big(\mathbf{L}_p \otimes \mathbf{I}_n\big)$ a positive definite and nonsingular M-matrix. A simple transformation of the above equation then leads to

$$\lim_{t\to+\infty} \mathbf{x}_r(t) = \lim_{t\to+\infty} P_{lr}\widehat{\mathbf{L}}_p^{-1}\boldsymbol{\Omega}^*\mathbb{I}^\mathsf{T}\mathbf{x}_l(t).$$

Given that $\omega_i^* = 1/|\mathcal{S}_w|$ for $i \in \mathcal{S}_w$ and $\omega_i^* = 0$ for $i \notin \mathcal{S}_w$, defining $\mathbf{x}_{wl}(t)$ by removing all $\mathbf{x}_{li}(t)$ with $i \notin \mathcal{S}_w$ from $\mathbf{x}_l(t)$ converts the above equation into

$$\lim_{t\to+\infty} \mathbf{x}_r(t) = \lim_{t\to+\infty} P_{lr}\widehat{\mathbf{L}}_p^{-1}\boldsymbol{\Omega}_w^*\mathbf{x}_{wl}(t) = \lim_{t\to+\infty} P_{lr}\left[\big(P_{lr}\boldsymbol{\Omega}^* + \mathbf{L}_p \otimes \mathbf{I}_n\big)^{-1}\boldsymbol{\Omega}_w^*\right]\mathbf{x}_{wl}(t),$$

where $\boldsymbol{\Omega}_w^*$ of dimension $N_r n \times |\mathcal{S}_w| n$ is obtained by deleting all columns with only zero elements from $\boldsymbol{\Omega}^*\mathbb{I}^\mathsf{T}$. It remains to prove that every row of the nonnegative matrix $\mathbf{H} = P_{lr}\big(P_{lr}\boldsymbol{\Omega}^* + \mathbf{L}_p \otimes \mathbf{I}_n\big)^{-1}\boldsymbol{\Omega}_w^*$ sums to 1. Post-multiply $\mathbf{H}$ by $\mathbf{1}$,

$$\mathbf{H1} = \frac{P_{lr}}{|\mathcal{S}_w|}\big(P_{lr}\boldsymbol{\Omega}^* + \mathbf{L}_p \otimes \mathbf{I}_n\big)^{-1}\sum_{i\in\mathcal{S}_w}\big(\mathbf{e}_i \otimes \mathbf{1}_n\big),$$

where $\mathbf{e}_i$ is the unit column vector of dimension N_r with the i-th element 1 and all other elements 0. Then, pre-multiply both sides by $\big(P_{lr}\boldsymbol{\Omega}^* + \mathbf{L}_p \otimes \mathbf{I}_n\big)$,

$$\big(P_{lr}\boldsymbol{\Omega}^* + \mathbf{L}_p \otimes \mathbf{I}_n\big)\mathbf{H}\mathbf{1} = \frac{P_{lr}}{|\mathcal{S}_w|}\sum_{i\in\mathcal{S}_w}\big(\mathbf{e}_i \otimes \mathbf{1}_n\big) = \big(P_{lr}\boldsymbol{\Omega}^* + \mathbf{L}_p \otimes \mathbf{I}_n\big)\mathbf{1}$$

after using $\mathbf{L}_p\mathbf{1} = \mathbf{0}$. Because $\big(P_{lr}\boldsymbol{\Omega}^* + \mathbf{L}_p \otimes \mathbf{I}_n\big)$ is full rank, the above equation implies that $\mathbf{H}\mathbf{1} = \mathbf{1}$ and further that the sum of each row of $\mathbf{H}$ equals 1. Hence, every $\mathbf{x}_{rj}(t)$ converges to $\mathcal{C}_{\mathbf{x}_r}$ as $t \to +\infty$.

4. Substitution from (5.39b) in (5.38b), pre-multiplication of (5.38b) by $\big(\mathbf{1} \otimes \mathbf{I}_n\big)^\mathsf{T}$ and $\{\dot{\mathbf{x}}_l, \dot{\mathbf{x}}_r, \ddot{\mathbf{x}}_l, \ddot{\mathbf{x}}_r\} \to \mathbf{0}$ imply

$$\begin{aligned}&\lim_{t\to+\infty} P_{lr}\big(\mathbf{1} \otimes \mathbf{I}_n\big)^\mathsf{T}\boldsymbol{\Omega}(t)\mathbb{I}^\mathsf{T}\big[\mathbf{x}_l(t) - \mathbb{I}\mathbf{x}_r(t)\big] - \lim_{t\to+\infty}\big(\mathbf{1} \otimes \mathbf{I}_n\big)^\mathsf{T}\big(\mathbf{L}_p \otimes \mathbf{I}_n\big)\mathbf{x}_r(t)\\ =&\lim_{t\to+\infty}\sum_{i\in\mathcal{S}_w} P_{lr}\omega_i^*\big[\mathbf{x}_{li}(t) - \mathbf{x}_{ri}(t)\big] = \mathbf{0},\end{aligned}$$

and substitution from (5.39a) in (5.38a) and pre-multiplication of (5.38a) by $\big(\boldsymbol{\omega}^* \otimes \mathbf{I}_n\big)^\mathsf{T}\mathbb{I}^\mathsf{T}$ lead to

$$\begin{aligned}&\lim_{t\to+\infty}\big(\boldsymbol{\omega}^* \otimes \mathbf{I}_n\big)^\mathsf{T}\mathbb{I}^\mathsf{T}\Big(P_{lr}\big[\mathbb{I}\mathbf{x}_r(t) - \mathbf{x}_l(t)\big] + \mathbf{f}_h(t)\Big)\\ =&\lim_{t\to+\infty}\sum_{i\in\mathcal{S}_w} P_{lr}\omega_i^*\big[\mathbf{x}_{ri}(t) - \mathbf{x}_{li}(t)\big] + \omega_i^*\mathbf{f}_{hi}(t) = \mathbf{0}.\end{aligned}$$

Because $\omega_i^* = 1/|\mathcal{S}_w|\ \forall i \in \mathcal{S}_w$, the sum of the two equations above proves that $\sum_{i\in\mathcal{S}_w}\mathbf{f}_{hi}(t) \to \mathbf{0}$, and, by (5.38a), that $\mathbf{f}_{li}(t) + \mathbf{f}_{hi}(t) \to \mathbf{0}\ \forall i = 1, \cdots, N_l$, and further that $\mathbf{f}_{li}(t) \to -\mathbf{f}_{hi}(t) \to \sum_{j\in\mathcal{S}_w-\{i\}}\mathbf{f}_{hj}(t)$ for all winners $i \in \mathcal{S}_w$ as $t \to +\infty$. In contrast, the force feedback $\mathbf{f}_{lk}(t)$ to every other user $k \notin \mathcal{S}_w$ approaches $P_{lr}[\mathbf{x}_{rk}(t) - \mathbf{x}_{lk}(t)]$ because $\dot{\mathbf{x}}_{lk}(t) \to \mathbf{0}$ in (5.39a) as $t \to +\infty$. Since $\mathbf{x}_{rk}(t) \to \mathcal{C}_{\mathbf{x}_r}$ (see item 3), it follows that all non-winning users $k \notin \mathcal{S}_w$ feel approximately a scaled average displacement of the winners' local robots from their remote robots

$$\lim_{t\to+\infty}\mathbf{f}_{lk}(t) \approx \lim_{t\to+\infty}\sum_{i\in\mathcal{S}_w}\frac{P_{lr}}{|\mathcal{S}_w|}\big[\mathbf{x}_{li}(t) - \mathbf{x}_{lk}(t)\big].$$

5. With no user-applied forces $\mathbf{f}_h = \mathbf{0}$, $\{\dot{\mathbf{x}}_l, \dot{\mathbf{x}}_r, \ddot{\mathbf{x}}_l, \ddot{\mathbf{x}}_r\} \to \mathbf{0}$ implies, by (5.38), that

$\mathbf{f}_l(t) \to \mathbf{0}$ and $\mathbf{f}_r(t) \to \mathbf{0}$ as $t \to +\infty$. Then, it can be concluded: from (5.39a) that $\mathbb{I}\mathbf{x}_r(t) - \mathbf{x}_l(t) \to \mathbf{0}$ and hence that $\mathbf{x}_{ri}(t) - \mathbf{x}_{li}(t) \to \mathbf{0}$ $\forall i = 1, \cdots, N_l$; and from (5.39b) that $\big(\mathbf{L}_p \otimes \mathbf{I}_n\big)\mathbf{x}_r(t) \to \mathbf{0}$ and hence that $\mathbf{x}_{ri}(t) - \mathbf{x}_{rj}(t) \to \mathbf{0}$ $\forall i, j = 1, \cdots, N_r$ because the remote robot network is connected. In other words, all robot positions are synchronized, $\mathbf{x}_{li}(t) - \mathbf{x}_{rj}(t) \to \mathbf{0}$ $\forall i = 1, \cdots, N_l$ and $\forall j = 1, \cdots, N_r$ as $t \to +\infty$.

■

Compared to Section 5.2.1, the feedback interconnections (5.42) and (5.44) of the physical robot dynamics (5.1)-(5.2) with the WTA authority dispatch algorithm (5.30) lend themselves to rigorous passivity and performance analysis in this section. Because it uses authority factors to smoothly regulate the local robot-remote robot couplings, instead of sharply turning them on/off, the design herein is compatible with prevailing position-position teleoperation architectures [90]. In the presence of multiple winners, the design permits to explicitly evaluate the steady-state teleoperation performance in terms of containment and force feedback. It guarantees that all winning users contribute to adjusting the spatial distribution of the remote robot network and receive informative force feedback.

5.4 Experimental Results

This section presents the experimental performance[1] of multi-user teleoperation of a P+d controlled multi-robot system without and with the proposed WTA authority dispatch strategy. In the experimental testbed, 4 Geomagic Touch robots are the local robots (L1-L4) and 10 Novint Falcon robots are the leader (R1-R4) and follower (R5-R10) remote robots. All robots are controlled locally and individually, via USB 2.0 by a C++ program running at 1 kHz on dedicated Ubuntu machines. The underlying tree communication network of the remote robot team is implemented using ROS, which supports inter-robot information exchanges, shown as the dark grey lines in Figure 5.4, at about 50 Hz. The 4 human users press buttons on their local robots, and thus submit piecewise constant bids to their associated remote robots, to request authority to teleoperate the remote robot team. The positions of all robot end-effectors are projected into a shared Cartesian space for users to observe their motions in real time throughout the teleoperation.

[1] `https://youtu.be/WOntg14HQjs`

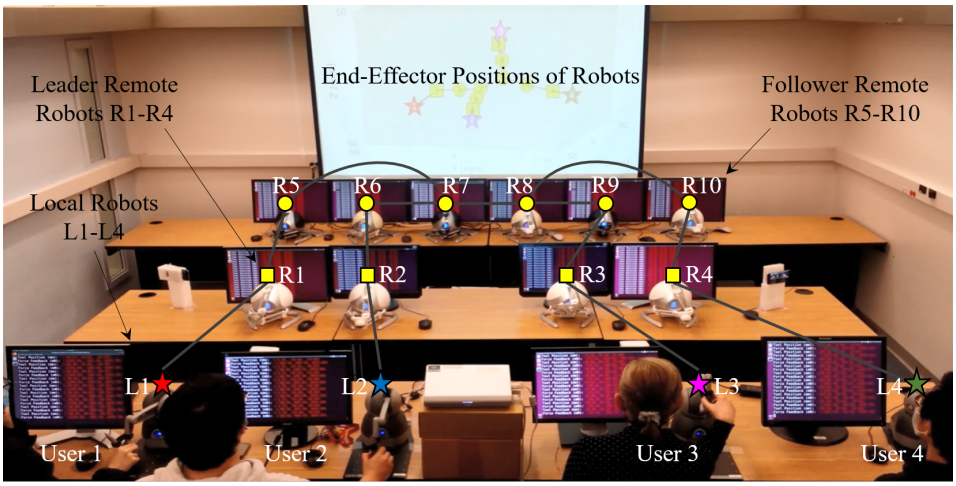

Figure 5.4: The experimental setup for distributed multi-user multi-robot teleoperation with online WTA authority dispatch.

Because of their limited performance, all robots are controlled via virtual 10 g point masses: the local robots are coupled to their respective point masses to tele-drive the group of the remote robots and to feedback forces to their users (upper bounded by 3 N for hardware safety); and the remote robots are unilaterally connected to their virtual masses for stable and precise position synchronization. The experimental P+d control gains are as follows: $P_{lr} = 100$ for the connections between the local and remote leader robots; $P_{ij} = 50$ for the connections between neighbouring remote robots; and $D_l = D_r = 1$ for damping throughout the teleoperator. In addition, the distributed algorithm (5.30) adapts the authority factors of the remote robots by $\epsilon = 0.1$, $\kappa = 200$, $\gamma = 2$ and $k_\omega = k_\eta = 1$ for WTA authority dispatch.

5.4.1 Teleoperation With No Authority Dispatch

In this first experiment, all users initially hold their local robots L1-L4, and then move their robots along closed paths in turn.

Figure 5.5 depicts the positions of all robot end-effectors at two instances while the user 1 moves the local robot L1 along the red path in the direction shown. It illustrates that P+d control maintains the remote robot network R1-R10 in the convex hull spanned by the local robots L1-L4 and thus, enables cooperative teleoperation. This feature becomes detrimental when the user 1 needs to tele-drive the remote robot network independently and the other users are unaware of this need.

Figure 5.6 compares, component-wise, the force feedback $\mathbf{f}_{li}$ to the user i and the

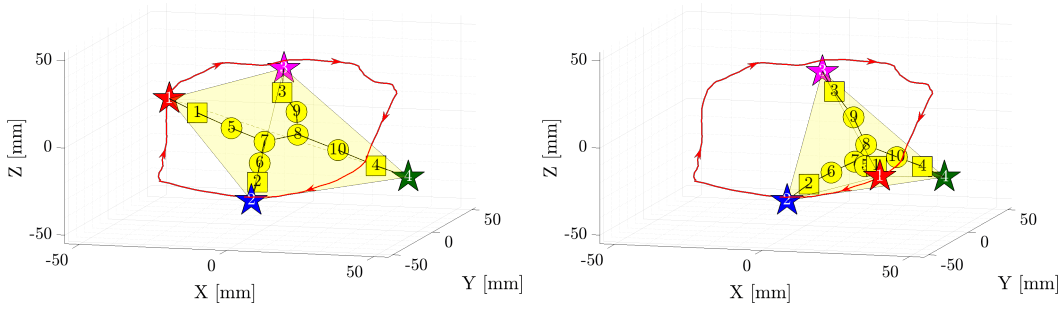

(a) $t = 44$ s. (b) $t = 48$ s.

Figure 5.5: Multi-user multi-robot teleoperation without authority dispatch: The end-effector positions of all robots when the local robot L1 moves along the red path in the direction shown and other local robots are stationary.

sum $\mathbf{f}_{h*} = \sum_{j \neq i} \mathbf{f}_{hj}$ of the forces $\mathbf{f}_{hj}$ of all other users $j \neq i$, from $t = 21$ s to $t = 52$ s. In the subplots, the coloured areas indicate the time periods when the users $4 - 1$ take turns moving their local robots L4-L1, and the two red dots mark the force feedback $\mathbf{f}_{l1}$ to the user 1 at the instances depicted in Figure 5.5. Figure 5.6 shows that P+d control with no authority dispatch can convey to each user the sum of all other user forces. The largest mismatches between $\mathbf{f}_{li}$ and $\mathbf{f}_{h*}$ are mainly caused by the 3 N-bounds imposed on the local robot force outputs. Despite the bounded actuation of their local robots, all users can perceive the tele-driving forces of all other users throughout the experiment.

5.4.2 Teleoperation With WTA Authority Dispatch

In the second experiment, the users change their bids to the remote network and the teleoperator behaviour changes in response to different authority distributions. Table 5.1 shows the user bids (u_1, u_2, u_3, u_4) and the corresponding allocated authority factors $(\omega_1, \omega_2, \omega_3, \omega_4)$ in chronological order. The experiment starts with all users sending unity bids and the WTA algorithm distributing equal authority factors to all leader remote robots. Then the users change their bid to 2 one by one, starting with the user 4 and ending with the user 1, and trigger the WTA algorithm to recognize them as winners and to enable them to teleoperate the remote robot group in cooperation with all other winners. Lastly, the users change their bids back to 1 in the same order, and trigger the WTA algorithm to remove them from the set of winners and to prevent them from teleoperating the remote robot group.

Note that the experimental steady-state authority factors $(\omega_1, \omega_2, \omega_3, \omega_4)$ do not

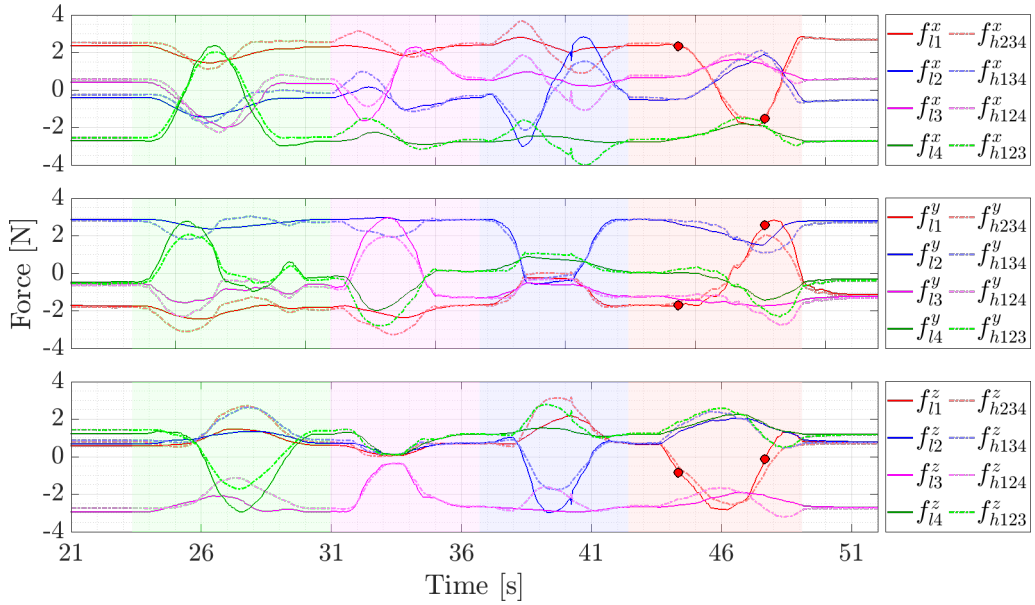

Figure 5.6: Multi-user multi-robot teleoperation without authority dispatch: The force feedback $\mathbf{f}_{li} = \left(f^x_{li}, f^y_{li}, f^z_{li}\right)^\mathsf{T}$ to the user i and the sum $\mathbf{f}_{h*} = \sum_{j\neq i} \mathbf{f}_{hj}$ of the forces $\mathbf{f}_{hj}$ of all other users $j \neq i$.

match their theoretical values exactly. For example, the experimental WTA algorithm dispatches $(\omega_1, \omega_2, \omega_3, \omega_4) = (0, 0, 0.52, 0.52)$ instead of the nominal $(\omega_1^*, \omega_2^*, \omega_3^*, \omega_4^*) = (0, 0, 0.5, 0.5)$. The authority distribution bias can possibly be attributed to three practical implementation issues: (i) the functions $\text{sign}(\alpha_i)$ in (5.30) output 0 for $|\alpha_i| \leq 0.01$ to overcome chattering; (ii) the initialization of $\boldsymbol{\eta}$ by a max-consensus protocol compromises the conditions in Proposition 5.3; and (iii) the additional damping $-\eta_i$ is injected in (5.30b) for practical robustness to communication delays. Nonetheless, the experimental algorithm fulfills the WTA authority dispatch function: it permits only winners to cooperatively tele-drive the remote robots and discards the teleoperation commands of other users.

Figure 5.7 depicts the positions of all robot end-effectors at different time instances during the experiment when all but one user keep their local robots stationary.

- Figures 5.7(a)-5.7(b) show two instances when $(u_1, u_2, u_3, u_4) = (2, 2, 2, 2)$ and the user 4 moves their local robot along the green path. The WTA algorithm recognizes all users as winners and distributes equal teleoperation authority to all: the control forces (5.4)-(5.5) keep the remote robot network in the tetrahedron formed by all local robots. Practically, the teleoperator behaves as under P+d control without authority dispatch.

Table 5.1: The time-varying user bids and the steady-state authority factors of the leader remote robots in the second experiment.

Time t	(u_1, u_2, u_3, u_4)	$(\omega_1, \omega_2, \omega_3, \omega_4)$
53 s-58 s	$(1, 1, 1, 1)$	$(0.25, 0.25, 0.25, 0.25)$
58 s-79 s	$(1, 1, 1, 2)$	$(0, 0, 0, 1)$
79 s-101 s	$(1, 1, 2, 2)$	$(0, 0, 0.52, 0.52)$
101 s-132 s	$(1, 2, 2, 2)$	$(0, 0.35, 0.35, 0.35)$
132 s-162 s	$(2, 2, 2, 2)$	$(0.26, 0.26, 0.26, 0.26)$
162 s-190 s	$(2, 2, 2, 1)$	$(0.35, 0.35, 0.35, 0)$
190 s-210 s	$(2, 2, 1, 1)$	$(0.52, 0.52, 0, 0)$
210 s-229 s	$(2, 1, 1, 1)$	$(1, 0, 0, 0)$
229 s-259 s	$(1, 1, 1, 1)$	$(0.25, 0.25, 0.25, 0.25)$

- Figures 5.7(c)-5.7(d) depict two instances when $(u_1, u_2, u_3, u_4) = (2, 2, 2, 1)$ and the user 3 moves their local robot along the pink path. The WTA algorithm enables the users $1-3$ to equally share the teleoperation authority, and prevents the user 4 from controlling the remote robot network: the spatial distribution of the network is determined by the locations of the local robots L1-L3, independently of the location of the local robot L4.

- Figures 5.7(e)-5.7(f) plot two instances when $(u_1, u_2, u_3, u_4) = (2, 2, 1, 1)$ and the user 2 moves their local robot along the blue path. The WTA algorithm allows only the users $1-2$ to equally share the teleoperation authority, and deprives the users $3-4$ of their teleoperation authority: the winning users $1-2$, cooperatively alter the placement of the remote robot network, while the users $3-4$ have no influence on it. The drift of the remote robots from the L1-L2 line segment is due to the delay in tracking the quickly moving robot L2 in Figure 5.7(e) and to R1 reaching the boundary of its workspace in Figure 5.7(f).

- Figures 5.7(g)-5.7(h) report two instances when $(u_1, u_2, u_3, u_4) = (2, 1, 1, 1)$ and the user 1 moves their local robot along the red path. The WTA algorithm assigns to the user 1 full, and to the users $2-4$ no, teleoperation authority. As shown by the coordination of the remote robots with the local robot L1, the single winner user 1 can tele-drive the remote robots regardless of other users' actions. The inexact coordination, caused by the inertia of the remote robots, is needed to convey the motion status of the remote fleet to the winning user 1.

Figures 5.8-5.11 demonstrate the forces during teleoperation with the following user bids: $(u_1, u_2, u_3, u_4) = (2, 2, 2, 2)$ in Figure 5.8; $(u_1, u_2, u_3, u_4) = (2, 2, 2, 1)$ in Figure 5.9; $(u_1, u_2, u_3, u_4) = (2, 2, 1, 1)$ in Figure 5.10; and $(u_1, u_2, u_3, u_4) = (2, 1, 1, 1)$ in Figure 5.11. The dots mark the time instances in Figure 5.7.

- Figure 5.8 compares the force feedback $\mathbf{f}_{li}$ to every user i to the sum $\mathbf{f}_{h*} = \sum_{j \in \mathcal{S}_w - \{i\}} \mathbf{f}_{hj}$ of all other user forces. In Figure 5.8, all users are winners and teleoperate the remote fleet in turn, during the periods lightly shaded in the colours of their local robots, e.g., the user 4 manipulates the robot L4 during the period shaded in light green. The match between $\mathbf{f}_{li}$ and $\mathbf{f}_{h*}$ at the ends of the coloured areas, when all local robots are at rest, validates that all users feel the sums of all other users' forces accurately in the steady state. The accuracy drops during telemanipulation because of the limited outputs of the local robots (3 N), but $\mathbf{f}_{li}$ still convey $\mathbf{f}_{h*}$ well throughout the interaction.

- Figure 5.9 contrasts: the force feedback to each winner $i = 1, 2, 3$ to the sum of the forces of the other two winners; and the force feedback to the user 4 to the saturated scaled average displacement $\mathbf{f}_{wch4} = \mathrm{S}_3\big(100\big[(\mathbf{x}_1 + \mathbf{x}_2 + \mathbf{x}_3)/3 - \mathbf{x}_4\big]\big)$ of winners' local robots L1-L3 from the local robot L4. Note that all winners hold L1-L3 motionless when the user 4 moves L4 and the force $\mathbf{f}_{l4}$ felt by the user 4 varies accordingly while the forces $\mathbf{f}_{l1}$-$\mathbf{f}_{l3}$ fed back to the winners are constant, see the light green area. Then, the winning users tele-alter the deployment of the remote robot group in sequence. Unless prevented by the limited actuation of their local robot, each winner feels roughly the sum of the forces applied by the other two winners and the user 4 feels roughly the scaled average displacement of L1-L3 from L4, $\mathbf{f}_{l1} \approx \mathbf{f}_{h23}$, $\mathbf{f}_{l2} \approx \mathbf{f}_{h13}$, $\mathbf{f}_{l3} \approx \mathbf{f}_{h12}$ and $\mathbf{f}_{l4} \approx \mathbf{f}_{wch4}$.

- Figure 5.10 compares: the force feedback to each winner $i \in \mathcal{S}_w = \{1, 2\}$ to the force applied by the other winner $j \in \mathcal{S}_w - \{i\}$; and the force feedback to the users $k = 3, 4$ to the saturated scaled average displacement $\mathbf{f}_{wchk} = \mathrm{S}_3\big(100\big[(\mathbf{x}_1 + \mathbf{x}_2)/2 - \mathbf{x}_k\big]\big)$ of the local robots L1 and L2 from their local robot Lk. Note, in the light green-grey shaded area, that, when the winners hold L1-L2 fixed while the users 3 and 4 move their local robots, the force feedback to the winners remains unchanged regardless of the variations of $\mathbf{f}_{l3}$ and $\mathbf{f}_{l4}$.

- Figure 5.11 compares: the force feedback $\mathbf{f}_{l1}$ to the winning user 1 to $\mathbf{0}$; and the force feedback $\mathbf{f}_{li}$ to the users $i = 2, 3, 4$ to the saturated scaled displace-

ment $\mathbf{f}_{wchj} = \mathrm{S}_3\big[100(\mathbf{x}_1 - \mathbf{x}_j)\big]$ of the robot L1 from their local robots. Note that the constant and almost zero $\mathbf{f}_{l1}$ - when the user 1 holds L1 fixed and the users $2-4$ move their local robots (the blue shaded area) - validates that the user 1 is the winner and that the other users have no teleoperation authority. When the winner manipulates L1 (pink shaded area), the remote robot fleet does not track L1 perfectly and $\mathbf{f}_{l1}$ informs them of its location.

In summary, the experimental results validate that the proposed authority dispatch strategy can enable WTA teleoperation of a tree network of the remote robots. The strategy permits all winners to cooperatively tele-guide the remote fleet, and to feel the sum of the forces applied by all other winners. It deprives the other users of their teleoperation authority, and lets them feel forces proportional to the average displacement of the remote fleet from their local robot.

5.5 Conclusion

This chapter has contrived two distributed WTA authority dispatch algorithms based on the Oja's rule for PCA and a constrained quadratic programming. Because conventional authority allocation strategies in the teleoperation setting have rarely accommodated distributed inter-robot communications, the first algorithm (5.6) advances them by deriving a dynamical network that endorses exponential convergence and distributed implementation. With endowed authority factors evolving into 1 and 0, the leader remote robots can functionally activate and deactivate their connections to the local robots of a single winner and other users, respectively. Given that adapting the couplings between the local and leader remote robots can possibly sabotage teleoperation stability, the second algorithm (5.30) proceeds to explore its intrinsic passivity while inheriting the exponential convergence and distributed feature of (5.6). On this basis, this chapter further passivates the teleoperator by interconnecting the second WTA algorithm and the physical robot network in a power-preserving way, and by updating the damping of each leader remote robot, from a switched system viewpoint. The comparative experiments have also practically corroborated that the proposed control with WTA authority dispatch outperforms P+d control with no authority dispatch in terms of teleoperation versatility.

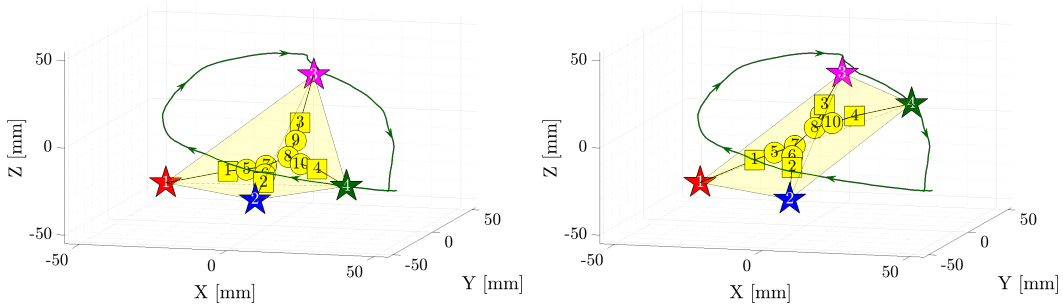

(a) $t = 137$ s, $(u_1, u_2, u_3, u_4) = (2, 2, 2, 2)$.

(b) $t = 141$ s, $(u_1, u_2, u_3, u_4) = (2, 2, 2, 2)$.

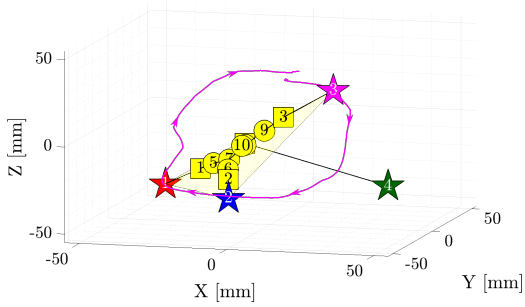

(c) $t = 171$ s, $(u_1, u_2, u_3, u_4) = (2, 2, 2, 1)$.

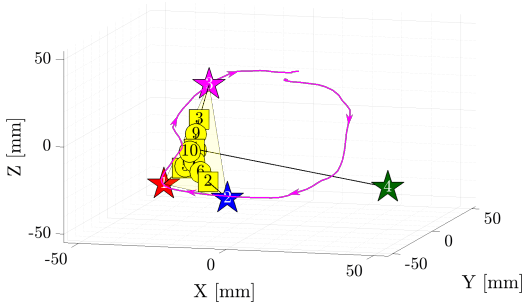

(d) $t = 175$ s, $(u_1, u_2, u_3, u_4) = (2, 2, 2, 1)$.

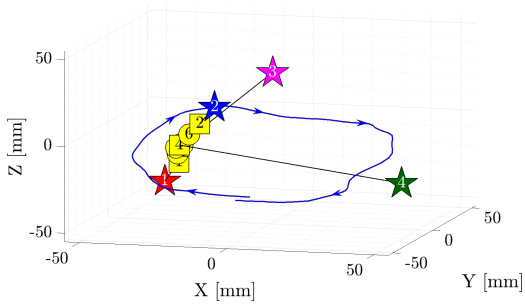

(e) $t = 200$ s, $(u_1, u_2, u_3, u_4) = (2, 2, 1, 1)$.

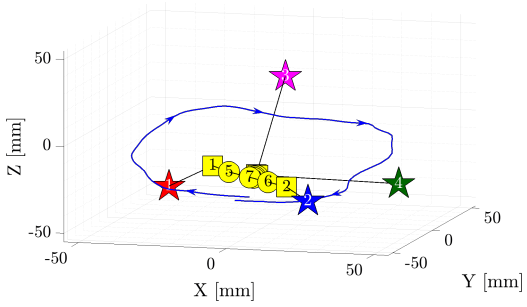

(f) $t = 202$ s, $(u_1, u_2, u_3, u_4) = (2, 2, 1, 1)$.

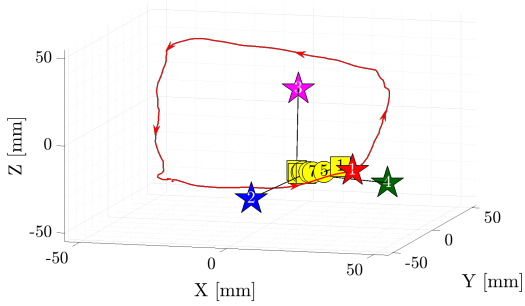

(g) $t = 222$ s, $(u_1, u_2, u_3, u_4) = (2, 1, 1, 1)$.

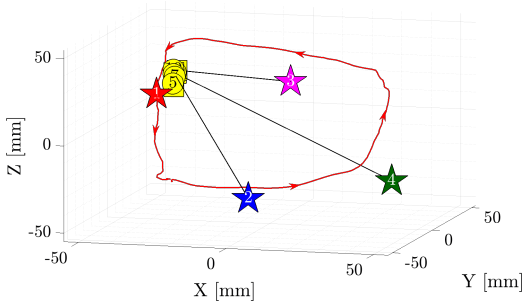

(h) $t = 226$ s, $(u_1, u_2, u_3, u_4) = (2, 1, 1, 1)$.

Figure 5.7: Multi-user multi-robot teleoperation with WTA authority dispatch: The end-effector positions of all robots at different time instances and for different user bids. All but one user keep their local robots stationary. The coloured curves indicate the path along, and the direction in, which the one user moves their local robot.

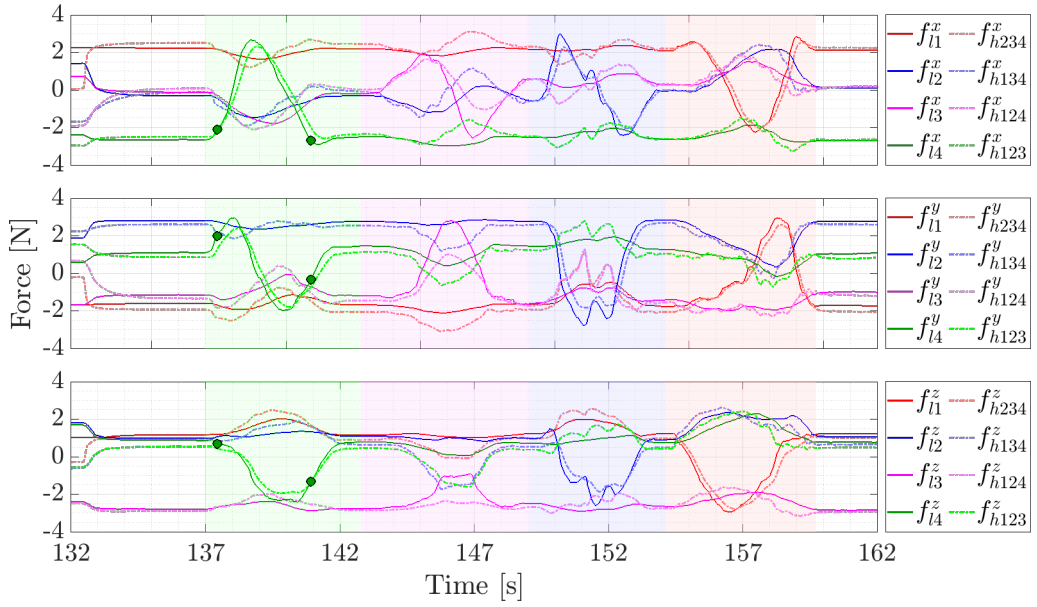

Figure 5.8: Multi-user multi-robot teleoperation with WTA authority dispatch for $(u_1, u_2, u_3, u_4) = (2, 2, 2, 2)$: The force feedback $\mathbf{f}_{li} = \left(f^x_{li}, f^y_{li}, f^z_{li}\right)^\mathsf{T}$ to the user i and the sum $\mathbf{f}_{h*} = \sum_{j \neq i} \mathbf{f}_{hj}$ of the forces $\mathbf{f}_{hj}$ of all other winning users $j \neq i$.

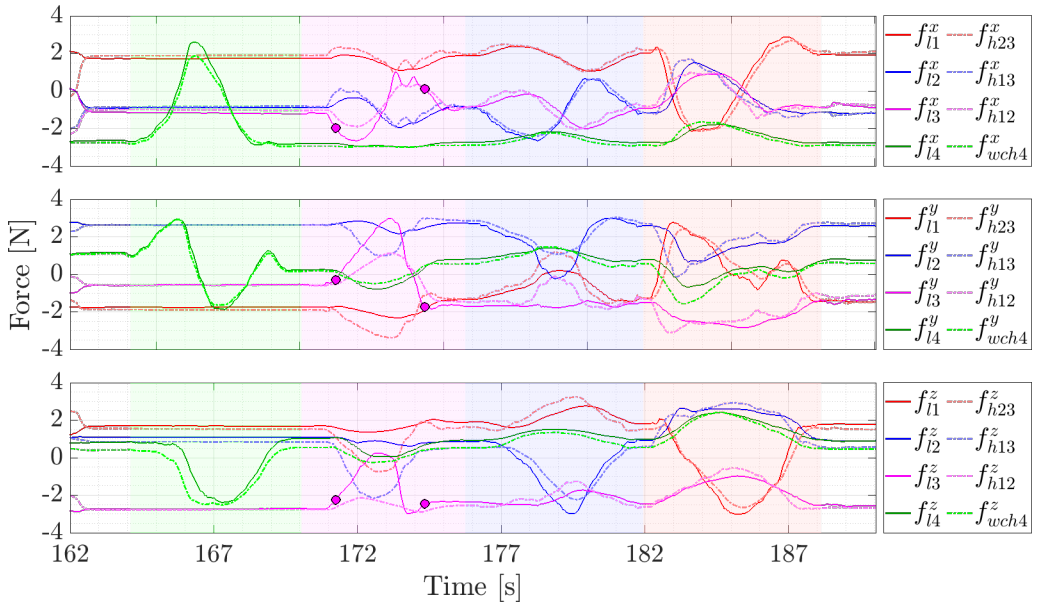

Figure 5.9: Multi-user multi-robot teleoperation with WTA authority dispatch for $(u_1, u_2, u_3, u_4) = (2, 2, 2, 1)$: The force feedback $\mathbf{f}_{li} = \left(f^x_{li}, f^y_{li}, f^z_{li}\right)^\mathsf{T}$ to the user i and the sum $\mathbf{f}_{h*} = \sum_{j \neq i} \mathbf{f}_{hj}$ of the forces $\mathbf{f}_{hj}$ of all other winning users $j \neq i$.

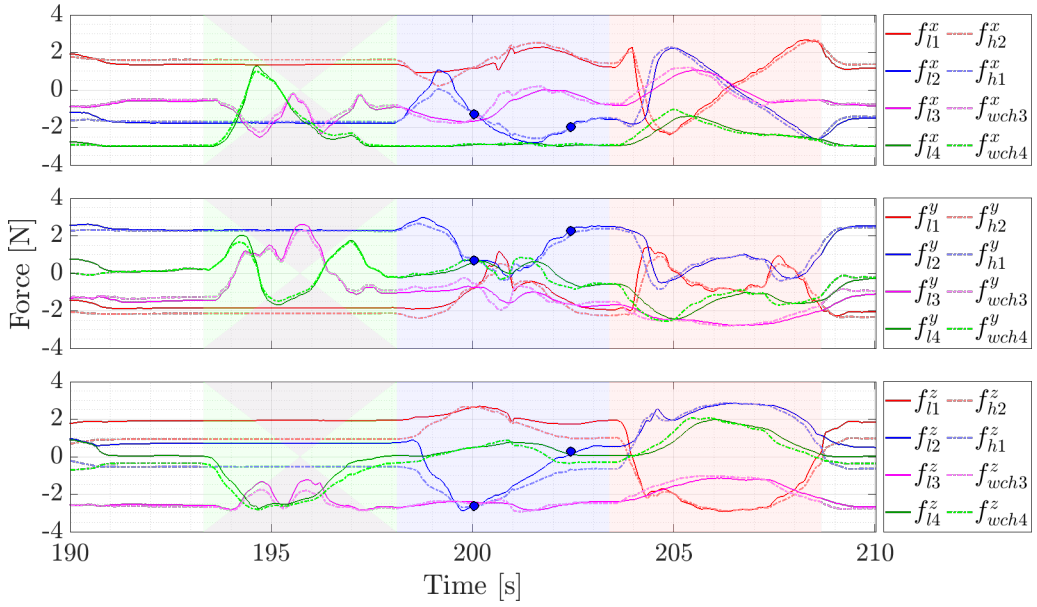

Figure 5.10: Multi-user multi-robot teleoperation with WTA authority dispatch for $(u_1, u_2, u_3, u_4) = (2, 2, 1, 1)$: The force feedback $\mathbf{f}_{li} = \left(f^x_{li}, f^y_{li}, f^z_{li}\right)^\mathsf{T}$ to the user i and the sum $\mathbf{f}_{h*} = \sum_{j \neq i} \mathbf{f}_{hj}$ of the forces $\mathbf{f}_{hj}$ of all other winning users $j \neq i$.

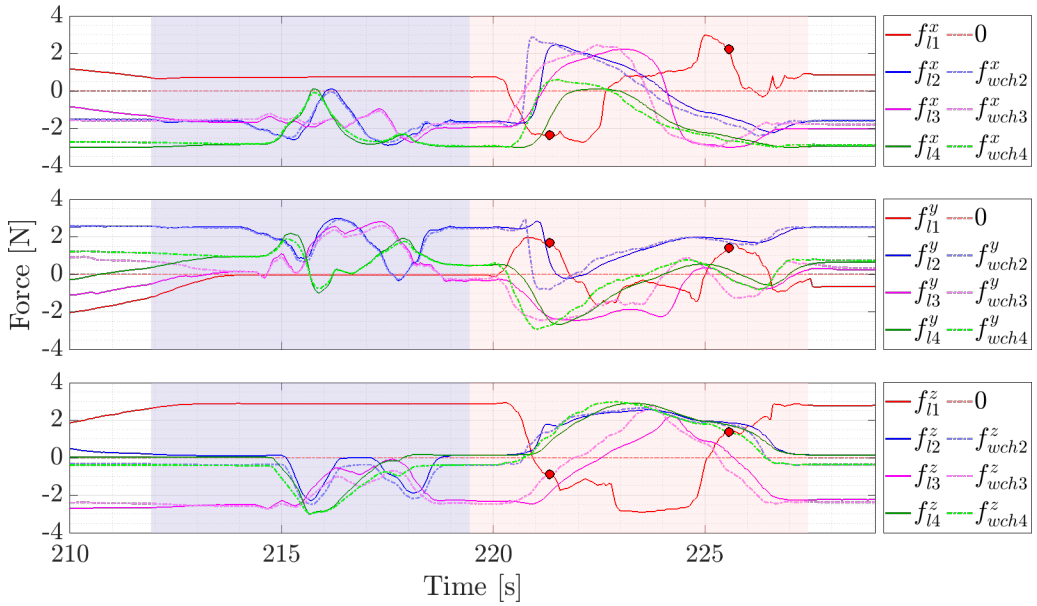

Figure 5.11: Multi-user multi-robot teleoperation with WTA authority dispatch for $(u_1, u_2, u_3, u_4) = (2, 1, 1, 1)$: The force feedback $\mathbf{f}_{li} = \left(f^x_{li}, f^y_{li}, f^z_{li}\right)^\mathsf{T}$ to the user i and the sum $\mathbf{f}_{h*} = \sum_{j \neq i} \mathbf{f}_{hj}$ of the forces $\mathbf{f}_{hj}$ of all other winning users $j \neq i$.

Chapter 6

Conclusions and Future Work

This thesis bases on an energy shaping design principle to tackle two problems facing multi-robot teleoperation: connectivity-preserving coordination at the bottom level and authority dispatch at the top level. In a distributed way, the former seeks to retain a minimal communication network for tele-driving a multi-robot group, while the latter allocates a unique amount of authority to every user as per the urgency levels of their requests. Each problem may endanger the passivity of bilateral teleoperation unless addressed appropriately. Connectivity-preserving coordination must limit the energy stored in the remote robot group to a certain threshold without knowing the energy injected by human users beforehand. Authority dispatch must augment the robot network with an auxiliary system, thereby inserting another source of energy. We have developed a dynamic feedforward-feedback passivation control and a WTA authority dispatch machine to transform the multi-robot teleoperator into a novel power-preserving interconnection of several subsystems, and to regulate their energy balances individually. We have also built an experimental multi-robot teleoperation platform to examine the proposed designs in practice.

6.1 Conclusions

Chapter 2 has designed a dynamic interconnection and damping injection strategy that can render a bilateral teleoperator exponentially ISS in the presence of time-varying communication delays. Given a pair of local and remote robots with EL dynamics, a sliding variable summing the velocity of, and the position error between, them has firstly transformed a delay-free teleoperator into a first-order system with

mismatched dynamics. An energy analysis reveals that suitably adapting the interconnection between, and the damping injection of, both robots using their own velocities can suppress state-dependent mismatches arising from the transformation of robot dynamics. With time-varying communication delays, the virtual inertia have further been integrated into the design to handle delay-induced instability via constant damping injection. An explicit law of updating the interconnection and damping gains has been derived to ensure exponentially ISS teleoperation. The experimental results have also validated that the proposed strategy can tightly constrain the position error between the local and remote robots in practical teleoperation.

Chapter 3 has established a connectivity-preserving synchronization control for autonomous multi-robot systems with both time-varying delays and bounded actuation. Due to time-delay information transmissions, every pair of initially adjacent robots can keep receiving messages from each other only if their maximum distance over the time-delay period is limited to the communication range. To this end, a specific criterion has firstly been proposed to select the parameters of a bounded potential function and the gains of a gradient plus damping control for every robot. However, actuator saturation can counterbalance the control by restricting the enhancement of inter-robot couplings and the injection of local damping, thereby endangering connectivity preservation. The virtual inertia have then been unified into the control to convert the constraint of bounded actuation into a constraint on their distances. The resulting indirect coupling scheme can address communication delays and actuator saturation by inter-proxy and robot-proxy couplings, separately. The rigorous energy analysis and experimental validations illustrate that the designed control can drive a time-delay robot network to connectivity-preserving synchronization even when actuators saturate.

Chapter 4 has formulated a distributed multi-robot teleoperator that can preserve the tree communication network of its remote robot group when interacting with multiple human users. Based on the control designs in Chapters 2 and 3, the gradient of a bounded potential function has been embedded into a sliding variable to decompose the remote robot dynamics into a power-preserving interconnection of two subsystems. An energy analysis has then derived two laws for selecting parameters and updating control gains for preserving the tree connectivity of the remote robot group, and for rendering it passive with respect to a customized power port. After that, saturated P+d control interconnects the local robots with their associated leader remote robots through the port in a power-preserving way, thereby passivating

the closed-loop teleoperator. Further, the kinematic virtual points have been implemented at every leader remote robots to transform their couplings with the local robots into a cyber component. By synthesizing the robot dynamics into a physical component, a dynamic feedforward-feedback passivation strategy has been formalized at last to passivate time-delay teleoperation of a connectivity-preserving remote robot network. The steady-state analysis has proved that the strategy enables every user to tele-alter the spatial deployment of the remote robots with containment control, and to perceive the sum of the forces of other users. The comparative experiments have also illustrated that the strategy outperforms P+d synchronization control in connectivity maintenance.

Chapter 5 has framed a WTA authority dispatch machinery for a distributed multi-robot teleoperator responding to multiple user requests simultaneously. Using Oja's rule for PCA, it has firstly contrived a distributed WTA algorithm, of which the exponential convergence is investigated by the conjunction of set invariance and a dedicated quotient function. However, incorporating the algorithm into fashionable passivity-based multi-robot teleoperation controls is nontrivial because its intrinsic passivity is uncertain. In view of this, it derives then a second WTA algorithm from a constrained quadratic programming, of which the projected primal-dual dynamics feature exponential convergence and distributed implementation as well. Most importantly, by energy analysis, the second algorithm has been proven output strictly passive with respect to a particular power port. It thus facilitates a further power-preserving interconnection with physical robot dynamics, and closed-loop passive teleoperation with online authority dispatch. Given that the set the winners varies with time, the teleoperator admits multiple albeit finite operation modes, it thus leverages multiple storage functions to study the passivity of the teleoperator from a switched system standpoint. The experimental validations have also substantiated the practical efficacy of the second WTA algorithm for authority allocation throughout multi-robot teleoperation.

6.2 Future Work

6.2.1 Global Connectivity Preservation

A conscious augmentation of the control design in Chapter 4 is global connectivity preservation of the teleoperated remote robot network with switching spanning trees.

Because a connected communication graph can have multiple spanning trees, the connectivity-preserving teleoperation control in Chapter 4, which maintains a single tree communication topology invariant, significantly restricts the mobility of the remote robots and further the flexibility of the entire teleoperator. Existing designs have preserved the global connectivity of a teleoperated multi-robot network by estimating and then rendering positive the algebraic eigenvalue of the Laplacian matrix associated with the underlying communication topology. However, they impose a stringent condition on the bandwidth of the communication network for algebric connectivity estimation. Thus, we formulate the following estimation-free global connectivity maintenance problem for distributed multi-robot teleoperation:

Problem 6.1. *Every pair of the remote robots that are within the communication distance r can automatically establish and then maintain a new communication link or voluntarily remove their current one with no algebraic connectivity estimation so long as a switching spanning tree exists in the underlying communication network of the whole remote robot group.*

Note that each remote robot performs two operations: creating new links with other remote robots whenever their distances become smaller than the communication range r and then preserving them; and deleting its connections with other remote robots if not destroying the global connectivity of the remote robot network. Because the first and second operations enhance and weaken the network connectivity, respectively, a key to solving Problem 6.1 is to design a local decision-making machine for every remote robot to determine the feasibility of deactivating proximity-constraining actions. Being unaware of the network connectivity and other robots' behaviours, every remote robots removing their couplings with neighbours individually can lead to multiple link deletions simultaneously and disconnect the network. A scheduling algorithm is thus required to make multiple link deletions asynchronous.

A multi-robot teleoperator can remove at most 2 communication links simultaneously from its remote robot network while maintaining it connected if its original communication topology is as in Figure 6.1(a). By simple enumerations, it can validate that the original communication graph has 12 spanning trees because of the two cycles $(5, 6, 7, 8, 5)$ and $(7, 8, 9, 10, 7)$. When 2 robot pairs from 2 different cycles delete their communication links simultaneously, the communication graph remains connected. For example, removing $(5, 6)$ and $(9, 10)$, and removing $(5, 8)$ and $(7, 8)$, simultaneously, result in two spaning trees in Figure 6.1(b) and Figure 6.1(c), respec-

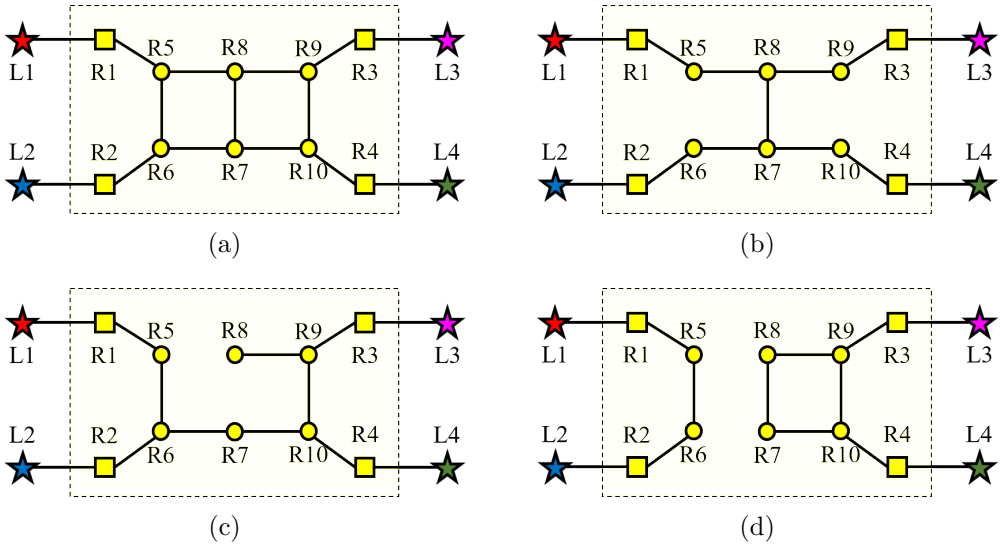

Figure 6.1: A communication network remains connected when deleting 2 links from 2 cycles respectively, while becomes disconnected when the 2 links belong to an exclusive cycle.

tively. However, when the robot pairs $(5, 8)$ and $(6, 7)$ delete their communication links, the graph becomes disconnected because both links belong to the only cycle $(5, 6, 7, 8, 5)$. The example thus implies that the scheduling algorithm permits the teleoperator to delete a maximal number of communication links simultaneously by informing all pairs of adjacent remote robots that if any two of their communication links to be deleted are from the same cycle.

6.2.2 Proportional-Prize Authority Dispatch

A natural extension of the control design in Chapter 5 is a proportional-prize multi-robot teleoperation problem in which the users tele-drive a number of the remote robots proportional to the urgencies of their requests. Given N_l user bids, the remote robot group is partitioned into N_l clusters $\mathcal{G}_c = \{\mathcal{V}_c, \mathcal{E}_c\}$ with $c = 1, \cdots, N_l$, each teleoperated by an individual user simultaneously with, and independently of, other clusters. To assign a number of the remote robots to the cluster $\mathcal{G}_c$ in response to the user bid $u_c(t_k)$, we formulate the following proportional-prize multi-robot teleoperation objective:

Problem 6.2. *The number of the remote robots allocated to the cluster $\mathcal{G}_c$ is propor-*

tional to the value of the user bid $u_c(t_k)$ *by*

$$r_c(t_k) = |\mathcal{V}_c(t_k)| = \frac{N_r u_c(t_k)}{u_1(t_k) + \cdots + u_{N_l}(t_k)} \in \mathbb{Z}_{\geq 0},$$

and the sum of their topological distances to the local robot c *in the remote robot network* $\mathcal{G}$ *is minimized. Here, we assume that every proportion* $r_c(t_k)$ *is an integer and* $r_1(t_k) + \cdots + r_{N_l}(t_k) = N_r$.

Following Chapter 5, let each remote robot $i = 1, \cdots, N_r$ be endowed with a vector of decision variables $\boldsymbol{\omega}_i = \left(\omega_i^1, \cdots, \omega_i^{N_l}\right)^\mathsf{T}$, where $\omega_i^c = 1$ if the remote robot i is to be assigned to the cluster $\mathcal{G}_c$, and $\omega_i^c = 0$ otherwise, for $c = 1, \cdots, N_l$. Suppose that each remote robot i is aware of its geodesic distance d_i^c to the leader remote robot c in $\mathcal{G}$. Then, the clustering of the remote robot group can be formulated as

$$\underset{\omega_i^c \in \mathbb{R}}{\text{minimize}} \ \sum_{i=1}^{N_r} \sum_{c=1}^{N_l} d_i^c \omega_i^c, \tag{6.1a}$$

$$\text{such that} \ \sum_{c=1}^{N_l} \omega_i^c = 1, \ i = 1, \cdots, N_r, \tag{6.1b}$$

$$\sum_{i=1}^{N_r} \omega_i^c = r_c, \ c = 1, \cdots, N_l, \tag{6.1c}$$

$$\omega_i^c \in \{0, 1\}, \ i = 1, \cdots, N_r, \ c = 1, \cdots, N_l. \tag{6.1d}$$

Here: the linear objective function in (6.1a) indicates that the clustering of all remote robots into $\mathcal{G}_c$, $c = 1, \cdots, N_l$, minimizes the sum of their geodesic distances in $\mathcal{G}$ to the leader remote robot c and thus to the local robot c; the constraint (6.1b) ensures that every remote robot i is assigned to a unique cluster; the constraint (6.1c) restricts the number of the remote robots grouped into every cluster $\mathcal{G}_c$ to be r_c; and the constraint (6.1d) compels all decision variables ω_i^c to be either 0 or 1.

Specifically, the evolving coefficients $\boldsymbol{\omega}_i^\mathsf{T} \boldsymbol{\omega}_j$ determines the status of the interconnections between the remote robots i and j. With (6.1), every remote robot i can select a cluster $\mathcal{G}_c$ by $\omega_i^c \to 1$ and abandon other clusters $\mathcal{G}_k$ with $k \neq c$ by $\omega_i^k \to 0$. Therefore, $\boldsymbol{\omega}_i^\mathsf{T} \boldsymbol{\omega}_j \to 1$ if the adjacent robots i and j belong to the same cluster, and $\boldsymbol{\omega}_i^\mathsf{T} \boldsymbol{\omega}_j \to 0$ otherwise.

However, the integer program (6.1) can possibly result in pathological clusters of the remote robots that cannot be teleoperated by the designated users over a

distributed communication network $\mathcal{G}$ in Figure 6.2(a). When $u_1(t_k) = 2u_2(t_k)$, it requires to allocate $r_1 = 8$ and $r_2 = 4$ remote robots to the clusters $\mathcal{G}_1$ and $\mathcal{G}_2$ to be teleoperated by the local robots 1 and 2, respectively. The user c can teleoperate the cluster $\mathcal{G}_c$ iff every remote robot in $\mathcal{G}_c$ is reachable from the local robot c for $c = 1, 2$. Yet, the integer program (6.1) has 3 minimizers leading to three possible clusterings of the remote robot team depicted in Figures 6.2(b)-6.2(d). In these figures, the red and blue vertices represent the remote robots assigned to the clusters $\mathcal{G}_1$ and $\mathcal{G}_2$, respectively. Because the remote robots R12 in Figure 6.2(c) and R10 in Figure 6.2(d) are unreachable from the local robot L2, the two clusterings prevent the user 2 from teleoperating the cluster $\mathcal{G}_2$. The remaining solution of the integer program (6.1) offers the only reachable clustering of the remote robot group in Figure 6.2(b).

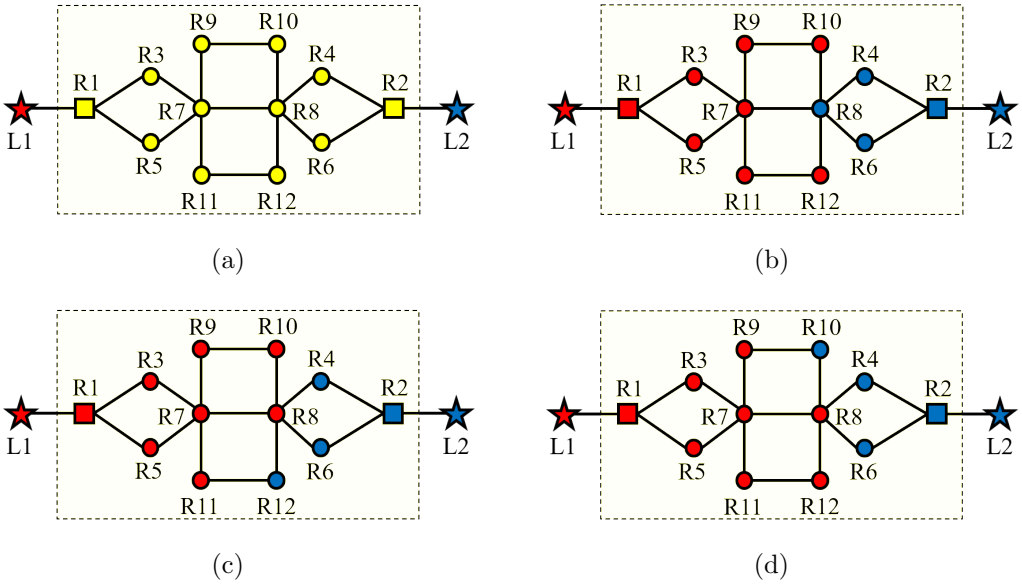

Figure 6.2: Under $r_1 = 8$ and $r_2 = 4$, the integer program (6.1) has 3 solutions, Figures 6.2(b)-6.2(d), for proportional-prize multi-robot teleoperation with the communication topology shown in Figure 6.2(a).

Therefore, the future study will solve Problem 6.2 in the following steps: (i) impose an indispensable reachability constraint on the integer program (6.1) to preclude pathological clusterings and to preserve reachable solutions; (ii) find a continuous-time algorithm to efficiently search a minimizer of (6.1) in a distributed manner; (iii) establish a power-preserving interconnection between the algorithm and physical robot dynamics to render multi-robot teleoperation passive; (iv) investigate the position synchronization and force feedback performance of the design in field trials.

Appendix A

Derivations of Equation (3.9)

$$
\begin{aligned}
&\dot{\mathbf{x}}_i^{\mathsf{T}}\nabla_i\psi(\|\mathbf{x}_{ij}\|) - \dot{\mathbf{x}}_i^{\mathsf{T}}\nabla_i\psi(\|\mathbf{x}_{ij}^d\|)\\
=&\frac{2P\left(r^2+Q\right)}{\left(r^2-\|\mathbf{x}_{ij}\|^2+Q\right)^2}\dot{\mathbf{x}}_i^{\mathsf{T}}\left(\mathbf{x}_i-\mathbf{x}_j\right) - \frac{2P\left(r^2+Q\right)}{\left(r^2-\|\mathbf{x}_{ij}^d\|^2+Q\right)^2}\dot{\mathbf{x}}_i^{\mathsf{T}}\left(\mathbf{x}_i-\mathbf{x}_{jd}\right)\\
=&\frac{2P\left(r^2+Q\right)\dot{\mathbf{x}}_i^{\mathsf{T}}\mathbf{x}_{ij}}{\left(r^2-\|\mathbf{x}_{ij}\|^2+Q\right)^2} - \frac{2P\left(r^2+Q\right)\dot{\mathbf{x}}_i^{\mathsf{T}}\mathbf{x}_{ij}}{\left(r^2-\|\mathbf{x}_{ij}^d\|^2+Q\right)^2} - \frac{2P\left(r^2+Q\right)\dot{\mathbf{x}}_i^{\mathsf{T}}(\mathbf{x}_j-\mathbf{x}_{jd})}{\left(r^2-\|\mathbf{x}_{ij}^d\|^2+Q\right)^2}\\
=&\frac{2P\left(r^2+Q\right)\dot{\mathbf{x}}_i^{\mathsf{T}}\mathbf{x}_{ij}}{\left(r^2-\|\mathbf{x}_{ij}\|^2+Q\right)^2\left(r^2-\|\mathbf{x}_{ij}^d\|^2+Q\right)^2}\left[\left(r^2-\|\mathbf{x}_{ij}^d\|^2+Q\right)^2-\left(r^2-\|\mathbf{x}_{ij}\|^2+Q\right)^2\right]\\
&-\frac{2P\left(r^2+Q\right)\dot{\mathbf{x}}_i^{\mathsf{T}}(\mathbf{x}_j-\mathbf{x}_{jd})}{\left(r^2-\|\mathbf{x}_{ij}^d\|^2+Q\right)^2}\\
\leq&\frac{2P\left(r^2+Q\right)|\dot{\mathbf{x}}_i^{\mathsf{T}}\mathbf{x}_{ij}|}{\left(r^2-\|\mathbf{x}_{ij}\|^2+Q\right)\left(r^2-\|\mathbf{x}_{ij}^d\|^2+Q\right)}\left(\frac{1}{r^2-\|\mathbf{x}_{ij}\|^2+Q}+\frac{1}{r^2-\|\mathbf{x}_{ij}^d\|^2+Q}\right)\\
&\cdot\left|\left(r^2-\|\mathbf{x}_{ij}^d\|^2+Q\right)-\left(r^2-\|\mathbf{x}_{ij}\|^2+Q\right)\right| + 2PQ^{-2}\left(r^2+Q\right)|\dot{\mathbf{x}}_i^{\mathsf{T}}\left(\mathbf{x}_j-\mathbf{x}_{jd}\right)|\\
\leq&\frac{4PQ^{-1}\left(r^2+Q\right)\left|\|\mathbf{x}_{ij}\|^2-\|\mathbf{x}_{ij}^d\|^2\right||\dot{\mathbf{x}}_i^{\mathsf{T}}\mathbf{x}_{ij}|}{\left(r^2-\|\mathbf{x}_{ij}\|^2+Q\right)\left(r^2-\|\mathbf{x}_{ij}^d\|^2+Q\right)} + 2PQ^{-2}\left(r^2+Q\right)\left|\dot{\mathbf{x}}_i^{\mathsf{T}}\left(\mathbf{x}_j-\mathbf{x}_{jd}\right)\right|\\
\leq&4PQ^{-3}\left(r^2+Q\right)\left|\|\mathbf{x}_{ij}\|^2-\|\mathbf{x}_{ij}^d\|^2\right||\dot{\mathbf{x}}_i^{\mathsf{T}}\mathbf{x}_{ij}| + 2PQ^{-2}\left(r^2+Q\right)|\dot{\mathbf{x}}_i^{\mathsf{T}}\left(\mathbf{x}_j-\mathbf{x}_{jd}\right)|\\
\leq&8rPQ^{-3}\left(r^2+Q\right)\|\mathbf{x}_{ij}-\mathbf{x}_{ij}^d\||\dot{\mathbf{x}}_i^{\mathsf{T}}\mathbf{x}_{ij}| + 2PQ^{-2}\left(r^2+Q\right)|\dot{\mathbf{x}}_i^{\mathsf{T}}\left(\mathbf{x}_j-\mathbf{x}_{jd}\right)|\\
\leq&2PQ^{-3}(r^2+Q)(4r^2+Q)\|\dot{\mathbf{x}}_i\|\|\mathbf{x}_j-\mathbf{x}_{jd}\|.
\end{aligned}
$$

Appendix B

Derivations of Equation (4.17)

$$
\begin{aligned}
V_1 =& \frac{\sigma}{2}\sum_{i=1}^{N_r}\sum_{j\in\mathcal{N}_i}\frac{(r^2-\|\mathbf{x}_{rij}\|^2+Q)^3}{4P(r^2+Q)^2}\frac{4P^2(r^2+Q)^2\|\mathbf{x}_{rij}\|^2}{(r^2-\|\mathbf{x}_{rij}\|^2+Q)^4}\\
=& \frac{\sigma}{2}\sum_{i=1}^{N_r}\sum_{j\in\mathcal{N}_i}\frac{(r^2-\|\mathbf{x}_{rij}\|^2+Q)^3}{4P(r^2+Q)^2}\left\|\nabla_i\psi(\|\mathbf{x}_{rij}\|)\right\|^2\\
=& \sum_{(i,j)\in\mathcal{E}}\frac{\sigma\,(r^2-\|\mathbf{x}_{rij}\|^2+Q)^3}{4P(r^2+Q)^2}\left\|\nabla_i\psi(\|\mathbf{x}_{rij}\|)\right\|^2\\
\leq& \sum_{(i,j)\in\mathcal{E}}\frac{\sigma(r^2+Q)}{4P}\left\|\nabla_i\psi(\|\mathbf{x}_{rij}\|)\right\|^2\\
=& \frac{\sigma(r^2+Q)}{4P}\sum_{(i,j)\in\mathcal{E}}\left\|l_{ij}(\mathbf{x}_r)(\mathbf{x}_{ri}-\mathbf{x}_{rj})\right\|^2\\
=& \frac{\sigma(r^2+Q)}{4P}\left\|\left[\mathbf{W}(\mathbf{x}_r)\otimes\mathbf{I}_n\right]\widetilde{\mathbf{x}}_r\right\|^2\\
=& \frac{\sigma(r^2+Q)}{4P}\widetilde{\mathbf{x}}_r^{\mathsf{T}}\left[\mathbf{W}(\mathbf{x}_r)\otimes\mathbf{I}_n\right]^{\mathsf{T}}\left[\mathbf{W}(\mathbf{x}_r)\otimes\mathbf{I}_n\right]\widetilde{\mathbf{x}}_r\\
\leq& \frac{\sigma(r^2+Q)}{4\lambda_L P}\widetilde{\mathbf{x}}_r^{\mathsf{T}}\left[\mathbf{W}^{\mathsf{T}}(\mathbf{x}_r)\mathbf{L}_e\mathbf{W}(\mathbf{x}_r)\otimes\mathbf{I}_n\right]\widetilde{\mathbf{x}}_r\\
=& \frac{\sigma(r^2+Q)}{4\lambda_L P}\mathbf{x}_r^{\mathsf{T}}\left[\mathbf{B}\mathbf{W}^{\mathsf{T}}(\mathbf{x}_r)\mathbf{B}^{\mathsf{T}}\mathbf{B}\mathbf{W}(\mathbf{x}_r)\mathbf{B}^{\mathsf{T}}\otimes\mathbf{I}_n\right]\mathbf{x}_r\\
=& \frac{\sigma(r^2+Q)}{4\lambda_L P}\mathbf{x}_r^{\mathsf{T}}\left[\mathbf{L}^{\mathsf{T}}(\mathbf{x}_r)\mathbf{L}(\mathbf{x}_r)\otimes\mathbf{I}_n\right]\mathbf{x}_r,
\end{aligned}
$$

Appendix C

Derivations of Equation (4.20)

By $\boldsymbol{\Delta}_{lri}$ given in (4.5),

$$\begin{aligned}\boldsymbol{\Delta}_{lri} =&\mathbf{M}_{ri}(\mathbf{x}_{ri})\dot{\boldsymbol{\theta}}_{lri} + \mathbf{C}_{ri}(\mathbf{x}_{ri},\dot{\mathbf{x}}_{ri})\boldsymbol{\theta}_{lri}\\ =&K_{lri}\mathbf{M}_{ri}(\mathbf{x}_{ri})\overline{\mathbf{F}}_{hi}\Big[\mathbf{I}_n - \mathrm{diag}\big\{\tanh^2[K_{lri}(\mathbf{x}_{ri}-\mathbf{x}_{li})]\big\}\Big]\big(\dot{\mathbf{x}}_{ri}-\dot{\mathbf{x}}_{li}\big)\\ &+\mathbf{C}_{ri}(\mathbf{x}_{ri},\dot{\mathbf{x}}_{ri})\overline{\mathbf{F}}_{hi}\cdot\tanh\big[K_{lri}(\mathbf{x}_{ri}-\mathbf{x}_{li})\big]\end{aligned}$$

for the leader remote robots $i = 1,\cdots,N_l$, while $\boldsymbol{\Delta}_{lri} = \mathbf{0}$ for the follower remote robots $i = N_l+1,\cdots,N_r$. It follows then that

$$\begin{aligned}\mathbf{s}_i^{\mathsf{T}}\boldsymbol{\Delta}_{lri} =&K_{lri}\mathbf{s}_i^{\mathsf{T}}\mathbf{M}_{ri}(\mathbf{x}_{ri})\overline{\mathbf{F}}_{hi}\Big[\mathbf{I}_n - \mathrm{diag}\big\{\tanh^2\big[K_{lri}(\mathbf{x}_{ri}-\mathbf{x}_{li})\big]\big\}\Big]\big(\dot{\mathbf{x}}_{ri}-\dot{\mathbf{x}}_{li}\big)\\ &+\mathbf{s}_i^{\mathsf{T}}\mathbf{C}_{ri}(\mathbf{x}_{ri},\dot{\mathbf{x}}_{ri})\overline{\mathbf{F}}_{hi}\cdot\tanh\big[K_{lri}(\mathbf{x}_{ri}-\mathbf{x}_{li})\big]\\ \le&\frac{\lambda_{ri}^2}{4\eta}K_{lri}^2\|\dot{\mathbf{x}}_{li}-\dot{\mathbf{x}}_{ri}\|^2\mathbf{s}_i^{\mathsf{T}}\Big[\mathbf{I}_n - \mathrm{diag}\big\{\tanh^2\big[K_{lri}(\mathbf{x}_{ri}-\mathbf{x}_{li})\big]\big\}\Big]^2\mathbf{s}_i + \eta\overline{\mathbf{f}}_{hi}^{\mathsf{T}}\overline{\mathbf{f}}_{hi}\\ &+\frac{c_{ri}^2}{4}\mathbf{s}_i^{\mathsf{T}}\overline{\mathbf{F}}_{hi}^2\cdot\mathrm{diag}\Big\{\tanh^2\big[K_{lri}(\mathbf{x}_{ri}-\mathbf{x}_{li})\big]\Big\}\mathbf{s}_i + \dot{\mathbf{x}}_{ri}^{\mathsf{T}}\dot{\mathbf{x}}_{ri}\\ =&\mathbf{s}_i^{\mathsf{T}}\boldsymbol{\Gamma}_{lri}^c(t)\mathbf{s}_i + \dot{\mathbf{x}}_{ri}^{\mathsf{T}}\dot{\mathbf{x}}_{ri} + \eta\overline{\mathbf{f}}_{hi}^{\mathsf{T}}\overline{\mathbf{f}}_{hi},\end{aligned}$$

for the leader remote robots $i = 1,\cdots,N_l$, where

$$\begin{aligned}\boldsymbol{\Gamma}_{lri}^c(t) =&\frac{\lambda_{ri}^2}{4\eta}K_{lri}^2\|\dot{\mathbf{x}}_{li}-\dot{\mathbf{x}}_{ri}\|^2\Big[\mathbf{I}_n - \mathrm{diag}\big\{\tanh^2\big[K_{lri}(\mathbf{x}_{ri}-\mathbf{x}_{li})\big]\big\}\Big]^2\\ &+\frac{c_{ri}^2}{4}\overline{\mathbf{F}}_{hi}^2\cdot\mathrm{diag}\Big\{\tanh^2\big[K_{lri}(\mathbf{x}_{ri}-\mathbf{x}_{li})\big]\Big\},\end{aligned}$$

and $\mathbf{s}_i^{\mathsf{T}}\boldsymbol{\Delta}_{lri}=0$ for the follower remote robots $i=N_l+1,\cdots,N_r$. Thus,

$$\begin{aligned}\sum_{i=1}^{N_r}\frac{\eta}{D_{ri}}\mathbf{s}_i^{\mathsf{T}}\boldsymbol{\Delta}_{lri}\leq&\sum_{i=1}^{N_l}\frac{\eta}{D_{ri}}\mathbf{s}_i^{\mathsf{T}}\boldsymbol{\Gamma}_{lri}^c(t)\mathbf{s}_i+\sum_{i=1}^{N_l}\frac{\eta}{D_{ri}}\dot{\mathbf{x}}_{ri}^{\mathsf{T}}\dot{\mathbf{x}}_{ri}+\sum_{i=1}^{N_l}\frac{\eta^2}{D_{ri}}\overline{\mathbf{f}}_{hi}^{\mathsf{T}}\overline{\mathbf{f}}_{hi}\\=&\eta\mathbf{s}^{\mathsf{T}}\mathbf{D}_r^{-1}\mathbb{I}^{\mathsf{T}}\boldsymbol{\Gamma}_{lr}^c(t)\mathbb{I}\mathbf{s}+\eta\dot{\mathbf{x}}_r^{\mathsf{T}}\mathbf{D}_r^{-1}\mathbb{I}^{\mathsf{T}}\mathbb{I}\dot{\mathbf{x}}_r+\eta^2\overline{\mathbf{f}}_h^{\mathsf{T}}\mathbb{I}\mathbf{D}_r^{-1}\mathbb{I}^{\mathsf{T}}\overline{\mathbf{f}}_h,\end{aligned}\tag{C.1}$$

where $\boldsymbol{\Gamma}_{lr}^c(t)=\mathrm{Diag}\big\{\boldsymbol{\Gamma}_{lri}^c(t)\big\}$ and $\overline{\mathbf{f}}_h=\left(\overline{\mathbf{f}}_{h1}^{\mathsf{T}},\cdots,\overline{\mathbf{f}}_{hN_l}^{\mathsf{T}}\right)^{\mathsf{T}}$.

Further, the time derivative of $\boldsymbol{\theta}_{ri}$ defined in (4.3) is

$$\begin{aligned}\dot{\boldsymbol{\theta}}_{ri}=&8P(r^2+Q)\sum_{j\in\mathcal{N}_i}\frac{(r^2-\|\mathbf{x}_{rij}\|^2+Q)\mathbf{x}_{rij}^{\mathsf{T}}\dot{\mathbf{x}}_{rij}(\mathbf{x}_{ri}-\mathbf{x}_{rj})}{(r^2-\|\mathbf{x}_{rij}\|^2+Q)^4}\\&+2P(r^2+Q)\sum_{j\in\mathcal{N}_i}\frac{(r^2-\|\mathbf{x}_{rij}\|^2+Q)^2(\dot{\mathbf{x}}_{ri}-\dot{\mathbf{x}}_{rj})}{(r^2-\|\mathbf{x}_{rij}\|^2+Q)^4}\\=&2P(r^2+Q)\sum_{j\in\mathcal{N}_i}\left[\frac{4(\mathbf{x}_{ri}-\mathbf{x}_{rj})^{\mathsf{T}}(\dot{\mathbf{x}}_{ri}-\dot{\mathbf{x}}_{rj})(\mathbf{x}_{ri}-\mathbf{x}_{rj})}{(r^2-\|\mathbf{x}_{rij}\|^2+Q)^3}+\frac{\dot{\mathbf{x}}_{ri}-\dot{\mathbf{x}}_{rj}}{(r^2-\|\mathbf{x}_{rij}\|^2+Q)^2}\right].\end{aligned}$$

It then results in

$$\begin{aligned}\mathbf{s}_i^{\mathsf{T}}\mathbf{M}_{ri}(\mathbf{x}_{ri})\dot{\boldsymbol{\theta}}_{ri}=&\sum_{j\in\mathcal{N}_i}\frac{8P(r^2+Q)}{(r^2-\|\mathbf{x}_{rij}\|^2+Q)^3}\mathbf{s}_i^{\mathsf{T}}\mathbf{M}_{ri}(\mathbf{x}_{ri})(\mathbf{x}_{ri}-\mathbf{x}_{rj})^{\mathsf{T}}(\dot{\mathbf{x}}_{ri}-\dot{\mathbf{x}}_{rj})(\mathbf{x}_{ri}-\mathbf{x}_{rj})\\&+\sum_{j\in\mathcal{N}_i}\frac{2P(r^2+Q)}{(r^2-\|\mathbf{x}_{rij}\|^2+Q)^2}\mathbf{s}_i^{\mathsf{T}}\mathbf{M}_{ri}(\mathbf{x}_{ri})(\dot{\mathbf{x}}_{ri}-\dot{\mathbf{x}}_{rj})\\\leq&+\sum_{j\in\mathcal{N}_i}\left[\frac{64P^2(r^2+Q)^2}{(r^2-\|\mathbf{x}_{rij}\|^2+Q)^6}\frac{\lambda_{ri}^2}{4}\|\mathbf{x}_{ri}-\mathbf{x}_{rj}\|^4\mathbf{s}_i^{\mathsf{T}}\mathbf{s}_i+\dot{\mathbf{x}}_{ri}^{\mathsf{T}}\dot{\mathbf{x}}_{ri}\right.\\&\qquad\left.+\frac{64P^2(r^2+Q)^2}{(r^2-\|\mathbf{x}_{rij}\|^2+Q)^6}\frac{\lambda_{ri}^2}{4}\|\mathbf{x}_{ri}-\mathbf{x}_{rj}\|^4\mathbf{s}_i^{\mathsf{T}}\mathbf{s}_i+\dot{\mathbf{x}}_{rj}^{\mathsf{T}}\dot{\mathbf{x}}_{rj}\right]\\&+\sum_{j\in\mathcal{N}_i}\left[\frac{4P^2(r^2+Q)^2}{(r^2-\|\mathbf{x}_{rij}\|^2+Q)^4}\frac{\lambda_{ri}^2}{4}\mathbf{s}_i^{\mathsf{T}}\mathbf{s}_i+\dot{\mathbf{x}}_{ri}^{\mathsf{T}}\dot{\mathbf{x}}_{ri}\right.\\&\qquad\left.+\frac{4P^2(r^2+Q)^2}{(r^2-\|\mathbf{x}_{rij}\|^2+Q)^4}\frac{\lambda_{ri}^2}{4}\mathbf{s}_i^{\mathsf{T}}\mathbf{s}_i+\dot{\mathbf{x}}_{rj}^{\mathsf{T}}\dot{\mathbf{x}}_{rj}\right]\\=&\sum_{j\in\mathcal{N}_i}\left[\frac{32\lambda_{ri}^2P^2(r^2+Q)^2\|\mathbf{x}_{rij}\|^4}{(r^2-\|\mathbf{x}_{rij}\|^2+Q)^6}\mathbf{s}_i^{\mathsf{T}}\mathbf{s}_i+\dot{\mathbf{x}}_{ri}^{\mathsf{T}}\dot{\mathbf{x}}_{ri}+\dot{\mathbf{x}}_{rj}^{\mathsf{T}}\dot{\mathbf{x}}_{rj}\right]\\&+\sum_{j\in\mathcal{N}_i}\left[\frac{2\lambda_{ri}^2P^2(r^2+Q)^2}{(r^2-\|\mathbf{x}_{rij}\|^2+Q)^4}\mathbf{s}_i^{\mathsf{T}}\mathbf{s}_i+\dot{\mathbf{x}}_{ri}^{\mathsf{T}}\dot{\mathbf{x}}_{ri}+\dot{\mathbf{x}}_{rj}^{\mathsf{T}}\dot{\mathbf{x}}_{rj}\right],\end{aligned}$$

and, similarly, the definition of $\boldsymbol{\theta}_{ri}$ implies that

$$\begin{aligned}\mathbf{s}_i^\mathsf{T}\mathbf{C}_{ri}(\mathbf{x}_{ri},\dot{\mathbf{x}}_{ri})\boldsymbol{\theta}_{ri} &= \sum_{j\in\mathcal{N}_i}\frac{2P(r^2+Q)}{(r^2-\|\mathbf{x}_{rij}\|^2+Q)^2}\mathbf{s}_i^\mathsf{T}\mathbf{C}_{ri}(\mathbf{x}_{ri},\dot{\mathbf{x}}_{ri})(\mathbf{x}_{ri}-\mathbf{x}_{rj})\\ &\le \sum_{j\in\mathcal{N}_i}\left[\frac{4P^2(r^2+Q)^2}{(r^2-\|\mathbf{x}_{rij}\|^2+Q)^4}\frac{c_{ri}^2}{4}\|\mathbf{x}_{ri}-\mathbf{x}_{rj}\|^2\mathbf{s}_i^\mathsf{T}\mathbf{s}_i+\dot{\mathbf{x}}_{ri}^\mathsf{T}\dot{\mathbf{x}}_{ri}\right]\\ &= \sum_{j\in\mathcal{N}_i}\left[\frac{c_{ri}^2P^2(r^2+Q)^2\|\mathbf{x}_{rij}\|^2}{(r^2-\|\mathbf{x}_{rij}\|^2+Q)^4}\mathbf{s}_i^\mathsf{T}\mathbf{s}_i+\dot{\mathbf{x}}_{ri}^\mathsf{T}\dot{\mathbf{x}}_{ri}\right],\end{aligned}$$

for every remote robot $i=1,\cdots,N_r$. The above two inequalities together lead to

$$\mathbf{s}_i^\mathsf{T}\boldsymbol{\Delta}_{rri}=\mathbf{s}_i^\mathsf{T}\mathbf{M}_{ri}(\mathbf{x}_{ri})\dot{\boldsymbol{\theta}}_{ri}+\mathbf{s}_i^\mathsf{T}\mathbf{C}_{ri}(\mathbf{x}_{ri},\dot{\mathbf{x}}_{ri})\boldsymbol{\theta}_{ri}\le\mathbf{s}_i^\mathsf{T}\boldsymbol{\Gamma}_{rri}(t)\mathbf{s}_i+\sum_{j\in\mathcal{N}_i}\left(3\dot{\mathbf{x}}_{ri}^\mathsf{T}\dot{\mathbf{x}}_{ri}+2\dot{\mathbf{x}}_{rj}^\mathsf{T}\dot{\mathbf{x}}_{rj}\right)$$

by $\boldsymbol{\Delta}_{rri}$ defined in (4.5), where $\boldsymbol{\Gamma}_{rri}(t)=\gamma_{rri}(t)\mathbf{I}_n$ with

$$\gamma_{rri}(t)=\sum_{j\in\mathcal{N}_i}\frac{P^2(r^2+Q)^2\left(2\lambda_{ri}^2+c_{ri}^2\|\mathbf{x}_{rij}\|^2\right)}{(r^2-\|\mathbf{x}_{rij}\|^2+Q)^4}+\frac{32\lambda_{ri}^2P^2(r^2+Q)^2\|\mathbf{x}_{rij}\|^4}{(r^2-\|\mathbf{x}_{rij}\|^2+Q)^6},$$

and thus the summation as follows

$$\begin{aligned}\sum_{i=1}^{N_r}\frac{\sigma}{D_{ri}}\mathbf{s}_i^\mathsf{T}\boldsymbol{\Delta}_{rri}\le&\sum_{i=1}^{N_r}\frac{\sigma}{D_{ri}}\mathbf{s}_i^\mathsf{T}\boldsymbol{\Gamma}_{rri}(t)\mathbf{s}_i+\sum_{i=1}^{N_r}\sum_{j\in\mathcal{N}_i}\frac{\sigma}{D_{ri}}\left(3\dot{\mathbf{x}}_{ri}^\mathsf{T}\dot{\mathbf{x}}_{ri}+2\dot{\mathbf{x}}_{rj}^\mathsf{T}\dot{\mathbf{x}}_{rj}\right)\\ =&\sigma\mathbf{s}^\mathsf{T}\mathbf{D}_r^{-1}\boldsymbol{\Gamma}_{rr}(t)\mathbf{s}+\sigma\mathbf{1}_{N_rn}^\mathsf{T}\mathbf{D}_r^{-1}\left[(3\mathbf{D}+2\mathbf{A})\otimes\mathbf{I}_n\right]\dot{\mathbf{x}}_r^2,\end{aligned}\tag{C.2}$$

where $\boldsymbol{\Gamma}_{rr}(t)=\mathrm{Diag}\{\boldsymbol{\Gamma}_{rri}(t)\}$.

The definition of $\boldsymbol{\Delta}_r$ in (4.7) implies that

$$\mathbf{s}^\mathsf{T}\mathbf{D}_r^{-1}\boldsymbol{\Delta}_r=\sum_{i=1}^{N_r}\frac{\eta}{D_{ri}}\mathbf{s}_i^\mathsf{T}\boldsymbol{\Delta}_{lri}+\sum_{i=1}^{N_r}\frac{\sigma}{D_{ri}}\mathbf{s}_i^\mathsf{T}\boldsymbol{\Delta}_{rri}.\tag{C.3}$$

Therefore, adding (C.1)-(C.2) up can bound (C.3) from above by

$$\begin{aligned}\mathbf{s}^\mathsf{T}\mathbf{D}_r^{-1}\boldsymbol{\Delta}_r\le&\eta\mathbf{s}^\mathsf{T}\mathbf{D}_r^{-1}\mathbb{I}^\mathsf{T}\boldsymbol{\Gamma}_{lr}^c(t)\mathbb{I}\mathbf{s}+\eta\dot{\mathbf{x}}_r^\mathsf{T}\mathbf{D}_r^{-1}\mathbb{I}^\mathsf{T}\mathbb{I}\dot{\mathbf{x}}_r+\eta^2\overline{\mathbf{f}}_h^\mathsf{T}\mathbb{I}\mathbf{D}_r^{-1}\mathbb{I}^\mathsf{T}\overline{\mathbf{f}}_h\\ &+\sigma\mathbf{s}^\mathsf{T}\mathbf{D}_r^{-1}\boldsymbol{\Gamma}_{rr}(t)\mathbf{s}+\sigma\mathbf{1}_{N_rn}^\mathsf{T}\mathbf{D}_r^{-1}\left[(3\mathbf{D}+2\mathbf{A})\otimes\mathbf{I}_n\right]\dot{\mathbf{x}}_r^2\\ =&\mathbf{1}_{N_rn}^\mathsf{T}\mathbf{D}_r^{-1}\left[\eta\mathbb{I}^\mathsf{T}\mathbb{I}+\sigma(3\mathbf{D}+2\mathbf{A})\otimes\mathbf{I}_n\right]\dot{\mathbf{x}}_r^2+\mathbf{s}^\mathsf{T}\mathbf{D}_r^{-1}\left[\eta\mathbb{I}^\mathsf{T}\boldsymbol{\Gamma}_{lr}^c(t)\mathbb{I}\right.\\ &\left.+\sigma\boldsymbol{\Gamma}_{rr}(t)\right]\mathbf{s}+\eta^2\overline{\mathbf{f}}_h^\mathsf{T}\mathbb{I}\mathbf{D}_r^{-1}\mathbb{I}^\mathsf{T}\overline{\mathbf{f}}_h.\end{aligned}$$

Appendix D

Derivations of Equation (4.21)

$$
\begin{aligned}
\dot{V}_3 =& \mathbf{s}^{\mathsf{T}}\mathbf{D}_r^{-1}\boldsymbol{\Delta}_r - \eta\dot{\mathbf{x}}_r^{\mathsf{T}}\mathbf{u}_{lr} - \dot{\mathbf{x}}_r^{\mathsf{T}}\dot{\mathbf{x}}_r - \mathbf{s}^{\mathsf{T}}\mathbf{D}_r^{-1}\mathbf{K}_r(t)\mathbf{s} \\
\leq& \mathbf{1}_{N_r n}^{\mathsf{T}}\mathbf{D}_r^{-1}\left[\eta\mathbb{I}^{\mathsf{T}}\mathbb{I} + \sigma(3\mathbf{D}+2\mathbf{A})\otimes\mathbf{I}_n\right]\dot{\mathbf{x}}_r^2 + \mathbf{s}^{\mathsf{T}}\mathbf{D}_r^{-1}\boldsymbol{\Gamma}_1^c(t)\mathbf{s} + \eta^2\overline{\mathbf{f}}_h^{\mathsf{T}}\mathbb{I}\mathbf{D}_r^{-1}\mathbb{I}^{\mathsf{T}}\overline{\mathbf{f}}_h \\
&+ \frac{1}{4}\dot{\mathbf{x}}_r^{\mathsf{T}}\dot{\mathbf{x}}_r + \eta^2\mathbf{u}_{lr}^{\mathsf{T}}\mathbf{u}_{lr} - \dot{\mathbf{x}}_r^{\mathsf{T}}\dot{\mathbf{x}}_r - \mathbf{s}^{\mathsf{T}}\mathbf{D}_r^{-1}\mathbf{K}_r(t)\mathbf{s} - \frac{\sigma\lambda_L}{4k_r}V_3 \\
&+ \frac{\sigma\lambda_L}{4k_r}\left[\frac{k_r}{2\sigma\lambda_L}(2\dot{\mathbf{x}}_r^{\mathsf{T}}\dot{\mathbf{x}}_r + 2\mathbf{s}^{\mathsf{T}}\mathbf{s} + \eta^2\mathbf{u}_{lr}^{\mathsf{T}}\mathbf{u}_{lr}) + \frac{1}{2}\mathbf{s}^{\mathsf{T}}\mathbf{D}_r^{-1}\boldsymbol{\Lambda}_r\mathbf{s}\right] \\
\leq& \eta^2\overline{\mathbf{f}}_h^{\mathsf{T}}\mathbb{I}\mathbf{D}_r^{-1}\mathbb{I}^{\mathsf{T}}\overline{\mathbf{f}}_h + \eta^2\overline{\mathbf{f}}_h^{\mathsf{T}}\mathbb{I}\mathbb{I}^{\mathsf{T}}\overline{\mathbf{f}}_h + \frac{\sigma\lambda_L}{4k_r}\frac{k_r}{2\sigma\lambda_L}\eta^2\overline{\mathbf{f}}_h^{\mathsf{T}}\mathbb{I}\mathbb{I}^{\mathsf{T}}\overline{\mathbf{f}}_h - \frac{\sigma\lambda_L}{4k_r}V_3 \\
&+ \mathbf{1}_{N_r n}^{\mathsf{T}}\mathbf{D}_r^{-1}\left[\eta\mathbb{I}^{\mathsf{T}}\mathbb{I} + \sigma(3\mathbf{D}+2\mathbf{A})\otimes\mathbf{I}_n\right]\dot{\mathbf{x}}_r^2 + \frac{1}{4}\dot{\mathbf{x}}_r^{\mathsf{T}}\dot{\mathbf{x}}_r - \dot{\mathbf{x}}_r^{\mathsf{T}}\dot{\mathbf{x}}_r + \frac{\sigma\lambda_L}{4k_r}\frac{k_r}{2\sigma\lambda_L}2\dot{\mathbf{x}}_r^{\mathsf{T}}\dot{\mathbf{x}}_r \\
&+ \mathbf{s}^{\mathsf{T}}\mathbf{D}_r^{-1}\boldsymbol{\Gamma}_1^c(t)\mathbf{s} - \mathbf{s}^{\mathsf{T}}\mathbf{D}_r^{-1}\mathbf{K}_r(t)\mathbf{s} + \frac{\sigma\lambda_L}{4k_r}\frac{k_r}{2\sigma\lambda_L}2\mathbf{s}^{\mathsf{T}}\mathbf{s} + \frac{\sigma\lambda_L}{4k_r}\frac{1}{2}\mathbf{s}^{\mathsf{T}}\mathbf{D}_r^{-1}\boldsymbol{\Lambda}_r\mathbf{s} \\
=& \overline{\mathbf{f}}_h^{\mathsf{T}}\mathbb{I}\left(\eta^2\mathbf{D}_r^{-1} + \eta^2\mathbf{I}_{N_r n} + \frac{\eta^2}{8}\mathbf{I}_{N_r n}\right)\mathbb{I}^{\mathsf{T}}\overline{\mathbf{f}}_h - \frac{\sigma\lambda_L}{4k_r}V_3 \\
&- \mathbf{s}^{\mathsf{T}}\mathbf{D}_r^{-1}\left[\mathbf{K}_r(t) - \frac{1}{4}\mathbf{D}_r - \frac{\sigma\lambda_L}{8k_r}\boldsymbol{\Lambda}_r - \boldsymbol{\Gamma}_1^c(t)\right]\mathbf{s} \\
&- \mathbf{1}_{N_r n}^{\mathsf{T}}\mathbf{D}_r^{-1}\left[\mathbf{D}_r - \frac{1}{4}\mathbf{D}_r - \frac{1}{4}\mathbf{D}_r - \eta\mathbb{I}^{\mathsf{T}}\mathbb{I} - \sigma(3\mathbf{D}+2\mathbf{A})\otimes\mathbf{I}_n\right]\dot{\mathbf{x}}_r^2 \\
=& \frac{\eta^2}{8}\overline{\mathbf{f}}_h^{\mathsf{T}}\mathbb{I}\left(9\mathbf{I}_{N_r n} + 8\mathbf{D}_r^{-1}\right)\mathbb{I}^{\mathsf{T}}\overline{\mathbf{f}}_h - \mathbf{s}^{\mathsf{T}}\mathbf{D}_r^{-1}\left[\mathbf{K}_r(t) - \frac{\sigma\lambda_L\boldsymbol{\Lambda}_r + 2k_r\mathbf{D}_r}{8k_r} - \boldsymbol{\Gamma}_1^c(t)\right]\mathbf{s} \\
&- \frac{\sigma\lambda_L}{4k_r}V_3 - \frac{1}{2}\mathbf{1}_{N_r n}^{\mathsf{T}}\mathbf{D}_r^{-1}\left[\mathbf{D}_r - 2\eta\mathbb{I}^{\mathsf{T}}\mathbb{I} - 2\sigma(3\mathbf{D}+2\mathbf{A})\otimes\mathbf{I}_n\right]\dot{\mathbf{x}}_r^2 \\
\leq& \frac{\eta^2}{8}\overline{\mathbf{f}}_h^{\mathsf{T}}\mathbb{I}\left(9\mathbf{I}_{N_r n} + 8\mathbf{D}_r^{-1}\right)\mathbb{I}^{\mathsf{T}}\overline{\mathbf{f}}_h - \frac{\sigma\lambda_L}{4k_r}V_3 - \frac{1}{2}\mathbf{1}_{N_r n}^{\mathsf{T}}\mathbf{D}_r^{-1}\mathbf{D}_{cr}\dot{\mathbf{x}}_r^2 - \mathbf{s}^{\mathsf{T}}\mathbf{D}_r^{-1}\mathbf{K}_{cr}(t)\mathbf{s},
\end{aligned}
$$

Appendix E

Feasibility Analysis of Lemma 4.1

Analogous to (4.17), lower bound V_1 by

$$\begin{aligned}
V_1 =& \sum_{(i,j)\in\mathcal{E}} \frac{\sigma(r^2-\|\mathbf{x}_{rij}\|^2+Q)^3}{4P(r^2+Q)^2}\left\|\nabla_i\psi(\|\mathbf{x}_{rij}\|)\right\|^2 \\
\geq& \frac{\sigma Q^3}{4P(r^2+Q)^2}\sum_{(i,j)\in\mathcal{E}}\left\|\nabla_i\psi(\|\mathbf{x}_{rij}\|)\right\|^2 \\
=& \frac{\sigma Q^3}{4P(r^2+Q)^2}\sum_{(i,j)\in\mathcal{E}}\left\|l_{ij}(\mathbf{x}_r)(\mathbf{x}_{ri}-\mathbf{x}_{rj})\right\|^2 \\
=& \frac{\sigma Q^3}{4P(r^2+Q)^2}\left\|\left[\mathbf{W}(\mathbf{x}_r)\otimes\mathbf{I}_n\right]\widetilde{\mathbf{x}}_r\right\|^2 \\
=& \frac{\sigma Q^3}{4P(r^2+Q)^2}\widetilde{\mathbf{x}}_r^{\mathsf{T}}\left[\mathbf{W}(\mathbf{x}_r)\otimes\mathbf{I}_n\right]^{\mathsf{T}}\left[\mathbf{W}(\mathbf{x}_r)\otimes\mathbf{I}_n\right]\widetilde{\mathbf{x}}_r \\
\geq& \frac{\sigma Q^3}{4\overline{\lambda}_L P(r^2+Q)^2}\widetilde{\mathbf{x}}_r^{\mathsf{T}}\left[\mathbf{W}^{\mathsf{T}}(\mathbf{x}_r)\mathbf{L}_e\mathbf{W}(\mathbf{x}_r)\otimes\mathbf{I}_n\right]\widetilde{\mathbf{x}}_r \\
=& \frac{\sigma\overline{k}_r Q}{4\overline{\lambda}_L P}\mathbf{x}_r^{\mathsf{T}}\left[\mathbf{B}\mathbf{W}^{\mathsf{T}}(\mathbf{x}_r)\mathbf{B}^{\mathsf{T}}\mathbf{B}\mathbf{W}(\mathbf{x}_r)\mathbf{B}^{\mathsf{T}}\otimes\mathbf{I}_n\right]\mathbf{x}_r \\
\geq& \frac{\sigma\overline{k}_r Q}{4\overline{\lambda}_L P}\mathbf{x}_r^{\mathsf{T}}\left[\mathbf{L}^{\mathsf{T}}(\mathbf{x}_r)\mathbf{L}(\mathbf{x}_r)\otimes\mathbf{I}_n\right]\mathbf{x}_r,
\end{aligned} \tag{E.1}$$

where $\overline{k}_r = Q^2/(r^2+Q)^2$ and $\overline{\lambda}_L$ is the maximum eigenvalue of $\mathbf{L}_e$. The dynamics (4.4) of Π_1 and the energy (4.13) of Π_2 together limit $V_3(0)$ by

$$V_3(0) \leq V_1(0) + \frac{\lambda_r}{2}\sum_{i=1}^{N_r}\frac{1}{D_{ri}}\mathbf{s}_i^{\mathsf{T}}(0)\mathbf{s}_i(0) = V_1(0) + \frac{\lambda_r}{2}\mathbf{s}^{\mathsf{T}}(0)\mathbf{D}_r^{-1}\mathbf{s}(0)$$

$$
\begin{aligned}
=&V_1(0)+\frac{\lambda_r}{2}\Big(\dot{\mathbf{x}}_r(0)+\sigma\big[\mathbf{L}(\mathbf{x}_r(0))\otimes\mathbf{I}_n\big]\mathbf{x}_r(0)+\eta\mathbf{u}_{lr}(0)\Big)^{\mathsf{T}}\\
&\cdot\mathbf{D}_r^{-1}\Big(\dot{\mathbf{x}}_r(0)+\sigma\big[\mathbf{L}(\mathbf{x}_r(0))\otimes\mathbf{I}_n\big]\mathbf{x}_r(0)+\eta\mathbf{u}_{lr}(0)\Big)\\
=&V_1(0)+\frac{\lambda_r}{2}\Big(\sigma\left[\mathbf{L}(\mathbf{x}_r(0))\otimes\mathbf{I}_n\right]\mathbf{x}_r(0)+\eta\mathbf{u}_{lr}(0)\Big)^{\mathsf{T}}\\
&\cdot\mathbf{D}_r^{-1}\Big(\sigma\left[\mathbf{L}(\mathbf{x}_r(0))\otimes\mathbf{I}_n\right]\mathbf{x}_r(0)+\eta\mathbf{u}_{lr}(0)\Big)\\
\leq&V_1(0)+\lambda_r\Big(\sigma\big[\mathbf{L}(\mathbf{x}_r(0))\otimes\mathbf{I}_n\big]\mathbf{x}_r(0)\Big)^{\mathsf{T}}\mathbf{D}_r^{-1}\Big(\sigma\big[\mathbf{L}(\mathbf{x}_r(0))\otimes\mathbf{I}_n\big]\mathbf{x}_r(0)\Big)\\
&+\lambda_r\big[\eta\mathbf{u}_{lr}(0)\big]^{\mathsf{T}}\mathbf{D}_r^{-1}\big[\eta\mathbf{u}_{lr}(0)\big]\\
\leq&V_1(0)+\frac{\sigma^2\lambda_r}{D_r}\mathbf{x}_r^{\mathsf{T}}(0)\big[\mathbf{L}^{\mathsf{T}}(\mathbf{x}_r(0))\mathbf{L}(\mathbf{x}_r(0))\otimes\mathbf{I}_n\big]\mathbf{x}_r(0)+\frac{\lambda_r\eta^2}{D_r}\mathbf{u}_{lr}^{\mathsf{T}}(0)\mathbf{u}_{lr}(0)\\
\leq&V_1(0)+\frac{\sigma^2\lambda_r}{D_r}\frac{4\overline{\lambda}_L P}{\sigma\overline{k}_r Q}V_1(0)+\frac{\lambda_r\eta^2}{D_r}\overline{\mathbf{f}}_h\mathbb{I}\mathbb{I}^{\mathsf{T}}\overline{\mathbf{f}}_h\\
\leq&\left(1+\frac{4\sigma\lambda_r\overline{\lambda}_L P}{\overline{k}_r D_r Q}\right)V_1(0)+\frac{\lambda_r\eta^2}{D_r}\overline{\mathbf{f}}_h^{\mathsf{T}}\overline{\mathbf{f}}_h
\end{aligned}
$$

with $\lambda_r\mathbf{I}_{N_r n}\succeq\mathbf{\Lambda}_r$ and $\mathbf{D}_r\succeq D_r\mathbf{I}_{N_r n}$. Then, the condition (4.22) can be ensured by

$$
\begin{aligned}
&V_3(0)+\frac{k_r\eta^2}{2\sigma\lambda_L}\overline{\mathbf{f}}_h^{\mathsf{T}}\mathbb{I}\left(9\mathbf{I}_{N_r n}+8\mathbf{D}_r^{-1}\right)\mathbb{I}^{\mathsf{T}}\overline{\mathbf{f}}_h\\
\leq&\left(1+\frac{4\sigma\lambda_r\overline{\lambda}_L P}{\overline{k}_r D_r Q}\right)V_1(0)+\frac{\lambda_r\eta^2}{D_r}\overline{\mathbf{f}}_h^{\mathsf{T}}\overline{\mathbf{f}}_h+\frac{k_r\eta^2}{2\sigma\lambda_L}\overline{\mathbf{f}}_h^{\mathsf{T}}\mathbb{I}\left(9+\frac{8}{D_r}\right)\mathbb{I}^{\mathsf{T}}\overline{\mathbf{f}}_h\\
=&\left(1+\frac{4\sigma\lambda_r\overline{\lambda}_L P}{\overline{k}_r D_r Q}\right)V_1(0)+\left[\frac{\lambda_r\eta^2}{D_r}+\frac{k_r\eta^2(9D_r+8)}{2\sigma\lambda_L D_r}\right]\overline{\mathbf{f}}_h^{\mathsf{T}}\overline{\mathbf{f}}_h<\sigma\psi_{\max},
\end{aligned}
$$

which is equivalent to

$$
V_1(0)+\frac{1}{\left(1+\frac{4\sigma\lambda_r\overline{\lambda}_L P}{\overline{k}_r D_r Q}\right)}\left[\frac{\lambda_r\eta^2}{D_r}+\frac{k_r\eta^2(9D_r+8)}{2\sigma\lambda_L D_r}\right]\overline{\mathbf{f}}_h^{\mathsf{T}}\overline{\mathbf{f}}_h<\frac{\sigma\psi_{\max}}{\left(1+\frac{4\sigma\lambda_r\overline{\lambda}_L P}{\overline{k}_r D_r Q}\right)}.
$$

In the above inequality, the left-hand side is upper-bounded by

$$
\begin{aligned}
&V_1(0)+\frac{1}{\frac{4\sigma\lambda_r\overline{\lambda}_L P}{\overline{k}_r D_r Q}}\frac{\lambda_r\eta^2}{D_r}\overline{\mathbf{f}}_h^{\mathsf{T}}\overline{\mathbf{f}}_h+\frac{k_r\eta^2(9D_r+8)}{2\sigma\lambda_L D_r}\overline{\mathbf{f}}_h^{\mathsf{T}}\overline{\mathbf{f}}_h\\
\leq&V_1(0)+\frac{\overline{k}_r D_r Q}{4\sigma\lambda_r\overline{\lambda}_L P}\frac{\lambda_r\eta^2}{D_r}\overline{\mathbf{f}}_h^{\mathsf{T}}\overline{\mathbf{f}}_h+\frac{k_r\eta^2(9D_r+8)}{2\sigma\lambda_L D_r}\overline{\mathbf{f}}_h^{\mathsf{T}}\overline{\mathbf{f}}_h\\
=&V_1(0)+\frac{\eta^2}{\sigma}\left[\frac{\overline{k}_r Q}{4\overline{\lambda}_L P}+\frac{k_r(9D_r+8)}{2\lambda_L D_r}\right]\overline{\mathbf{f}}_h^{\mathsf{T}}\overline{\mathbf{f}}_h,
\end{aligned}
$$

while the right-hand side approaches $\sigma\psi_{\max}$ as D_r increases. Therefore, the condition (4.22) can be guaranteed by

$$V_1(0) + \alpha \overline{\mathbf{f}}_h^{\mathsf{T}} \overline{\mathbf{f}}_h < \widehat{\sigma}\psi_{\max}, \tag{E.2}$$

where α is upper-bounded by

$$\alpha \leq \frac{\eta^2}{\sigma}\left[\frac{\overline{k}_r Q}{4\overline{\lambda}_L P} + \frac{k_r(9D_r+8)}{2\lambda_L D_r}\right] = \overline{\alpha},$$

and $\widehat{\sigma}$ approaches σ as D_r increases:

$$\widehat{\sigma} = \frac{\sigma \overline{k}_r D_r Q}{\overline{k}_r D_r Q + 4\sigma\lambda_r \overline{\lambda}_L P}.$$

Therefore, after choosing σ and η and letting $\Delta = \overline{\alpha}\overline{\mathbf{f}}_h^{\mathsf{T}}\overline{\mathbf{f}}_h$, Proposition 4.1 shows how to select P and Q such that $V_1(0) + \Delta < \sigma\psi_{\max}$. Then, there exist some damping gains $\mathbf{D}_r$ with D_r sufficiently large to ensure (E.2), and thus (4.22), and $\mathbf{D}_{cr} \succeq \mathbf{0}$.

Appendix F

Derivations of Equation (4.29)

By the definition of $\mathbf{\Delta}_{lri}$ in (4.5), its impact on the closed-loop passivity can be requantified by

$$\begin{aligned}
\mathbf{s}_i^{\mathsf{T}}\mathbf{\Delta}_{lri} =& K_{lri}\mathbf{s}_i^{\mathsf{T}}\mathbf{M}_{ri}(\mathbf{x}_{ri})\overline{\mathbf{F}}_{hi}\Big[\mathbf{I}_n - \mathrm{diag}\big\{\tanh^2\big[K_{lri}(\mathbf{x}_{ri}-\mathbf{x}_{li})\big]\big\}\Big]\big(\dot{\mathbf{x}}_{ri}-\dot{\mathbf{x}}_{li}\big)\\
&+\mathbf{s}_i^{\mathsf{T}}\mathbf{C}_{ri}(\mathbf{x}_{ri},\dot{\mathbf{x}}_{ri})\overline{\mathbf{F}}_{hi}\cdot\tanh\big[K_{lri}(\mathbf{x}_{ri}-\mathbf{x}_{li})\big]\\
\le& \frac{\lambda_{ri}^2}{4}K_{lri}^2\mathbf{s}_i^{\mathsf{T}}\overline{\mathbf{F}}_{hi}^2\Big[\mathbf{I}_n - \mathrm{diag}\big\{\tanh^2\big[K_{lri}(\mathbf{x}_{ri}-\mathbf{x}_{li})\big]\big\}\Big]^2\mathbf{s}_i + \dot{\mathbf{x}}_{ri}^{\mathsf{T}}\dot{\mathbf{x}}_{ri}\\
&+\frac{\lambda_{ri}^2}{4}K_{lri}^2\mathbf{s}_i^{\mathsf{T}}\overline{\mathbf{F}}_{hi}^2\Big[\mathbf{I}_n - \mathrm{diag}\big\{\tanh^2\big[K_{lri}(\mathbf{x}_{ri}-\mathbf{x}_{li})\big]\big\}\Big]^2\mathbf{s}_i + \dot{\mathbf{x}}_{li}^{\mathsf{T}}\dot{\mathbf{x}}_{li}\\
&+\frac{c_{ri}^2}{4}\mathbf{s}_i^{\mathsf{T}}\overline{\mathbf{F}}_{hi}^2\cdot\mathrm{diag}\Big\{\tanh^2\big[K_{lri}(\mathbf{x}_{ri}-\mathbf{x}_{li})\big]\Big\}\mathbf{s}_i + \dot{\mathbf{x}}_{ri}^{\mathsf{T}}\dot{\mathbf{x}}_{ri}\\
=& \mathbf{s}_i^{\mathsf{T}}\mathbf{\Gamma}_{lri}^p(t)\mathbf{s}_i + \dot{\mathbf{x}}_{li}^{\mathsf{T}}\dot{\mathbf{x}}_{li} + 2\dot{\mathbf{x}}_{ri}^{\mathsf{T}}\dot{\mathbf{x}}_{ri}
\end{aligned}$$

for the leader remote robots $i = 1, \cdots, N_l$, where

$$\begin{aligned}
\mathbf{\Gamma}_{lri}^p(t) =& \frac{\lambda_{ri}^2}{2}K_{lri}^2\overline{\mathbf{F}}_{hi}^2\Big[\mathbf{I}_n - \mathrm{diag}\big\{\tanh^2\big[K_{lri}(\mathbf{x}_{ri}-\mathbf{x}_{li})\big]\big\}\Big]^2\\
&+\frac{c_{ri}^2}{4}\overline{\mathbf{F}}_{hi}^2\cdot\mathrm{diag}\Big\{\tanh^2\big[K_{lri}(\mathbf{x}_{ri}-\mathbf{x}_{li})\big]\Big\},
\end{aligned}$$

and $\mathbf{s}_i^{\mathsf{T}}\mathbf{\Delta}_{lri} = 0$ for the follower remote robots $i = N_l+1, \cdots, N_r$. It follows then that

$$\begin{aligned}
\sum_{i=1}^{N_r}\frac{\eta}{D_{ri}}\mathbf{s}_i^{\mathsf{T}}\mathbf{\Delta}_{lri} \le& \sum_{i=1}^{N_l}\frac{\eta}{D_{ri}}\mathbf{s}_i^{\mathsf{T}}\mathbf{\Gamma}_{lri}^p(t)\mathbf{s}_i + \sum_{i=1}^{N_l}\frac{\eta}{D_{ri}}\dot{\mathbf{x}}_{li}^{\mathsf{T}}\dot{\mathbf{x}}_{li} + \sum_{i=1}^{N_l}\frac{2\eta}{D_{ri}}\dot{\mathbf{x}}_{ri}^{\mathsf{T}}\dot{\mathbf{x}}_{ri}\\
=& \eta\mathbf{s}^{\mathsf{T}}\mathbf{D}_r^{-1}\mathbb{I}^{\mathsf{T}}\mathbf{\Gamma}_{lr}^p(t)\mathbb{I}\mathbf{s} + \eta\dot{\mathbf{x}}_l^{\mathsf{T}}\mathbb{I}\mathbf{D}_r^{-1}\mathbb{I}^{\mathsf{T}}\dot{\mathbf{x}}_l + 2\eta\dot{\mathbf{x}}_r^{\mathsf{T}}\mathbf{D}_r^{-1}\mathbb{I}^{\mathsf{T}}\mathbb{I}\dot{\mathbf{x}}_r,
\end{aligned} \tag{F.1}$$

where $\mathbf{\Gamma}_{lr}^{p}(t) = \mathrm{Diag}\big\{\mathbf{\Gamma}_{lri}^{p}(t)\big\}$.

Using (C.3), the sum of (C.2) and (F.1) gives that

$$\begin{aligned}
\mathbf{s}^{\mathsf{T}}\mathbf{D}_r^{-1}\mathbf{\Delta}_r \leq & \eta\mathbf{s}^{\mathsf{T}}\mathbf{D}_r^{-1}\mathbb{I}^{\mathsf{T}}\mathbf{\Gamma}_{lr}^{p}(t)\mathbb{I}\mathbf{s} + \eta\dot{\mathbf{x}}_l^{\mathsf{T}}\mathbb{I}\mathbf{D}_r^{-1}\mathbb{I}^{\mathsf{T}}\dot{\mathbf{x}}_l + 2\eta\dot{\mathbf{x}}_r^{\mathsf{T}}\mathbf{D}_r^{-1}\mathbb{I}^{\mathsf{T}}\mathbb{I}\dot{\mathbf{x}}_r \\
& + \sigma\mathbf{s}^{\mathsf{T}}\mathbf{D}_r^{-1}\mathbf{\Gamma}_{rr}(t)\mathbf{s} + \sigma\mathbf{1}_{N_r n}^{\mathsf{T}}\mathbf{D}_r^{-1}\big[(3\mathbf{D}+2\mathbf{A})\otimes\mathbf{I}_n\big]\dot{\mathbf{x}}_r^2 \\
= & \eta\dot{\mathbf{x}}_l^{\mathsf{T}}\mathbb{I}\mathbf{D}_r^{-1}\mathbb{I}^{\mathsf{T}}\dot{\mathbf{x}}_l + \mathbf{1}_{N_r n}^{\mathsf{T}}\mathbf{D}_r^{-1}\big[2\eta\mathbb{I}^{\mathsf{T}}\mathbb{I} + \sigma(3\mathbf{D}+2\mathbf{A})\otimes\mathbf{I}_n\big]\dot{\mathbf{x}}_r^2 \\
& + \mathbf{s}^{\mathsf{T}}\mathbf{D}_r^{-1}\Big[\eta\mathbb{I}^{\mathsf{T}}\mathbf{\Gamma}_{lr}^{p}(t)\mathbb{I} + \sigma\mathbf{\Gamma}_{rr}(t)\Big]\mathbf{s}
\end{aligned}$$

Appendix G

Derivations of Equation (4.40)

By the definition of $\boldsymbol{\Delta}_{cri}$ given in (4.33),

$$\begin{aligned}\boldsymbol{\Delta}_{cri} =&\mathbf{M}_{ri}(\mathbf{x}_{ri})\dot{\boldsymbol{\theta}}_{cri} + \mathbf{C}_{ri}(\mathbf{x}_{ri},\dot{\mathbf{x}}_{ri})\boldsymbol{\theta}_{cri}\\ =&K_{cri}\mathbf{M}_{ri}(\mathbf{x}_{ri})\overline{\mathbf{F}}_{hi}\Big[\mathbf{I}_n - \mathrm{diag}\big\{\tanh^2[K_{cri}(\mathbf{x}_{ri}-\boldsymbol{\xi}_i)]\big\}\Big]\big(\dot{\mathbf{x}}_{ri}-\dot{\boldsymbol{\xi}}_i\big)\\ &+\mathbf{C}_{ri}(\mathbf{x}_{ri},\dot{\mathbf{x}}_{ri})\overline{\mathbf{F}}_{hi}\cdot\tanh[K_{cri}(\mathbf{x}_{ri}-\boldsymbol{\xi}_i)]\end{aligned}$$

for the leader remote robots $i = 1,\cdots,N_l$, while $\boldsymbol{\Delta}_{cri} = \mathbf{0}$ for the follower remote robots $i = N_l+1,\cdots,N_r$. As a result,

$$\begin{aligned}\mathbf{s}_i^{\mathsf{T}}\boldsymbol{\Delta}_{cri} =&K_{cri}\mathbf{s}_i^{\mathsf{T}}\mathbf{M}_{ri}(\mathbf{x}_{ri})\overline{\mathbf{F}}_{hi}\Big[\mathbf{I}_n - \mathrm{diag}\big\{\tanh^2[K_{cri}(\mathbf{x}_{ri}-\boldsymbol{\xi}_i)]\big\}\Big]\big(\dot{\mathbf{x}}_{ri}-\dot{\boldsymbol{\xi}}_i\big)\\ &+\mathbf{s}_i^{\mathsf{T}}\mathbf{C}_{ri}(\mathbf{x}_{ri},\dot{\mathbf{x}}_{ri})\overline{\mathbf{F}}_{hi}\cdot\tanh[K_{cri}(\mathbf{x}_{ri}-\boldsymbol{\xi}_i)]\\ \le&\frac{\lambda_{ri}^2}{4\eta}K_{cri}^2\big\|\dot{\mathbf{x}}_{ri}-\dot{\boldsymbol{\xi}}_i\big\|^2\mathbf{s}_i^{\mathsf{T}}\Big[\mathbf{I}_n - \mathrm{diag}\big\{\tanh^2[K_{cri}(\mathbf{x}_{ri}-\boldsymbol{\xi}_i)]\big\}\Big]^2\mathbf{s}_i + \eta\overline{\mathbf{f}}_{hi}^{\mathsf{T}}\overline{\mathbf{f}}_{hi}\\ &+\frac{c_{ri}^2}{4}\mathbf{s}_i^{\mathsf{T}}\overline{\mathbf{F}}_{hi}^2\cdot\mathrm{diag}\big\{\tanh^2[K_{cri}(\mathbf{x}_{ri}-\boldsymbol{\xi}_i)]\big\}\mathbf{s}_i + \dot{\mathbf{x}}_{ri}^{\mathsf{T}}\dot{\mathbf{x}}_{ri}\\ =&\mathbf{s}_i^{\mathsf{T}}\boldsymbol{\Gamma}_{cri}^c(t)\mathbf{s}_i + \dot{\mathbf{x}}_{ri}^{\mathsf{T}}\dot{\mathbf{x}}_{ri} + \eta\overline{\mathbf{f}}_{hi}\overline{\mathbf{f}}_{hi}\end{aligned}$$

for the leader remote robots $i = 1,\cdots,N_l$, where

$$\begin{aligned}\boldsymbol{\Gamma}_{cri}^c(t) =&\frac{\lambda_{ri}^2}{4\eta}K_{cri}^2\big\|\dot{\mathbf{x}}_{ri}-\dot{\boldsymbol{\xi}}_i\big\|^2\Big[\mathbf{I}_n - \mathrm{diag}\big\{\tanh^2[K_{cri}(\mathbf{x}_{ri}-\boldsymbol{\xi}_i)]\big\}\Big]^2\\ &+\frac{c_{ri}^2}{4}\overline{\mathbf{F}}_{hi}^2\cdot\mathrm{diag}\big\{\tanh^2[K_{cri}(\mathbf{x}_{ri}-\boldsymbol{\xi}_i)]\big\},\end{aligned}$$

while $\mathbf{s}_i^\mathsf{T}\boldsymbol{\Delta}_{cri}=0$ for the follower remote robots $i=N_l+1,\cdots,N_r$. It gives, in sum, that

$$\begin{aligned}\sum_{i=1}^{N_r}\frac{\eta}{D_{ri}}\mathbf{s}_i^\mathsf{T}\boldsymbol{\Delta}_{cri}\leq&\sum_{i=1}^{N_l}\frac{\eta}{D_{ri}}\mathbf{s}_i^\mathsf{T}\boldsymbol{\Gamma}_{cri}^c(t)\mathbf{s}_i+\sum_{i=1}^{N_l}\frac{\eta}{D_{ri}}\dot{\mathbf{x}}_{ri}^\mathsf{T}\dot{\mathbf{x}}_{ri}+\sum_{i=1}^{N_l}\frac{\eta^2}{D_{ri}}\overline{\mathbf{f}}_{hi}^\mathsf{T}\overline{\mathbf{f}}_{hi}\\=&\eta\mathbf{s}^\mathsf{T}\mathbf{D}_r^{-1}\mathbb{I}^\mathsf{T}\boldsymbol{\Gamma}_{cr}^c(t)\mathbb{I}\mathbf{s}+\eta\dot{\mathbf{x}}_r^\mathsf{T}\mathbf{D}_r^{-1}\mathbb{I}^\mathsf{T}\mathbb{I}\dot{\mathbf{x}}_r+\eta^2\overline{\mathbf{f}}_h^\mathsf{T}\mathbb{I}\mathbf{D}_r^{-1}\mathbb{I}^\mathsf{T}\overline{\mathbf{f}}_h,\end{aligned}\tag{G.1}$$

where $\boldsymbol{\Gamma}_{cr}^c(t)=\mathrm{Diag}\big\{\boldsymbol{\Gamma}_{cri}^c(t)\big\}$.

With $\widehat{\boldsymbol{\Delta}}_r$ defined in (4.35), it follows that

$$\mathbf{s}^\mathsf{T}\mathbf{D}_r^{-1}\widehat{\boldsymbol{\Delta}}_r=\sum_{i=1}^{N_r}\frac{\eta}{D_{ri}}\mathbf{s}_i^\mathsf{T}\boldsymbol{\Delta}_{cri}+\sum_{i=1}^{N_r}\frac{\sigma}{D_{ri}}\mathbf{s}_i^\mathsf{T}\boldsymbol{\Delta}_{rri},\tag{G.2}$$

and further, by (C.2) and (G.1), that

$$\begin{aligned}\mathbf{s}^\mathsf{T}\mathbf{D}_r^{-1}\widehat{\boldsymbol{\Delta}}_r\leq&\eta\mathbf{s}^\mathsf{T}\mathbf{D}_r^{-1}\mathbb{I}^\mathsf{T}\boldsymbol{\Gamma}_{cr}^c(t)\mathbb{I}\mathbf{s}+\eta\dot{\mathbf{x}}_r^\mathsf{T}\mathbf{D}_r^{-1}\mathbb{I}^\mathsf{T}\mathbb{I}\dot{\mathbf{x}}_r+\eta^2\overline{\mathbf{f}}_h^\mathsf{T}\mathbb{I}\mathbf{D}_r^{-1}\mathbb{I}^\mathsf{T}\overline{\mathbf{f}}_h\\&+\sigma\mathbf{s}^\mathsf{T}\mathbf{D}_r^{-1}\boldsymbol{\Gamma}_{rr}(t)\mathbf{s}+\sigma\mathbf{1}_{N_rn}^\mathsf{T}\mathbf{D}_r^{-1}\big[(3\mathbf{D}+2\mathbf{A})\otimes\mathbf{I}_n\big]\dot{\mathbf{x}}_r^2\\=&\mathbf{1}_{N_rn}^\mathsf{T}\mathbf{D}_r^{-1}\big[\eta\mathbb{I}^\mathsf{T}\mathbb{I}+\sigma(3\mathbf{D}+2\mathbf{A})\otimes\mathbf{I}_n\big]\dot{\mathbf{x}}_r^2\\&+\mathbf{s}^\mathsf{T}\mathbf{D}_r^{-1}\Big[\eta\mathbb{I}^\mathsf{T}\boldsymbol{\Gamma}_{cr}^c(t)\mathbb{I}+\sigma\boldsymbol{\Gamma}_{rr}(t)\Big]\mathbf{s}+\eta^2\overline{\mathbf{f}}_h^\mathsf{T}\mathbb{I}\mathbf{D}_r^{-1}\mathbb{I}^\mathsf{T}\overline{\mathbf{f}}_h.\end{aligned}$$

Appendix H

Derivations of Equation (4.43)

$$
\begin{aligned}
\dot{V}_3 \leq & \mathbf{1}_{N_r n}^{\mathsf{T}} \mathbf{D}_r^{-1} \left[\eta \mathbb{I}^{\mathsf{T}} \mathbb{I} + \sigma(3\mathbf{D} + 2\mathbf{A}) \otimes \mathbf{I}_n\right] \dot{\mathbf{x}}_r^2 + \mathbf{s}^{\mathsf{T}} \mathbf{D}_r^{-1} \boldsymbol{\Gamma}_2^c(t) \mathbf{s} + \eta^2 \overline{\mathbf{f}}_h^{\mathsf{T}} \mathbb{I} \mathbf{D}_r^{-1} \mathbb{I}^{\mathsf{T}} \overline{\mathbf{f}}_h \\
& + \frac{1}{4} \dot{\mathbf{x}}_r^{\mathsf{T}} \dot{\mathbf{x}}_r + \eta^2 \mathbf{u}_{cr}^{\mathsf{T}} \mathbf{u}_{cr} - \dot{\mathbf{x}}_r^{\mathsf{T}} \dot{\mathbf{x}}_r - \mathbf{s}^{\mathsf{T}} \mathbf{D}_r^{-1} \mathbf{K}_r(t) \mathbf{s} - \frac{\sigma \lambda_L}{4 k_r} V_3 \\
& + \frac{\sigma \lambda_L}{4 k_r} \left[\frac{k_r}{2 \sigma \lambda_L} \left(2 \dot{\mathbf{x}}_r^{\mathsf{T}} \dot{\mathbf{x}}_r + 2 \mathbf{s}^{\mathsf{T}} \mathbf{s} + \eta^2 \mathbf{u}_{cr}^{\mathsf{T}} \mathbf{u}_{cr} \right) + \frac{1}{2} \mathbf{s}^{\mathsf{T}} \mathbf{D}_r^{-1} \boldsymbol{\Lambda}_r \mathbf{s} \right] \\
\leq & \eta^2 \overline{\mathbf{f}}_h^{\mathsf{T}} \mathbb{I} \mathbf{D}_r^{-1} \mathbb{I}^{\mathsf{T}} \overline{\mathbf{f}}_h + \eta^2 \overline{\mathbf{f}}_h^{\mathsf{T}} \mathbb{I} \mathbb{I}^{\mathsf{T}} \overline{\mathbf{f}}_h + \frac{\sigma \lambda_L}{4 k_r} \frac{k_r}{2 \sigma \lambda_L} \eta^2 \overline{\mathbf{f}}_h^{\mathsf{T}} \mathbb{I} \mathbb{I}^{\mathsf{T}} \overline{\mathbf{f}}_h - \frac{\sigma \lambda_L}{4 k_r} V_3 \\
& + \mathbf{1}_{N_r n}^{\mathsf{T}} \mathbf{D}_r^{-1} \left[\eta \mathbb{I}^{\mathsf{T}} \mathbb{I} + \sigma(3\mathbf{D} + 2\mathbf{A}) \otimes \mathbf{I}_n\right] \dot{\mathbf{x}}_r^2 + \frac{1}{4} \dot{\mathbf{x}}_r^{\mathsf{T}} \dot{\mathbf{x}}_r - \dot{\mathbf{x}}_r^{\mathsf{T}} \dot{\mathbf{x}}_r + \frac{\sigma \lambda_L}{4 k_r} \frac{k_r}{2 \sigma \lambda_L} 2 \dot{\mathbf{x}}_r^{\mathsf{T}} \dot{\mathbf{x}}_r \\
& + \mathbf{s}^{\mathsf{T}} \mathbf{D}_r^{-1} \boldsymbol{\Gamma}_2^c(t) \mathbf{s} - \mathbf{s}^{\mathsf{T}} \mathbf{D}_r^{-1} \mathbf{K}_r(t) \mathbf{s} + \frac{\sigma \lambda_L}{4 k_r} \frac{k_r}{2 \sigma \lambda_L} 2 \mathbf{s}^{\mathsf{T}} \mathbf{s} + \frac{\sigma \lambda_L}{4 k_r} \frac{1}{2} \mathbf{s}^{\mathsf{T}} \mathbf{D}_r^{-1} \boldsymbol{\Lambda}_r \mathbf{s} \\
= & \overline{\mathbf{f}}_h^{\mathsf{T}} \mathbb{I} \left(\eta^2 \mathbf{D}_r^{-1} + \eta^2 \mathbf{I}_{N_r n} + \frac{\eta^2}{8} \mathbf{I}_{N_r n} \right) \mathbb{I}^{\mathsf{T}} \overline{\mathbf{f}}_h - \frac{\sigma \lambda_L}{4 k_r} V_3 \\
& - \mathbf{1}_{N_r n}^{\mathsf{T}} \mathbf{D}_r^{-1} \left[\mathbf{D}_r - \frac{1}{4} \mathbf{D}_r - \frac{1}{4} \mathbf{D}_r - \eta \mathbb{I}^{\mathsf{T}} \mathbb{I} - \sigma(3\mathbf{D} + 2\mathbf{A}) \otimes \mathbf{I}_n \right] \dot{\mathbf{x}}_r^2 \\
& - \mathbf{s}^{\mathsf{T}} \mathbf{D}_r^{-1} \Big[\mathbf{K}_r(t) - \frac{1}{4} \mathbf{D}_r - \frac{\sigma \lambda_L}{8 k_r} \boldsymbol{\Lambda}_r - \boldsymbol{\Gamma}_2^c(t) \Big] \mathbf{s} \\
= & \frac{\eta^2}{8} \overline{\mathbf{f}}_h^{\mathsf{T}} \mathbb{I} \big(9 \mathbf{I}_{N_r n} + 8 \mathbf{D}_r^{-1} \big) \mathbb{I}^{\mathsf{T}} \overline{\mathbf{f}}_h - \frac{\sigma \lambda_L}{4 k_r} V_3 \\
& - \frac{1}{2} \mathbf{1}_{N_r n}^{\mathsf{T}} \mathbf{D}_r^{-1} \Big[\mathbf{D}_r - 2 \eta \mathbb{I}^{\mathsf{T}} \mathbb{I} - 2 \sigma (3\mathbf{D} + 2\mathbf{A}) \otimes \mathbf{I}_n \Big] \dot{\mathbf{x}}_r^2 \\
& - \mathbf{s}^{\mathsf{T}} \mathbf{D}_r^{-1} \left[\mathbf{K}_r(t) - \frac{\sigma \lambda_L \boldsymbol{\Lambda}_r + 2 k_r \mathbf{D}_r}{8 k_r} - \boldsymbol{\Gamma}_2^c(t) \right] \mathbf{s} \\
\leq & \frac{\eta^2}{8} \overline{\mathbf{f}}_h^{\mathsf{T}} \mathbb{I} \left(9 \mathbf{I}_{N_r n} + 8 \mathbf{D}_r^{-1} \right) \mathbb{I}^{\mathsf{T}} \overline{\mathbf{f}}_h - \frac{\sigma \lambda_L}{4 k_r} V_3 - \frac{1}{2} \mathbf{1}_{N_r n}^{\mathsf{T}} \mathbf{D}_r^{-1} \widehat{\mathbf{D}}_{cr} \dot{\mathbf{x}}_r^2 - \mathbf{s}^{\mathsf{T}} \mathbf{D}_r^{-1} \widehat{\mathbf{K}}_{cr}(t) \mathbf{s},
\end{aligned}
$$

Appendix I

Derivations of Equation (4.45)

The impact of $\boldsymbol{\Delta}_{cri}$ on the closed-loop passivity is assessed as follows:

$$\begin{aligned}
\mathbf{s}_i^{\mathsf{T}}\boldsymbol{\Delta}_{cri} =& K_{cri}\mathbf{s}_i^{\mathsf{T}}\mathbf{M}_{ri}(\mathbf{x}_{ri})\overline{\mathbf{F}}_{hi}\Big[\mathbf{I}_n - \mathrm{diag}\big\{\tanh^2[K_{cri}(\mathbf{x}_{ri}-\boldsymbol{\xi}_i)]\big\}\Big](\dot{\mathbf{x}}_{ri}-\dot{\boldsymbol{\xi}}_i)\\
&+\mathbf{s}_i^{\mathsf{T}}\mathbf{C}_{ri}(\mathbf{x}_{ri},\dot{\mathbf{x}}_{ri})\overline{\mathbf{F}}_{hi}\cdot\tanh[K_{cri}(\mathbf{x}_{ri}-\boldsymbol{\xi}_i)]\\
\leq& \frac{\lambda_{ri}^2}{4}K_{cri}^2\mathbf{s}_i^{\mathsf{T}}\overline{\mathbf{F}}_{hi}^2\Big[\mathbf{I}_n - \mathrm{diag}\big\{\tanh^2[K_{cri}(\mathbf{x}_{ri}-\boldsymbol{\xi}_i)]\big\}\Big]^2\mathbf{s}_i + \dot{\mathbf{x}}_{ri}^{\mathsf{T}}\dot{\mathbf{x}}_{ri}\\
&+\frac{\lambda_{ri}^2}{4}K_{cri}^2\mathbf{s}_i^{\mathsf{T}}\overline{\mathbf{F}}_{hi}^2\Big[\mathbf{I}_n - \mathrm{diag}\big\{\tanh^2[K_{cri}(\mathbf{x}_{ri}-\boldsymbol{\xi}_i)]\big\}\Big]^2\mathbf{s}_i + \dot{\boldsymbol{\xi}}_i^{\mathsf{T}}\dot{\boldsymbol{\xi}}_i\\
&+\frac{c_{ri}^2}{4}\mathbf{s}_i^{\mathsf{T}}\overline{\mathbf{F}}_{hi}^2\cdot\mathrm{diag}\big\{\tanh^2[K_{cri}(\mathbf{x}_{ri}-\boldsymbol{\xi}_i)]\big\}\mathbf{s}_i + \dot{\mathbf{x}}_{ri}^{\mathsf{T}}\dot{\mathbf{x}}_{ri}\\
=& \mathbf{s}_i^{\mathsf{T}}\boldsymbol{\Gamma}_{cri}^p(t)\mathbf{s}_i + 2\dot{\mathbf{x}}_{ri}^{\mathsf{T}}\dot{\mathbf{x}}_{ri} + \dot{\boldsymbol{\xi}}_i^{\mathsf{T}}\dot{\boldsymbol{\xi}}_i
\end{aligned}$$

for the leader remote robots $i = 1, \cdots, N_l$, where

$$\begin{aligned}
\boldsymbol{\Gamma}_{cri}^p(t) =& \frac{\lambda_{ri}^2}{2}K_{cri}^2\overline{\mathbf{F}}_{hi}^2\Big[\mathbf{I}_n - \mathrm{diag}\big\{\tanh^2[K_{cri}(\mathbf{x}_{ri}-\boldsymbol{\xi}_i)]\big\}\Big]^2\\
&+\frac{c_{ri}^2}{4}\overline{\mathbf{F}}_{hi}^2\cdot\mathrm{diag}\big\{\tanh^2[K_{cri}(\mathbf{x}_{ri}-\boldsymbol{\xi}_i)]\big\},
\end{aligned}$$

while $\mathbf{s}_i^{\mathsf{T}}\boldsymbol{\Delta}_{cri} = 0$ for the follower remote robots $i = N_l+1, \cdots, N_r$. And, in total,

$$\begin{aligned}
\sum_{i=1}^{N_r}\frac{\eta}{D_{ri}}\mathbf{s}_i^{\mathsf{T}}\boldsymbol{\Delta}_{cri} \leq& \sum_{i=1}^{N_l}\frac{\eta}{D_{ri}}\mathbf{s}_i^{\mathsf{T}}\boldsymbol{\Gamma}_{cri}^p(t)\mathbf{s}_i + \sum_{i=1}^{N_l}\frac{2\eta}{D_{ri}}\dot{\mathbf{x}}_{ri}^{\mathsf{T}}\dot{\mathbf{x}}_{ri} + \sum_{i=1}^{N_l}\frac{\eta}{D_{ri}}\dot{\boldsymbol{\xi}}_i^{\mathsf{T}}\dot{\boldsymbol{\xi}}_i\\
=& \eta\mathbf{s}^{\mathsf{T}}\mathbf{D}_r^{-1}\mathbb{I}^{\mathsf{T}}\boldsymbol{\Gamma}_{cr}^p(t)\mathbb{I}\mathbf{s} + 2\eta\dot{\mathbf{x}}_r^{\mathsf{T}}\mathbf{D}_r^{-1}\mathbb{I}^{\mathsf{T}}\mathbb{I}\dot{\mathbf{x}}_r + \eta\dot{\boldsymbol{\xi}}^{\mathsf{T}}\mathbb{I}\mathbf{D}_r^{-1}\mathbb{I}^{\mathsf{T}}\dot{\boldsymbol{\xi}},
\end{aligned} \tag{I.1}$$

where $\boldsymbol{\Gamma}_{cr}^p(t) = \mathrm{Diag}\big\{\boldsymbol{\Gamma}_{cri}^p(t)\big\}$.

Together, (C.2) and (I.1) bound (G.2) from above by

$$\begin{aligned}\mathbf{s}^\intercal \mathbf{D}_r^{-1} \widehat{\boldsymbol{\Delta}}_r \leq & \eta \mathbf{s}^\intercal \mathbf{D}_r^{-1} \mathbb{I}^\intercal \boldsymbol{\Gamma}_{cr}^p(t) \mathbb{I}\mathbf{s} + 2\eta \dot{\mathbf{x}}_r^\intercal \mathbf{D}_r^{-1} \mathbb{I}^\intercal \mathbb{I} \dot{\mathbf{x}}_r + \eta \dot{\boldsymbol{\xi}}^\intercal \mathbb{I} \mathbf{D}_r^{-1} \mathbb{I}^\intercal \dot{\boldsymbol{\xi}} \\ & + \sigma \mathbf{s}^\intercal \mathbf{D}_r^{-1} \boldsymbol{\Gamma}_{rr}(t) \mathbf{s} + \sigma \mathbf{1}_{N_r n}^\intercal \mathbf{D}_r^{-1} \big[(3\mathbf{D} + 2\mathbf{A}) \otimes \mathbf{I}_n \big] \dot{\mathbf{x}}_r^2 \\ = & \eta \dot{\boldsymbol{\xi}}^\intercal \mathbb{I} \mathbf{D}_r^{-1} \mathbb{I}^\intercal \dot{\boldsymbol{\xi}} + \mathbf{1}_{N_r n}^\intercal \mathbf{D}_r^{-1} \big[2\eta \mathbb{I}^\intercal \mathbb{I} + \sigma (3\mathbf{D} + 2\mathbf{A}) \otimes \mathbf{I}_n \big] \dot{\mathbf{x}}_r^2 \\ & + \mathbf{s}^\intercal \mathbf{D}_r^{-1} \Big[\eta \mathbb{I}^\intercal \boldsymbol{\Gamma}_{cr}^p(t) \mathbb{I} + \sigma \boldsymbol{\Gamma}_{rr}(t) \Big] \mathbf{s}.\end{aligned}$$

Appendix J

Derivations of Equation (5.11)

Notice that $\mathbf{u}_{tk} \circ \boldsymbol{\omega}$ can be geometrically decomposed into $\mathbf{u}_{tk} \circ \boldsymbol{\omega} = \boldsymbol{\omega}^{\|} + \boldsymbol{\omega}^{\perp}$, where

$$\boldsymbol{\omega}^{\|} = \frac{\boldsymbol{\omega}\boldsymbol{\omega}^{\mathsf{T}}}{\|\boldsymbol{\omega}\|^2}(\mathbf{u}_{tk} \circ \boldsymbol{\omega}), \quad \text{and} \quad \boldsymbol{\omega}^{\perp} = \left(\mathbf{I} - \frac{\boldsymbol{\omega}\boldsymbol{\omega}^{\mathsf{T}}}{\|\boldsymbol{\omega}\|^2}\right)(\mathbf{u}_{tk} \circ \boldsymbol{\omega}).$$

It then follows that

$$(\mathbf{I} - \boldsymbol{\omega}\boldsymbol{\omega}^{\mathsf{T}})\boldsymbol{\omega}^{\|} = (\mathbf{I} - \boldsymbol{\omega}\boldsymbol{\omega}^{\mathsf{T}})\frac{\boldsymbol{\omega}\boldsymbol{\omega}^{\mathsf{T}}}{\|\boldsymbol{\omega}\|^2}(\mathbf{u}_{tk} \circ \boldsymbol{\omega}) = (1 - \boldsymbol{\omega}^{\mathsf{T}}\boldsymbol{\omega})\frac{\boldsymbol{\omega}\boldsymbol{\omega}^{\mathsf{T}}}{\|\boldsymbol{\omega}\|^2}(\mathbf{u}_{tk} \circ \boldsymbol{\omega}) = (1 - \boldsymbol{\omega}^{\mathsf{T}}\boldsymbol{\omega})\boldsymbol{\omega}^{\|}$$

and that

$$(\mathbf{I} - \boldsymbol{\omega}\boldsymbol{\omega}^{\mathsf{T}})\boldsymbol{\omega}^{\perp} = (\mathbf{I} - \boldsymbol{\omega}\boldsymbol{\omega}^{\mathsf{T}})\left(\mathbf{I} - \frac{\boldsymbol{\omega}\boldsymbol{\omega}^{\mathsf{T}}}{\|\boldsymbol{\omega}\|^2}\right)(\mathbf{u}_{tk} \circ \boldsymbol{\omega}) = \left(\mathbf{I} - \frac{\boldsymbol{\omega}\boldsymbol{\omega}^{T}}{\|\boldsymbol{\omega}\|^2}\right)(\mathbf{u}_{tk} \circ \boldsymbol{\omega}) = \boldsymbol{\omega}^{\perp}.$$

Using the above two equations, it derives that

$$\begin{aligned}
&2\sigma\boldsymbol{\delta}^{\mathsf{T}}\big(\mathbf{u}_{tk} \circ \boldsymbol{\omega} \circ \big[(\mathbf{I} - \boldsymbol{\omega}\boldsymbol{\omega}^{\mathsf{T}})\boldsymbol{\omega}^{\|}\big]\,\big) = 2\sigma\boldsymbol{\delta}^{\mathsf{T}}\big(\mathbf{u}_{tk} \circ \boldsymbol{\omega} \circ \big[(1 - \boldsymbol{\omega}^{\mathsf{T}}\boldsymbol{\omega})\boldsymbol{\omega}^{\|}\big]\,\big) \\
\leq &\frac{\sigma}{4\kappa}(1 - \boldsymbol{\omega}^{\mathsf{T}}\boldsymbol{\omega})^2\boldsymbol{\omega}^{\mathsf{T}}\mathbf{U}_{tk}\boldsymbol{\omega} + 4\sigma\kappa\boldsymbol{\delta}^{\mathsf{T}} \cdot \mathrm{diag}\{\boldsymbol{\omega}^{\|}\} \cdot \mathbf{U}_{tk} \cdot \mathrm{diag}\{\boldsymbol{\omega}^{\|}\} \cdot \boldsymbol{\delta} \\
\leq &\frac{\sigma}{4\kappa}(1 - \boldsymbol{\omega}^{\mathsf{T}}\boldsymbol{\omega})^2\mathbf{u}_{tk}^{\mathsf{T}}\boldsymbol{\omega}^2 + 4\sigma\kappa\boldsymbol{\delta}^{\mathsf{T}} \cdot \mathrm{diag}\{b_m\boldsymbol{\omega}\} \cdot \mathbf{U}_{tk} \cdot \mathrm{diag}\{b_m\boldsymbol{\omega}\} \cdot \boldsymbol{\delta} \\
= &\frac{\sigma}{4\kappa}(1 - \boldsymbol{\omega}^{\mathsf{T}}\boldsymbol{\omega})^2\mathbf{u}_{tk}^{\mathsf{T}}\boldsymbol{\omega}^2 + 4\sigma\kappa b_m^2\boldsymbol{\delta}^{\mathsf{T}}\boldsymbol{\Omega}\mathbf{U}_{tk}\boldsymbol{\Omega}\boldsymbol{\delta}
\end{aligned}$$

where $u_i(t_k) \leq b_m$ for any $i = 1, \cdots, N_r$ has been applied, and also that

$$\begin{aligned}
&2\sigma\boldsymbol{\delta}^{\mathsf{T}}\big(\mathbf{u}_{tk} \circ \boldsymbol{\omega} \circ \big[(\mathbf{I} - \boldsymbol{\omega}\boldsymbol{\omega}^{\mathsf{T}})\boldsymbol{\omega}^{\perp}\big]\,\big) = 2\sigma\boldsymbol{\delta}^{\mathsf{T}}\mathbf{L}_c(\mathbf{u}_{tk} \circ \boldsymbol{\omega} \circ \boldsymbol{\omega}^{\perp}) \\
= &2\sigma\boldsymbol{\delta}^{\mathsf{T}}\mathbf{B}\mathbf{T}\mathbf{B}^{\mathsf{T}}(\mathbf{u}_{tk} \circ \boldsymbol{\omega} \circ \boldsymbol{\omega}^{\perp}) \leq 2\sigma\left|\widetilde{\boldsymbol{\delta}}\right|^{\mathsf{T}}\left|\mathbf{T}\mathbf{B}^{\mathsf{T}}(\mathbf{u}_{tk} \circ \boldsymbol{\omega} \circ \boldsymbol{\omega}^{\perp})\right|
\end{aligned}$$

$$
\begin{aligned}
=&2\sigma \left|\widetilde{\boldsymbol{\delta}}\right|^{\mathsf{T}} \left|\mathbf{T}\mathbf{B}^{\mathsf{T}} \left(\mathbf{u}_{tk} \circ \boldsymbol{\omega} \circ \left[\left(\mathbf{I} - \frac{\boldsymbol{\omega}\boldsymbol{\omega}^{\mathsf{T}}}{\|\boldsymbol{\omega}\|^2}\right)(\mathbf{u}_{tk} \circ \boldsymbol{\omega})\right]\right)\right| \\
=&2\sigma \left|\widetilde{\boldsymbol{\delta}}\right|^{\mathsf{T}} \left|\mathbf{T}\mathbf{B}^{\mathsf{T}} \left[\left(\mathbf{u}_{tk} - \frac{\mathbf{u}_{tk}^{\mathsf{T}}\boldsymbol{\omega}^2}{\|\boldsymbol{\omega}\|^2}\mathbf{1}\right) \circ \mathbf{u}_{tk} \circ \boldsymbol{\omega}^2\right]\right| \\
\leq&2\sigma(b_m - b_1) \left|\widetilde{\boldsymbol{\delta}}\right|^{\mathsf{T}} \left|\boldsymbol{\upsilon}\mathbf{1}^{\mathsf{T}}(\mathbf{u}_{tk} \circ \boldsymbol{\omega}^2)\right| \\
=&2\sigma(b_m - b_1)(\mathbf{u}_{tk}^{\mathsf{T}}\boldsymbol{\omega}^2) \left|\widetilde{\boldsymbol{\delta}}\right|^{\mathsf{T}} \boldsymbol{\upsilon} = \sigma N_r(b_m - b_1) \left|\widetilde{\boldsymbol{\delta}}\right|^{\mathsf{T}} \left(\boldsymbol{\upsilon} \circ \left[|\mathbf{B}|^{\mathsf{T}}(\boldsymbol{\eta} - \boldsymbol{\delta})\right]\right) \\
\leq&\sigma N_r(b_m - b_1) \left|\widetilde{\boldsymbol{\delta}}\right|^{\mathsf{T}} \boldsymbol{\Upsilon}|\mathbf{B}|^{\mathsf{T}}\boldsymbol{\eta} + \sigma N_r(b_m - b_1)\widetilde{\boldsymbol{\delta}}^{\mathsf{T}}\boldsymbol{\Upsilon}^2\widetilde{\boldsymbol{\delta}} + \sigma N_r(b_m - b_1)\boldsymbol{\delta}^{\mathsf{T}}|\mathbf{B}||\mathbf{B}|^{\mathsf{T}}\boldsymbol{\delta},
\end{aligned}
$$

where $u_i\omega_i^2 > 0$, and $|u_i - \mathbf{u}^{\mathsf{T}}\boldsymbol{\omega}^2/\|\boldsymbol{\omega}\|^2| \leq b_m - b_1$ and $2\mathbf{u}^{\mathsf{T}}\boldsymbol{\omega}^2\mathbf{1} = N_r|\mathbf{B}|^{\mathsf{T}}(\boldsymbol{\eta} - \boldsymbol{\delta})$ by (5.8) have been employed in the fifth and sixth lines.

Because $\mathbf{u} \circ \boldsymbol{\omega} = \boldsymbol{\omega}^{\parallel} + \boldsymbol{\omega}^{\perp}$, the summation of the above two equations gives (5.11).

Appendix K

Derivations of Equation (5.15)

Notice firstly that

$$\begin{aligned}
&\boldsymbol{\delta}^{\mathsf{T}}\boldsymbol{\Lambda}(t)\boldsymbol{\delta} = \boldsymbol{\delta}^{\mathsf{T}}\mathbf{L}_c\boldsymbol{\Lambda}(t)\mathbf{L}_c\boldsymbol{\delta} = \boldsymbol{\delta}^{\mathsf{T}}\mathbf{B}\mathbf{T}\mathbf{B}^{\mathsf{T}}\boldsymbol{\Lambda}(t)\mathbf{B}\mathbf{T}\mathbf{B}^{\mathsf{T}}\boldsymbol{\delta} \\
=&\widetilde{\boldsymbol{\delta}}^{\mathsf{T}}\mathbf{T}\mathbf{B}^{\mathsf{T}}\boldsymbol{\Lambda}(t)\mathbf{B}\mathbf{T}\widetilde{\boldsymbol{\delta}} \leq \left|\widetilde{\boldsymbol{\delta}}\right|^{\mathsf{T}}\boldsymbol{\upsilon}\mathbf{1}^{\mathsf{T}}\boldsymbol{\Lambda}(t)\mathbf{1}\boldsymbol{\upsilon}^{\mathsf{T}}\left|\widetilde{\boldsymbol{\delta}}\right| \\
=&\left(\frac{\kappa}{2}N_r\mathbf{u}_{tk}^{\mathsf{T}}\boldsymbol{\omega}^2 + \frac{1}{2}N_r^2\mathbf{1}^{\mathsf{T}}\boldsymbol{\Omega}\mathbf{U}_{tk}^{-1}\boldsymbol{\Omega}\mathbf{1}\right)\left(\boldsymbol{\upsilon}^{\mathsf{T}}\left|\widetilde{\boldsymbol{\delta}}\right|\right)^2 \\
&+\kappa\mathbf{1}^{\mathsf{T}}\left[(4\kappa b_m^2 - 2N_r)\boldsymbol{\Omega}\mathbf{U}_{tk}\boldsymbol{\Omega} + N_r(b_m - b_1)|\mathbf{B}||\mathbf{B}|^{\mathsf{T}}\right]\mathbf{1}\left(\boldsymbol{\upsilon}^{\mathsf{T}}\left|\widetilde{\boldsymbol{\delta}}\right|\right)^2 \\
\leq&\left(\frac{\kappa}{2}N_r\mathbf{u}_{tk}^{\mathsf{T}}\boldsymbol{\omega}^2 + \frac{N_r^2}{2b_1^2}\mathbf{u}_{tk}^{\mathsf{T}}\boldsymbol{\omega}^2\right)\widetilde{\boldsymbol{\delta}}^{\mathsf{T}}\boldsymbol{\Upsilon}^2\widetilde{\boldsymbol{\delta}} \\
&+\kappa\left[(4\kappa b_m^2 - 2N_r)\mathbf{u}_{tk}^{\mathsf{T}}\boldsymbol{\omega}^2 + 4N_r(N_r-1)(b_m - b_1)\right]\widetilde{\boldsymbol{\delta}}^{\mathsf{T}}\boldsymbol{\Upsilon}^2\widetilde{\boldsymbol{\delta}} \\
=&\left[\left(\frac{N_r^2}{4b_1^2} - \frac{3}{4}\kappa N_r + 2\kappa^2 b_m^2\right)2\mathbf{u}_{tk}^{\mathsf{T}}\boldsymbol{\omega}^2 + 4N_r(N_r-1)(b_m - b_1)\right]\widetilde{\boldsymbol{\delta}}^{\mathsf{T}}\boldsymbol{\Upsilon}^2\widetilde{\boldsymbol{\delta}}
\end{aligned} \tag{K.1}$$

Using (5.8), $2\mathbf{u}_{tk}^{\mathsf{T}}\boldsymbol{\omega}^2\widetilde{\boldsymbol{\delta}}^{\mathsf{T}}\boldsymbol{\Upsilon}^2\widetilde{\boldsymbol{\delta}}$ in the above can be rewritten as

$$\begin{aligned}
2\mathbf{u}_{tk}^{\mathsf{T}}\boldsymbol{\omega}^2\widetilde{\boldsymbol{\delta}}^{\mathsf{T}}\boldsymbol{\Upsilon}^2\widetilde{\boldsymbol{\delta}} &= N_r\widetilde{\boldsymbol{\delta}}^{\mathsf{T}}\boldsymbol{\Upsilon}\cdot\mathrm{diag}\{|\mathbf{B}|^{\mathsf{T}}\boldsymbol{\eta} - \boldsymbol{\delta}\}\cdot\boldsymbol{\Upsilon}\widetilde{\boldsymbol{\delta}} \\
=&N_r\widetilde{\boldsymbol{\delta}}^{\mathsf{T}}\boldsymbol{\Upsilon}\cdot\mathrm{diag}\{|\mathbf{B}|^{\mathsf{T}}\boldsymbol{\eta}\}\cdot\boldsymbol{\Upsilon}\widetilde{\boldsymbol{\delta}} - N_r\widetilde{\boldsymbol{\delta}}^{\mathsf{T}}\boldsymbol{\Upsilon}\cdot\mathrm{diag}\{|\mathbf{B}|^{\mathsf{T}}\boldsymbol{\delta}\}\cdot\boldsymbol{\Upsilon}\widetilde{\boldsymbol{\delta}}
\end{aligned} \tag{K.2}$$

Because $\mathbf{L}_c\boldsymbol{\delta} = \boldsymbol{\delta}$ by Proposition 5.1, the errors of estimation $\boldsymbol{\delta}$ can be upper-bounded by the difference $\widetilde{\boldsymbol{\delta}}$ between the errors of estimation by

$$\boldsymbol{\delta}^{\mathsf{T}}\boldsymbol{\delta} = \boldsymbol{\delta}^{\mathsf{T}}\mathbf{L}_c\mathbf{L}_c\boldsymbol{\delta} = \boldsymbol{\delta}^{\mathsf{T}}\mathbf{B}\mathbf{T}\mathbf{B}^{\mathsf{T}}\mathbf{B}\mathbf{T}\mathbf{B}^{\mathsf{T}}\boldsymbol{\delta} = \widetilde{\boldsymbol{\delta}}^{\mathsf{T}}\mathbf{T}\mathbf{B}^{\mathsf{T}}\mathbf{B}\mathbf{T}\widetilde{\boldsymbol{\delta}} \leq K_c^2\widetilde{\boldsymbol{\delta}}^{\mathsf{T}}\widetilde{\boldsymbol{\delta}},$$

where K_c is given in (5.13). Using (5.8), it further derives that

$$\begin{aligned}
&-N_r\widetilde{\boldsymbol{\delta}}^{\mathsf{T}}\boldsymbol{\Upsilon}\cdot\mathrm{diag}\{|\mathbf{B}|^{\mathsf{T}}\boldsymbol{\delta}\}\cdot\boldsymbol{\Upsilon}\widetilde{\boldsymbol{\delta}}\leq 2N_r|\boldsymbol{\delta}|_\infty\widetilde{\boldsymbol{\delta}}^{\mathsf{T}}\boldsymbol{\Upsilon}^2\widetilde{\boldsymbol{\delta}}\leq 2N_r\|\boldsymbol{\delta}\|\widetilde{\boldsymbol{\delta}}^{\mathsf{T}}\boldsymbol{\Upsilon}^2\widetilde{\boldsymbol{\delta}}\\
\leq&2N_rK_c\left\|\widetilde{\boldsymbol{\delta}}\right\|\widetilde{\boldsymbol{\delta}}^{\mathsf{T}}\boldsymbol{\Upsilon}^2\widetilde{\boldsymbol{\delta}}\leq N_rK_c\left\|\widetilde{\boldsymbol{\delta}}\right\|^2\widetilde{\boldsymbol{\delta}}^{\mathsf{T}}\widetilde{\boldsymbol{\delta}}+N_rK_c\widetilde{\boldsymbol{\delta}}^{\mathsf{T}}\boldsymbol{\Upsilon}^4\widetilde{\boldsymbol{\delta}}\\
=&N_rK_c\widetilde{\boldsymbol{\delta}}^{\mathsf{T}}\widetilde{\boldsymbol{\delta}}\widetilde{\boldsymbol{\delta}}^{\mathsf{T}}\widetilde{\boldsymbol{\delta}}+N_rK_c\widetilde{\boldsymbol{\delta}}^{\mathsf{T}}\boldsymbol{\Upsilon}^4\widetilde{\boldsymbol{\delta}}=N_rK_c\widetilde{\boldsymbol{\delta}}^{\mathsf{T}}\left(\mathbf{B}^{\mathsf{T}}\boldsymbol{\delta}\right)\left(\boldsymbol{\delta}^{\mathsf{T}}\mathbf{B}\right)\widetilde{\boldsymbol{\delta}}+N_rK_c\widetilde{\boldsymbol{\delta}}^{\mathsf{T}}\boldsymbol{\Upsilon}^4\widetilde{\boldsymbol{\delta}}\\
=&N_rK_c\widetilde{\boldsymbol{\delta}}^{\mathsf{T}}\left[\mathbf{B}^{\mathsf{T}}\left(\boldsymbol{\eta}-\mathbf{u}_{tk}^{\mathsf{T}}\boldsymbol{\omega}^2\frac{\mathbf{1}}{N_r}\right)\right]\left[\left(\boldsymbol{\eta}-\mathbf{u}_{tk}^{\mathsf{T}}\boldsymbol{\omega}^2\frac{\mathbf{1}}{N_r}\right)^{\mathsf{T}}\mathbf{B}\right]\widetilde{\boldsymbol{\delta}}+N_rK_c\widetilde{\boldsymbol{\delta}}^{\mathsf{T}}\boldsymbol{\Upsilon}^4\widetilde{\boldsymbol{\delta}}\\
=&N_rK_c\widetilde{\boldsymbol{\delta}}^{\mathsf{T}}\left(\mathbf{B}^{\mathsf{T}}\boldsymbol{\eta}\right)\left(\boldsymbol{\eta}^{\mathsf{T}}\mathbf{B}\right)\widetilde{\boldsymbol{\delta}}+N_rK_c\widetilde{\boldsymbol{\delta}}^{\mathsf{T}}\boldsymbol{\Upsilon}^4\widetilde{\boldsymbol{\delta}}\\
\leq&N_rK_c(N_r-1)\widetilde{\boldsymbol{\delta}}^{\mathsf{T}}\cdot\mathrm{diag}\left\{\left(\mathbf{B}^{\mathsf{T}}\boldsymbol{\eta}\right)^2\right\}\widetilde{\boldsymbol{\delta}}+N_rK_c\widetilde{\boldsymbol{\delta}}^{\mathsf{T}}\boldsymbol{\Upsilon}^4\widetilde{\boldsymbol{\delta}}.
\end{aligned}\tag{K.3}$$

Thus, the substitutions of (K.3) in (K.2), and of (K.2) in (K.1), lead to (5.14).

Appendix L

Publications

- **Refereed journal papers that have been published or accepted**

  J1. **Y. Yang**, D. Constantinescu and Y. Shi, "Input-to-state stable bilateral teleoperation by dynamic interconnection and damping injection: Theory and experiments," *IEEE Transactions on Industrial Electronics*, vol. 67, no. 1, pp. 790-799, Jan. 2020.
  (This work is presented in Chapter 2.)

  J2. **Y. Yang**, Y. Shi and D. Constantinescu, "Connectivity-preserving synchronization of time-delay Euler-Lagrange networks with bounded actuation," *IEEE Transactions on Cybernetics*, accepted for publication, 2019, doi: 10.1109/TCYB.2019.2914403.
  (This work is presented in Chapter 3.)

- **Refereed journal papers that have been conditionally accepted**

  J3. **Y. Yang**, D. Constantinescu and Y. Shi, "Passive multi-user teleoperation of a multi-robot system with connectivity-preserving containment," conditionally accepted, *IEEE Transactions on Robotics*.
  (This work is presented in Chapter 4.)

- **Refereed journal papers that are under review**

  J4. **Y. Yang**, D. Constantinescu and Y. Shi, "Distributed multi-robot teleoperation with winners-take-all authority dispatch," submitted.
  (This work is presented in Chapter 5.)

- **Refereed conference papers that have appeared**

  C1. **Y. Yang**, D. Constantinescu and Y. Shi, "Distributed winner-take-all teleoperation of a multi-robot system," *2020 IEEE International Conference on Robotics and Automation (ICRA)*, Paris, France, 2020, pp. 9171-9177.
  (This work is presented in Chapter 5.)

  C2. **Y. Yang**, D. Constantinescu and Y. Shi, "Connectivity-preserving swarm teleoperation with a tree network," *2019 IEEE/RSJ International Conference on Intelligent Robots and Systems (IROS)*, Macau, China, 2019, pp. 3624-3629.
  (This work is presented in Chapter 4.)

  C3. **Y. Yang**, D. Constantinescu, and Y. Shi, "Distributed connectivity-preserving coordination of multi-agent systems with bounded velocities," *2019 International Conference on Human Interaction and Emerging Technologies (IHIET)*, August, 2019.

- **Refereed conference papers that have been accepted**

  C4. **Y. Yang**, D. Constantinescu and Y. Shi, "Proportional and reachable cluster teleoperation of a distributed multi-robot system," accepted, *2021 IEEE International Conference on Robotics and Automation (ICRA)*, Xi'an, China, 2021.
  (This work is presented in Chapter 6.)

Bibliography

[1] Centre for Research on the Epidemiology of Disasters CRED, "2015 disasters in numbers," Available at http://cred.be/sites/default/files/2015_DisastersInNumbers.pdf, 2016.

[2] ——, "Cred crunch 60 - technological disasters," Available at https://cred.be/sites/default/files/CC60.pdf, 2020.

[3] Wikipedia contributors, "2008 sichuan earthquake — Wikipedia, the free encyclopedia," https://en.wikipedia.org/w/index.php?title=2008_Sichuan_earthquake&oldid=1001773312, 2021.

[4] ——, "Mv doña paz — Wikipedia, the free encyclopedia," https://en.wikipedia.org/w/index.php?title=MV_Do%C3%B1a_Paz&oldid=1004482947, 2021.

[5] J. Casper and R. R. Murphy, "Human-robot interactions during the robot-assisted urban search and rescue response at the world trade center," *IEEE Transactions on Systems, Man, and Cybernetics, Part B (Cybernetics)*, vol. 33, no. 3, pp. 367–385, 2003.

[6] R. R. Murphy, "Human-robot interaction in rescue robotics," *IEEE Transactions on Systems, Man, and Cybernetics, Part C (Applications and Reviews)*, vol. 34, no. 2, pp. 138–153, 2004.

[7] I. R. Nourbakhsh, K. Sycara, M. Koes, M. Yong, M. Lewis, and S. Burion, "Human-robot teaming for search and rescue," *IEEE Pervasive Computing*, vol. 4, no. 1, pp. 72–79, 2005.

[8] M. Bernard, K. Kondak, I. Maza, and A. Ollero, "Autonomous transportation and deployment with aerial robots for search and rescue missions," *Journal of Field Robotics*, vol. 28, no. 6, pp. 914–931, 2011.

[9] J. Wang, Y. Guo, M. Fahad, and B. Bingham, "Dynamic plume tracking by cooperative robots," *IEEE/ASME Transactions on Mechatronics*, vol. 24, no. 2, pp. 609–620, 2019.

[10] E. M. Fischell, N. R. Rypkema, and H. Schmidt, "Relative autonomy and navigation for command and control of low-cost autonomous underwater vehicles," *IEEE Robotics and Automation Letters*, vol. 4, no. 2, pp. 1800–1806, 2019.

[11] E. M. Fischell, A. R. Kroo, and B. W. O'Neill, "Single-hydrophone low-cost underwater vehicle swarming," *IEEE Robotics and Automation Letters*, vol. 5, no. 2, pp. 354–361, 2020.

[12] G. Vasiljević, T. Petrović, B. Arbanas, and S. Bogdan, "Dynamic median consensus for marine multi-robot systems using acoustic communication," *IEEE Robotics and Automation Letters*, vol. 5, no. 4, pp. 5299–5306, 2020.

[13] A. Babić, G. Vasiljević, and N. Mišković, "Vehicle-in-the-loop framework for testing long-term autonomy in a heterogeneous marine robot swarm," *IEEE Robotics and Automation Letters*, vol. 5, no. 3, pp. 4439–4446, 2020.

[14] S. Musić and S. Hirche, "Control sharing in human-robot team interaction," *Annual Reviews in Control*, vol. 44, pp. 342–354, 2017.

[15] W. Lo, Y. Liu, I. H. Elhajj, N. Xi, Y. Wang, and T. Fukuda, "Cooperative teleoperation of a multirobot system with force reflection via internet," *IEEE/ASME Transactions on Mechatronics*, vol. 9, no. 4, pp. 661–670, 2004.

[16] M. Shahbazi, S. F. Atashzar, and R. V. Patel, "A systematic review of multilateral teleoperation systems," *IEEE Transactions on Haptics*, vol. 11, no. 3, pp. 338–356, July 2018.

[17] S. Sirouspour, "Modeling and control of cooperative teleoperation systems," *IEEE Transactions on Robotics*, vol. 21, no. 6, pp. 1220–1225, Dec 2005.

[18] I. G. Polushin, S. N. Dashkovskiy, A. Takhmar, and R. V. Patel, "A small gain framework for networked cooperative force-reflecting teleoperation," *Automatica*, vol. 49, no. 2, pp. 338–348, 2013.

[19] A. Takhmar, I. G. Polushin, A. Talasaz, and R. V. Patel, "Cooperative teleoperation with projection-based force reflection for MIS," *IEEE Transactions on Control Systems Technology*, vol. 23, no. 4, pp. 1411–1426, 2015.

[20] M. Geravand, E. Shahriari, A. De Luca, and A. Peer, "Port-based modeling of human-robot collaboration towards safety-enhancing energy shaping control," in *2016 IEEE International Conference on Robotics and Automation (ICRA)*, 2016, pp. 3075–3082.

[21] M. Minelli, F. Ferraguti, N. Piccinelli, R. Muradore, and C. Secchi, "An energy-shared two-layer approach for multi-master-multi-slave bilateral teleoperation systems," in *2019 International Conference on Robotics and Automation (ICRA)*, May 2019, pp. 423–429.

[22] M. Panzirsch, R. Balachandran, J. Artigas, C. Riecke, M. Ferre, and A. Albu-Schaeffer, "Haptic intention augmentation for cooperative teleoperation," in *2017 IEEE International Conference on Robotics and Automation (ICRA)*, 2017, pp. 5335–5341.

[23] J. H. Ryu, Q. Ha-Van, and A. Jafari, "Multilateral teleoperation over communication time delay using the time-domain passivity approach," *IEEE Transactions on Control Systems Technology*, vol. 28, no. 6, pp. 2705–2712, 2020.

[24] D. Lee and M. W. Spong, "Bilateral teleoperation of multiple cooperative robots over delayed communication networks: Theory," in *Proceedings of the 2005 IEEE International Conference on Robotics and Automation (ICRA)*, April 2005, pp. 360–365.

[25] D. Lee, "Semi-autonomous teleoperation of multiple wheeled mobile robots over the Internet," in *ASME 2008 Dynamic Systems and Control Conference*. American Society of Mechanical Engineers Digital Collection, 2008, pp. 147–154.

[26] G. Hwang and H. Hashimoto, "Development of a human-robot-shared controlled teletweezing system," *IEEE Transactions on Control Systems Technology*, vol. 15, no. 5, pp. 960–966, 2007.

[27] K. Y. Lui, H. Cho, C. Ha, and D. Lee, "First-person view semi-autonomous teleoperation of cooperative wheeled mobile robots with visuo-haptic feedback,"

The International Journal of Robotics Research, vol. 36, no. 5-7, pp. 840–860, 2017.

[28] C. Lin, M. Khong, and Y. Liu, "Experiments on human-in-the-loop coordination for multirobot system with task abstraction," *IEEE Transactions on Automation Science and Engineering*, vol. 12, no. 3, pp. 981–989, 2015.

[29] S. Musić, G. Salvietti, P. B. g. Dohmann, F. Chinello, D. Prattichizzo, and S. Hirche, "Human–robot team interaction through wearable haptics for cooperative manipulation," *IEEE Transactions on Haptics*, vol. 12, no. 3, pp. 350–362, 2019.

[30] D. Sieber and S. Hirche, "Human-guided multirobot cooperative manipulation," *IEEE Transactions on Control Systems Technology*, vol. 27, no. 4, pp. 1492–1509, 2019.

[31] Z. Wang and M. Schwager, "Force-Amplifying N-robot Transport System (Force-ANTS) for cooperative planar manipulation without communication," *The International Journal of Robotics Research*, vol. 35, no. 13, pp. 1564–1586, 2016.

[32] D. Sun, Q. Liao, and A. Loutfi, "Single master bimanual teleoperation system with efficient regulation," *IEEE Transactions on Robotics*, vol. 36, no. 4, pp. 1022–1037, 2020.

[33] E. J. Rodríguez-Seda, J. J. Troy, C. A. Erignac, P. Murray, D. M. Stipanović, and M. W. Spong, "Bilateral teleoperation of multiple mobile agents: Coordinated motion and collision avoidance," *IEEE Transactions on Control Systems Technology*, vol. 18, no. 4, pp. 984–992, July 2010.

[34] J. Yan, Y. Wan, X. Luo, C. Chen, C. Hua, and X. Guan, "Formation control of teleoperating cyber-physical system with time delay and actuator saturation," *IEEE Transactions on Control Systems Technology*, vol. 26, no. 4, pp. 1458–1467, 2018.

[35] A. Franchi, C. Masone, V. Grabe, M. Ryll, H. H. Bülthoff, and P. Robuffo Giordano, "Modeling and control of UAV bearing formations with bilateral high-level steering," *The International Journal of Robotics Research*, vol. 31, no. 12, pp. 1504–1525, 2012.

[36] D. Zhou, Z. Wang, and M. Schwager, "Agile coordination and assistive collision avoidance for quadrotor swarms using virtual structures," *IEEE Transactions on Robotics*, vol. 34, no. 4, pp. 916–923, Aug 2018.

[37] C. Ha and D. Lee, "Vision-based teleoperation of unmanned aerial and ground vehicles," in *2013 IEEE International Conference on Robotics and Automation*, 2013, pp. 1465–1470.

[38] H. Saeidi, J. R. Wagner, and Y. Wang, "A mixed-initiative haptic teleoperation strategy for mobile robotic systems based on bidirectional computational trust analysis," *IEEE Transactions on Robotics*, vol. 33, no. 6, pp. 1500–1507, Dec 2017.

[39] H. Saeidi and Y. Wang, "Incorporating trust and self-confidence analysis in the guidance and control of (semi)autonomous mobile robotic systems," *IEEE Robotics and Automation Letters*, vol. 4, no. 2, pp. 239–246, April 2019.

[40] H. Saeidi, D. G. Mikulski, and Y. Wang, "Trust-based leader selection for bilateral haptic teleoperation of multi-robot systems," in *2017 IEEE/RSJ International Conference on Intelligent Robots and Systems (IROS)*, Sep 2017, pp. 6575–6581.

[41] A. Franchi and P. Robuffo Giordano, "Online leader selection for improved collective tracking and formation maintenance," *IEEE Transactions on Control of Network Systems*, vol. 5, no. 1, pp. 3–13, March 2018.

[42] A. Franchi, P. Robuffo Giordano, and G. Michieletto, "Online leader selection for collective tracking and formation control: The second-order case," *IEEE Transactions on Control of Network Systems*, vol. 6, no. 4, pp. 1415–1425, Dec 2019.

[43] T. Hatanaka, N. Chopra, and M. Fujita, "Passivity-based bilateral human-swarm-interactions for cooperative robotic networks and human passivity analysis," in *2015 54th IEEE Conference on Decision and Control (CDC)*, 2015, pp. 1033–1039.

[44] A. Franchi, C. Secchi, M. Ryll, H. H. Bülthoff, and P. Robuffo Giordano, "Shared control : Balancing autonomy and human assistance with a group

of quadrotor UAVs," *IEEE Robotics Automation Magazine*, vol. 19, no. 3, pp. 57–68, Sep 2012.

[45] A. Franchi, C. Secchi, H. I. Son, H. H. Bülthoff, and P. Robuffo Giordano, "Bilateral teleoperation of groups of mobile robots with time-varying topology," *IEEE Transactions on Robotics*, vol. 28, no. 5, pp. 1019–1033, Oct 2012.

[46] C. Secchi, A. Franchi, H. H. Bülthoff, and P. Robuffo Giordano, "Bilateral teleoperation of a group of UAVs with communication delays and switching topology," in *2012 IEEE International Conference on Robotics and Automation (ICRA)*, May 2012, pp. 4307–4314.

[47] L. Sabattini, C. Secchi, B. Capelli, and C. Fantuzzi, "Passivity preserving force scaling for enhanced teleoperation of multirobot systems," *IEEE Robotics and Automation Letters*, vol. 3, no. 3, pp. 1925–1932, July 2018.

[48] L. Sabattini, C. Secchi, and C. Fantuzzi, "Controlling the interaction of a multi-robot system with external entities," in *2018 IEEE International Conference on Robotics and Automation (ICRA)*, 2018, pp. 7654–7659.

[49] L. Sabattini, B. Capelli, C. Fantuzzi, and C. Secchi, "Teleoperation of multi-robot systems to relax topological constraints," in *2020 IEEE International Conference on Robotics and Automation (ICRA)*, 2020, pp. 4558–4564.

[50] D. Lee, A. Franchi, H. I. Son, C. Ha, H. H. Bülthoff, and P. Robuffo Giordano, "Semiautonomous haptic teleoperation control architecture of multiple unmanned aerial vehicles," *IEEE/ASME Transactions on Mechatronics*, vol. 18, no. 4, pp. 1334–1345, Aug 2013.

[51] H. I. Son, A. Franchi, L. L. Chuang, J. Kim, H. H. Bülthoff, and P. Robuffo Giordano, "Human-centered design and evaluation of haptic cueing for teleoperation of multiple mobile robots," *IEEE Transactions on Cybernetics*, vol. 43, no. 2, pp. 597–609, 2013.

[52] P. Robuffo Giordano, A. Franchi, C. Secchi, and H. H. Bülthoff, "A passivity-based decentralized strategy for generalized connectivity maintenance," *The International Journal of Robotics Research*, vol. 32, no. 3, pp. 299–323, 2013.

[53] C. Secchi, A. Franchi, H. H. Bülthoff, and P. Robuffo Giordano, "Bilateral control of the degree of connectivity in multiple mobile-robot teleoperation," in *2013 IEEE International Conference on Robotics and Automation (ICRA)*, May 2013, pp. 3645–3652.

[54] M. Aggravi, C. Pacchierotti, and P. Robuffo Giordano, "Connectivity-maintenance teleoperation of a UAV fleet with wearable haptic feedback," *IEEE Transactions on Automation Science and Engineering*, pp. 1–20, 2020.

[55] C. Secchi, S. Stramigioli, and C. Fantuzzi, *Control of Interactive Robotic Interfaces: A port-Hamiltonian Approach*. Springer Science & Business Media, 2007, vol. 29.

[56] M. A. Hsieh, A. Cowley, V. Kumar, and C. J. Taylor, "Maintaining network connectivity and performance in robot teams," *Journal of Field Robotics*, vol. 25, no. 1-2, pp. 111–131, 2008.

[57] S. Chung, A. A. Paranjape, P. Dames, S. Shen, and V. Kumar, "A survey on aerial swarm robotics," *IEEE Transactions on Robotics*, vol. 34, no. 4, pp. 837–855, Aug 2018.

[58] X. Yu and M. A. Hsieh, "Synthesis of a time-varying communication network by robot teams with information propagation guarantees," *IEEE Robotics and Automation Letters*, vol. 5, no. 2, pp. 1413–1420, 2020.

[59] A. J. van der Schaft, *L2-Gain and Passivity Techniques in Nonlinear Control*. Springer Science & Business Media, 2017.

[60] I. G. Polushin, P. X. Liu, and C. Lung, "A force-reflection algorithm for improved transparency in bilateral teleoperation with communication delay," *IEEE/ASME Transactions on Mechatronics*, vol. 12, no. 3, pp. 361–374, 2007.

[61] ——, "Projection-based force reflection algorithm for stable bilateral teleoperation over networks," *IEEE Transactions on Instrumentation and Measurement*, vol. 57, no. 9, pp. 1854–1865, 2008.

[62] ——, "Stability of bilateral teleoperators with generalized projection-based force reflection algorithms," *Automatica*, vol. 48, no. 6, pp. 1005–1016, 2012.

[63] I. G. Polushin, A. Takhmar, and R. V. Patel, "Projection-based force-reflection algorithms with frequency separation for bilateral teleoperation," *IEEE/ASME Transactions on Mechatronics*, vol. 20, no. 1, pp. 143–154, 2015.

[64] S. F. Atashzar, I. G. Polushin, and R. V. Patel, "A small-gain approach for nonpassive bilateral telerobotic rehabilitation: Stability analysis and controller synthesis," *IEEE Transactions on Robotics*, vol. 33, no. 1, pp. 49–66, Feb 2017.

[65] S. Hirche and M. Buss, "Human-oriented control for haptic teleoperation," *Proceedings of the IEEE*, vol. 100, no. 3, pp. 623–647, March 2012.

[66] D. B. Venkateswaran and Z. Qu, "A passivity-shortage based control design for teleoperation with time-varying delays," *IEEE Robotics and Automation Letters*, vol. 5, no. 3, pp. 4070–4077, 2020.

[67] J. E. Colgate and N. Hogan, "Robust control of dynamically interacting systems," *International Journal of Control*, vol. 48, no. 1, pp. 65–88, 1988.

[68] M. Xia, A. Rahnama, S. Wang, and P. J. Antsaklis, "Control design using passivation for stability and performance," *IEEE Transactions on Automatic Control*, vol. 63, no. 9, pp. 2987–2993, Sep. 2018.

[69] J. H. Ryu, Dong-Soo Kwon, and B. Hannaford, "Stable teleoperation with time-domain passivity control," *IEEE Transactions on Robotics and Automation*, vol. 20, no. 2, pp. 365–373, April 2004.

[70] J. H. Ryu, J. Artigas, and C. Preusche, "A passive bilateral control scheme for a teleoperator with time-varying communication delay," *Mechatronics*, vol. 20, no. 7, pp. 812–823, 2010.

[71] V. Chawda and M. K. O'Malley, "Position synchronization in bilateral teleoperation under time-varying communication delays," *IEEE/ASME Transactions on Mechatronics*, vol. 20, no. 1, pp. 245–253, 2015.

[72] H. Singh, M. Panzirsch, A. Coelho, and C. Ott, "Proxy-based approach for position synchronization of delayed robot coupling without sacrificing performance," *IEEE Robotics and Automation Letters*, vol. 5, no. 4, pp. 6599–6606, 2020.

[73] M. Laghi, A. Ajoudani, M. G. Catalano, and A. Bicchi, "Unifying bilateral teleoperation and tele-impedance for enhanced user experience," *The International Journal of Robotics Research*, vol. 39, no. 4, pp. 514–539, 2020.

[74] D. Lee and K. Huang, "Passive-set-position-modulation framework for interactive robotic systems," *IEEE Transactions on Robotics*, vol. 26, no. 2, pp. 354–369, April 2010.

[75] C. Secchi, S. Stramigioli, and C. Fantuzzi, "Position drift compensation in port-Hamiltonian based telemanipulation," in *2006 IEEE/RSJ International Conference on Intelligent Robots and Systems (IROS)*, Oct 2006, pp. 4211–4216.

[76] F. Ferraguti, N. Preda, A. Manurung, M. Bonfè, O. Lambercy, R. Gassert, R. Muradore, P. Fiorini, and C. Secchi, "An energy tank-based interactive control architecture for autonomous and teleoperated robotic surgery," *IEEE Transactions on Robotics*, vol. 31, no. 5, pp. 1073–1088, Oct 2015.

[77] M. Franken, S. Stramigioli, S. Misra, C. Secchi, and A. Macchelli, "Bilateral telemanipulation with time delays: A two-layer approach combining passivity and transparency," *IEEE Transactions on Robotics*, vol. 27, no. 4, pp. 741–756, Aug 2011.

[78] D. Heck, A. Saccon, R. Beerens, and H. Nijmeijer, "Direct force-reflecting two-layer approach for passive bilateral teleoperation with time delays," *IEEE Transactions on Robotics*, vol. 34, no. 1, pp. 194–206, Feb 2018.

[79] R. J. Anderson and M. W. Spong, "Bilateral control of teleoperators with time delay," *IEEE Transactions on Automatic Control*, vol. 34, no. 5, pp. 494–501, 1989.

[80] G. Niemeyer and J.-J. E. Slotine, "Stable adaptive teleoperation," *IEEE Journal of Oceanic Engineering*, vol. 16, no. 1, pp. 152–162, 1991.

[81] C. Secchi, S. Stramigioli, and C. Fantuzzi, "Transparency in port-Hamiltonian-based telemanipulation," *IEEE Transactions on Robotics*, vol. 24, no. 4, pp. 903–910, 2008.

[82] F. Ferraguti, M. Bonfè, C. Fantuzzi, and C. Secchi, "Optimized power modulation in wave based bilateral teleoperation," *IEEE/ASME Transactions on Mechatronics*, 2020, doi: 10.1109/TMECH.2020.3013978.

[83] D. Lee and M. W. Spong, "Passive bilateral teleoperation with constant time delay," *IEEE Transactions on Robotics*, vol. 22, no. 2, pp. 269–281, April 2006.

[84] E. Nuño, R. Ortega, N. Barabanov, and L. Basañez, "A globally stable PD controller for bilateral teleoperators," *IEEE Transactions on Robotics*, vol. 24, no. 3, pp. 753–758, June 2008.

[85] C. Hua and P. X. Liu, "Delay-dependent stability criteria of teleoperation systems with asymmetric time-varying delays," *IEEE Transactions on Robotics*, vol. 26, no. 5, pp. 925–932, 2010.

[86] N. Chopra, M. W. Spong, and R. Lozano, "Synchronization of bilateral teleoperators with time delay," *Automatica*, vol. 44, no. 8, pp. 2142–2148, 2008.

[87] E. Nuño, R. Ortega, and L. Basañez, "An adaptive controller for nonlinear teleoperators," *Automatica*, vol. 46, no. 1, pp. 155–159, 2010.

[88] Y. Liu and N. Chopra, "Control of semi-autonomous teleoperation system with time delays," *Automatica*, vol. 49, no. 6, pp. 1553–1565, 2013.

[89] Y. Liu and M. Khong, "Adaptive control for nonlinear teleoperators with uncertain kinematics and dynamics," *IEEE/ASME Transactions on Mechatronics*, vol. 20, no. 5, pp. 2550–2562, 2015.

[90] E. Nuño, L. Basañez, R. Ortega, and M. W. Spong, "Position tracking for non-linear teleoperators with variable time delay," *The International Journal of Robotics Research*, vol. 28, no. 7, pp. 895–910, 2009.

[91] E. Nuño, L. Basañez, and R. Ortega, "Passivity-based control for bilateral teleoperation: A tutorial," *Automatica*, vol. 47, no. 3, pp. 485–495, 2011.

[92] M. Ji and M. Egerstedt, "Distributed coordination control of multiagent systems while preserving connectedness," *IEEE Transactions on Robotics*, vol. 23, no. 4, pp. 693–703, Aug 2007.

[93] D. V. Dimarogonas and K. J. Kyriakopoulos, "Connectedness preserving distributed swarm aggregation for multiple kinematic robots," *IEEE Transactions on Robotics*, vol. 24, no. 5, pp. 1213–1223, 2008.

[94] D. V. Dimarogonas and K. H. Johansson, "Decentralized connectivity maintenance in mobile networks with bounded inputs," in *2008 IEEE International Conference on Robotics and Automation*, 2008, pp. 1507–1512.

[95] Z. Kan, A. P. Dani, J. M. Shea, and W. E. Dixon, "Network connectivity preserving formation stabilization and obstacle avoidance via a decentralized controller," *IEEE Transactions on Automatic Control*, vol. 57, no. 7, pp. 1827–1832, 2012.

[96] A. Ajorlou, A. Momeni, and A. G. Aghdam, "A class of bounded distributed control strategies for connectivity preservation in multi-agent systems," *IEEE Transactions on Automatic Control*, vol. 55, no. 12, pp. 2828–2833, 2010.

[97] A. Ajorlou and A. G. Aghdam, "Connectivity preservation in nonholonomic multi-agent systems: A bounded distributed control strategy," *IEEE Transactions on Automatic Control*, vol. 58, no. 9, pp. 2366–2371, 2013.

[98] H. Su, X. Wang, and G. Chen, "Rendezvous of multiple mobile agents with preserved network connectivity," *Systems & Control Letters*, vol. 59, no. 5, pp. 313–322, 2010.

[99] Z. Feng, G. Hu, Y. Sun, and J. Soon, "An overview of collaborative robotic manipulation in multi-robot systems," *Annual Reviews in Control*, 2020.

[100] M. C. De Gennaro and A. Jadbabaie, "Decentralized control of connectivity for multi-agent systems," in *Proceedings of the 45th IEEE Conference on Decision and Control (CDC)*, Dec 2006, pp. 3628–3633.

[101] P. Yang, R. Freeman, G. Gordon, K. Lynch, S. Srinivasa, and R. Sukthankar, "Decentralized estimation and control of graph connectivity for mobile sensor networks," *Automatica*, vol. 46, no. 2, pp. 390–396, 2010.

[102] L. Sabattini, N. Chopra, and C. Secchi, "Decentralized connectivity maintenance for cooperative control of mobile robotic systems," *The International Journal of Robotics Research*, vol. 32, no. 12, pp. 1411–1423, 2013.

[103] L. Sabattini, C. Secchi, N. Chopra, and A. Gasparri, "Distributed control of multirobot systems with global connectivity maintenance," *IEEE Transactions on Robotics*, vol. 29, no. 5, pp. 1326–1332, Oct 2013.

[104] A. Gasparri, L. Sabattini, and G. Ulivi, "Bounded control law for global connectivity maintenance in cooperative multirobot systems," *IEEE Transactions on Robotics*, vol. 33, no. 3, pp. 700–717, June 2017.

[105] M. M. Zavlanos and G. J. Pappas, "Distributed connectivity control of mobile networks," *IEEE Transactions on Robotics*, vol. 24, no. 6, pp. 1416–1428, Dec 2008.

[106] M. M. Zavlanos, H. G. Tanner, A. Jadbabaie, and G. J. Pappas, "Hybrid control for connectivity preserving flocking," *IEEE Transactions on Automatic Control*, vol. 54, no. 12, pp. 2869–2875, 2009.

[107] R. K. Williams and G. S. Sukhatme, "Constrained interaction and coordination in proximity-limited multiagent systems," *IEEE Transactions on Robotics*, vol. 29, no. 4, pp. 930–944, Aug 2013.

[108] R. K. Williams, A. Gasparri, G. Ulivi, and G. S. Sukhatme, "Generalized topology control for nonholonomic teams with discontinuous interactions," *IEEE Transactions on Robotics*, vol. 33, no. 4, pp. 994–1001, Aug 2017.

[109] K. Khateri, M. Pourgholi, M. Montazeri, and L. Sabattini, "A comparison between decentralized local and global methods for connectivity maintenance of multi-robot networks," *IEEE Robotics and Automation Letters*, vol. 4, no. 2, pp. 633–640, April 2019.

[110] ——, "Decentralized local-global connectivity maintenance for networked robotic teams," *European Journal of Control*, vol. 51, pp. 110–121, 2020.

[111] K. Khateri, M. Pourgholi, M. Montazeri, and L. Sabattini, "A connectivity preserving node permutation local method in limited range robotic networks," *Robotics and Autonomous Systems*, vol. 129, p. 103540, 2020.

[112] Z. Kan, E. A. Doucette, and W. E. Dixon, "Distributed connectivity preserving target tracking with random sensing," *IEEE Transactions on Automatic Control*, vol. 64, no. 5, pp. 2166–2173, May 2019.

[113] M. Zareh, L. Sabattini, and C. Secchi, "Decentralized biconnectivity conditions in multi-robot systems," in *2016 IEEE 55th Conference on Decision and Control (CDC)*, 2016, pp. 99–104.

[114] ——, "Enforcing biconnectivity in multi-robot systems," in *2016 IEEE 55th Conference on Decision and Control (CDC)*, 2016, pp. 1800–1805.

[115] M. Minelli, J. Panerati, M. Kaufmann, C. Ghedini, G. Beltrame, and L. Sabattini, "Self-optimization of resilient topologies for fallible multi-robots," *Robotics and Autonomous Systems*, vol. 124, p. 103384, 2020.

[116] W. Luo and K. Sycara, "Minimum k-connectivity maintenance for robust multi-robot systems," in *2019 IEEE/RSJ International Conference on Intelligent Robots and Systems (IROS)*, 2019, pp. 7370–7377.

[117] W. Luo, S. Yi, and K. Sycara, "Behavior mixing with minimum global and subgroup connectivity maintenance for large-scale multi-robot systems," in *2020 IEEE International Conference on Robotics and Automation (ICRA)*, 2020, pp. 9845–9851.

[118] W. Luo, N. Chakraborty, and K. Sycara, "Minimally disruptive connectivity enhancement for resilient multi-robot teams," in *2020 IEEE/RSJ International Conference on Intelligent Robots and Systems (IROS)*, 2020, pp. 11 809–11 816.

[119] G. A. Hollinger and S. Singh, "Multirobot coordination with periodic connectivity: Theory and experiments," *IEEE Transactions on Robotics*, vol. 28, no. 4, pp. 967–973, 2012.

[120] Y. Kantaros and M. M. Zavlanos, "Distributed intermittent connectivity control of mobile robot networks," *IEEE Transactions on Automatic Control*, vol. 62, no. 7, pp. 3109–3121, 2017.

[121] R. Aragues, D. V. Dimarogonas, P. Guallar, and C. Sagues, "Intermittent connectivity maintenance with heterogeneous robots," *IEEE Transactions on Robotics*, vol. 37, no. 1, pp. 225–245, 2021.

[122] Y. Kantaros, M. Guo, and M. M. Zavlanos, "Temporal logic task planning and intermittent connectivity control of mobile robot networks," *IEEE Transactions on Automatic Control*, vol. 64, no. 10, pp. 4105–4120, 2019.

[123] R. Khodayi-mehr, Y. Kantaros, and M. M. Zavlanos, "Distributed state estimation using intermittently connected robot networks," *IEEE Transactions on Robotics*, vol. 35, no. 3, pp. 709–724, 2019.

[124] M. Motaharifar, H. D. Taghirad, K. Hashtrudi-Zaad, and S. F. Mohammadi, "Control synthesis and ISS stability analysis of a dual-user haptic training system based on S-shaped function," *IEEE/ASME Transactions on Mechatronics*, vol. 24, no. 4, pp. 1553–1564, 2019.

[125] S. S. Nudehi, R. Mukherjee, and M. Ghodoussi, "A shared-control approach to haptic interface design for minimally invasive telesurgical training," *IEEE Transactions on Control Systems Technology*, vol. 13, no. 4, pp. 588–592, 2005.

[126] B. Khademian and K. Hashtrudi-Zaad, "Shared control architectures for haptic training: Performance and coupled stability analysis," *The International Journal of Robotics Research*, vol. 30, no. 13, pp. 1627–1642, 2011.

[127] ——, "Dual-user teleoperation systems: New multilateral shared control architecture and kinesthetic performance measures," *IEEE/ASME Transactions on Mechatronics*, vol. 17, no. 5, pp. 895–906, 2012.

[128] K. Razi and K. Hashtrudi-Zaad, "Analysis of coupled stability in multilateral dual-user teleoperation systems," *IEEE Transactions on Robotics*, vol. 30, no. 3, pp. 631–641, 2014.

[129] B. Khademian and K. Hashtrudi-Zaad, "A framework for unconditional stability analysis of multimaster/multislave teleoperation systems," *IEEE Transactions on Robotics*, vol. 29, no. 3, pp. 684–694, 2013.

[130] M. Shahbazi, S. F. Atashzar, H. A. Talebi, and R. V. Patel, "Novel cooperative teleoperation framework: Multi-master/single-slave system," *IEEE/ASME Transactions on Mechatronics*, vol. 20, no. 4, pp. 1668–1679, 2015.

[131] N. A. Usmani, T. Kim, and J. H. Ryu, "Dynamic authority distribution for cooperative teleoperation," in *2015 IEEE/RSJ International Conference on Intelligent Robots and Systems (IROS)*, 2015, pp. 5222–5227.

[132] F. Liu, A. Lelevé, D. Eberard, and T. Redarce, "An energy based approach for passive dual-user haptic training systems," in *2016 IEEE/RSJ International Conference on Intelligent Robots and Systems (IROS)*, 2016, pp. 5246–5251.

[133] A. R. Licona, A. Lelevé, M. T. Pham, and D. Eberard, "A multi-trainee architecture for haptic hands-on training," in *2019 IEEE/RSJ International Conference on Intelligent Robots and Systems (IROS)*, 2019, pp. 7314–7320.

[134] M. Shahbazi, S. F. Atashzar, C. Ward, H. A. Talebi, and R. V. Patel, "Multimodal sensorimotor integration for expert-in-the-loop telerobotic surgical training," *IEEE Transactions on Robotics*, vol. 34, no. 6, pp. 1549–1564, 2018.

[135] M. Motaharifar, H. D. Taghirad, K. Hashtrudi-Zaad, and S. F. Mohammadi, "Control of dual-user haptic training system with online authority adjustment: An observer-based adaptive robust scheme," *IEEE Transactions on Control Systems Technology*, vol. 28, no. 6, pp. 2404–2415, 2020.

[136] K. Urahama and T. Nagao, "K-winners-take-all circuit with O(N) complexity," *IEEE Transactions on Neural Networks*, vol. 6, no. 3, pp. 776–778, 1995.

[137] X. Hu and B. Zhang, "A new recurrent neural network for solving convex quadratic programming problems with an application to the k-winners-take-all problem," *IEEE Transactions on Neural Networks*, vol. 20, no. 4, pp. 654–664, 2009.

[138] S. Liu and J. Wang, "A simplified dual neural network for quadratic programming with its KWTA application," *IEEE Transactions on Neural Networks*, vol. 17, no. 6, pp. 1500–1510, 2006.

[139] S. Li, B. Liu, and Y. Li, "Selective positive–negative feedback produces the winner-take-all competition in recurrent neural networks," *IEEE Transactions on Neural Networks and Learning Systems*, vol. 24, no. 2, pp. 301–309, 2013.

[140] S. Li, M. Zhou, X. Luo, and Z. You, "Distributed winner-take-all in dynamic networks," *IEEE Transactions on Automatic Control*, vol. 62, no. 2, pp. 577–589, 2017.

[141] Y. Zhang, S. Li, B. Xu, and Y. Yang, "Analysis and design of a distributed k-winners-take-all model," *Automatica*, vol. 115, p. 108868, 2020.

[142] L. Jin and S. Li, "Distributed task allocation of multiple robots: A control perspective," *IEEE Transactions on Systems, Man, and Cybernetics: Systems*, vol. 48, no. 5, pp. 693–701, 2018.

[143] L. Jin, S. Li, H. M. La, X. Zhang, and B. Hu, "Dynamic task allocation in multi-robot coordination for moving target tracking: A distributed approach," *Automatica*, vol. 100, pp. 75–81, 2019.

[144] A. Cherukuri and J. Cortés, "Distributed generator coordination for initialization and anytime optimization in economic dispatch," *IEEE Transactions on Control of Network Systems*, vol. 2, no. 3, pp. 226–237, 2015.

[145] ——, "Initialization-free distributed coordination for economic dispatch under varying loads and generator commitment," *Automatica*, vol. 74, pp. 183–193, 2016.

[146] P. Yi, Y. Hong, and F. Liu, "Initialization-free distributed algorithms for optimal resource allocation with feasibility constraints and application to economic dispatch of power systems," *Automatica*, vol. 74, pp. 259–269, 2016.

[147] G. Chen, Q. Yang, Y. Song, and F. L. Lewis, "A distributed continuous-time algorithm for nonsmooth constrained optimization," *IEEE Transactions on Automatic Control*, vol. 65, no. 11, pp. 4914–4921, 2020.

[148] H. Yun, H. Shim, and H.-S. Ahn, "Initialization-free privacy-guaranteed distributed algorithm for economic dispatch problem," *Automatica*, vol. 102, pp. 86–93, 2019.

[149] S. Liang, X. Zeng, G. Chen, and Y. Hong, "Distributed sub-optimal resource allocation via a projected form of singular perturbation," *Automatica*, vol. 121, p. 109180, 2020.

[150] R. Li, "Distributed algorithm design for optimal resource allocation problems via incremental passivity theory," *Systems & Control Letters*, vol. 138, p. 104650, 2020.

[151] X. Zhang and A. Papachristodoulou, "A real-time control framework for smart power networks: Design methodology and stability," *Automatica*, vol. 58, pp. 43–50, 2015.

[152] N. Li, C. Zhao, and L. Chen, "Connecting automatic generation control and economic dispatch from an optimization view," *IEEE Transactions on Control of Network Systems*, vol. 3, no. 3, pp. 254–264, 2016.

[153] T. Stegink, C. De Persis, and A. van der Schaft, "A unifying energy-based approach to stability of power grids with market dynamics," *IEEE Transactions on Automatic Control*, vol. 62, no. 6, pp. 2612–2622, 2017.

[154] D. Feijer and F. Paganini, "Stability of primal–dual gradient dynamics and applications to network optimization," *Automatica*, vol. 46, no. 12, pp. 1974–1981, 2010.

[155] K. C. Kosaraju, V. Chinde, R. Pasumarthy, A. Kelkar, and N. M. Singh, "Stability analysis of constrained optimization dynamics via passivity techniques," *IEEE Control Systems Letters*, vol. 2, no. 1, pp. 91–96, 2018.

[156] K. C. Kosaraju, M. Cucuzzella, and J. M. A. Scherpen, "Distributed control of dc microgrids using primal-dual dynamics," in *2019 IEEE 58th Conference on Decision and Control (CDC)*, 2019, pp. 6215–6220.

[157] Y. Kawano, K. C. Kosaraju, and J. M. A. Scherpen, "Krasovskii and shifted passivity based control," *IEEE Transactions on Automatic Control*, 2020.

[158] G. H. Hines, M. Arcak, and A. K. Packard, "Equilibrium-independent passivity: A new definition and numerical certification," *Automatica*, vol. 47, no. 9, pp. 1949–1956, 2011.

[159] J. T. Wen and M. Arcak, "A unifying passivity framework for network flow control," *IEEE Transactions on Automatic Control*, vol. 49, no. 2, pp. 162–174, 2004.

[160] J. Wang and N. Elia, "A control perspective for centralized and distributed convex optimization," in *2011 50th IEEE Conference on Decision and Control and European Control Conference*, 2011, pp. 3800–3805.

[161] A. Cherukuri, E. Mallada, and J. Cortés, "Asymptotic convergence of constrained primal–dual dynamics," *Systems & Control Letters*, vol. 87, pp. 10–15, 2016.

[162] T. Hatanaka, N. Chopra, T. Ishizaki, and N. Li, "Passivity-based distributed optimization with communication delays using PI consensus algorithm," *IEEE Transactions on Automatic Control*, vol. 63, no. 12, pp. 4421–4428, 2018.

[163] M. Li, G. Chesi, and Y. Hong, "Input-feedforward-passivity-based distributed optimization over jointly connected balanced digraphs," *IEEE Transactions on Automatic Control*, 2020.

[164] S. Yamashita, T. Hatanaka, J. Yamauchi, and M. Fujita, "Passivity-based generalization of primal–dual dynamics for non-strictly convex cost functions," *Automatica*, vol. 112, p. 108712, 2020.

[165] M. Li, S. Yamashita, T. Hatanaka, and G. Chesi, "Smooth dynamics for distributed constrained optimization with heterogeneous delays," *IEEE Control Systems Letters*, vol. 4, no. 3, pp. 626–631, 2020.

[166] D. Gadjov and L. Pavel, "A passivity-based approach to Nash equilibrium seeking over networks," *IEEE Transactions on Automatic Control*, vol. 64, no. 3, pp. 1077–1092, 2019.

[167] C. De Persis and S. Grammatico, "Distributed averaging integral Nash equilibrium seeking on networks," *Automatica*, vol. 110, p. 108548, 2019.

[168] E. D. Sontag, "Input to state stability: Basic concepts and results," in *Nonlinear and Optimal Control Theory*. Springer, 2008, pp. 163–220.

[169] P. Pepe and Z.-P. Jiang, "A lyapunov–krasovskii methodology for ISS and iISS of time-delay systems," *Systems & Control Letters*, vol. 55, no. 12, pp. 1006–1014, 2006.

[170] R. Ortega, J. A. L. Perez, P. J. Nicklasson, and H. J. Sira-Ramirez, *Passivity-Based Control of Euler-Lagrange Systems: Mechanical, Electrical and Electromechanical Applications*. Springer Science & Business Media, 2013.

[171] M. Mesbahi and M. Egerstedt, *Graph Theoretic Methods in Multiagent Networks*. Princeton University Press, 2010.

[172] I. Karafyllis, P. Pepe, and Z.-P. Jiang, "Input-to-output stability for systems described by retarded functional differential equations," *European Journal of Control*, vol. 14, no. 6, p. 539, 2008.

[173] A. Nygaard, "High-level control system for remote controlled surgical robots: Haptic guidance of surgical robot," Master's thesis, Norwegian University of Science and Technology, 2008.

[174] E. Nuño, I. Sarras, and L. Basañez, "Consensus in networks of nonidentical Euler–Lagrange systems using P+d controllers," *IEEE Transactions on Robotics*, vol. 29, no. 6, pp. 1503–1508, 2013.

[175] F. Blanchini, "Set invariance in control," *Automatica*, vol. 35, no. 11, pp. 1747–1767, 1999.

[176] M. M. Zavlanos, M. B. Egerstedt, and G. J. Pappas, "Graph-theoretic connectivity control of mobile robot networks," *Proceedings of the IEEE*, vol. 99, no. 9, pp. 1525–1540, 2011.

[177] A. Zavala-Río and V. Sántibañez, "A natural saturating extension of the PD-with-desired-gravity-compensation control law for robot manipulators with bounded inputs," *IEEE Transactions on Robotics*, vol. 23, no. 2, pp. 386–391, 2007.

[178] F. Morabito, A. R. Teel, and L. Zaccarian, "Nonlinear antiwindup applied to Euler-Lagrange systems," *IEEE Transactions on Robotics and Automation*, vol. 20, no. 3, pp. 526–537, 2004.

[179] A. Zavala-Río and V. Santibáñez, "Simple extensions of the PD-with-gravity-compensation control law for robot manipulators with bounded inputs," *IEEE Transactions on Control Systems Technology*, vol. 14, no. 5, pp. 958–965, 2006.

[180] K. J. Kuchenbecker and G. Niemeyer, "Modeling induced master motion in force-reflecting teleoperation," in *Proceedings of the 2005 IEEE International Conference on Robotics and Automation (ICRA)*, April 2005, pp. 348–353.

[181] M. Panzirsch, H. Singh, and C. Ott, "The 6-DoF implementation of the energy-reflection based time domain passivity approach with preservation of physical coupling behavior," *IEEE Robotics and Automation Letters*, vol. 5, no. 4, pp. 6756–6763, 2020.

[182] K. I. Diamantaras and S. Y. Kung, *Principal Component Neural Networks: Theory and Applications*. John Wiley & Sons, Inc., 1996.

[183] D. P. Bertsekas, *Nonlinear Programming*. Athena Scientific, 1999.

[184] J. Zhao and D. J. Hill, "Dissipativity theory for switched systems," *IEEE Transactions on Automatic Control*, vol. 53, no. 4, pp. 941–953, 2008.